# TUNING MECHANICAL PROPERTIES OF HYDROGELS

**OYA USTAHÜSEYİN**

Max Planck Graduate Center
mit der Johannes Gutenberg-Universität Mainz


DISSERTATION

Zur Erlangung des Grade eines
„Doctor rerum naturalium (Dr. rer. nat.)“
der Fachbereiche:
• 08 – Physik, Mathematik und Informatik
• 09 – Chemie, Pharmazie und Geowissenschaften
• 10 – Biologie
• Universitätsmedizin
der Johannes Gutenberg-Universität

Mainz, July 2017

# TUNING MECHANICAL PROPERTIES OF HYDROGELS

**Oya USTAHÜSEYİN**

**geb. in İstanbul i. d. Türkei**

Dissertation

Max Planck Institut für Polymerforschung

Mainz, July 2017

*Dedicated to my family*

I hereby declare that I wrote this dissertation submitted without any unauthorized external assistance and used only sources acknowledged in the work. All textual passages which are appropriated verbatim or paraphrased from published and unpublished texts as well as all information obtained from oral sources are duly indicated and listed in accordance with bibliographical rules. In carrying out this research, I complied with the rules of standard scientific practice as formulated in the statutes of the Johannes Gutenberg-University Mainz to insure standard scientific practice.

Oya USTAHÜSEYİN

# Abstract

The properties of the cellular microenvironment are critical for cellular behaviour and are dynamically regulated in living tissues. The mechanical properties of the extracellular matrix (ECM), in particular, are relevant cues influencing attachment, spreading, and phenotypic differentiation of cells. These properties change during healing, aging, or disease states. Natural and synthetic hydrogels used to mimic the extracellular matrix in *in vitro* cultures need to capture the mechanical properties of the ECM and their changes. In this thesis, different strategies to adjust and dynamically tune the stiffness of synthetic poly(ethyleneglycol) and natural alginate based hydrogels within physiologically relevant ranges are presented. They include different tunable crosslinking mechanisms (catechol chemistry, ionic crosslinking and photoactivatable strategies), polymer architectures (single and interpenetrating networks) and morphologies (hydrogel films and 3D bioprinted scaffolds).

Catechol-terminated poly(ethyleneglycol) (PEG) hydrogels with tunable mechanical properties were developed by introducing electron-donating or electron-withdrawing substituents on the catechol ring. Gel mechanics during gelation was characterized by rheology measurements. The effect of substitution in the final stiffness and the crosslinking kinetics of the hydrogels was studied. Independently variation of these two parameters within desired ranges was successfully achieved by mixing different catechol derivatives and oxidative conditions.

Light-based dynamic regulation of the mechanical properties of catechol-derivatized PEG hydrogels was attempted using photosensitive nitrocatechol derivatives. Synthetic effort was devoted to obtain chromophores with high photosensitivity in order to allow changes in the mechanical properties in the presence of living cells without causing photodamage. Nitrobenzyl chemistry was also applied to dynamically regulate the mechanics of soft alginate hydrogels by using a phototunable calcium chelator. *In situ* variations in the ionic crosslinking degree of the alginate upon light-induced changes in the concentration of $Ca^{2+}$ ions was demonstrated.

The long term mechanical stability of ionically crosslinked alginate in cell culture conditions was studied by rheology. Interpenetrating networks (IPNs) of ionically crosslinked alginate and covalently crosslinked polyacrylamide hydrogels with different compositions were developed and the mechanical properties during incubation in different conditions were studied. Stable network compositions with mechanical properties within physiologically relevant ranges were obtained.

Mechanically tunable 3D alginate scaffolds were developed by 3D bioprinting Alginate/Gelatin mixtures. Parameter windows for printability using different compositions, temperature and ionic concentration of the printing bath were identified. 3D scaffolds with enhanced stability in watery media were achieved by using chitosan to build polyionic complex coatings on the scaffold. The physical properties of scaffold were monitored over different temperature ranges.

# Zusammenfassung

Die Eigenschaften der zellulären Mikroumgebung sind entscheidend für das Zellverhalten und sind in lebendem Gewebe dynamisch reguliert. Insbesondere die mechanischen Eigenschaften der extrazellulären Matrix (EZM) sind relevante Faktoren, die das Anhaften, Ausbreiten und die phänotypische Differenzierung von Zellen beeinflussen. Diese Eigenschaften verändern sich während eines Heilungsprozesses, der Alterung oder einer Erkrankung. Natürliche sowie synthetische Hydrogele, die genutzt werden um extrazelluläre Matrix in *in vitro* Zellkulturen nachzuahmen, müssen die mechanischen Eigenschaften der EZM und ihre Veränderungen nachbilden können. In dieser Arbeit werden verschiedene Strategien präsentiert, mit denen die Steifheit von synthetischen polyethylenglycolbasierten und natürlichen alginatbasierten Hydrogelen im physiologisch relevanten Bereich eingestellt und dynamisch angepasst werden kann. Diese beinhalten verschiedene einstellbare Vernetzungsmechanismen (Brenzcatechin Chemie, ionische Vernetzung und photoaktivierbare Strategien), Polymergebilde (einfache und interpenetrierende Netzwerke) und Morphologien (Hydrogelfilme und mithilfe eines Bioprinters hergestellte 3D Gerüste).

Mit Brenzcatechin als Endgruppe versehene Polyethylenglycolhydrogele mit verstellbaren mechanischen Eigenschaften wurden durch Elektronen abgebende, beziehungsweise Elektonen entziehendeSubstituenten im Brenzcatechinring hergestellt. Die mechanischen Eigenschaften wurden während der Gelierung mittels rheologischer Messungen charakterisiert. Der Einfluss von Substitution auf die endgültige Steifheit und die Vernetzungskinetiken der Hydrogele wurde analysiert. Eine individuelle Variierung dieser beiden Parameter innerhalb des gewünschten Bereiches wurde durch das Mischen verschiedener Brenzcatechinderivate und Abänderung oxidativer Bedingungen erreicht.

Lichtbasierte dynamische Regulierung der mechanischen Eigenschaften von Brenzcatechin derivatisierten Polyethylenglycolhydrogelen wurde mittels photosensitiver Nitrocatecholderivate versucht. Bei der Synthese der Chromophore wurde besonderer Wert auf hohe Photosensitivität gelegt um eine Veränderung der mechanischen Eigenschaften zu ermöglichen ohne dabei vorhandene lebende Zellen bei der Bestrahlung zu schädigen. Nitrobenzylierungen wurden angewendet um die mechanischen Eigenschaften von Alginathydrogelen dynamisch zu regulieren, wobei ein lichtabhängiger Calciumchelator eingesetzt wurde. Abänderungen des ionischen Vernetzungsgrades des Alginats nach lichtinduzierten Veränderungen der $Ca^{2+}$ Ionenkonzentration konnte *in situ* gezeigt werden.

Die mechanische Langzeitstabilität von ionisch vernetztem Alginat unter Zellkulturbedingungen wurde mittels rheologischer Messungen analysiert. Interpenetrierende Netzwerke (IPNs) aus ionisch vernetztem Alginat und kovalent vernetzten Polyacrylamidhydrogelen mit unterschiedlicher Zusammensetzung wurden hergestellt und auf ihre mechanischen Eigenschaften während der Inkubation unter verschiedenen Bedingungen untersucht. Es konnten stabile Netzwerkzusammensetzungen mit mechanischen Eigenschaften innerhalb der physiologisch relevanten Bereiche hergestellt werden.

Mechanisch veränderbare 3D Alginatgerüste wurden mithilfe eines 3D Bioprinters aus Alginat/Gelatinlösungen hergestellt. Spezifische Parameterbereiche für verschiedene Zusammensetzungen, Temperatur und Ionenkonzentrationen des Druckerbades wurden für den 3D-

Druck wurden identifiziert. 3D Gerüste mit verbesserter Stabilität in wässrigem Medium konnten mittels polyionischer komplexer Beschichtung mit Chitosan hergestellt werden. Die physikalischen Eigenschaften des Gerüsts wurden bei verschiedenen Temperaturbereichen gemessen.

# Abbreviations

| | |
|---|---|
| α | Hydrodynamic radius of diffusing solute |
| γ | Frequency |
| δ | Chemical shift |
| Σ | Molar extinction coefficient |
| Y | Free volume theory diffusion parameter, |
| E | Young's modulus or modulus of elasticity |
| G | Shear modulus |
| Q | Swelling ratio |
| γ | Strain |
| η | Shear viscosity |
| ξ | Mesh size |
| σ | Stress |
| $\upsilon$ | Polymer volume fraction |
| $M_c$ | Molecular weight between elastically-active crosslinking points |
| $\dot{\gamma}$ | Shear rate |
| $\rho_x$ | Crosslinking density |
| °C | Degree Celsius |
| | |
| µm | Micrometre |
| 13C-NMR | Carbon NMR spectroscopy |
| 1H-NMR | Proton NMR spectroscopy |
| AD | anno Domini; beforeChrist |
| BAPTA | 1,2-bis(*o*-aminophenoxy)ethane-N,N,N′,N′-tetraacetic acid |
| bFGF | Basic fibroblast growth factor |
| boc-Osu | *N*-(tert-Butoxycarbonyloxy) succinimide |
| C2C12 | Mouse myoblast cell line |
| | |
| ca. | Circa, meaning *approximately* |
| CH | Methine |
| $CH_2$ | Methylene |
| CT | Computed tomography |
| d | Day |
| DBTDL | Dibutyltin dilaurate |
| DBU | 1,8-Diazabicyclo[5.4.0]undec-7-ene |
| $D_{gel}$ | Diffusion coefficient in hydrogel |
| DHI | 5,6-dihydroxyindole |
| DMF | N,N-Dimethylformamide |
| DMP | 2,2-dimethoxypropane |
| DNA | Deoxyribonucleic acid |
| ECM | Extracellular matrix |
| EDC | *N*-(3-dimethylaminopropyl)-*N′*-ethylcarbodiimide |
| FAK | Focal adhesıon kinase |
| Fmoc-Osu | 9-fluorenylmethyl N-succinimidyl carbonate |
| g $moL^{-1}$ | Gram per moL |
| $G'$ | Storage modulus |
| $G''$ | Loss Modulus |
| GDL | D-glucono-δ-lactone |

| | |
|---|---|
| GelMA | Gelatin methacrylate |
| GO | Graphene oxide |
| GPC | Gel permeation chromatography |
| GTPase | A family of enzymes that hydrolyze guanosine triphosphate |
| h | Hour |
| hFOB | Human fetal osteoblastic cell line |
| HPLC | High-performance liquid chromatography |
| HRP | horseradish peroxidase |
| Hz | Hertz |
| i.e. | In other words |
| IKVAV | Isoleucine-lysine-valine-alanine-valine |
| ILK | Integrin-linked kinase |
| IQGAP1 | Ras GTPase-activating-like protein |
| $J/m^2$ | Joule per square metre |
| $kJm^{-2}$ | KiloJoule per square metre |
| kPa | KiloPascal |
| LAP | Lithium phenyl-2,4,6-trimethylbenzoylphosphinate |
| LED | Light-emitting diode |
| M | Molarity (mol/L) |
| m | Multiplett (NMR) |
| MeHA | Methacrylated hyaluronic acid |
| min | Minute |
| mm | Milimeter |
| mM | Milimolar |
| MMPs | Metalloproteinases |
| $M_n$ | Average number molecular weight |
| MOM | Methoxymethyl |
| MPa | MegaPascal |
| MTFA | Methyl trifluoroacetate |
| $M_w$ | Molecular weight |
| $mW\ cm^{-2}$ | MilliWatt per square centimetre |
| NHS | *N*-hydroxysuccinimide |
| NIH-3T3 | Cell line of mouse embryonic fibroblasts |
| nm | Nanometer |
| nN | NanoNewton |
| NNEN | Nitro-norepinephrine |
| *o* | Ortho |
| OH | Hydroxyl |
| OMe | Methoxy |
| ONC | Cyanate |
| *p* | Para |
| p130Cas | A focal adhesion protein; Crk-associated substrate |
| Pa | Pascal |
| pAMPS | Poly(2-acrylamido-2-methyl-1-propanesulfonic acid) |
| PBS | Phosphate buffered saline |
| PCL | Poly(caprolactone) |
| PDGF | Platelet-derived growth factor |
| PDMS | Poly(dimethylsiloxane) |
| PEG | Polyethylene glycol |
| PGA | Polyglycolic acid |
| pN | PicoNewton |

| | |
|---|---|
| ppm | Parts per million |
| PVA | Poly(vinyl alcohol) |
| R | Universal gas constant |
| RACK1 | Receptor for activated C kinase 1 |
| Ras | Rat sarcoma |
| s | Second |
| SD | Standard deviation |
| SEM | Scanning electron microscope |
| T | Temperature |
| TBD | 1,5,7-Triazabicyclo[4.4.0]dec-5-ene |
| TBDMS-Cl | *tert*-Butyldimethylsilyl chloride |
| TFA | Trifluoroacetic acid |
| TGF-β | Tissue growth factor |
| UV | Ultraviolet |
| V | Volume |
| VEGF | Vascular endothelial growth factor |
| VIC | Valvular interstitial cell |
| vs. | Versus |
| wt% | Weight percentage |
| $\nu$ | Poisson's ratio |

All other abbreviations, as physical and chemical units, have their usual meaning if not stated otherwise.

## INDEX

# Motivation

The mechanical properties of living tissues are different depending on tissue function and mechanical solicitations to which they are exposed. For example, bone is a hard tissue that provides mechanical stability to the body; lung is a soft, elastic tissue that has to support cyclic deformation during breathing. Cells within the different tissues are therefore attached to environments of different stiffness. Mechanical aspects have not been taken into account in biomaterials supporting in vitro cell cultures until recently. Polystyrene tissue culture plates are the gold standard substrates for 2D cell culture. In 2006, a study showed that mesenchymal stem cells (MSCs) can differentiate into different phenotypes depending on the Young's Modulus of the culture substrate. That seminal study was followed by many others demonstrating that the mechanical properties of the cellular microenvironment in vitro affect short and long term cell functions such as adhesion, self-renewal, migration or differentiation.

The mechanical properties of living tissues change during aging and healing processes and in pathological states like tumour formation. Typical substrates for cell culture in 2D and 3D present a constant stiffness and do not capture the dynamic evolution of mechanics in tissues. New biomaterials with tunable mechanical properties and able to undergo controlled mechanical changes in tihe presence of cells need to be developed in order to understand and reproduce mechanical effects in in vitro cultures and tissue models. This PhD Thesis presents different strategies to tune mechanics of hydrogel based biomaterials.

The thesis is organized as follows. *Chapter 1 (Background and Literature Review)* describes the state-of-the-art of literature concerning cell-biomaterials interactions, hydrogel based biomaterials and strategies to control their mechanical properties.

*Chapter 2* presents a strategy to tune the polymerization kinetics and the mechanical properties of PEG hydrogels functionalized with catechols for crosslinking.

*Chapter 3* two chemical strategies were introduced to change the mechanical properties of PEG or alginate gels using light. The first one includes the increase the crosslinking density in alginate hydrogel by light with the help of a photoactivatable calcium chelator, Nitr-T. The second strategy is the photodegradation of PEG hydrogels functionalized with nitrocatechol derivatives

*Chapter 4* describes alginate/pAAm interpenetrating networks and formulation strategies to control their short-term and long-term mechanical stability.

In *Chapter 5,* describes a strategy for 3D printing of alginate/gelatin scaffolds with high fidelity by printing in $CaCl_2$/chitosan crosslinking bath..

In *Chapter 6* the most important conclusions of the work will be stated and a brief outlook is provided.

*Chapter 7 (Appendix)* provides supplementary data of Chapters 2-5.

# 1

# Background and Literature Review

## 1.1 The Natural Cellular Environment

Tissues are mainly composed of cells and extracellular matrix (ECM). ECM is the scaffold where the cells are embedded. It is secreted by the cells and provides mechanical support and anchoring for cells to stabilize and form tissues. The composition of the ECM is specific for each tissue type[2].(Figure 1.1) The ECM contains important cues to regulate tissue morphogenesis and homeostasis. Moreover, ECM is highly dynamic and is remodeled by the cells biochemically and mechanically. In the cellular microenvironment, there are also soluble factors secreted by the cells (growth factory, cytokines etc).

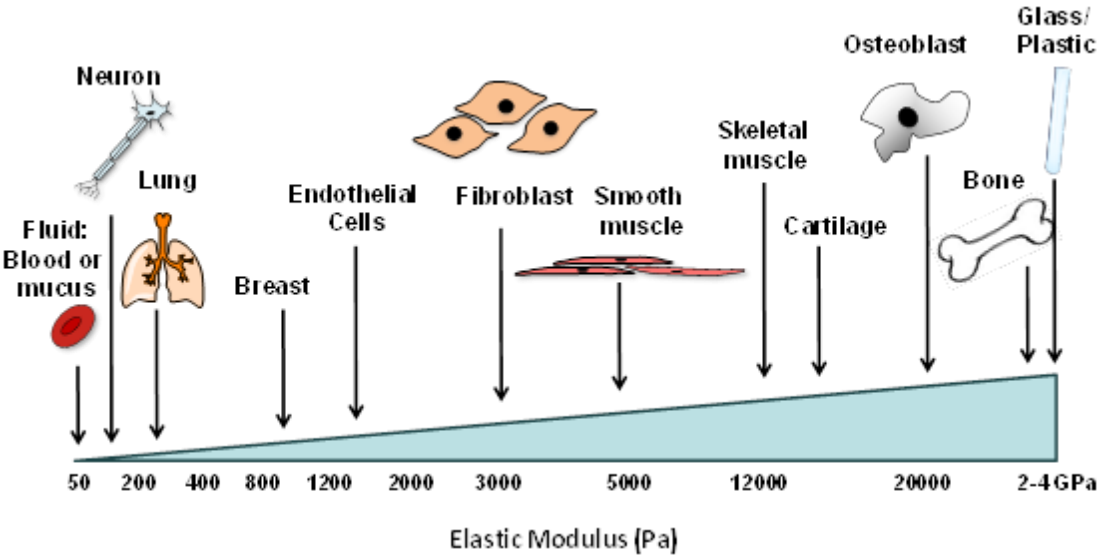


**Figure 1.1** Mechanical properties of tissues in different parts of body. Reproduced with permission from [3] Copyright Nature publishing group.

The ECM has two main components: 1) *proteoglycans* and 2) fibrous proteins (Figure 1.2). Proteoglycans are *glycosaminoglycans* (GAGs) covalently attached to a specific core protein (with exception of the GAG hyaluronic acid). They can be classified in three main families: modular proteoglycans, small leucine-rich proteoglycans and cell-surface proteoglycans.[4] The GAG chains are unbranched polysaccharides consisting of sulfated or nonsulfated disaccharide units. The GAGs chains are hydrophilic and capable of absorb water in high extend. Fibrous proteins are relevant for the mechanical properties of the tissue. Collagen, elastin, resilin, fibronectin or laminin are important ECM proteins. The most abundant fibrous protein in ECM is collagen. It forms 30% of the total protein mass of multicellular animal. ECM proteins offer adhesive cues to embedded cells to regulate cell functions such as cell migration, cell adhesion, differentiation and proliferation.[5] For instance, it has been shown that fibronectin suppresses

differentiation and promotes proliferation of myoblast or human umbilical cord blood derived neural stem cells, (nSCs) and laminin stimulates differentiation of embryonic stem cell lines or cortical neural progenitors.[6-9] Collagen fibers assist migration along the fiber direction and direct tissue formation. [10]

The composition of the ECM varies during aging, healing or during tissue pathologies like cancer. During aging process, elastin network gets degenerated, the amount of fibronectin and decorin increases whereas total number of proteoglycans decrease. Collagen fibers get more crosslinked.[11] the basal membrane, the ECM layer supporting epithelial layers, weakens and its thickness decreases probably because of increase in activity of matrix metalloproteinases (MMPs).[12] As a result of these changes, tensile strength decreases and stiffness increases in tissue. In wound healing process, the most significant change is the increase in the amount of Collagen I and III, fibcronectin, hyaluronic acid and fibrin around the wound. It leads to an increase in stiffness and a decrease in mechanical stability, tensile strength and elasticity. The increase in mechanical stress related with change in ECM composition, initiates the epithelial-to-mesenchymal transition of epithelial cells or transdifferentiation of fibroblasts.[13, 14] Also, the levels of growth factors (GFs) such as TGF-β, PDGF, bFGF, and VEGF, increase to promote healing of the wound. Additionally, it was reported that an unresolved wound can resemble the characteristics of a tumor.[15] Tumorigenic tissue is stiffer than normal tissue. It is caused by remodeling of ECM by neighboring fibroblast and elevated contractility of ECM by transdifferentiated fibroblasts into myofibroblasts and expanding epithelium. Elevated levels of chemokines and GFs in ECM cause inflammation. It follows increase in levels of collagen type I, III and IV, fibronectin, elastin, PGs such as decorin, biglycan and lumican in ECM secreted by transdifferentiated myofibroblasts.[2]

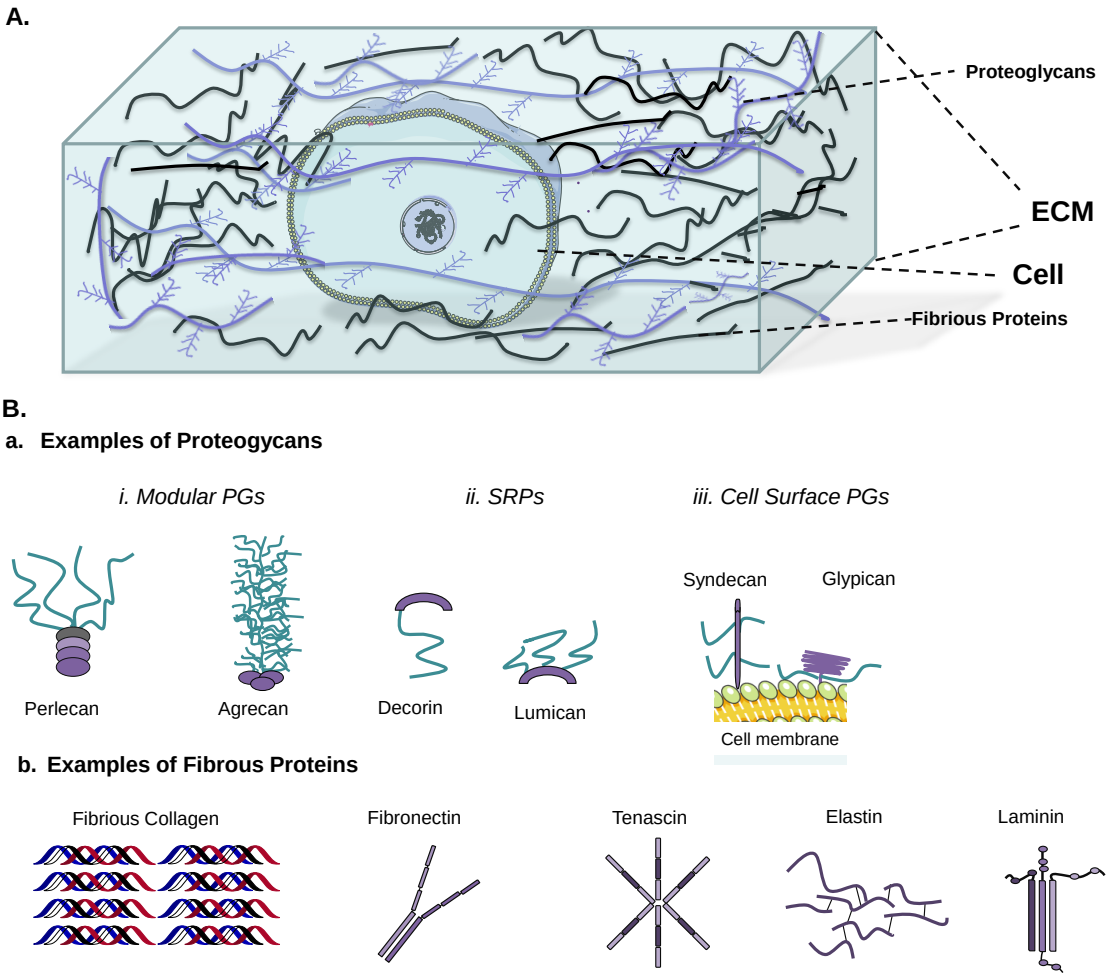


**Figure 1.2 A.** Representation of a cell in ECM. **B.** Schematic showing components of ECM. **a.** Examples of various proteoglycans, **b.** Examples of fibrous proteins. Reprinted with permission from (1). Copyright (2010) Company of Biologists LTD.

The interactions between the ECM and the embedded cells in a tissue are mediated by cell adhesion molecules (CAMs) located at the cellular membrane. Most important CAMs regulating fundamental cellular functions are integrins, selectins and syndecan proteoglycans.[16-18] The integrin family includes 24 heterodimers with α and β subunits.[19] 18 types of α subunits and 8 types of β subunits exist in mammals. A single β chain can interact with several α chains increasing diversity of integrins and creating specificity for cells to migrate to the correct direction during tissue morphogenesis. The size of integrins varies from 750 to 1000 amino acids typically.[18]

All five αV integrins, two β1 integrins (α5, α8), and αIIbβ3 recognize ligands at the ECM containing the tripeptide arginine-glycine-aspartic acid (RGD). The Interaction of αVβ3 and

αIIbβ3 with RGD ligands has been studied in crystal structures.[20, 21] The interaction site has an interface with α and β subunits, with the basic residue fitting into a cleft in a β-propeller module in the α subunit, and the acidic residue coordinating a cation bound in the β-I-domain. RGD is a widely used cell adhesive peptide to mediate the interaction of membrane integrins to synthetic biomaterials.

Integrins have different structural forms depending on their activity state. Integrins can be in low, intermediate or high ligand affinity state.[22] In low ligand affinity state, the integrin exists in bent V-shape.[23] When the integrin recognizes an interaction site at the ECM, it goes through rapid conformational changes to the “activated” form.[24] Activation of integrin might lead to formation of focal adhesions and thus attachment of the cell. The formation of focal adhesions includes sequential steps: 1) Recognition and binding of receptor to ligand, 2) Recruitment of additional integrins to form a focal adhesion complex and connection to the actin cytoskeleton, 3) Initiation of signal transduction and 4) Actin polymerization and regulation of cellular activity.[25] (Figure 1.3) Focal adhesion complexes include proteins such as talin, tensin, plectin, filamin, α-actinin or kindlin-ILK-parvin complex. The proteins focal adhesion kinase (FAK), receptor for activated C kinase 1 (RACK1), integrin-linked kinase (ILK), paxillin, p130Cas, and Ras GTPase–activating–like protein IQGAP1 are involved in regulation of signal transduction processes. [26-30] The last step is actin polymerization. Cooperation between actin and myosin within cell generates contractile forces. It is created by stepping of the motor proteins from the myosin family on the actin filaments. These steps are regulated with the mechanical tension formed by motors pulling on their filaments in the lamella from lamellipodium. Whereas contractile forces are formed by myosins in lamella, protrusive forces are created by polymerization of actin network in the lamellipodium. These two forces move the cell membrane forward.[31] There are studies indicating that the generation of this mechanical force depends on the rigidity of substrate that the cell attaches.[32]

It should be noted that the experimental demonstration that cells are able to apply forces is already 40 years old, when researchers observed that cells exerted wrinkles on elastic substrates.[33] This study made the anchorage between cell and substrate visible. The response of the cells was characterized with spreading area, cytoskeletal polarization, adhesion strength and cellular traction forces.[34]

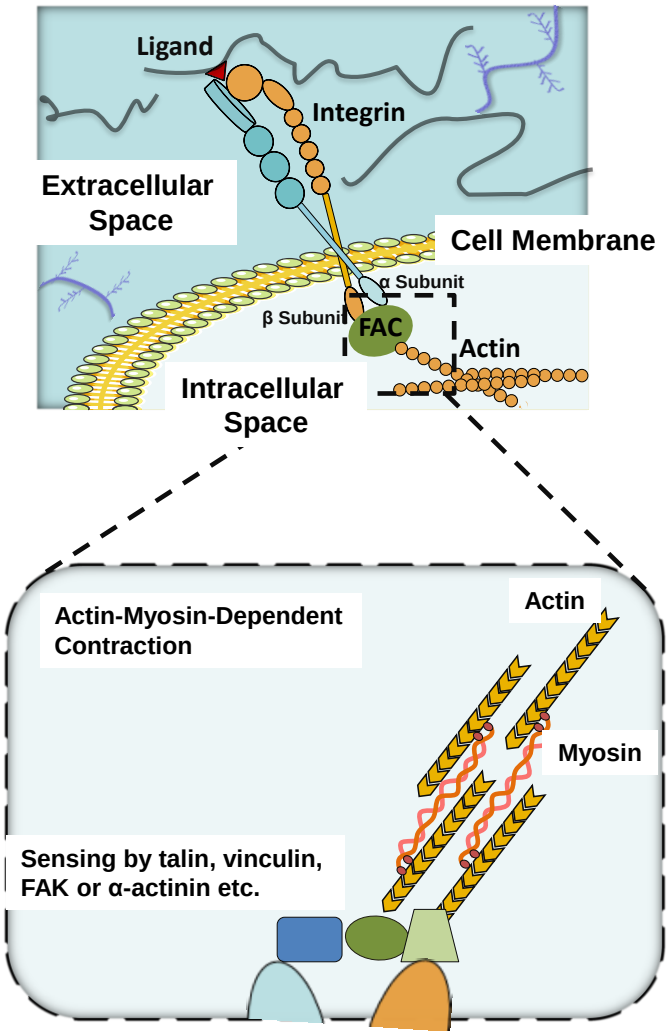


**Figure 1.3** Representation of integrin in cell membrane. Different colors show different subunits of integrin. Interaction of integrin with a ligand (soluble or part of ECM) changes actin cytoskeleton through focal adhesion complexes (FACs).

In human body, cells are exposed to different types of mechanical stimuli; shear, compressive, and tensile stress during daily life.[3] In recent years, researchers have found out that cells are able to sense mechanical stimuli and also the mechanical properties of the extracellular matrix.[35-39] The term *mechanotransduction* has been developed to describe the response of cells to the mechanical properties of the cellular microenvironment. Cells and sub cellular structures can experience mechanical stresses from many sources. Stress might occur through external forces applied to the tissue, or through endogenous forces generated by the cellular cytoskeleton. External forces range from stresses on the musculoskeletal system to microscopic forces exerted by contracting cells in the surrounding extra cellular matrix (ECM). Such forces

generate many different cellular responses and can be transduced through different mechanisms. The threshold magnitude of external forces that trigger cellular response appears to be in the pN to nN range.[40, 41] Cells generate forces of magnitudes from 1-100nN per focal adhesion.[42-44] Myosin generated forces are almost always contractile i.e. Cell is under tension and forces are applied towards the centroid of the cell.[42, 43] Blocking cell generated forces can alter many basic cellular functions, such as proliferation differentiation sorting and migration.[45-49]

The ability of cells to sense and respond to the mechanical properties of their microenvironment opens the possibility of directing cell behavior by using biomaterials with different physical and chemical properties depending on purpose of application.[50] Recent studies have shown that the differentiation pathway of stem cells (SCs) *in vitro* depends on the mechanical properties of the substrate or biomaterial used for their culture. *In vivo*, the stiffness of the ECM varies with the type of tissue, from ca. 30 kPa in the case of bone, to 5 kPa in fat tissue. *In vitro* cultures of mesenchymal stem cells (MSCs) on planar substrates with different stiffness (from 1 to 100kPa) showed that osteoblasts were obtained on stiff surfaces and adipocytes were obtained on substrates with lower stiffness. [51] Similar studies on 3D stem cell cultures on hydrogels with different stiffness also showed that cells differentiation was also dependent on the crosslinking density and matrix stiffness. [52-55] Studies of stem cell lineage commitment in an ionically-crosslinked alginate hydrogel with different rigidities showed a clear tendency of human and murine MSCs to undergo adipogenic commitment within soft hydrogels (2.5-5 kPa) and osteogenic commitment within rigid hydrogels (11-100 kPa).[53] Similar experiments were performed by a different group on polydimethylsiloxane (PDMS) and polyacrylamide (pAAm) gels with comparable mechanical properties.[54] Whereas hMSCs showed different commitments on pAAm hydrogels with different rigidity, this was not observed on PDMS gels. This apparent inconsistency was justified by the fact that adsorption of cell anchoring proteins on the different materials is different. Cells sense the mechanical properties of the matrix through the linkage between membrane receptors and ECM proteins and, therefore, not only the matrix stiffness but also the type and concentration of anchoring proteins available for the cell to build up adhesion complexes and the way they are linked to the matrix or biomaterial, influence differentiation.

*In vivo*, cells continuously remodel the properties of the ECM. This raises the question of what happens to SCs during differentiation when the mechanical properties of their environment are dynamically changed. Regulation of stem cell differentiation by in-situ changing the matrix

rigidity has also been examined. Using a photodegradable polymer, Anseth et al.[56] differentiated hMSCs into chondrocytes upon *in-situ* light irradiation. However, the photodegradation changed both the stiffness and the availability of anchoring proteins in the matrix at the same time and, therefore, the real role of the mechanical cue cannot be assessed. It has also been demonstrated that temporal rigidification of ECM altered the lineage commitment of hMSCs. [57] Hyaluronic acid functionalized with methacrylate side groups (MeHA) and a photoinitiator was used and the stiffness of the material was increased by light exposure. hMSCs cultured on these gels showed differences in differentiation upon short and long term (minutes to hours or days to weeks) stiffening. Eventually, the cells preferentially underwent adipogenic lineage in later stiffening and into osteogenic lineage in earlier stiffening on the surface. According a recent study by Anseth et al, hMSCs have mechanical memory. When they are treated on stiff surface and then softer surface, reversible or irreversible (depending on mechanical dose) differentiation starts. [58]

These studies clearly show the relevance that the mechanical properties of the cell microenvironment might have in cellular processes. They also highlight the need of well-established hydrogels for 3D culture protocols with tunable stiffness to study these processes. On the other hand, it is clear that cells response to the mechanical cue is highly dependent on the status of the adhesive complexes (integrin-ECM), i.e. the availability of adhesive binding motifs of tethered proteins to the scaffold, the nature of their linkage to it, and most probably their temporal variation. In order to understand this interplay, biomaterials that allow individual, independent and spatiotemporal controlled changes of the stiffness within physiologically relevant ranges (1-100 kPa) and the presence and availability of adhesive ligands are required. Responsive hydrogels for biomedical applications typically undergo crosslinking or swelling changes in response to the temperature or pH variations.[59] However, these changes are also associated to changes in the polarity of the chains and cannot be spatially localized. These limitations can be overcome with light responsive hydrogels.[60]

Beyond biochemical composition and mechanical properties, the structural organization of the ECM is also a relevant parameter to which cells respond. Organization of the components of ECM is tissue specific. [61] For instance in muscle tissue, collagen fibers are aligned whereas in small intestinal submucosa collagens are in spiral arrangement with adjacent smooth muscle cells. The alignment of collagen fibers in muscle provides high tensile strength to the tissue.[62] The spiral arrangement of collagen fibers enables efficient transport of biomass. Also this spiral arrangement of collagen fibers causes anisotropic biomechanical behavior of small intestinal

submucosa ECM.[63] 3D structure of ECM alters mechanical behavior. Moreover, spatial arrangement of ECM influences migratory decisions of cells in regard of porosity, network density and alignment of adhesive receptors.[64]

## 1.2 Hydrogels as Biomimetic Cellular Microenvironments

Researchers have used a wide range of materials including synthetic or bio- polymers, metals, ceramics, or composite materials designed to replace tissues in human body. [65] In tissue engineering, biopolymers are used to mimic characteristics of ECM and provide a minimal scaffold to study and analyze the behavior of living cells or tissues *in vitro*. The compositional, mechanical and structural properties of the scaffold are important for the recreating natural ECM environment. (Figure 1.4) For example, it has been showed that the surface to volume ratio, polarity, and rigidity of the cells were similar to their natural properties when they were cultured in hydrogels compared to tissue culture plates.[66] In particular, there is a growing literature in studying the relation between cell behavior and the material where cells are cultured. For instance, in 3D cell culture conditions, mammary epithelial cells responded similar to their response in *in vivo* unlike their response in 2D cell culture conditions. [67] Additionally, the features of native ECM are quite dynamic. Therefore, the need of dynamically tunable ECM mimics has been ascending to study the interplay between cells and their microenvironment.

**Properties of Biomimetic Materials Affecting Cell Behavior:**

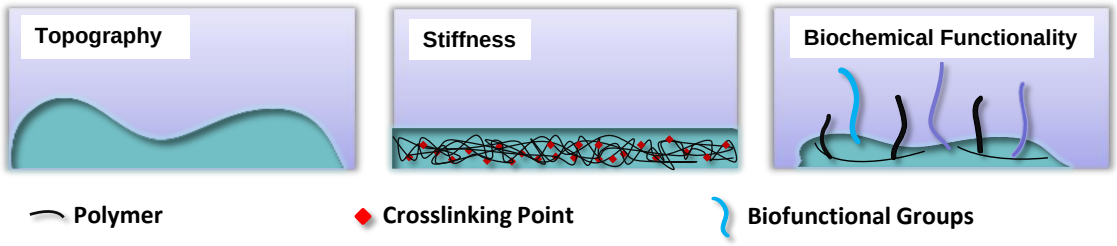


**Figure 1.4**Features of biomimetic materials affecting cell behavior.

Hydrogels are polymeric networks which can absorb up to 99 wt.% of water and find application for ECM replacement. They can be biocompatible and easily tunable in terms of their mechanical properties. They are of interest for medical applications such as wound healing ,[68] drug delivery,[69] scaffold for tissue engineering,[70],[71] or prosthetics[72]. Hydrogels can be based on natural or synthetic polymers. Most commonly used natural polymers are alginate, chitosan, collagen, and gelatin. In synthetic polymers, polyethylene glycol (PEG), and pAAm, poly(2-hydroxyethyl methacrylate) (pHEMA), poly(*N*-isopropylacrylamide) (pNIPAM) and peptide

amphiphiles are the most commonly used ones. The properties and chemical structure of some of these hydrogels are discussed in the next section.

A material should not only be non-toxic but also have biochemically functional cues depending on purpose in order to be used with targeted cells. In the use of bioplatform application, it is particularly important to provide cells with adhesive signals for interaction and attachment. For this purpose, hydrogels are modified with ECM adhesive proteins or peptidomimetics. Examples of peptide sequences are RGD, [73] KQAGDV, [74] REDV, [75] GFOGER, [74] YIGSR[76] The studies involved insertion of adhesive moieties and change in density of RGD ligands. [77-79] Besides, specific amino acid sequences were inserted to promote vascularization,[80] neuroregeneration[81] etc.

### 1.2.1 Relevant Hydrogels for Cell Culture

Hydrogels can be made out of synthetic or natural polymers. Synthetic polymers offer different advantages over natural polymers. Their chemical structures are easily tailorable. They can be non-toxic or non-inflammatory. Synthetic polymers can be functionalized chemically depending on the purpose of application. In contrast, natural polymers have batch to batch variation in chemical structure and molecular weight. They contain biologically active groups that might trigger host immune response. Introduction of modifications in the chemical structure is not necessarily straightforward and often not selective. In addition, the chemical structure is not necessarily well known and side reactions are unforeseen.

In general, there are two ways to form hydrogels from polymeric structures: 1) using long chain precursors with reactive end functionalization for chemical or physical crosslinking ie. poly(ethyleneglycol) methacrylate (PEG-MA),[82] and poly(ethyleneglycol) modified with dopamine (PEG-Dop),[83] or 2) using bifunctional monomers that can be polymerized to form a crosslinked network ie. polyacrylamide[84]. Their gelation mechanisms vary with type of crosslinker.

#### a. Alginate

Alginate is a negatively charged linear polysaccharide. It contains two types of uronic acid units: guluronic (G) and mannuronic (M) acids. The G/M ratio of the alginate depends on the natural source. Typically M-rich alginates can be isolated from bacteria and G-rich alginates can be extracted from particular algal tissues.[85]

Alginate can form hydrogels when crosslinked. Two crosslinking ways are possible: chemical covalent or physical crosslinking. (Figure 1.5) For covalent crosslinking the alginate polymer has to be functionalized by attaching reactive monomers, such as catechol or methacrylate groups.[86, 87] (Figure 1.5a and 1.5b) Advantage of catechol mediated crosslinking is that it results in hydrogels with biocompatible crosslinking. [88] Methacrylate functionalization of alginate has limited biocompatibility due to the need of initiators or strong light exposure for initiating the radical polymerization reaction. For applications as biomaterial, alginate is preferentially crosslinked via physical interaction of the negatively charged carboxyl groups in G units with divalent cations. It is proposed that divalent cations form a complex with GG sequence.[85, 89] (Figure 1.5c) Thus, hydrogel prepared with alginates of high G residues results to higher mechanical strength than those with lower G residues. [90] Divalent cations with different binding affinities can be used to crosslink alginate: Pb >Cu > Cd > Ba > Sr > Ca > Co, Ni, Zn > Mn. [91, 92] The mechanical strength of resulting alginate hydrogel depends on type of divalent cation. Traditionally, $Ca^{2+}$ ion is widely used to form alginate hydrogel since it is biocompatible at certain concentration and easily available able to form hydrogel with alginate. [89] However, in human body, when serum calcium concentration is above 2.63 mmol $L^{-1}$, it causes hypercalcemia. It is a disease leading renal insufficiency, vascular and soft tissue calcification.[93] This issue might limit *in vivo* applications of calcium crosslinked hydrogels. Another alternative to physically crosslink alginate is to mix it with positively charged chitosan. The oppositely charged polymer chains form a macromolecular complex through positively charged amine group of chitosan and negatively charged carboxyl groups of alginate at pH values between 5 and 9. [94](Figure 1.5d)

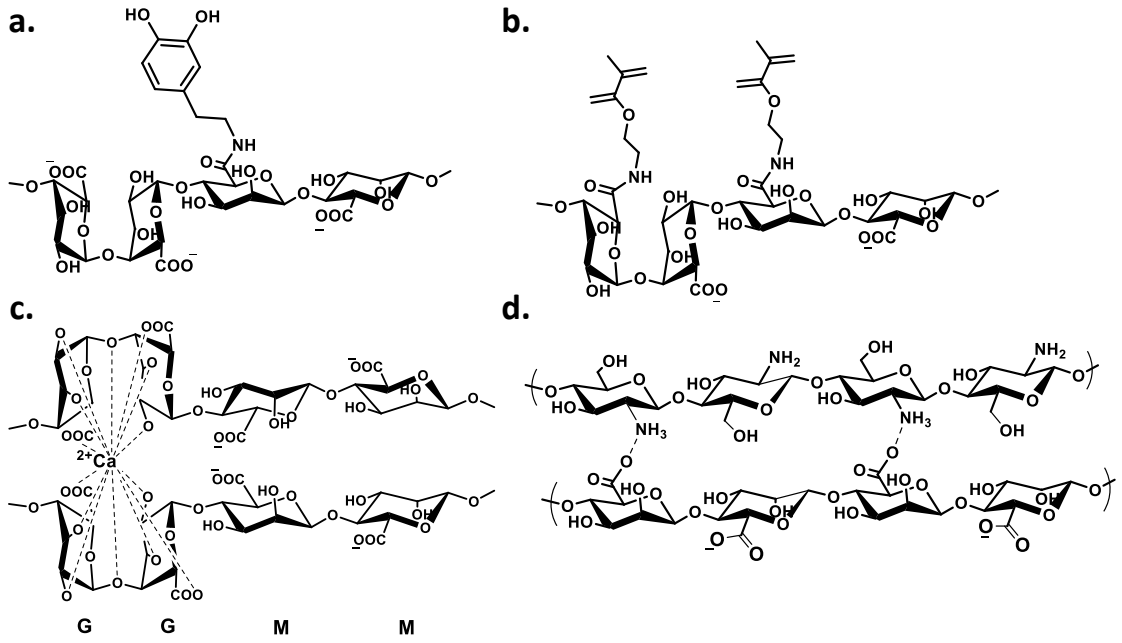


**Figure 1.5** *Schematic showing chemical and physical crosslinking mechanisms of alginate*. **a.** Alginate functionalized with dopamine **b.** alginate functionalized with 2-amine-ethyl methacrylate.**c.** Interaction of alginate with a divalent cation, $Ca^{2+}$ **d.** Interaction of negatively charged alginate with positively charged chitosan.

Alginate hydrogels with different stiffness can be prepared by varying the alginate G/M relationship (by changing the alginate source), the branching degree and the molecular weight. The stiffness can also be tuned by varying the crosslinking degree with the concentration of divalent cations. $Ca^{2+}$ ions can be added to the alginate as solution or as suspension of a $Ca^{2+}$ salt. Gelation of alginate with $CaCl_2$ solution occurs very fast is difficult to control, leading to inhomogeneous hydrogels.[95] Suspensions of calcium salts with low solubility, such as $CaSO_4$ or $CaCO_3$, can be used to extend the gelation time and obtain more homogeneous hydrogels.[96]

Alginate hydrogels have been used in biomedical applications due to their low toxicity, biocompatibility, low cost, and mechanically tunable nature. [97] Examples of alginate hydrogels applications in wound healing, [98] delivery of small biochemical molecules such as drugs or proteins,[99] tissue regeneration with cell delivery,[100] and biomimetic cellular microenvironments in 2D and 3D cell culture studies[101] have been reported.

### b. Gelatin

Gelatin is the hydrolyzed and thermally denatured form of collagen. It is obtained with acidic or basic solutions as a result of hydrolysis of collagen. The properties of gelatin depend on the

type of collagen from which it is formed and the processing method used for extraction. Gelatin for biomedical applications is typically prepared from Type I collagen, which is extracted from connective tissue of animals, skin, bone and tendons. [102] Gelatin is rich in glycine, hydroxyproline and proline. It has no tryptophan and trace amount of cysteine, and methionine.[102]

In the preparation process of gelatin, collagen can be processed either in basic conditions yielding acidic gelatin, Type A gelatin, or in acidic conditions yielding basic gelatin, Type B gelatin. (Figure 1.6) Amino acid sequence of gelatin might have minor variations due to process type. [103] In collagen, 35% of aspartic and glutamic acid is amidated form of asparagine and glutamine. In alkaline preparation method, they are converted into aspartic and glutamic acid. In the acidic preparation method, this conversion is very low and chemical structure is preserved. Therefore, isoelectric point (IEP) of type A gelatin is 5 and it is 9 for type B gelatin.

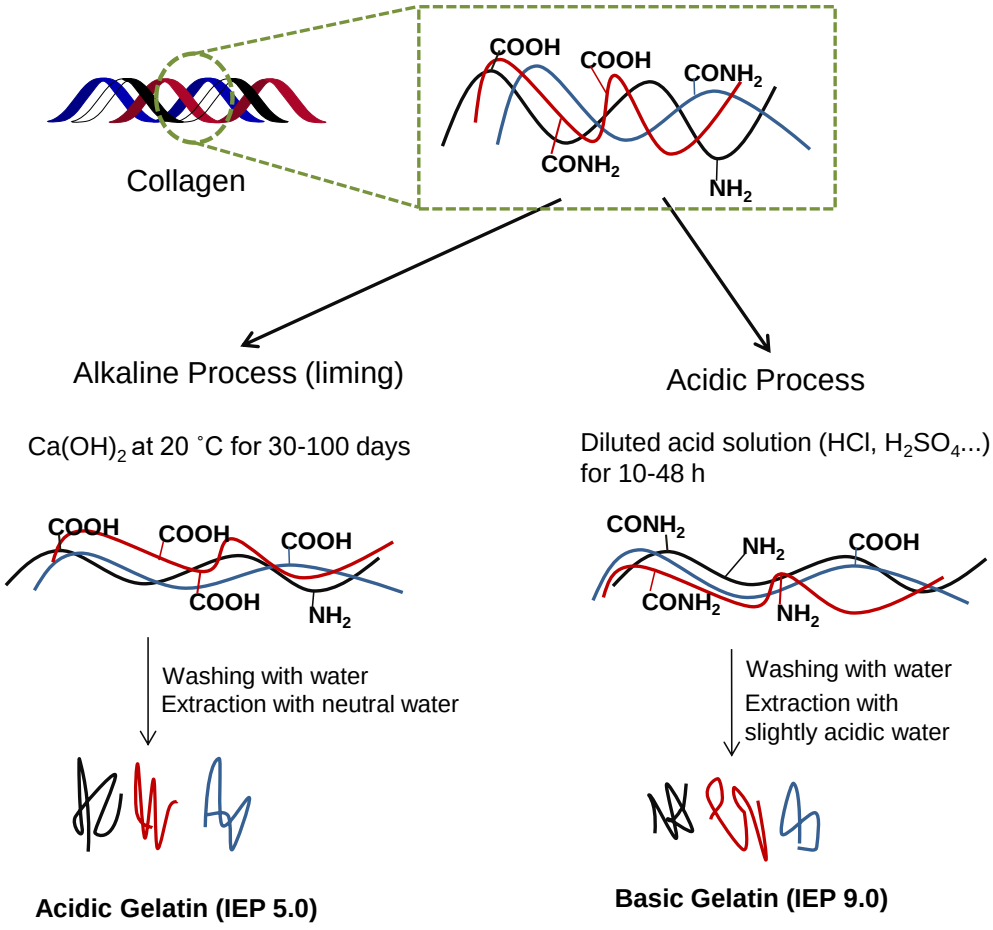


**Figure 1.6** Gelatin preparation methods; alkaline and acidic process. Reprinted with permission from (102). Copyright (2011) Intech Publishing Group.

Gelatin forms physical hydrogels at concentrations above 2 wt.% in water. The gel strength is independent of pH changes between 4.2 and 9.5. [104] The temperature of the solution affects gelation process as well. Gelatin molecules self-organize and form a triple helix superstructure and random coils at temperatures above 30 ˚C. [105, 106] (Figure 1.7) Triple helices are stabilized through intermolecular hydrogen bonds and can eventually assemble in bundled structures (nanofibrils).

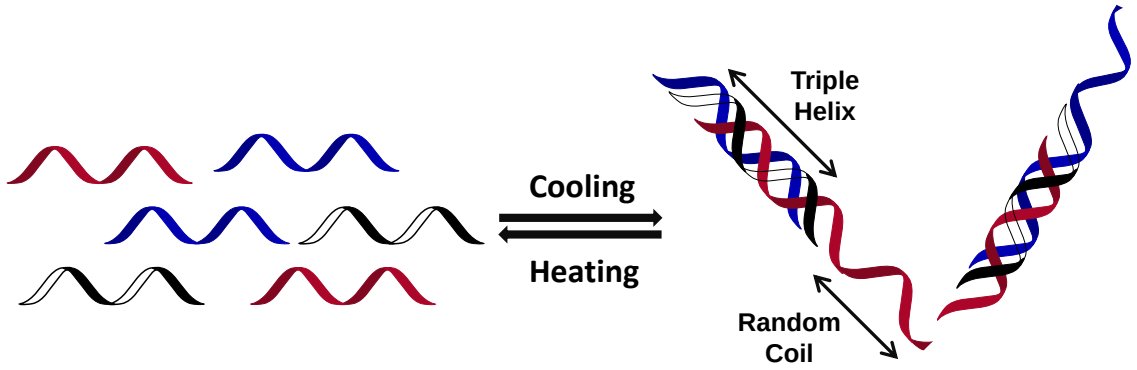


**Figure 1.7** Self-assembly proteins in gelatin.

In order to stabilize gelatin hydrogels, chemical, enzymatic and physical crosslinking methods can be used. Gelatin can be chemically crosslinked using difunctional crosslinkers like glutaraldehyde,[107, 108] dialdehyde starch,[109] carbodiimides, [110-112] or ethylene glycol diglycidyl ether[113]. Alternatively, phenolic compounds, [114, 115] genipin, [116-118] and citric acid derivatives [119] can also be used. In enzymatic crosslinking method, transglutaminase,[120, 121] and tyrosinase[122] have been used to produce mechanically stable and cell-friendly hydrogels. Transglutaminase formed peptide bond between amine group at the side chain of lysine and acyl group at side chain of glutamine. In this way, gelatin was covalently crosslinked.[121] Tyrosinase converted the tyrosine residues on gelatin into L-3,4-dihydroxyphenylalanine, DOPA. With the addition of $Fe^{3+}$ ions, DOPA was crosslinked with $Fe^{3+}$ molecules and, thereby, gelatin was crosslinked. [122]

Gelatin has been used to build scaffolds for drug and gene delivery vehicles[123, 124] or endovascular embolization,[125] in tissue engineering and as substrates in tissue engineering for example to engineer contractile skeletal muscle tissue,[126] or as hemostatic dressing[127] to accelerate healing rate of wounds etc. In addition, gelatin has been used with combination of natural synthetic polymers such as alginate,[128] chitosan,[129] or PEG[130, 131] to enhance biocompatibility.

### c. Poly(acrylamide)

One of the most commonly used synthetic polymers is poly(acrylamide), pAAm. Its easy synthesis and commercially available reagents make poly(acrylamide) preferable in many applications from wastewater treatment[132] to molecular biology laboratory methods such as sodium dodecyl sulfate poly(acrylamide) gel electrophoresis (SDS PAGE) of proteins[133].

Poly(acrylamide) was synthesized by C. Moureu in 1893. [134] 60 years after its synthesis, it became commercially available and widely used.[135] pAAm gels are obtained by copolymerization of acrylamide monomer and a crosslinker, as shown in Figure 1.8. It is a vinyl addition reaction initiated by a free radical. Ammonium persulfate and tetramethylenediamine, TEMED, are typically used for thermal initiation of acrylamide polymerization.(Figure 1.9) Alternatively, riboflavin or riboflavin-5'-phosphate in addition to TEMED/ammonium persulfate mixture can be used as photoinitiator. PAAm can be crosslinked with N,N'-methylenebisacrylamide piperazine di-acrylamide, [136] diallyl-tartardiamide, dihydroxyethylene-bis-acrylamide or bis-acrylylcystamine. [137] Piperazine di-acrylamide is advantageous for application in SDS PAGE separation of proteins because it leads to hydrogels with improved strength, minimized nonspecific silver staining for proteins,[138] and higher resolution in SDS PAGE protocol[139]. Besides, the amount of crosslinker and ratio between crosslinker and monomer determines the mechanical strength of resulting hydrogel. One of the biggest advantageous of pAAm hydrogels as biomaterials for cell culture is its well-established tunability of mechanical properties. [140]

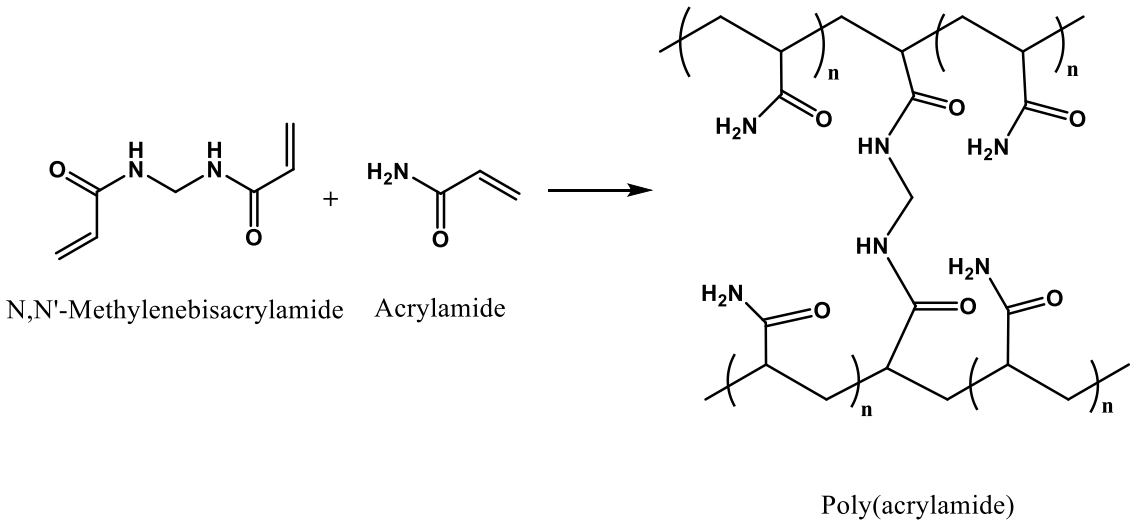


**Figure 1.8**Polymerization reaction of acrylamide with crosslinker N,N'-Methylenebisacrylamide

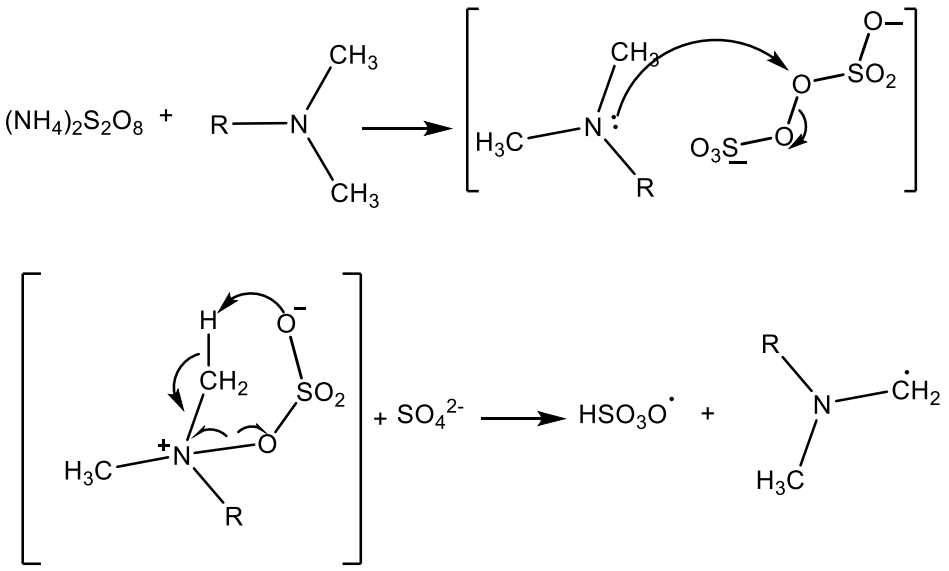

**Figure 1.9** Radial formation from ammonium persulfate by tertiary amine of TEMED to initiate acrylamide polymerization.[141]

Poly(acrylamide) hydrogels show little interaction with proteins. In order to be used for cell culture, chemical synthetic steps are necessary to bioconjugate cell adhesive molecules to the pAAm gel.[142] A commonly used method involves the photoreactive linker sulfosuccinimidyl-6-(4′-azido-2′-nitrophenylamino) hexanoate), sulfo-SANPAH.[142, 143] Upon light irradiation, the aryl-azide moiety reacts with pAAm backbone. On the other hand, activated ester reacts with amine groups on proteins. This method results in poor control over immobilization step due to the poor specificity of the coupling reaction. However, it has been used widely for functionalization of polyacrylamide with collagen, fibronection etc.[143, 144]. Acrylamide has

also been copolymerized with other reactive nomoners such as N-hydroxyethylacrylamide,[145, 146] acrylic acid, [147] 2-pyridinecarboxaldehyde,[148] phenyl oxadiazole methylsulfone acrylate, or benzothiazol methylsulfone acrylate [84] in order to add reactive groups for coupling of adhesive ligands. The comonomers can then react with thiols or amines at the protein surface.

Poly(acrylamide) hydrogels are used as cell culture substrates to investigate influence of substrate stiffness on cell motility,[149] spreading,[149] and differentiation[51]. Although pAAm is nontoxic, the acrylamide monomer is toxic.[150] Therefore, pAAm hydrogel is not suitable for 3D cell culture. In 2D cell culture proper washing steps need to be applied to discard unreacted monomers before contact with the living cells.

### d. Poly(ethylene glycol)

Poly(ethylene glycol), PEG, is an important hydrophilic polymer for biomedical applications. It shows low nonspecific adsorption of proteins and is widely used as 3D matrix for cell culture studies. PEG is commercially available as linear, and branched (4-arm or 8-arm) polymer. (Figure 1.10)

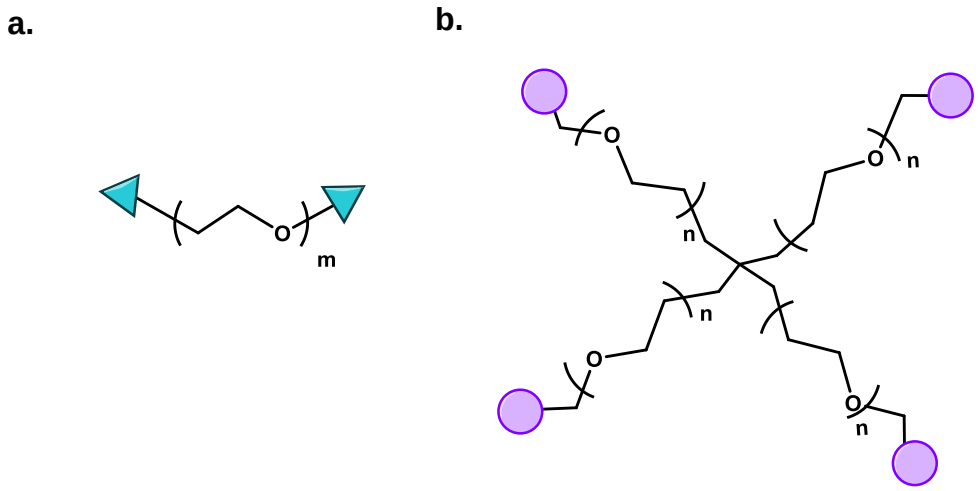


**Figure 1.10** Chemical structures of **a.** linear and **b.** four-armed PEGs which can be functionalized with different groups for different crosslinking types.

In order to build a stable hydrogel, reactive functionalities for crosslinking have to be introduced at the PEG hydroxyl end groups. This can be achieved bythree major crosslinking methods of linear or branched PEGs; ɣ-radiation or electron beam radiation, [151] or by functionalization

with acrylic derivatives[152] acrylate and thiols groups for Michael-type addition crosslinking, [153] acetylene and azide groups for click-based crosslinking, , [154] or with catechol groups for self-polymerization at physiological conditions [155, 156]. The end-functional groups can also be used to introduce cell adhesive molecules for cell culture.[157]

PEG hydrogels have been used as cell adhesive, [158, 159] enzyme sensitive, [160] growth factor bearing or binding,[161] matrix protein binding,[162] immuno-isolating,[163] nitric oxide-bearing[164] scaffolds in tissue engineering. Moreover, PEG hydrogels have been used in drug delivery [165] and other related biomedical applications with their tailorable chemistry and biofunctional groups.

## 1.3 General Physicochemical Properties of Hydrogels

In general, hydrogels are soft, highly hydrated materials. A relevant feature of hydrogels for their application as scaffolds for cell culture is their good mass transport capabilities. Cells rely on diffusive mass transport of nutrients and oxygen through hydrogel in order to pursue on their regular metabolic activities.

Important factors in the design of hydrogels as biomaterials are the crosslinking density ($\rho_x$), swelling ratio ($Q$), mesh size ($\xi$), molecular weight between elastically-active crosslinking points ($M_c$), the shear modulus ($G$) and the elastic modulus ($E$).(Figure 1.11) These properties are interrelated. Crosslinking density is number of chain segments between crosslinks, swelling ratio is the ratio of swollen weight to dry weight, mesh size is the chain length between the crosslinks, shear modulus is the ratio of shear force per unit area (stress) to the ratio of shear deformation over initial length (strain) and elastic modulus is the ratio of the stress to the strain along that axis.

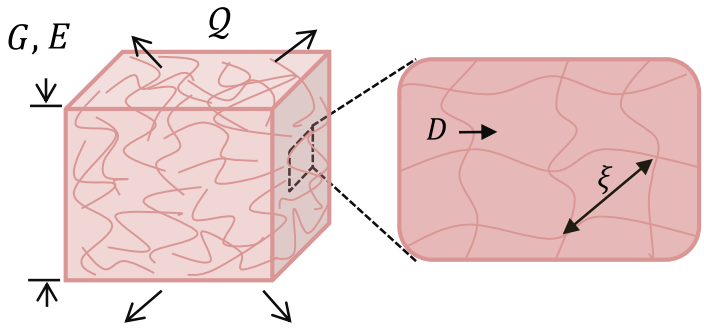


**Figure 1.11** Crucial features of hydrogels; elastic and shear moduli, swelling ratio, diffusivity and pore size.

The relation between swelling ratio and shear modulus and crosslinking density is described below in Eq. 1:

$$G = RT\rho_x Q^{-1/3} \quad (1)$$

Universal gas constant and temperature are shown as R and T, respectively.

Swelling ratio is inversely proportional to shear modulus and crosslinking density. The relation between crosslinking density and elastic modulus is also established by Eq. 2 [166]:

$$E = (3\rho_x RT)/M_c \quad (2)$$

As crosslinking density increases, the elastic modulus increases and the molecular weight between elastically-active crosslinking points decreases. The diffusion of solute molecules in hydrogel can be described by the diffusion coefficient, $D_{gel}$, following Lustig Peppas model[167] as stated in Equation 3.

$$D_{gel} = D_0\left(1 - \frac{\alpha}{\xi(t)}\right)e^{-\Upsilon(t)\left(\frac{\upsilon(t)}{\upsilon(t)-1}\right)} \quad (3)$$

The diffusion coefficient is related to the distance between crosslinks, $\xi(t)$, the polymer volume fraction, $\upsilon(t)$, and the free volume theory diffusion parameter, $\Upsilon(t)$, depending on time. α represents the hydrodynamic radius of diffusing solute. Equation 3 can be simplified in the case of highly swollen hydrogels, when the volume fraction is approximated as zero, to Equation 4:[168]

$$1 - \frac{D_{gel}}{D_0} \approx (Q(t))^{-7/6} \quad (4)$$

## 1.4 Responsive Hydrogels with Phototunable Mechanical Properties

In recent years there has been an increasing interest in developing responsive hydrogels with *in situ* tunable mechanical properties. These biomaterials should mimic the dynamic changes in mechanical properties that occur in natural tissues during ageing or pathological processes (cancer). From a chemical point of view, the design of such responsive biomaterials is

challenging, since the stimulus for the mechanical change should neither compromise the viability of the embedded cells, nor interfere with cellular processes. Pressure, temperature or pH responsive systems are useless for this type of designs. Light-responsive hydrogels, with the ability to change properties upon exposure, are most appropriate. , Photo-assisted stiffening and softening hydrogels have been developed, i.e. gelatin methacrylate (GelMA), methacrylated hyaluronic acid (MeHA), alginate, pAAm, and PEG. [48, 57, 86, 169-175]

One distinct example is the light controlled stiffening of gelatin-methacrylate hydrogel. (Figure 1.12a) The methacrylate units can undergo photoinitiated radical polymerization in the presence of cells. Graphene oxide (GO) incorporated to the GelMA enhanced spreading, viability, and proliferation of cells and facilitated the alignment of cells. Yet, the mechanism behind this outcome was not completely known, it is proposed that it is related with interaction of cells with GO and its high UV absorption. Moreover, GO enhances compressive strength and range of compressive modulus of GO-GelMA. It was proposed that enhancement arose from strong adhesion between GelMA coated on GOs to the acrylic group on GelMA chains. A change in the elastic modulus of the gel between 4 and 24 kPa was achieved with the light irradiation. 3D multilayered tissue constructs with controllable thickness and stiffness (1-6 kPa) were created to mimic the multilayer structure and gradient properties of skin tissue or blood vessels.[173]

A similar photocrosslinking approach was applied to stiffen alginate hydrogels.[86] Alginate polymer was functionalized with 2-aminoethyl methacrylate by reaction carboxyl groups of guluronic acid residues. In the presence of a photoinitiator (Irgacure D-2959), the biopolymer was covalently crosslinked upon light irradiation at 365 nm. This approach gave opportunity to tailor mechanical properties and degradation rates. Moreover, it showed low cytotoxicity and high metabolic activity with primary bovine chrondrocytes encapsulated in *in situ* photocrosslinked alginate hydrogel after 2 and 7 days. Another approach to tune mechanical properties of the alginate hydrogel, was by light-triggered release of $Ca^{2+}$ ions from embedded liposomes containing gold nanoparticles.[170] (Figure 1.12b)Upon irradiation at 800 nm, liposomes were ruptured due to heating of gold nanoparticles, called surface plasmon resonance, and released $Ca^{2+}$ ions, leading to a local increase in the crosslinking degree of alginate and a macroscopic increase in the modulus of elasticity of alginate hydrogel. For softening of alginate hydrogel, the $Ca^{2+}$ chelator, DTPA, was also encapsulated. Light-triggered release of DTPA lead to a decrease in the elastic modulus of alginate. Dynamic modulation of stiffness of alginate hydrogel was applied to investigate morphological changes of fibroblasts

upon stiffening of the hydrogel. A transition in the migration mode from mesenchymal to amoeboid was observed.[176]

Another biopolymer, hyaluronic acid was functionalized with methacrylic acid groups and stiffness of hyaluronic acid hydrogel was phototuned.[57] Modulus of elasticity was tuned from 3 to 30 kPa in the presence of the cells. Cellular response to the change in modulus was investigated in short term, minutes to hours or long term, days to weeks. In short term; human mesenchymal stem cells (hMSCs) increased their spreading area and exhibit greater traction forces upon stiffening. In long term, they preferred adipogenic differentiation path in early stiffening and osteogenic differentiation in later stiffening. (Figure 1.12c)

Previous work in the group A. del Campo demonstrated a light-based stiffening of alginate hydrogels by using Nitr-T (Figure 1.12f), a phototriggerable chelator of the $Ca^{2+}$ cation. [177] Nitr-T has two *o*-nitrobenzhydryl groups attached to 1,2-bis(*o*-aminophenoxy)ethane-N,N,N′,N′-tetraacetic acid, BAPTA, that can form a complex with $Ca^{2+}$ ions. BAPTA groups are insensitive to pH changes in physiological pH range (6.5-7.5), so that the complex is farely stable with the pH under physiological conditions. Moreover, they have high $Ca^{2+}/Mg^{2+}$ selectivity. Photosensitive *o*-nitrobenzhydryl groups attached to BAPTA in *p*-positions increase the affinity of BAPTA for $Ca^{2+}$. The *o*-nitrobenzyl group is photosensitive. Under light exposure, it converts into a nitrosobenzo ketone derivative. These molecular changes reduce the affinity of the chelator for $Ca^{2+}$ and allow release of the cation from the chelator in solution after exposure. Light exposure also decreases the buffering capacity of Nitr-T for $Ca^{2+}$ ions because electron withdrawing moieties are formed on the aromatic ring.[178] This approach has been used to tune stiffness of alginate hydrogel in this thesis.

In PEG hydrogel systems, a variety of approaches have been applied to tune stiffness, softening and stiffening. Anseth et al. reported a photodegradable nitrobenzyl ether-derived photocleavable PEG-diacrylate macromer. [56] [171] (Figure 1.12e) Upon light irradiation, the photocleavage of the PEG chain lead to a decrease in the modulus of elasticity from 5 kPa to complete erosion. These gels were used to encapsulate hMSCs and study the effect of stiffness in their differentiation phenotype. When the modulus of the photodegradable PEG was decreased, chondrogenesis was promoted. In 2014 Linyong Zhu reported a strategy for photostiffening of PEG hydrogel via photo-uncaged-thiol Michael addition reaction.[175] (Figure 1.12g) A methacylate monomer with a macrocyclic coumarin-caged thiol was copolymerized

with PEG-methacylate (PEG-MA) to generate a photosensitive macromolecule. Upon light irradiation, thiol groups were uncaged and reacted with another macromolecule possessing maleimide groups and underwent thiol Michael addition to create hydrogels. Three cell lines, hFOB, C2C12, NIH-3T3, were test in the cell encapsulation experiments resulting in a high cell viability, >95%. In a different study, PEG-norbornene was crosslinked with matrix metalloprotein degradable peptide with cysteine and adhesive peptide with the help of a photoinitiator, lithium phenyl-2,4,6-trimethylbenzoylphosphinate, LAP, to undergo photoinitiated thiol-ene reaction.[174] (Figure 1.12h) Hydrogels were produced with elastic modulus of 0.24, 4 and 12 kPa. The effect of stiffness on valvular interstitial cells (VICs) was studied with the encapsulation of the cells in the hydrogels. In softer gels, VICs exhibited 40% less α-smooth muscle actin fibers. In stiffened gels, VICs became deactivated to a fibroblast phenotype.

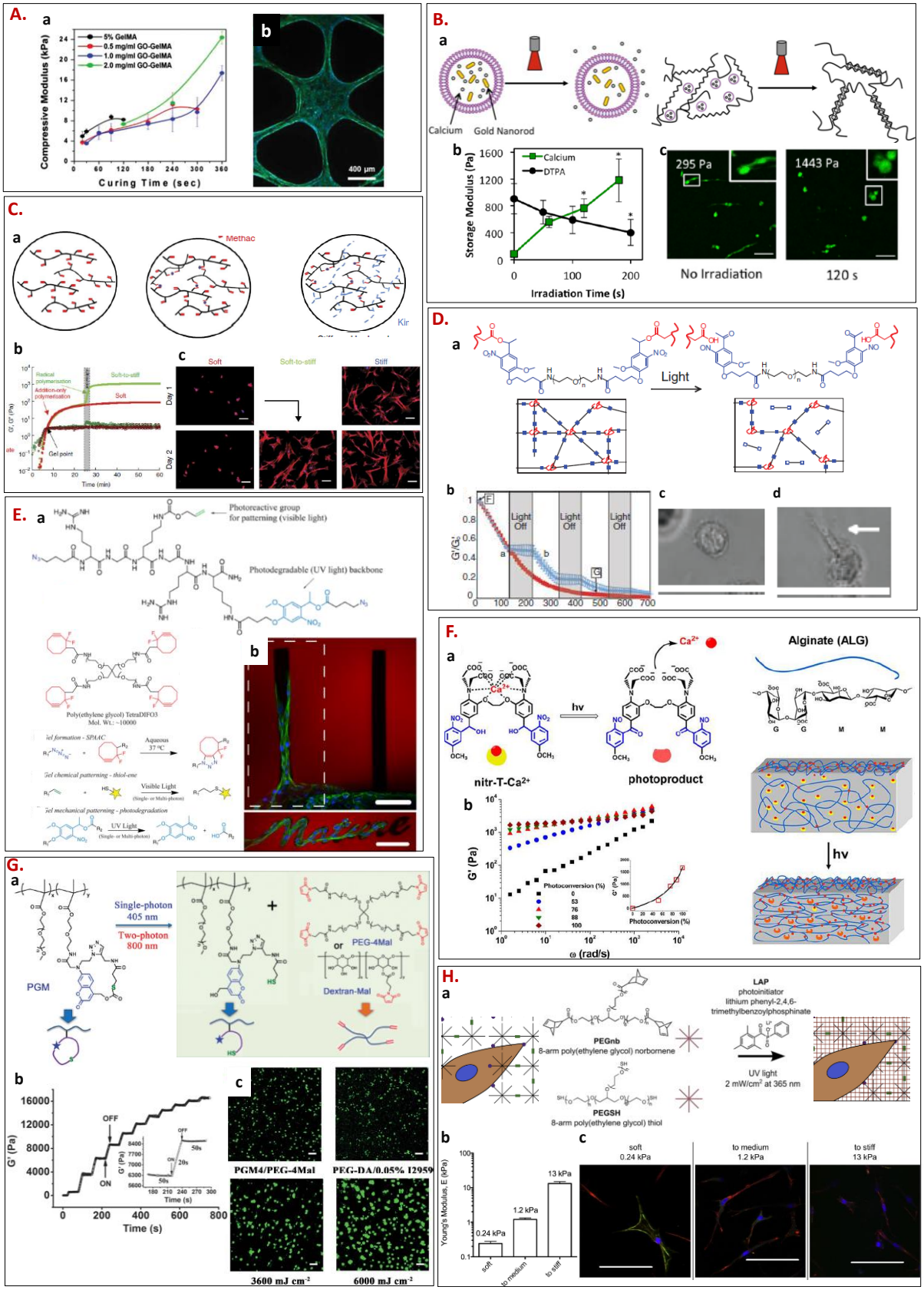
A.
a
5% GelMA
0.5 mg/ml GO-GelMA
1.0 mg/ml GO-GelMA
2.0 mg/ml GO-GelMA
Compressive Modulus (kPa)
Curing Time (sec)
b
400 μm
B.
a
Calcium
Gold Nanorod
b
Calcium
DTPA
Storage Modulus (Pa)
Irradiation Time (s)
c
295 Pa
1443 Pa
No Irradiation
120 s
C.
a
Methac
Kir
b
Radical polymerisation
Addition-only polymerisation
Soft-to-stiff
Soft
Gel point
Time (min)
c
Soft
Soft-to-stiff
Stiff
Day 1
Day 2
D.
a
Light
b
Light Off
Light Off
Light Off
G'/G'0
c
d
E.
a
Photoreactive group for patterning (visible light)
Photodegradable (UV light) backbone
Poly(ethylene glycol) TetraDIFO3
Mol. Wt.: ~10000
Gel formation - SPAAC
Aqueous
37 °C
Gel chemical patterning - thiol-ene
Visible Light
Gel mechanical patterning - photodegradation
UV Light
b
Nature
F.
a
Ca2+
hv
nitr-T-Ca2+
photoproduct
Alginate (ALG)
b
G' (Pa)
Photoconversion (%)
ω (rad/s)
hv
G.
a
Single-photon
405 nm
Two-photon
800 nm
PGM
or
PEG-4Mal
Dextran-Mal
b
G' (Pa)
OFF
ON
Time (s)
c
PGM4/PEG-4Mal
PEG-DA/0.05% I2959
3600 mJ cm-2
6000 mJ cm-2
H.
a
LAP
photoinitiator
lithium phenyl-2,4,6-trimethylbenzoylphosphinate
PEGnb
8-arm poly(ethylene glycol) norbornene
PEGSH
8-arm poly(ethylene glycol) thiol
UV light
2 mW/cm2 at 365 nm
b
Young's Modulus, E (kPa)
0.24 kPa
1.2 kPa
13 kPa
soft
to medium
to stiff
c
soft
0.24 kPa
to medium
1.2 kPa
to stiff
13 kPa

**Figure 1.12** Examples of light responsive hydrogels from the literature. Reprinted with permission from **A.** (172) Copyright (2013).John Wiley and Sons, **B.** (169) Copyright (2015) National Academy of Sciences, **C.** (56) Copyright (2012) Nature publishing group, **D.** (55) Copyright (2009) American Association for the Advancement of Science, **E.** (170) Copyright (2011) Nature Publishing Group, **F.** (82) Copyright (2015) American Chemical Society, **G.** (174) Copyright (2014) WILEY-VCH Verlag GmbH& Co. KGaA Weinheim, **H.** (173) Copyright (2015) Elsevier.

## 1.5 Mechanical Properties of Materials

The mechanical properties of a material can be described as stiffness, elasticity, toughness, tensile properties, ductility, and fracture strength. Elasticity is the measure of a material's ability to return to its original shape after application of a force. Ductility is the ability to deform before complete rupture. Toughness is ability of a material to absorb energy up to its failure point. Fracture strength is the stress of a material at its failure point. Upon axial or lateral application of force (stress), a material stores or dissipates energy through displacement of molecules (strain). (Figure 1.13) Energy storage does not permanently disturb the shape of the material, i.e. the initial shape is recovered when the stress is released. This is called elastic deformation. At higher applied stress values, materials might be deformed irreversibly. This is called plastic deformation and in polymer materials it involves flow of the polymeric chains. The stress value at which a polymer material starts plastic deformation is called yield stress. At higher applied stress, the materials might rupture (point of failure).

The mechanical behavior of a material is typically visualized in stress-strain curves as in Figure 1.13, brittle material shows little plastic deformation region and small strains before fracture. A ductile material shows an elastic deformation region followed by a plastic deformation region. In polymer materials necking behavior (large amounts of strain localizing in disproportionately in small region) often occurs.

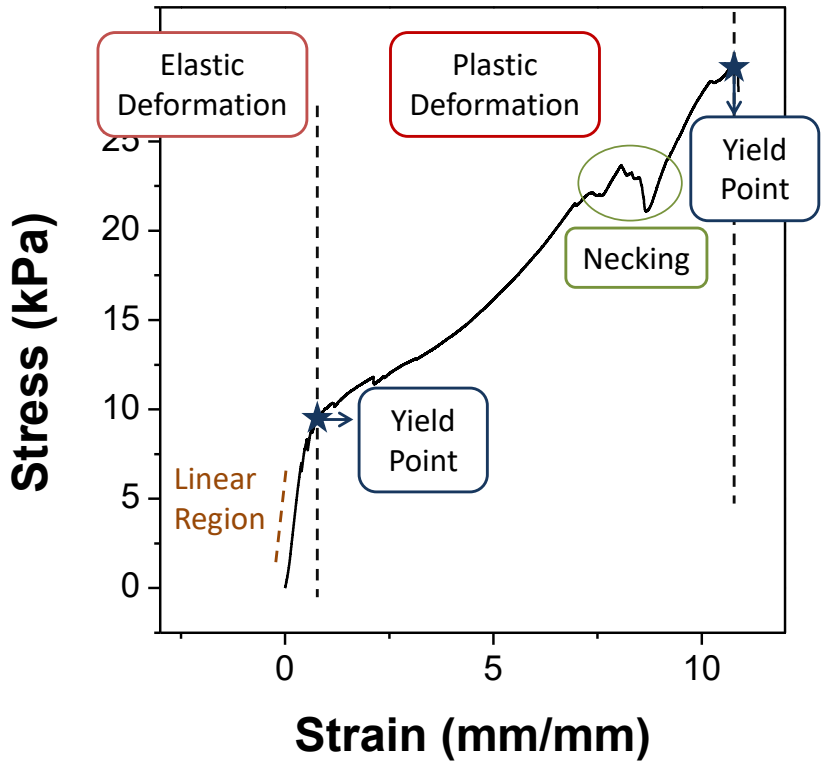


**Figure 1.13** Representative stress vs. strain curve for an example of alginate/pAAm interpenetrating network (IPN) used in the context of this thesis.

In tensile tests, the applied force is uniaxial. In the linear elastic deformation region, the stress, $\sigma$, strain, $\gamma$, relationship is defined with Hooke's law:

$$\sigma = E \times \gamma \tag{5}$$

Stress is defined as applied force per unit area (Eq. 6) and strain is defined as displacement during measurement.

$$\sigma = \frac{Load}{Area} = \frac{F}{A} \tag{6}$$

The slope of linear region of stress vs. strain curve is called as Young's modulus or modulus of elasticity, *E*.

If the applied force is lateral, shear stresses produce strain according to[179]

$$\sigma = G \times \gamma \tag{7}$$

In the equation, *G* is called as shear modulus.

The elastic modulus quantifies the stiffness of the material. In general, ceramics, and metals have higher elastic modulus than polymer based materials. As a rule of thumb, as crosslinker concentration increases in hydrogels, elastic modulus increases.

When materials are subject to axial force, they shrink laterally. The ratio of lateral and axial strains is called as Poisson's ratio, $n$.

$$n = \gamma_{lateral}/\gamma_{axial} \tag{8}$$

Therefore, we can express the relation between elastic and shear modulus using Poisson's ratio:

$$E = 2G(1 + n) \tag{9}$$

For hydrogels, $n$ is accepted as 0.5. Equation 9 is particularly important in this thesis because it was used convert shear modulus to modulus of elasticity.

## 1.6 Mechanical Characterization Techniques

In mechanical characterization of soft materials, various types of methods are available. Most commonly used techniques are tensile tester, compression tester, rheometer, optical tweezer, nanoindentation and atomic force microscope. In the context of this thesis, tensile tester, oscillatory rheometer, and piezorheometer were used in mechanical characterization of materials. (Figure 1.14)

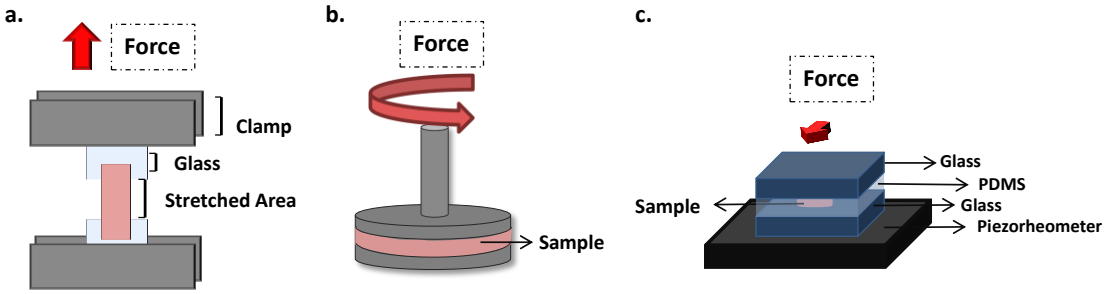


**Figure 1.14** Hydrogel measuring set-ups for **a.** tensile testing, **b.** oscillatory rheology and **c.** piezorheometer.

### a. Tensile Testing

Tensile testing is one of the most commonly used methods for characterization of materials. A uniaxial load is applied to a sample of known dimensions with a given velocity and the deformation is recorded. An example of tensile testing of a hydrogel specimen is shown at rest

and stretched position in Figure 1.15. This test gives information about a material's strength, failure point, ultimate tensile strength, yield strength, maximum strain and thus, ductility. It is advantageous because of being inexpensive, fully standardized, and informative about broad mechanical properties of a material, provider of quick results.

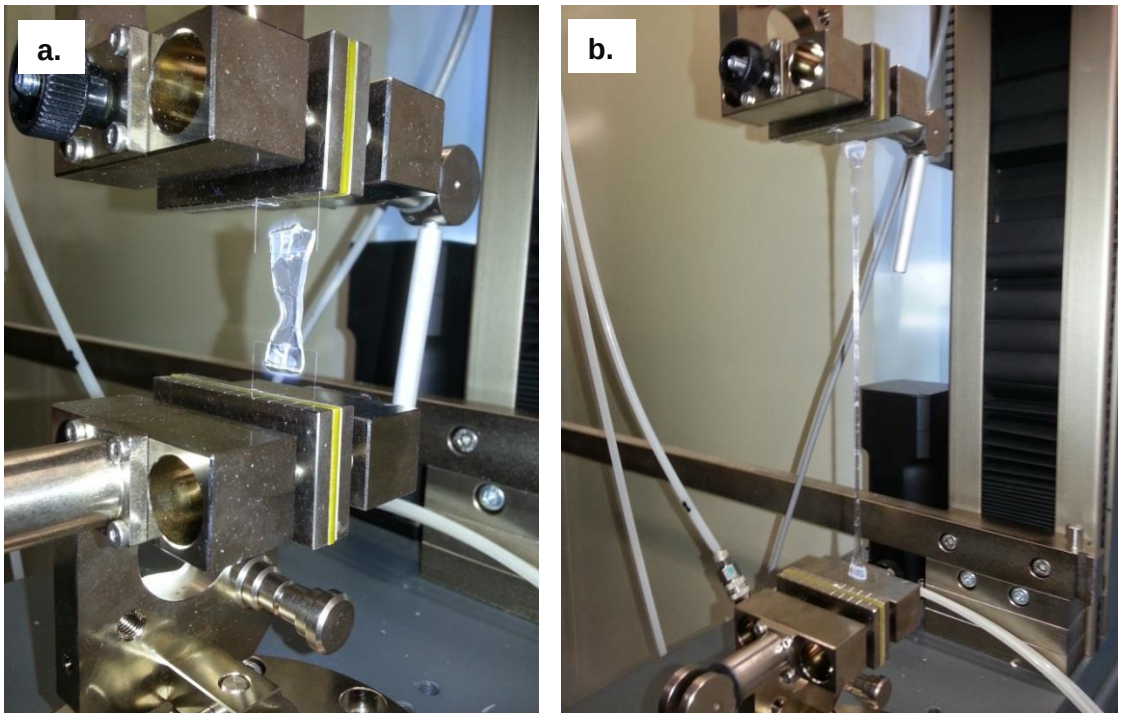


**Figure 1.15** Alginate/pAAm IPN hydrogel **a.** at rest position, before starting measurement **b.** at stretched position, before failure.

Shapes of specimens for tensile testing are particularly important in tensile testing. Fracture shouldn't place close to attachment positions to the instrument. Therefore, cross-sectional area or diameter of sample should be less than the length of stretched area. It would increase the stress in the stretched area since cross-sectional area is inversely proportional to stress.

The most critical concern when measuring soft materials is gripping of the sample in order to avoid slipping or fracture at the gripping point. In this thesis, specimens were glued to glass cover slips since hydrogels were too slippery to clamp. Clamping would squeeze hydrogels, decrease water content and cause undesirable change in elastic properties.

Vertical alignment of the specimen to the instrument is another crucial factor affecting the measurement. An unaligned sample might cause side loading or bending. Therefore, the best

way to attach a specimen is to grip the sample from the upper side and let it hang. Then, grip the lower part of the specimen.

Tensile testing is a destructive characterization method. It requires plastic deformation or complete rupture of sample depending on measurement type. Moreover, sample should be self-supportive enough to attach the sample. (Figure 1.15)

### b. Oscillatory Rheology

Another commonly used mechanical characterization method is oscillatory rheology. Rheology means study of deformation and flow of a material under applied shear forces measured with help of a rheometer.

In an oscillatory rheometer, the sample is placed between two plates and subjected to shear deformation. The stress occurred on the sample depends on time, frequency oscillation, and shear deformation. (Figure 1.16) Strain is applied by rotation of one of the plates while the other plate is fixed (Figure 1.14b). The torque measured in response to displacement on sample on stationary plate. Elastic solids display stress and strain which are in phase (Eq.5). Viscous liquid exhibits stress and strain which are 90° out of phase. The relation between stress, $\sigma$, and shear viscosity, $\eta$ depends on shear rate, $\dot{\gamma}$. (Eq. 10)

$$\sigma = \dot{\gamma}\eta \tag{10}$$

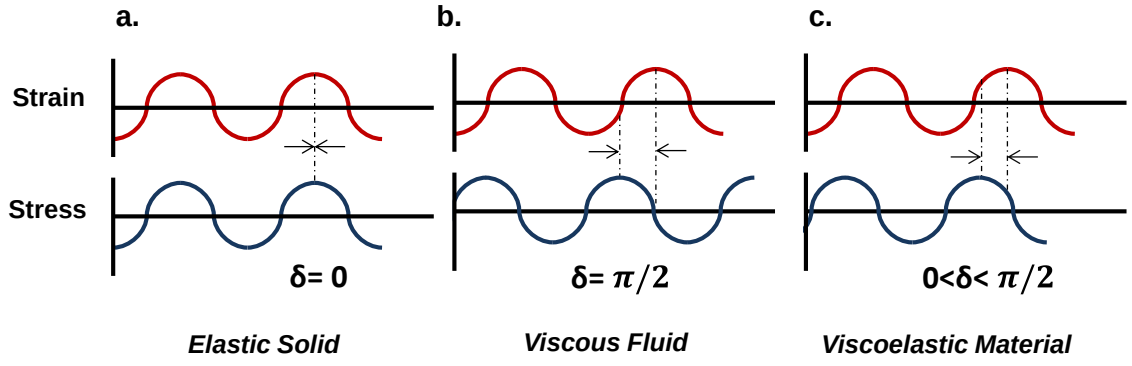


**Figure 1.16** Stress measured on different types of materials as a result of strain. Depending on shear stress, material can be classified as elastic solid, viscous fluid or viscoelastic material.

If the response of material is in between, the material has both viscous and elastic characteristic. Mathematically, it is defined by *equation 11*.

$$\sigma = \mathrm{G}'\gamma_0 \sin(\omega t) + \mathrm{G}''\gamma_0 \cos(\omega t) \quad (11)$$

Fundamental data obtained from rheological measurements are shear storage modulus, $\mathrm{G}'$, (elastic character of a material), shear loss modulus, $\mathrm{G}''$, (viscous character of a material) and loss factor, tanδ, ratio of liquid-like behavior to solid- like behavior. They can be obtained as a function of time, oscillatory frequency and oscillatory strain.

Rheology measurements can be applied to follow the change in mechanical properties of a gel during crosslinking. The measurement over time of an uncrosslinked polymer solution shows a decrease in the viscous character and an increase in the elastic character with increasing crosslinking. In other words, $\mathrm{G}'$ will be lower than $\mathrm{G}''$ in a time sweep measurement at constant strain and angular frequency. As crosslinking is initiated, elastic character will be more dominant. $\mathrm{G}'$ will be higher than $\mathrm{G}''$. After completion of crosslinking, $\mathrm{G}'$ and $\mathrm{G}''$ stay constant. It forms a viscoelastic material. For the characterization of strength of polymer, strain can be increased to point strain where crosslinking points are broken and polymer is plastically deformed. In this case,$\mathrm{G}'$, elastic behavior of polymer decreases and $\mathrm{G}''$, viscous behavior of polymer increases.

Rheological measurements in plate-plate, cone-plate and coquette geometries can be used depending on the material. Parallel plate geometry is useful when non-uniform strain is applied, or when adjustable gap height is desired to adapt to sample volume or when boundary effects like slip, are tested. The disadvantage of this geometry is the nonuniform strain distribution. Also, solvent evaporation can be a problem depending on type of sample, measurement time, or environment. Cone-plate geometries are useful for measuring samples with high viscosity and avoid slipping effects. One drawback of geometry is the positioning of the cone. The other commonly used geometry is coquette. It is suitable for measurement of sample with low viscosity at high shear rates. Evaporation is limited in this geometry. However, it requires high volume of sample and nonuniform strain field can be observed if ratio of diameter of sample to diameter of cylinder is higher than 0.15.

Rheology measurements provide information about the mechanical and viscoelastic properties of a material, they allow to follow gelation, polymerization or depolymerization kinetics over time and the behavior of hydrogels during or after flow. Currently, there are two types of rheometers mainly used, stress-controlled and strain-controlled. In general, strain-controlled mode is accepted as better defined. Stress-controlled instruments are only applied when high torque sensitivity is required.

Recently, developments of materials with light- and temperature-controlled stiffness led advancement of rheometers with high variety of accessories. In the market, there are rheometers which can perform measurements during light exposure at a specific wavelength and temperature control. (Figure 1.17)

**Figure 1.17** Photograph of TA-DHR3 rheometer with upper-heating plate for temperature control and UV curing plate.

### c. Piezorheology

Piezorheometers are similar in terms of set-up with classical oscillatory rheometers. The difference comes from signal generation and detection with piezoelectric actuators by means of the piezoelectric and inverse piezo-electric effect. Piezorheometers has advantages on generation small strain amplitudes in the rage of $10^{-4}$. It is important to rheological properties of soft and fragile materials without creating a plastic deformation. The other advantage comes from small sample volume ie. 10 µl, required for measurement. Therefore, it is possible to study rheological properties of very expensive materials with moderate cost. Finally, confocal microscopy or light irradiation can be combined with system with the help of transparent sample holder.

The first piezorheometer was designed by Durand and Bartolino. [180] Rigidity of a smectic-*A* liquid crystal was measured at low strain amplitude. The set-up had a temperature controller, as well. After the design of first piezorheometer, set-up has developed on the base of the first design. [181-184]

Sample holder set-up consists of two piezo-ceramic plates glued to glass plates where sample is placed and massive glass holders. Glass holders are screwed together in a way that gap be adjusted by turning the screws. This design gives the opportunity to change the gap from 10 μm to 1 mm with the accuracy of 3 μm. (Figure 1.14c)

In this thesis, a home-made piezorheometer was used designed in the lab of Dr. Günter K. Auernhammer in Max-Planck Institute for Polymer Research, Mainz.[185] (Figure 1.18) In this instrument, frequency is generated by a frequency generator 33220A, Agilent, to apply a voltage to piezo-ceramic. It can be varied in the range of 0.1 Hz to 1000 Hz and the peak-to-peak amplitude can be set in the range of 0.2 to 18 V. Due to inverse piezo effect and specific polarization of ceramics, a shear deformation can be generated, Complex shear modulus at a specific frequency, $G^*$, can be calculated with resulting stress σ(t) at the upper glass substrate the generation of free charges $Q_D(t)$, shear deformation s(t), sample thickness D. (Eq. 12)

$$Q_D(t) = d_{pc} \times \sigma(t) = d_{pc} \times G^*(\omega) \times \frac{s(t)}{D} \qquad (12)$$

$d_{pc}$ is proportionality constant between electric displacement and strain for a shear displacement of minimum 7nm to maximum 600 nm.

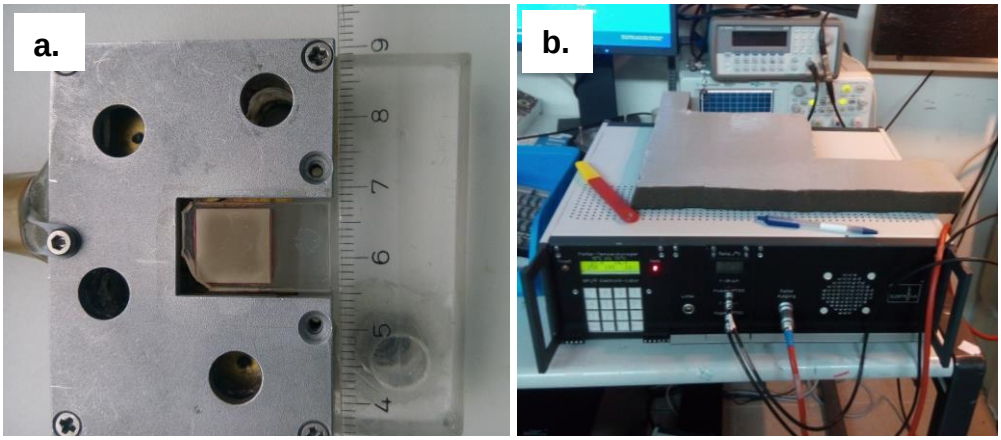


**Figure 1.18 a.** Photograph of lower part of sample holder of piezorheometer. **b.** Electronic components of piezorheometer.

In the concept of this chapter, calculation of all rheological properties was made with parameters designed by Marcel Roth.[185]

## 1.7 Interpenetrating Polymer Network Hydrogels

A hydrogel is considered as a tough hydrogel if tensile stress is 0.1-1 MPa and fracture energy is $10^2$-$10^3$ J/m$^2$.[186] The enhanced mechanical properties of tough hydrogels originate from integrated mechanisms to dissipate energy while maintaining high elasticity under deformation. [187] These two points have to be included in the molecular design of the hydrogel1) mechanisms to release mechanical energy upon crack propagation, 2) preservation of original shape even at large deformations.

Single network hydrogels have been limited by their brittle nature and poor mechanical robustness. Hydrogels offer a tunable range of stiffness similar to that found in extracellular matrices and tissues, Most hydrogels offer a tensile stress of sub-MPa although biological structures can reach tensile strength of 50 MPa.[188]

Recently, the development of interpenetrating networks (IPNs) has proven to be an effective route towards expanding the range of mechanical properties.[189, 190] As a result of recent studies, IPNs have developed to possess elastic modulus of 0.1-1 MPa, tensile strength up to 10 MPa, compressive failure strength up to 60 MPa and tearing fracture energy of 100-1000 J/m$^2$.[187] (Figure 1.19)

Different molecular mechanisms have been suggested to dissipate mechanical energy in polymer networks: the introduction of sacrificial bonds on loosely crosslinked polymer chains,[191] the use of reversible crosslinking chemistries,[192] the exploitation of secondary transformation or folding or unfolding of polymer chains,[193] or the fracture and pullout of reinforcing fibers or fillers in a bridging zone in front of the crack[194].

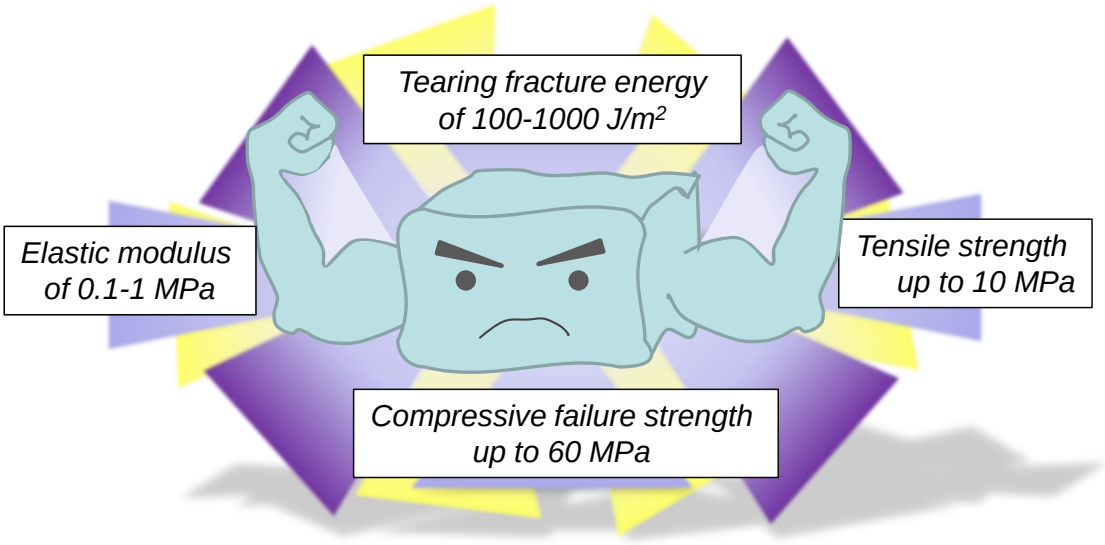


**Figure 1.19** Schematic showing of mechanical properties of tough hydrogels.

To retain the original form of hydrogel after deformation, long chain networks [195], physical and chemical crosslinkers [196], high functionality crosslinkers [197], monodisperse polymer networks [198], or meso-/macro scale composites[194] can be used.

A common strategy to strengthen the mechanical properties of a hydrogel is by fusing two polymer networks into one macrostructure. These system are called interpenetrating networks (IPNs). They can be prepared in different ways: [199] 1)the classical two-step sequential polymerization, 2) the molecular stent method, 3) the simultaneous polymerization of two different networks, 4) Extrusion 3D-printing method, and 5) Free-shapeable method. The two-step polymerization method was applied to prepare poly(2-acrylamido-2-methyl-1-propanesulfonic acid), pAMPS, interpenetrated with pAAm hydrogels by Gong et al. in 2003. [190] The first step was the UV-initiated polymerization of pAMPS to form a highly crosslinked and swellable network made of a strong polyelectrolyte, which was rigid and brittle. This network was swollen with a solution of AAm as neutral monomer, crosslinkers and initiators of second network. Polymerization occurred to form a soft and loosely crosslinked second network. In the molecular stent method the first network has a neutral character, for example poly(2-hydroxyethylacrylate), with low swelling degree and is swollen using a strong polyelectrolyte (pAMPS) as second gel, [200, 201] the so-called “stent-gel”. Alternatively, two networks can be crosslinked at the same time, in a one-pot synthesis. Comparing to multi-step synthesis, it is time-saving. However, it requires orthogonal crosslinking mechanisms which do not interfere

with each other. Physically/chemically crosslinked agar/pAAm or alginate/pAAm are tough hydrogels prepared in this method.[202, 203]

When the IPN is required to be formed in a particular shape, advanced manufacturing technologies like 3D printing can be combined with IPN systems to produce complex tough hydrogels structures.[204-208] In general, the gel precursor solution for the first network is printed into a mold (ie. pAAm) and polymerized via light, thermal or chemical activation. Afterwards, the printed structure is immersed in a solution of the second precursor (alginate) followed by crosslinking. An alternative method was developed by Nakajima et al.[209] In this method a complex 3D structure was prepared with cc, which is physically crosslinked, soft and flexible. 3D printed PVA structure was used as an internal mold which an interpenetrating network of pAMPS/pAAm which can be constructed with classical preparation method. In addition to PVA, particles of pAMPS and agar were used as internal mold to form tough hydrogels.[210-212]

Tough hydrogels find applications for tissue engineering[213], drug and biomolecule delivery,[214] antifouling materials,[215] and sensors and actuators,[216].[199] Their superior mechanical properties have been exploited in tissue engineering area especially as cartilage tissue mimics.[217-220]

Tough hydrogels are great interest of scientist not only because of sustaining mechanical stress precisely but also their intrinsic biocompatible and printability properties. Yet, there is a long way to develop ultimate material including stepwise energy dissipation mechanisms, as well as possessing characteristics suitable for cell studies and 3D printing.

## 1.8 3D Bioprinting of Hydrogels

The idea of sharing knowledge resulted in the development of the woodblock printing in China even before 220 AD.[221-223] It involved printing of texts or images with the help of a woodblock on textiles, and later paper. Printing remained a 2D process for very long time until of the concept of 3D printing was developed in the late 90's. The ancestor of 3D printing is high resolution stereolitography, invented by Charles Hull in 1983 mainly in the microelectronics field.[224] Additive manufacturing has been used in the industry mainly for prototyping. In the last decade, printing has been extended to the deposition of biomaterials to build up scaffolds,

eventually containing living cells. 3D bioprinting enables to create completed with spatial control of cells, biomolecules and scaffolding material.

3D printing entered the tissue engineering area, around 2001, when the first attempt to create an artificial organ (bladder) was reported.[225] A composite scaffold of made of collagen-polyglycolic acid (PGA) was prepared in the shape of a bladder using polyglycolic suturing material. The size of bladder was determined with a CT scan of each patient. Smooth muscle cells and urothelial cells extracted from each patient were seeded to scaffold. Engineered bladders were successfully implanted to 7 patients aged between 4 to 19 years old. Implanted bladders showed functional parameters over five years. This study exhibited ground-breaking advancements that can be achieved by deposition of materials with or without living cells in 3D.

There are three most commonly used 3D bioprinting techniques: 1) inkjet, 2) microextrusion, and 3) laser assisted bioprinting. (Figure 1.20) Inkjet bioprinting works with principle of deposition of bioink droplets via a piezo or thermal actuator. (Fig. 1.20a) It allows printing at high speed (1-10000 drops/s), low printing costs, and at high resolution (1-300 pL droplet size, 50 μm wide printed strands). On the other hand, it requires using low viscosity bioink, 3.5–12 mPa/s. Inkjet printing was successfully used for printing cartilage, liver skin with hydrogels; fibrin, soy agar or collagen .[226, 227]

Microextrusion bioprinting is the most commonly used technique for tissue engineering. It usually consists of a temperature controller dispensing system and stage with moving one or both capable of movement in x, y, z direction to print continuous deposition of bioink under constant pressure or mechanical force.(Fig. 1.20b) It requires high viscosity (30 mPa/s up to $6x10^7$ mPa/s) bioinks which can be printed with resolution up to 5 μm. A drawback of the pressure used for material extrusion, in decreased cell survival (40-80 %). However, recently usage of microextrusion bioprinter could result 90% cell viability. [228] Commonly used bioinks for extrusion printing are hyaluronic acid, alginate, gelatin, collagen, fibrin, polycaprolactone (PCL), and Pluronic 127.[226] The successful bioprinting of complex structures such as aortic valves and branched vessels and stromal vascular fraction was achieved.[229-231]

Laser-assisted bioprinting is printing technique involving a laser beam, a focusing system, a donor transport support. The donor transport support is basically a glass covered with a layer of laser-energy-absorbing and a layer of biological material (ink with or without cells) and receiving

substrate. It is based on working principle of generation of a high pressure bubble propelling biological material toward collector substrate with the help of focused laser pulse on absorbing layer. (Fig. 1.20c) It allows depositing low viscosity bioink with high cell densities at high printing speed is one of the advantages over other techniques. Collagen and nanohydroxyapatite are examples of bioinks used for this technique. [232, 233]

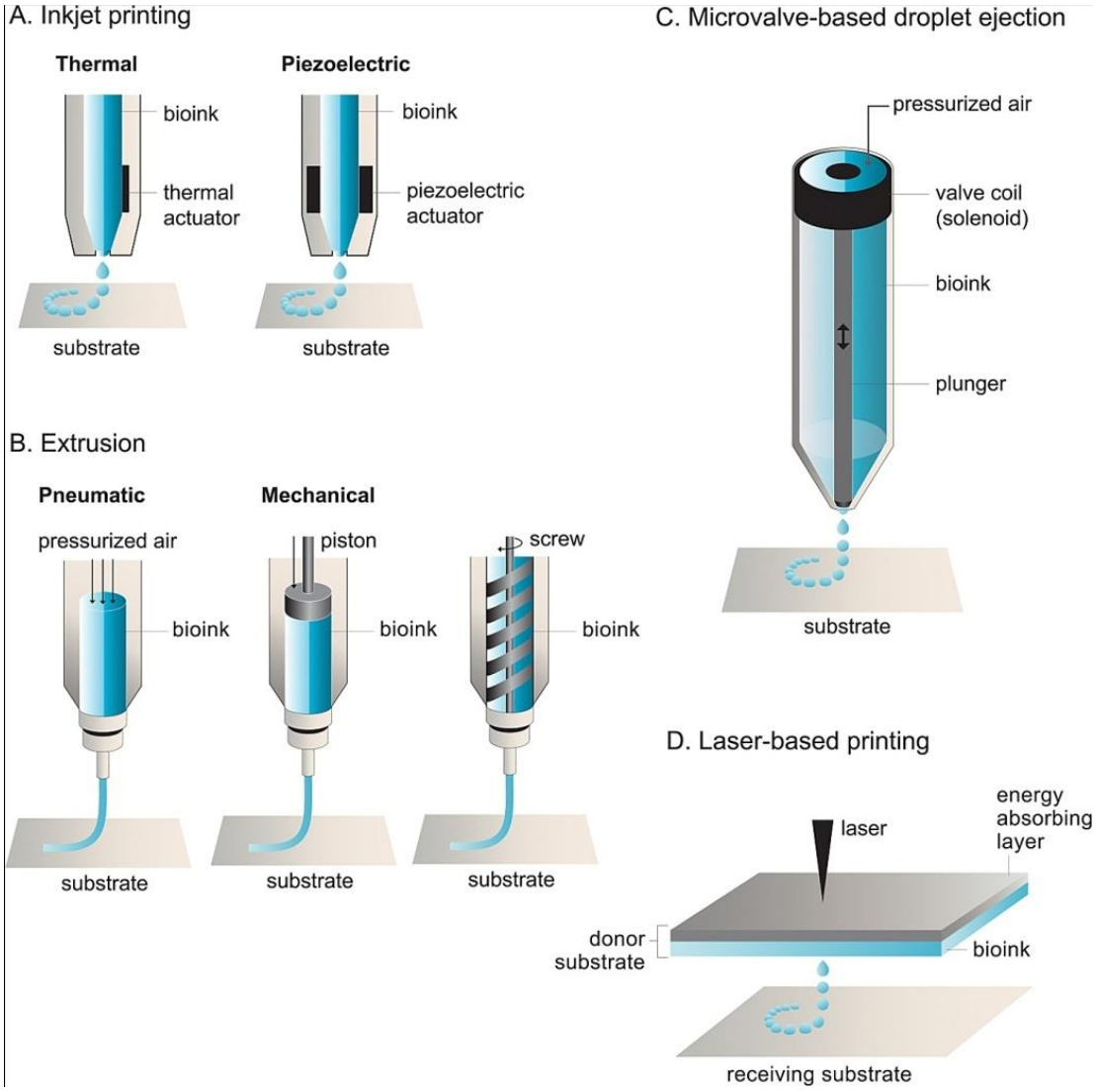


**Figure 1.20** Types of bioprinters according to printing methods, **a.** inkjet, **b.** microextrusion and **c.** laser assisted bioprinting. Reprinted with permission from ref.[64]. Copyright (2017) Elsevier.

The ideal material for bioprinting is defined with multiple parameters [234] Viscosity, gelation kinetic and rheological properties of bioink should be suitable for type of bioprinter. Not only printing material but also 3D structure after crosslinking with its degradation byproducts should be biocompatible. Degradation kinetic should be compatible with properties of targeted application. It should have mechanical properties of targeted organ for replacement or

mechanical properties of desirable tissue for healing. It can be chosen as degradable or nondegradable depending on purpose. Additionally, 3D bioprinted material should mimic targeted structure not only mechanically but also biochemically. It should possess tissue specific functional and dynamic properties. [234]

Several inks are developed with taking into account of properties mentioned above. Commonly used bioinks are naturally derived polymers like gelatin, collagen, fibrin, hyaluronic acid alginate or chitosan, or synthetic polymers like PEG or PCL.[235-238]

3D bioprinting field has been developing in the last 30 years. Comparing to other disciplines, the field is young and advancements are required for preparation of ultimate materials. Higher printing resolution and printing speed are required to obtain more complex structures within reasonable printing time scales. The combination of different bioprinting methods and technologies will be necessary for cost effective manufacturing of bioprinted structures. Beyond printing techniques, the development of advanced bioinks is required to assist high cell viability. Hydrogels with low viscosity are necessary to minimize shear stress on cells during printing. On the other hand, rapid gelation mechanisms are required in order to obtain self-supporting printed structures at high precision. Currently, this stands as a challenge in development of bioinks. Inks prepared with natural polymers are favorable in terms of biocompatibility and biomimicry. On the other hand, synthetic polymers are easier to print, control and preserve structure in higher precision.

### a. Printing Alginate

Alginate hydrogels are one of the most preferred bioinks. Printed alginate can be crosslinked *in situ* by printing in a $Ca^{2+}$ solution or post-printing by dropping or spraying a $Ca^{2+}$ solution on the printed structure after deposition of each layer. Alternatively, alginate can be printed upon mixing with gelatin at temperatures above 30 °C and printing on a cooled stage. [239] In this case gelatin gelifies immediately and the printed alginate /gelatin structure keeps its shape. Afterwards, alginate was crosslinked by immersion in a $Ca^{2+}$ solution. The mixture with gelatin provides adhesive cues for cells and a faster printing process compared to deposition of only alginate. Mixtures of alginate with other polymers have also been printed, i.e. highly stretchable, tough PEG-diacrylate/alginate hydrogel,[207] alginate/pAAm, alginate/pNIPAm, or alginate/poly(dihydroxyethyl acrylate). [207, 240]

## References


1. Frantz, C., K.M. Stewart, and V.M. Weaver, *The extracellular matrix at a glance.* Journal of Cell Science, 2010. 123(24): p. 4195-4200.
2. Butcher, D.T., T. Alliston, and V.M. Weaver, *A tense situation: forcing tumour progression.* Nature Reviews Cancer, 2009. 9(2): p. 108-122.
3. Schaefer, L. and R.M. Schaefer, *Proteoglycans: from structural compounds to signaling molecules.* Cell and Tissue Research, 2010. 339(1): p. 237-246.
4. Wojcik-Stanaszek, L., A. Gregor, and T. Zalewska, *Regulation of neurogenesis by extracellular matrix and integrins.* Acta Neurobiologiae Experimentalis, 2011. 71(1): p. 103-112.
5. Vondermark, K. and M. Ocalan, *Antagonistic Effects of Laminin and Fibronectin on the Expression of the Myogenic Phenotype.* Differentiation, 1989. 40(2): p. 150-157.
6. Buzanska, L., et al., *Patterned growth and differentiation of human cord blood-derived neural stem cells on bio-functionalized surfaces.* Acta Neurobiol Exp (Wars), 2009. 69(1): p. 24-36.
7. Szymczak, P., et al., *Effect of matrix metalloproteinases inhibition on the proliferation and differentiation of HUCB-NSCs cultured in the presence of adhesive substrates.* Acta Neurobiol Exp (Wars), 2010. 70(4): p. 325-36.
8. Andressen, C., et al., *The contribution of beta 1 integrins to neuronal migration and differentiation depends on extracellular matrix molecules.* European Journal of Cell Biology, 2005. 84(12): p. 973-982.
9. Rozario, T. and D.W. DeSimone, *The extracellular matrix in development and morphogenesis: a dynamic view.* Dev Biol, 2010. 341(1): p. 126-40.
10. Robins, S.P., *Biochemistry and functional significance of collagen cross-linking.* Biochemical Society Transactions, 2007. 35(5): p. 849-852.
11. Callaghan, T.M. and K.P. Wilhelm, *A review of ageing and an examination of clinical methods in the assessment of ageing skin. Part 2: Clinical perspectives and clinical methods in the evaluation of ageing skin.* International Journal of Cosmetic Science, 2008. 30(5): p. 323-332.
12. Velnar, T., T. Bailey, and V. Smrkoli, *The Wound Healing Process: an Overview of the Cellular and Molecular Mechanisms.* Journal of International Medical Research, 2009. 37(5): p. 1528-1542.
13. Schultz, G.S. and A. Wysocki, *Interactions between extracellular matrix and growth factors in wound healing.* Wound Repair and Regeneration, 2009. 17(2): p. 153-162.
14. Schafer, M. and S. Werner, *Cancer as an overhealing wound: an old hypothesis revisited.* Nature Reviews Molecular Cell Biology, 2008. 9(8): p. 628-638.
15. Morgan, M.R., M.J. Humphries, and M.D. Bass, *Synergistic control of cell adhesion by integrins and syndecans.* Nature reviews. Molecular cell biology, 2007. 8(12): p. 957-969.
16. Tedder, T.F., et al., *The selectins: vascular adhesion molecules.* The FASEB Journal, 1995. 9(10): p. 866-73.
17. Campbell, I.D. and M.J. Humphries, *Integrin Structure, Activation, and Interactions.* Cold Spring Harbor Perspectives in Biology, 2011. 3(3).
18. Petrie, T.A. and A.J. García, *Extracellular Matrix-derived Ligand for Selective Integrin Binding to Control Cell Function*, in *Biological Interactions on Materials Surfaces: Understanding and Controlling Protein, Cell, and Tissue Responses*, A.D. Puleo and R. Bizios, Editors. 2009, Springer US: New York, NY. p. 133-156.
19. Xiong, J.P., et al., *Crystal structure of the extracellular segment of integrin alpha Vbeta3 in complex with an Arg-Gly-Asp ligand.* Science, 2002. 296(5565): p. 151-5.

20. Xiao, T., et al., *Structural basis for allostery in integrins and binding to fibrinogen-mimetic therapeutics.* Nature, 2004. 432(7013): p. 59-67.
21. Luo, B.H., C.V. Carman, and T.A. Springer, *Structural basis of integrin regulation and signaling.* Annual Review of Immunology, 2007. 25: p. 619-647.
22. Xiong, J.P., et al., *Crystal structure of the extracellular segment of integrin alpha V beta 3.* Science, 2001. 294(5541): p. 339-345.
23. Calderwood, D.A., *Integrin activation.* Journal of Cell Science, 2004. 117(5): p. 657-666.
24. Zaidel-Bar, R., et al., *Hierarchical assembly of cell-matrix adhesion complexes.* Biochemical Society Transactions, 2004. 32: p. 416-420.
25. Zaidel-Bar, R., et al., *Functional atlas of the integrin adhesome.* Nat Cell Biol, 2007. 9(8): p. 858-67.
26. Ren, X.D., et al., *Focal adhesion kinase suppresses Rho activity to promote focal adhesion turnover.* Journal of Cell Science, 2000. 113(20): p. 3673-3678.
27. Brown, M.C., J.A. Perrotta, and C.E. Turner, *Identification of LIM3 as the principal determinant of paxillin focal adhesion localization and characterization of a novel motif on paxillin directing vinculin and focal adhesion kinase binding.* Journal of Cell Biology, 1996. 135(4): p. 1109-1123.
28. Zhou, J., et al., *Mechanism of Focal Adhesion Kinase Mechanosensing.* PLOS Computational Biology, 2015. 11(11): p. e1004593.
29. Arias-Salgado, E.G., et al., *Src kinase activation by direct interaction with the integrin beta cytoplasmic domain.* Proceedings of the National Academy of Sciences of the United States of America, 2003. 100(23): p. 13298-13302.
30. Schoen, I., B.L. Pruitt, and V. Vogel, *The Yin-Yang of Rigidity Sensing: How Forces and Mechanical Properties Regulate the Cellular Response to Materials.* Annual Review of Materials Research, Vol 43, 2013. 43: p. 589-618.
31. Walcott, S., et al., *Nucleation and Decay Initiation Are the Stiffness-Sensitive Phases of Focal Adhesion Maturation.* Biophysical Journal, 2011. 101(12): p. 2919-2928.
32. Harris, A.K., P. Wild, and D. Stopak, *Silicone rubber substrata: a new wrinkle in the study of cell locomotion.* Science, 1980. 208(4440): p. 177-9.
33. Geiger, B., J.P. Spatz, and A.D. Bershadsky, *Environmental sensing through focal adhesions.* Nat Rev Mol Cell Biol, 2009. 10(1): p. 21-33.
34. Austen, K., et al., *Extracellular rigidity sensing by talin isoform-specific mechanical linkages.* Nat Cell Biol, 2015. 17(12): p. 1597-1606.
35. Elosegui-Artola, A., et al., *Rigidity sensing and adaptation through regulation of integrin types.* Nat Mater, 2014. 13(6): p. 631-637.
36. Du, J., et al., *Integrin activation and internalization on soft ECM as a mechanism of induction of stem cell differentiation by ECM elasticity.* Proceedings of the National Academy of Sciences, 2011. 108(23): p. 9466-9471.
37. Dumbauld, D.W., et al., *How vinculin regulates force transmission.* Proceedings of the National Academy of Sciences, 2013. 110(24): p. 9788-9793.
38. Dupont, S., et al., *Role of YAP/TAZ in mechanotransduction.* Nature, 2011. 474(7350): p. 179-183.
39. Choquet, D., D.P. Felsenfeld, and M.P. Sheetz, *Extracellular matrix rigidity causes strengthening of integrin-cytoskeleton linkages.* Cell, 1997. 88(1): p. 39-48.
40. Jiang, Y.X., et al., *The principle of gating charge movement in a voltage-dependent K+ channel.* Nature, 2003. 423(6935): p. 42-48.
41. Tan, J.L., et al., *Cells lying on a bed of microneedles: An approach to isolate mechanical force.* Proceedings of the National Academy of Sciences of the United States of America, 2003. 100(4): p. 1484-1489.

42. Dembo, M. and Y.L. Wang, *Stresses at the cell-to-substrate interface during locomotion of fibroblasts.* Biophysical Journal, 1999. 76(4): p. 2307-2316.
43. Balaban, N.Q., et al., *Force and focal adhesion assembly: a close relationship studied using elastic micropatterned substrates.* Nature Cell Biology, 2001. 3(5): p. 466-472.
44. McBeath, R., et al., *Cell shape, cytoskeletal tension, and RhoA regulate stem cell lineage commitment.* Developmental Cell, 2004. 6(4): p. 483-495.
45. Sordella, R., et al., *Modulation of rho GTPase signaling regulates a switch between adipogenesis and myogenesis.* Cell, 2003. 113(2): p. 147-158.
46. Krieg, M., et al., *Tensile forces govern germ-layer organization in zebrafish.* Nature Cell Biology, 2008. 10(4): p. 429-U122.
47. Lo, C.M., et al., *Cell movement is guided by the rigidity of the substrate.* Biophysical Journal, 2000. 79(1): p. 144-152.
48. Huang, S. and D.E. Ingber, *The structural and mechanical complexity of cell-growth control.* Nature Cell Biology, 1999. 1(5): p. E131-E138.
49. Dvir, T., et al., *Nanotechnological strategies for engineering complex tissues.* Nature Nanotechnology, 2011. 6(1): p. 13-22.
50. Engler, A.J., et al., *Matrix elasticity directs stem cell lineage specification.* Cell, 2006. 126(4): p. 677-689.
51. Gilbert, P.M., et al., *Substrate elasticity regulates skeletal muscle stem cell self-renewal in culture.* Science, 2010. 329(5995): p. 1078-81.
52. Huebsch, N., et al., *Harnessing traction-mediated manipulation of the cell/matrix interface to control stem-cell fate.* Nat Mater, 2010. 9(6): p. 518-26.
53. Khetan, S., et al., *Degradation-mediated cellular traction directs stem cell fate in covalently crosslinked three-dimensional hydrogels.* Nat Mater, 2013. 12(5): p. 458-65.
54. Trappmann, B., et al., *Extracellular-matrix tethering regulates stem-cell fate.* Nat Mater, 2012. 11(7): p. 642-9.
55. Kloxin, A.M., et al., *Photodegradable hydrogels for dynamic tuning of physical and chemical properties.* Science, 2009. 324(5923): p. 59-63.
56. Guvendiren, M. and J.A. Burdick, *Stiffening hydrogels to probe short- and long-term cellular responses to dynamic mechanics.* Nat Commun, 2012. 3: p. 792.
57. Yang, C., et al., *Mechanical memory and dosing influence stem cell fate.* Nature Materials, 2014. 13(6): p. 645-652.
58. Rehmann, M.S. and A.M. Kloxin, *Tunable and dynamic soft materials for three-dimensional cell culture.* Soft Matter, 2013. 9(29): p. 6737-6746.
59. Higuchi, A., et al., *Design of polymeric materials for culturing human pluripotent stem cells: Progress toward feeder-free and xeno-free culturing.* Progress in Polymer Science, 2014. 39(7): p. 1348-1374.
60. Badylak, S.F., D.O. Freytes, and T.W. Gilbert, *Extracellular matrix as a biological scaffold material: Structure and function.* Acta Biomaterialia, 2009. 5(1): p. 1-13.
61. Gillies, A.R. and R.L. Lieber, *Structure and Function of the Skeletal Muscle Extracellular Matrix.* Muscle & nerve, 2011. 44(3): p. 318-331.
62. Sacks, M.S. and D.C. Gloeckner, *Quantification of the fiber architecture and biaxial mechanical behavior of porcine intestinal submucosa.* Journal of Biomedical Materials Research, 1999. 46(1): p. 1-10.
63. Wlodarczyk-Biegun, M.K. and A. del Campo, *3D bioprinting of structural proteins.* Biomaterials, 2017. 134: p. 180-201.
64. Santos, E., et al., *Cell-Biomaterial Interaction: Strategies To Mimic The Extracellular Matrix*, in *On Biomimetics*, D.L. Pramatarova, Editor 2011, InTech.
65. Adeloew, C., et al., *The effect of enzymatically degradable poly(ethylene glycol) hydrogels on smooth muscle cell phenotype.* Biomaterials, 2008. 29(3): p. 314-326.

66. Schmeichel, K.L. and M.J. Bissell, *Modeling tissue-specific signaling and organ function in three dimensions.* Journal of Cell Science, 2003. 116(12): p. 2377-2388.
67. Gaston, J. and S.L. Thibeault, *Hyaluronic acid hydrogels for vocal fold wound healing.* Biomatter, 2013. 3(1): p. e23799.
68. Li, J. and D.J. Mooney, *Designing hydrogels for controlled drug delivery.* Nature Reviews Materials, 2016. 1: p. 16071.
69. Khademhosseini, A. and R. Langer, *Microengineered hydrogels for tissue engineering.* Biomaterials, 2007. 28(34): p. 5087-5092.
70. Green, J.J. and J.H. Elisseeff, *Mimicking biological functionality with polymers for biomedical applications.* Nature, 2016. 540(7633): p. 386-394.
71. Poitout, D.G., *Biomechanics and Biomaterials in Orthopedics*2016: Springer London.
72. Ehrbar, M., et al., *Biomolecular hydrogels formed and degraded via site-specific enzymatic reactions.* Biomacromolecules, 2007. 8(10): p. 3000-3007.
73. Tsang, V.L., et al., *Fabrication of 3D hepatic tissues by additive photopatterning of cellular hydrogels.* Faseb Journal, 2007. 21(3): p. 790-801.
74. Girotti, A., et al., *Design and bioproduction of a recombinant multi(bio)functional elastin-like protein polymer containing cell adhesion sequences for tissue engineering purposes.* Journal of Materials Science-Materials in Medicine, 2004. 15(4): p. 479-484.
75. Fittkau, M.H., et al., *The selective modulation of endothelial cell mobility on RGD peptide containing surfaces by YIGSR peptides.* Biomaterials, 2005. 26(2): p. 167-174.
76. Wen, J.H., et al., *Interplay of matrix stiffness and protein tethering in stem cell differentiation.* Nature Materials, 2014. 13(10): p. 979-987.
77. Connelly, J.T., A.J. García, and M.E. Levenston, *Interactions between integrin ligand density and cytoskeletal integrity regulate BMSC chondrogenesis.* Journal of Cellular Physiology, 2008. 217(1): p. 145-154.
78. Kong, F., et al., *Cyclic Mechanical Reinforcement of Integrin-Ligand Interactions.* Molecular Cell, 2013. 49(6): p. 1060-1068.
79. Novosel, E.C., C. Kleinhans, and P.J. Kluger, *Vascularization is the key challenge in tissue engineering.* Advanced Drug Delivery Reviews, 2011. 63(4–5): p. 300-311.
80. Gage, Fred H. and S. Temple, *Neural Stem Cells: Generating and Regenerating the Brain.* Neuron. 80(3): p. 588-601.
81. Liu, S.Q., et al., *Synthetic hydrogels for controlled stem cell differentiation.* Soft Matter, 2010. 6(1): p. 67-81.
82. Paez, J.I., et al., *Gauging and Tuning Cross-Linking Kinetics of Catechol-PEG Adhesives via Catecholamine Functionalization.* Biomacromolecules, 2015. 16(12): p. 3811-3818.
83. Farrukh, A., et al., *Bioconjugating Thiols to Poly(acrylamide) Gels for Cell Culture Using Methylsulfonyl Co-monomers.* Angewandte Chemie-International Edition, 2016. 55(6): p. 2092-2096.
84. Steinbüchel, A., *Polysaccharides and polyamides in the food industry: properties, production, and patents*2005: Wiley-VCH-Verlag.
85. Jeon, O., et al., *Photocrosslinked alginate hydrogels with tunable biodegradation rates and mechanical properties.* Biomaterials, 2009. 30(14): p. 2724-2734.
86. Lee, C., et al., *Bioinspired, Calcium-Free Alginate Hydrogels with Tunable Physical and Mechanical Properties and Improved Biocompatibility.* Biomacromolecules, 2013. 14(6): p. 2004-2013.
87. Li, L., W. Smitthipong, and H.B. Zeng, *Mussel-inspired hydrogels for biomedical and environmental applications.* Polymer Chemistry, 2015. 6(3): p. 353-358.
88. Morch, Y.A., et al., *Effect of Ca2+, Ba2+, and Sr2+ on alginate microbeads.* Biomacromolecules, 2006. 7(5): p. 1471-1480.

89. Augst, A.D., H.J. Kong, and D.J. Mooney, *Alginate hydrogels as biomaterials.* Macromolecular Bioscience, 2006. 6(8): p. 623-633.
90. Haug, A., *The affinity of some divalent metals for different types of alginates.* Acta Chem Scand, 1961. 15: p. 1794-1795.
91. Haug, A. and O. Smidsrod, *Selectivity of some anionic polymers for divalent metal ions.* Acta Chem Scand, 1970. 24: p. 843-845.
92. Committee, I.o.M.U., *Tolerable Upper Intake Levels: Calcium and Vitamin D*, in *Dietary Reference Intakes for Calcium and Vitamin D*, A.C. Ross, C.L. Taylor, and A.L.e.a. Yaktine, Editors. 2011, National Academies Press (US): Washington (DC).
93. Saether, H.V., et al., *Polyelectrolyte complex formation using alginate and chitosan.* Carbohydrate Polymers, 2008. 74(4): p. 813-821.
94. Kuo, C.K. and P.X. Ma, *Maintaining dimensions and mechanical properties of ionically crosslinked alginate hydrogel scaffolds in vitro.* J Biomed Mater Res A, 2008. 84(4): p. 899-907.
95. Kuo, C.K. and P.X. Ma, *Ionically crosslinked alginate hydrogels as scaffolds for tissue engineering: Part 1. Structure, gelation rate and mechanical properties.* Biomaterials, 2001. 22(6): p. 511-521.
96. Lee, K.Y. and D.J. Mooney, *Alginate: Properties and biomedical applications.* Progress in Polymer Science, 2012. 37(1): p. 106-126.
97. Rabbany, S.Y., et al., *Continuous Delivery of Stromal Cell-Derived Factor-1 From Alginate Scaffolds Accelerates Wound Healing.* Cell Transplantation, 2010. 19(4): p. 399-408.
98. Maiti, S., et al., *Adipic acid dihydrazide treated partially oxidized alginate beads for sustained oral delivery of flurbiprofen.* Pharmaceutical Development and Technology, 2009. 14(5): p. 461-470.
99. Weir, M.D., H.H.K. Xu, and C.G. Simon, *Strong calcium phosphate cement-chitosan-mesh construct containing cell-encapsulating hydrogel beads for bone tissue engineering.* Journal of Biomedical Materials Research Part A, 2006. 77A(3): p. 487-496.
100. Chueh, B.H., et al., *Patterning alginate hydrogels using light-directed release of caged calcium in a microfluidic device.* Biomedical Microdevices, 2010. 12(1): p. 145-151.
101. Schrieber, R. and H. Gareis, *Gelatine Handbook: Theory and Industrial Practice*2007: Wiley.
102. Gorgieva, S. and V. Kokol, *Collagen- vs. Gelatine-Based Biomaterials and Their Biocompatibility: Review and Perspectives*, in *Biomaterials Applications for Nanomedicine*, R. Pignatello, Editor 2011, InTech.
103. Bello, J., H.R. Bello, and J.R. Vinograd, *The mechanism of gelation of gelatin. The influence of pH, concentration, time and dilute electrolyte on the gelation of gelatin and modified gelatins.* Biochim Biophys Acta, 1962. 57: p. 214-21.
104. Bello, J., H.C.A. Riese, and J.R. Vinograd, *Mechanism of Gelation of Gelatin. Influence of Certain Electrolytes on the Melting Points of Gels of Gelatin and Chemically Modified Gelatins.* The Journal of Physical Chemistry, 1956. 60(9): p. 1299-1306.
105. Djabourov, M., J. Leblond, and P. Papon, *Gelation of Aqueous Gelatin Solutions .1. Structural Investigation.* Journal De Physique, 1988. 49(2): p. 319-332.
106. Sisson, K., et al., *Evaluation of Cross-Linking Methods for Electrospun Gelatin on Cell Growth and Viability.* Biomacromolecules, 2009. 10(7): p. 1675-1680.
107. Farris, S., J. Song, and Q. Huang, *Alternative Reaction Mechanism for the Cross-Linking of Gelatin with Glutaraldehyde.* Journal of Agricultural and Food Chemistry, 2010. 58(2): p. 998-1003.

108. Martucci, J.F. and R.A. Ruseckaite, *Biodegradation of three-layer laminate films based on gelatin under indoor soil conditions.* Polymer Degradation and Stability, 2009. 94(8): p. 1307-1313.
109. Barbetta, A., et al., *Porous gelatin hydrogels by gas-in-liquid foam templating.* Soft Matter, 2010. 6(8): p. 1785-1792.
110. Chang, M.C. and W.H. Douglas, *Cross-linkage of hydroxyapatite/gelatin nanocomposite using imide-based zero-length cross-linker.* Journal of Materials Science-Materials in Medicine, 2007. 18(10): p. 2045-2051.
111. Kuijpers, A.J., et al., *Cross-linking and characterisation of gelatin matrices for biomedical applications.* Journal of Biomaterials Science-Polymer Edition, 2000. 11(3): p. 225-243.
112. Vargas, G., et al., *Study of cross-linking of gelatin by ethylene glycol diglycidyl ether.* Materials Letters, 2008. 62(21-22): p. 3656-3658.
113. Kim, S., et al., *Chitosan/gelatin-based films crosslinked by proanthocyanidin.* Journal of Biomedical Materials Research Part B-Applied Biomaterials, 2005. 75B(2): p. 442-450.
114. Zhang, X., et al., *Chemical Cross-Linking Gelatin with Natural Phenolic Compounds as Studied by High-Resolution NMR Spectroscopy.* Biomacromolecules, 2010. 11(4): p. 1125-1132.
115. Bigi, A., et al., *Stabilization of gelatin films by crosslinking with genipin.* Biomaterials, 2002. 23(24): p. 4827-4832.
116. Solorio, L., et al., *Gelatin microspheres crosslinked with genipin for local delivery of growth factors.* Journal of tissue engineering and regenerative medicine, 2010. 4(7): p. 514-523.
117. Liang, H.-C., et al., *Crosslinking structures of gelatin hydrogels crosslinked with genipin or a water-soluble carbodiimide.* Journal of Applied Polymer Science, 2004. 91(6): p. 4017-4026.
118. Inoue, M., et al., *An Antithrombogenic Citric Acid-Crosslinked Gelatin with Endothelialization Activity.* Advanced Healthcare Materials, 2012. 1(5): p. 573-581.
119. Paguirigan, A.L. and D.J. Beebe, *Protocol for the fabrication of enzymatically crosslinked gelatin microchannels for microfluidic cell culture.* Nat. Protocols, 2007. 2(7): p. 1782-1788.
120. Fang, J.Y., et al., *Tumor Bioengineering Using a Transglutaminase Crosslinked Hydrogel.* Plos One, 2014. 9(8).
121. Choi, Y.C., et al., *Human gelatin tissue-adhesive hydrogels prepared by enzyme-mediated biosynthesis of DOPA and Fe3+ ion crosslinking.* Journal of Materials Chemistry B, 2014. 2(2): p. 201-209.
122. Elzoghby, A.O., *Gelatin-based nanoparticles as drug and gene delivery systems: Reviewing three decades of research.* Journal of Controlled Release, 2013. 172(3): p. 1075-1091.
123. Suarasan, S., et al., *Doxorubicin-Incorporated Nanotherapeutic Delivery System Based on Gelatin-Coated Gold Nanoparticles: Formulation, Drug Release, and Multimodal Imaging of Cellular Internalization.* Acs Applied Materials & Interfaces, 2016. 8(35): p. 22900-22913.
124. Avery, R.K., et al., *An injectable shear-thinning biomaterial for endovascular embolization.* Science Translational Medicine, 2016. 8(365).
125. Hosseini, V., et al., *Engineered Contractile Skeletal Muscle Tissue on a Microgrooved Methacrylated Gelatin Substrate.* Tissue Engineering Part A, 2012. 18(23-24): p. 2453-2465.
126. Gaharwar, A.K., et al., *Shear-Thinning Nanocomposite Hydrogels for the Treatment of Hemorrhage.* Acs Nano, 2014. 8(10): p. 9833-9842.

127. Rosellini, E., et al., *Preparation and characterization of alginate/gelatin blend films for cardiac tissue engineering.* Journal of Biomedical Materials Research Part A, 2009. 91A(2): p. 447-453.
128. Huang, Y., et al., *In vitro characterization of chitosan-gelatin scaffolds for tissue engineering.* Biomaterials, 2005. 26(36): p. 7616-7627.
129. Hong, H., C.S. Liu, and W.J. Wu, *Preparation and Characterization of Chitosan/PEG/Gelatin Composites for Tissue Engineering.* Journal of Applied Polymer Science, 2009. 114(2): p. 1220-1225.
130. Truong, V.X., K.M. Tsang, and J.S. Forsythe, *Nonswelling Click-Cross-Linked Gelatin and PEG Hydrogels with Tunable Properties Using Pluronic Linkers.* Biomacromolecules, 2017. 18(3): p. 757-766.
131. Moody, G.M., *Role of Polyacrylamides and Related Products in Treatment of Mineral Processing Effluent.* Transactions of the Institution of Mining and Metallurgy Section C-Mineral Processing and Extractive Metallurgy, 1990. 99: p. C137-C141.
132. Smith, B.J., *SDS Polyacrylamide Gel Electrophoresis of Proteins*, in *Proteins*, J.M. Walker, Editor 1984, Humana Press: Totowa, NJ. p. 41-55.
133. Caulfield, M.J., G.G. Qiao, and D.H. Solomon, *Some aspects of the properties and degradation of polyacrylamides.* Chemical Reviews, 2002. 102(9): p. 3067-3083.
134. Williams, M., *The Merck Index: An Encyclopedia of Chemicals, Drugs, and Biologicals, 15th Edition Edited by M.J. O'Neil , PB - Royal Society of Chemistry , Cambridge, UK ISBN 9781849736701; 2708 pages. April 2013, $150 with 1-year free access to The Merck Index Online.* Drug Development Research, 2013. 74(5): p. 339-339.
135. Wiersma, J.A., M. Bos, and A.J. Pennings, *High strength poly(meth)acrylamide copolymer hydrogels.* Polymer Bulletin, 1994. 33(6): p. 615-622.
136. Gelfi, C. and P.G. Righetti, *Polymerization Kinetics of Polyacrylamide Gels .1. Effect of Different Cross-Linkers.* Electrophoresis, 1981. 2(4): p. 213-219.
137. Rabilloud, T., et al., *Silver-Staining of Proteins in Polyacrylamide Gels - a General Overview.* Cellular and Molecular Biology, 1994. 40(1): p. 57-75.
138. Martinez, I., T.J. Friis, and M. Seppola, *Requirements for the application of protein sodium dodecyl sulfate-polyacrylamide gel electrophoresis and randomly amplified polymorphic DNA analyses to product speciation.* Electrophoresis, 2001. 22(8): p. 1526-1533.
139. Caliari, S.R. and J.A. Burdick, *A practical guide to hydrogels for cell culture.* Nature Methods, 2016. 13(5): p. 405-414.
140. Zhang, S., et al., *Revisiting the mechanism of redox-polymerization to build the hydrogel with excellent properties using a novel initiator.* Soft Matter, 2016. 12(9): p. 2575-2582.
141. Tse, J.R. and A.J. Engler, *Preparation of hydrogel substrates with tunable mechanical properties.* Curr Protoc Cell Biol, 2010. Chapter 10: p. Unit 10 16.
142. Trappmann, B., et al., *Extracellular-matrix tethering regulates stem-cell fate.* Nature Materials, 2012. 11(7): p. 642-649.
143. Sunyer, R., et al., *Fabrication of Hydrogels with Steep Stiffness Gradients for Studying Cell Mechanical Response.* PLoS ONE, 2012. 7(10): p. e46107.
144. Grevesse, T. and S. Gabriele, *Micro-engineered hydrogels*, 2013, Google Patents.
145. Grevesse, T., et al., *A simple route to functionalize polyacrylamide hydrogels for the independent tuning of mechanotransduction cues.* Lab on a Chip, 2013. 13(5): p. 777-780.
146. Klein, J. and R. Heitzmann, *Preparation and Characterization of Poly(Acrylamide-Co-Acrylic Acid).* Makromolekulare Chemie-Macromolecular Chemistry and Physics, 1978. 179(8): p. 1895-1904.

147. Lee, J.P., et al., *N-terminal specific conjugation of extracellular matrix proteins to 2-pyridinecarboxaldehyde functionalized polyacrylamide hydrogels.* Biomaterials, 2016. 102: p. 268-276.
148. Pelham, R.J. and Y.L. Wang, *Cell locomotion and focal adhesions are regulated by substrate flexibility.* Proceedings of the National Academy of Sciences of the United States of America, 1997. 94(25): p. 13661-13665.
149. Hjortso, M., *Cell Adhesion in Bioprocessing and Biotechnology*1994: Taylor & Francis.
150. Keys, K.B., F.M. Andreopoulos, and N.A. Peppas, *Poly(ethylene glycol) star polymer hydrogels.* Macromolecules, 1998. 31(23): p. 8149-8156.
151. Hubbell, J.A., *Synthetic biodegradable polymers for tissue engineering and drug delivery.* Current Opinion in Solid State & Materials Science, 1998. 3(3): p. 246-251.
152. Metters, A. and J. Hubbell, *Network formation and degradation behavior of hydrogels formed by Michael-type addition reactions.* Biomacromolecules, 2005. 6(1): p. 290-301.
153. Polizzotti, B.D., B.D. Fairbanks, and K.S. Anseth, *Three-dimensional biochemical patterning of click-based composite hydrogels via thiolene photopolymerization.* Biomacromolecules, 2008. 9(4): p. 1084-1087.
154. Cui, J.X., et al., *Dopamine-Based Coatings and Hydrogels: Toward Substitution-Related Structure-Property Relationships.* Macromolecular Chemistry and Physics, 2014. 215(24): p. 2403-2413.
155. Cencer, M., et al., *Effect of pH on the Rate of Curing and Bioadhesive Properties of Dopamine Functionalized Poly(ethylene glycol) Hydrogels.* Biomacromolecules, 2014. 15(8): p. 2861-2869.
156. Hamley, I.W., *PEG-Peptide Conjugates.* Biomacromolecules, 2014. 15(5): p. 1543-1559.
157. Zhu, J.M., et al., *Extracellular matrix-like cell-adhesive hydrogels from RGD-containing poly(ethylene glycol) diacrylate.* Macromolecules, 2006. 39(4): p. 1305-1307.
158. Hern, D.L. and J.A. Hubbell, *Incorporation of adhesion peptides into nonadhesive hydrogels useful for tissue resurfacing.* Journal of Biomedical Materials Research, 1998. 39(2): p. 266-276.
159. Mann, B.K., et al., *Smooth muscle cell growth in photopolymerized hydrogels with cell adhesive and proteolytically degradable domains: synthetic ECM analogs for tissue engineering.* Biomaterials, 2001. 22(22): p. 3045-3051.
160. Seliktar, D., et al., *MMP-2 sensitive, VEGF-bearing bioactive hydrogels for promotion of vascular healing.* Journal of Biomedical Materials Research Part A, 2004. 68A(4): p. 704-716.
161. Lee, H.J., et al., *Collagen mimetic peptide-conjugated photopolymerizable PEG hydrogel.* Biomaterials, 2006. 27(30): p. 5268-5276.
162. Lin, C.C., A.T. Metters, and K.S. Anseth, *Functional PEG-peptide hydrogels to modulate local inflammation induced by the pro-inflammatory cytokine TNF alpha.* Biomaterials, 2009. 30(28): p. 4907-4914.
163. Bohl, K.S. and J.L. West, *Nitric oxide-generating polymers reduce platelet adhesion and smooth muscle cell proliferation.* Biomaterials, 2000. 21(22): p. 2273-2278.
164. Knop, K., et al., *Poly(ethylene glycol) in Drug Delivery: Pros and Cons as Well as Potential Alternatives.* Angewandte Chemie International Edition, 2010. 49(36): p. 6288-6308.
165. Zaikov, G.E., I.U.B. Monakov, and A. Jiménez, *Trends in Molecular and High Molecular Science*2005: Nova Science Publishers.
166. Lustig, S.R. and N.A. Peppas, *Solute Diffusion in Swollen Membranes .9. Scaling Laws for Solute Diffusion in Gels.* Journal of Applied Polymer Science, 1988. 36(4): p. 735-747.

167. Parlato, M. and W. Murphy, *Chapter 1 Soluble Molecule Transport Within Synthetic Hydrogels in Comparison to the Native Extracellular Matrix*, in *Hydrogels in Cell-Based Therapies*2014, The Royal Society of Chemistry. p. 1-30.
168. Zaari, N., et al., *Photopolymerization in microfluidic gradient generators: Microscale control of substrate compliance to manipulate cell response.* Advanced Materials, 2004. 16(23-24): p. 2133-+.
169. Stowers, R.S., S.C. Allen, and L.J. Suggs, *Dynamic phototuning of 3D hydrogel stiffness.* Proceedings of the National Academy of Sciences, 2015. 112(7): p. 1953-1958.
170. DeForest, C.A. and K.S. Anseth, *Cytocompatible click-based hydrogels with dynamically tunable properties through orthogonal photoconjugation and photocleavage reactions.* Nat Chem, 2011. 3(12): p. 925-31.
171. Khetan, S., et al., *Degradation-mediated cellular traction directs stem cell fate in covalently crosslinked three-dimensional hydrogels.* Nat Mater, 2013. 12(5): p. 458-465.
172. Shin, S.R., et al., *Cell-laden microengineered and mechanically tunable hybrid hydrogels of gelatin and graphene oxide.* Advanced Materials, 2013. 25(44): p. 6385-91.
173. Mabry, K.M., R.L. Lawrence, and K.S. Anseth, *Dynamic stiffening of poly(ethylene glycol)-based hydrogels to direct valvular interstitial cell phenotype in a three-dimensional environment.* Biomaterials, 2015. 49: p. 47-56.
174. Liu, Z.Z., et al., *Spatiotemporally Controllable and Cytocompatible Approach Builds 3D Cell Culture Matrix by Photo-Uncaged-Thiol Michael Addition Reaction.* Advanced Materials, 2014. 26(23): p. 3912-3917.
175. Stowers, R.S., S.C. Allen, and L.J. Suggs, *Dynamic phototuning of 3D hydrogel stiffness.* Proceedings of the National Academy of Sciences of the United States of America, 2015. 112(7): p. 1953-1958.
176. Cui, J.X., et al., *Light-Triggered Cross-Linking of Alginates with Caged Ca2+.* Biomacromolecules, 2013. 14(5): p. 1251-1256.
177. Ellis-Davies, G.C.R., *Neurobiology with caged calcium.* Chemical Reviews, 2008. 108(5): p. 1603-1613.
178. Hardin, B.O. and V.P. Drnevich, *Shear modulus and damping in soils: design equations and curves.* Journal of Geotechnical Engineering, 1972. 98(7): p. 25.
179. Bartolino, R. and G. Durand, *Plasticity in a Smectic-A Liquid Crystal.* Physical Review Letters, 1977. 39(21): p. 1346-1349.
180. Cagnon, M. and G. Durand, *Mechanical Shear of Layers in Smectic-A and Smectic-B Liquid Crystal.* Physical Review Letters, 1980. 45(17): p. 1418-1421.
181. Martinoty, P., J.L. Gallani, and D. Collin, *Hydrodynamic and Nonhydrodynamic Behavior of Layer-Compression Modulus B at the Nematic- Smectic- A Phase Transition in 8 OCB.* Physical Review Letters, 1998. 81(1): p. 144-147.
182. Auernhammer, G.K., D. Collin, and P. Martinoty, *Viscoelasticity of suspensions of magnetic particles in a polymer: Effect of confinement and external field.* The Journal of Chemical Physics, 2006. 124(20): p. 204907.
183. Jun, Y., N. Haruki, and O. Koji, *Apparatus for Measurement of Complex Shear Modulus of Liquid Crystals at Low Frequencies.* Japanese Journal of Applied Physics, 1987. 26(S1): p. 29.
184. Roth, M., et al., *Viscoelastic rheology of colloid-liquid crystal composites.* The Journal of Chemical Physics, 2010. 132(12): p. 124702.
185. Chen, Q., et al., *Engineering of Tough Double Network Hydrogels.* Macromolecular Chemistry and Physics, 2016. 217(9): p. 1022-1036.
186. Zhao, X.H., *Multi-scale multi-mechanism design of tough hydrogels: building dissipation into stretchy networks.* Soft Matter, 2014. 10(5): p. 672-687.

187. Fung, Y.C., *Biomechanics: Mechanical Properties of Living Tissues*2013: Springer New York.
188. Sun, J.Y., et al., *Highly stretchable and tough hydrogels.* Nature, 2012. 489(7414): p. 133-136.
189. Gong, J.P., et al., *Double-network hydrogels with extremely high mechanical strength.* Advanced Materials, 2003. 15(14): p. 1155-+.
190. Zhao, X.H., *A theory for large deformation and damage of interpenetrating polymer networks.* Journal of the Mechanics and Physics of Solids, 2012. 60(2): p. 319-332.
191. Sun, T.L., et al., *Physical hydrogels composed of polyampholytes demonstrate high toughness and viscoelasticity.* Nature Materials, 2013. 12(10): p. 932-7.
192. Brown, A.E., et al., *Multiscale mechanics of fibrin polymer: gel stretching with protein unfolding and loss of water.* Science, 2009. 325(5941): p. 741-4.
193. Agrawal, A., N. Rahbar, and P.D. Calvert, *Strong fiber-reinforced hydrogel.* Acta Biomater, 2013. 9(2): p. 5313-8.
194. Shin, H., B.D. Olsen, and A. Khademhosseini, *The mechanical properties and cytotoxicity of cell-laden double-network hydrogels based on photocrosslinkable gelatin and gellan gum biomacromolecules.* Biomaterials, 2012. 33(11): p. 3143-52.
195. Abdurrahmanoglu, S., V. Can, and O. Okay, *Design of high-toughness polyacrylamide hydrogels by hydrophobic modification.* Polymer, 2009. 50(23): p. 5449-5455.
196. Wang, Q., et al., *High-water-content mouldable hydrogels by mixing clay and a dendritic molecular binder.* Nature, 2010. 463(7279): p. 339-43.
197. Sakai, T., et al., *Highly Elastic and Deformable Hydrogel Formed from Tetra-arm Polymers.* Macromolecular Rapid Communications, 2010. 31(22): p. 1954-1959.
198. Chen, Q., et al., *Fundamentals of double network hydrogels.* Journal of Materials Chemistry B, 2015. 3(18): p. 3654-3676.
199. Nakajima, T., et al., *A Universal Molecular Stent Method to Toughen any Hydrogels Based on Double Network Concept.* Advanced Functional Materials, 2012. 22(21): p. 4426-4432.
200. Nakajima, T., et al., *Synthesis and Fracture Process Analysis of Double Network Hydrogels with a Well-Defined First Network.* Acs Macro Letters, 2013. 2(6): p. 518-521.
201. Sun, J.Y., et al., *Highly stretchable and tough hydrogels.* Nature, 2012. 489(7414): p. 133-6.
202. Chen, Q., et al., *A Robust, One-Pot Synthesis of Highly Mechanical and Recoverable Double Network Hydrogels Using Thermoreversible Sol-Gel Polysaccharide.* Advanced Materials, 2013. 25(30): p. 4171-4176.
203. Bakarich, S.E., et al., *Printed ionic-covalent entanglement hydrogels from carrageenan and an epoxy amine.* RSC Advances, 2014. 4(72): p. 38088-38092.
204. Bakarich, S.E., et al., *Extrusion printing of ionic-covalent entanglement hydrogels with high toughness.* Journal of Materials Chemistry B, 2013. 1(38): p. 4939-4946.
205. Bakarich, S.E., et al., *Three-Dimensional Printing Fiber Reinforced Hydrogel Composites.* Acs Applied Materials & Interfaces, 2014. 6(18): p. 15998-16006.
206. Hong, S.M., et al., *3D Printing of Highly Stretchable and Tough Hydrogels into Complex, Cellularized Structures.* Advanced Materials, 2015. 27(27): p. 4035-4040.
207. Jiang, Y.H. and Q.M. Wang, *Highly-stretchable 3D-architected Mechanical Metamaterials.* Scientific Reports, 2016. 6.
208. Nakajima, T., et al., *A facile method for synthesizing free-shaped and tough double network hydrogels using physically crosslinked poly(vinyl alcohol) as an internal mold.* Polymer Chemistry, 2010. 1(5): p. 693-697.

209. Tang, T. and A. Takasu, *Facile synthesis of unsaturated polyester-based double-network gels via chemoselective cross-linking using Michael addition and subsequent UV-initiated radical polymerization.* RSC Advances, 2015. 5(2): p. 819-829.
210. Saito, J., et al., *Robust bonding and one-step facile synthesis of tough hydrogels with desirable shape by virtue of the double network structure.* Polymer Chemistry, 2011. 2(3): p. 575-580.
211. Li, Y.L., et al., *Preparation and Characterization of PAM/SA Tough Hydrogels Reinforced by IPN Technique Based on Covalent/Ionic Crosslinking.* Journal of Applied Polymer Science, 2015. 132(4).
212. Mehrali, M., et al., *Nanoreinforced Hydrogels for Tissue Engineering: Biomaterials that are Compatible with Load-Bearing and Electroactive Tissues.* Advanced Materials, 2017. 29(8).
213. Lohani, A., et al., *Interpenetrating Polymer Networks as Innovative Drug Delivery Systems.* Journal of Drug Delivery, 2014. 2014: p. 11.
214. Shen, C., et al., *Mechanically strong interpenetrating network hydrogels for differential cellular adhesion.* RSC Advances, 2017. 7(29): p. 18046-18053.
215. Zheng, W.J., et al., *Tough Al-alginate/Poly(N-isopropylacrylamide) Hydrogel with Tunable LCST for Soft Robotics.* Acs Applied Materials & Interfaces, 2015. 7(3): p. 1758-1764.
216. Yoshikawa, K., et al., *Hyaluronic acid affects the in vitro induction effects of Synthetic PAMPS and PDMAAm hydrogels on chondrogenic differentiation of ATDC5 cells, depending on the level of concentration.* BMC Musculoskeletal Disorders, 2013. 14(1): p. 56.
217. Fukui, T., et al., *Intra-articular administration of hyaluronic acid increases the volume of the hyaline cartilage regenerated in a large osteochondral defect by implantation of a double-network gel.* Journal of Materials Science: Materials in Medicine, 2014. 25(4): p. 1173-1182.
218. Rennerfeldt, D.A., et al., *Tuning mechanical performance of poly(ethylene glycol) and agarose interpenetrating network hydrogels for cartilage tissue engineering.* Biomaterials, 2013. 34(33): p. 8241-8257.
219. Liao, I.C., et al., *Composite Three-Dimensional Woven Scaffolds with Interpenetrating Network Hydrogels to Create Functional Synthetic Articular Cartilage.* Advanced Functional Materials, 2013. 23(47): p. 5833-5839.
220. Filippini, G., et al., *Sperm DNA fragmentation as a prognostic factor of pregnancy outcome after ART: a study on 816 couples and 1200 cycles.* Human Reproduction, 2011. 26: p. I8-I8.
221. Pan, J., *On the origin of printing in the light of new archaeological discoveries.* Chinese Science Bulletin, 1997. 42(12): p. 976-981.
222. Whitfield, R., et al., *Caves of the Thousand Buddhas: Chinese Art from the Silk Route*1990: British Museum Publications for the Trustees of the British Museum.
223. Hull, C.W., *Apparatus for production of three-dimensional objects by stereolithography*, 1986, Google Patents.
224. Atala, A., et al., *Tissue-engineered autologous bladders for patients needing cystoplasty.* The Lancet. 367(9518): p. 1241-1246.
225. Zhang, X. and Y. Zhang, *Tissue Engineering Applications of Three-Dimensional Bioprinting.* Cell Biochemistry and Biophysics, 2015. 72(3): p. 777-782.
226. Cui, X., et al., *Direct Human Cartilage Repair Using Three-Dimensional Bioprinting Technology.* Tissue Engineering. Part A, 2012. 18(11-12): p. 1304-1312.

227. Rhee, S., et al., *3D Bioprinting of Spatially Heterogeneous Collagen Constructs for Cartilage Tissue Engineering.* Acs Biomaterials Science & Engineering, 2016. 2(10): p. 1800-1805.
228. Duan, B., et al., *3D Bioprinting of Heterogeneous Aortic Valve Conduits with Alginate/Gelatin Hydrogels.* Journal of biomedical materials research. Part A, 2013. 101(5): p. 1255-1264.
229. Williams, S.K., et al., *Encapsulation of Adipose Stromal Vascular Fraction Cells in Alginate Hydrogel Spheroids Using a Direct-Write Three-Dimensional Printing System.* BioResearch Open Access, 2013. 2(6): p. 448-454.
230. Norotte, C., et al., *Scaffold-Free Vascular Tissue Engineering Using Bioprinting.* Biomaterials, 2009. 30(30): p. 5910-5917.
231. Michael, S., et al., *Tissue Engineered Skin Substitutes Created by Laser-Assisted Bioprinting Form Skin-Like Structures in the Dorsal Skin Fold Chamber in Mice.* PLoS ONE, 2013. 8(3): p. e57741.
232. Virginie, K., et al., *In vivo bioprinting for computer- and robotic-assisted medical intervention: preliminary study in mice.* Biofabrication, 2010. 2(1): p. 014101.
233. Murphy, S.V. and A. Atala, *3D bioprinting of tissues and organs.* Nat Biotech, 2014. 32(8): p. 773-785.
234. Kang, H.-W., et al., *A 3D bioprinting system to produce human-scale tissue constructs with structural integrity.* Nat Biotech, 2016. 34(3): p. 312-319.
235. Derby, B., *Printing and Prototyping of Tissues and Scaffolds.* Science, 2012. 338(6109): p. 921-926.
236. Skardal, A., J. Zhang, and G.D. Prestwich, *Bioprinting vessel-like constructs using hyaluronan hydrogels crosslinked with tetrahedral polyethylene glycol tetracrylates.* Biomaterials, 2010. 31(24): p. 6173-6181.
237. Lei, M.J. and X.H. Wang, *Biodegradable Polymers and Stem Cells for Bioprinting.* Molecules, 2016. 21(5).
238. Wen, C., L.L. Lu, and X.S. Li, *Mechanically Robust Gelatin-Alginate IPN Hydrogels by a Combination of Enzymatic and Ionic Crosslinking Approaches.* Macromolecular Materials and Engineering, 2014. 299(4): p. 504-513.
239. Bootsma, K., et al., *3D printing of an interpenetrating network hydrogel material with tunable viscoelastic properties.* Journal of the Mechanical Behavior of Biomedical Materials, 2017. 70: p. 84-94.

# 2

# Approaches to Adjust the Mechanical Properties and Curing Kinetics of PEG-Catechol Hydrogels

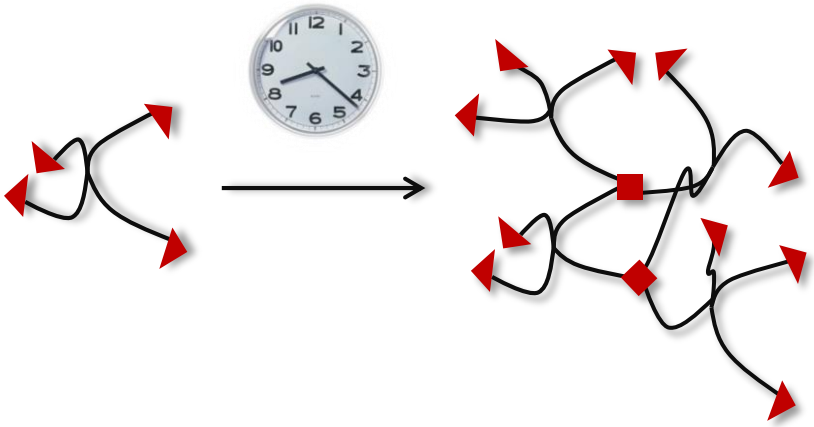

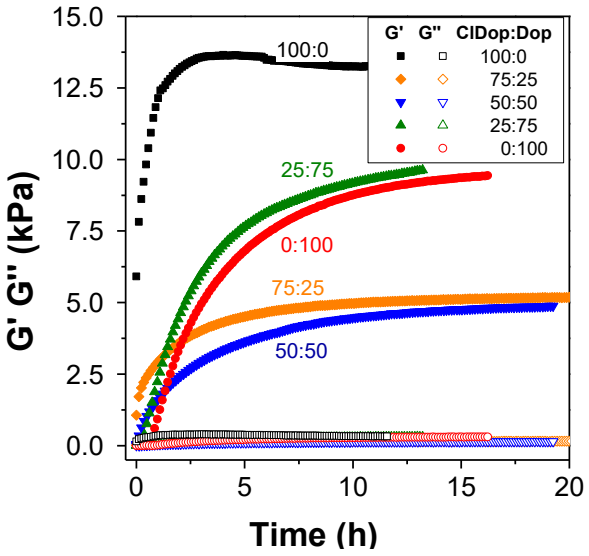


The contents of this chapter were published in Paez, J.I., Ustahuseyin, O., Serrano, C., Ton, X.A., Shafiq, Z., Auernhammer, G.K., d'Ischia, M., and del Campo, A. (2015). Gauging and Tuning Cross-Linking Kinetics of Catechol-PEG Adhesives via Catecholamine Functionalization. Biomacromolecules 16 3811-3818 with permission.

## 2.1 Abstract

Polyethylene(glycol) (PEG) hydrogels functionalized with catechol derivatives were used to create a system with tunable mechanical properties. Catechol derivatives had substituents with different electron withdrawing substituents. Also, they are biocompatible. In that way, the final moduli and crosslinking kinetics of the PEG hydrogels varied. Moreover, mixing two different PEG-catechol derivatives generated a hydrogel system with controlled final moduli and crosslinking kinetics. This strategy can be used in biomedical applications which require long or short curing time or high or low modulus.

## 2.2 Introduction

In tissue engineering, the ultimate goal is to create a personalized and implantable material which mimics the mechanical and biochemical properties of the targeted tissue. In that sense, poly(ethylene glycol) (PEG) hydrogels are promising and widely used biomaterials. They are synthetic, highly hydrophilic polymers with tailorable mechanical properties and the possibility of being biofunctionalized. They are non-immunogenic and do not support protein adsorption.[1] Depending on the purpose of application, PEGs have been functionalized with short bioactive peptide sequences such as RGD, KQAGDV, REDV, YIGSR, IKVAV, and GFOGER.[1-3]

PEG is commercially available in linear or star shaped forms.(Section 1.2.1) Star shaped PEG is a branched polymer which has linear arms derived from a core. In the market, three, four, six, and eight armed PEGs are available in the different molecular weight. The hydroxyl end groups can be reacted, and converted into carboxyl, amine, thiol, azide, vinyl sulfone, azide, acetylene, or acrylate groups for crosslinking or biofunctionalization of the PEG chains. [4]

In order to form PEG hydrogels, linear or star shaped PEGs chains have to be crosslinked. There are different chemistries that can be used to form crosslinked PEG hydrogels; such as free-radical polymerization of vinyl functionalized PEGs,[5, 6] Michael type addition of thiol and vinyl end-functionalized PEGs,[7, 8] click chemistry with acetylene groups with azide functionalized PEGs,[9] native chemical ligation of thiolester end group functionalized PEG with PEG-thiol[10] and enzymatic reaction between peptide functionalized PEGs[11]. When PEG is used for cell encapsulation, a biocompatible crosslinking mechanism able to maintain the viability of embedded cells is required. Not all crosslinking mechanism satisfies this condition.

In the last years, catecholamine-terminated PEGs have been used to form PEG hydrogels. Catechol containing molecules are widely present in biology.[12-14] A few examples are the

amino acid 3,4-dihydroxyphenylalanine (DOPA) as relevant component of proteinaceous glue of mussels, the neurotransmitter norepinephrine (NE), the amino acid 2-chloro-4,5-dihydroxyphenylalanine (ClDOPA) existing in proteinaceous glue of sandcastle worm Phragmatopama californica or the competitive enzyme inhibitor 6-nitro dopamine (NDop) [15, 16].

Catecholamines present an interesting reactivity under physiological conditions. The catechol group can oxidize to quinone, it can undergo self-reaction and self-polymerization, it can form metal-complexes with metal ions e.g. $Fe^{3+}$, or it can react with nucleophiles present in proteins. [17] The reaction pathway depends on the type of catecholamine and the specific reaction conditions (concentration, pH, buffer, presence of oxidants etc.).

The most commonly used catecholamine is dopamine. At basic conditions, dopamine undergoes oxidative self-polymerization to form polydopamine, PDA, an insoluble aggregate that can be deposited on any type of substrate in the form of a reactive thin film. [1, 18] Despite the extensive effort to explain the reaction mechanism behind the self-oxidation of dopamine and to identify the chemical structure of reaction intermediates and products, the detailed structure of PDA is still not completely understood and proved. The insolubility of PDA and the multiple reaction possibilities complicate these investigations. Proposed polymerization mechanisms involve covalent reactions and or noncovalent interactions. PDA polymerization was initially related to the formation mechanism of melanin in living organisms. [19] Dopamine oxidizes to form dopaminequinone followed by intramolecular cyclization to leukodopaminechrome. The reaction path then involves oxidation to dopaminechrome and rearrangement to form 5,6-dihydroxyindole (DHI) which oxidizes to 5,6-indolequinone. Formation of PDA/melanin was proposed to occur by crosslinks of DHI and 5,6-indolequinone. A different proposed mechanism consists of aggregation of monomers, mainly DHI and its dione derivatives through hydrogen bonding, $\pi$-stacking, and charge transfer. [20] Other authors have proposed that noncovalent interactions to form DHI aggregates are not related with PDA formation. [21] (Figure 2.1)

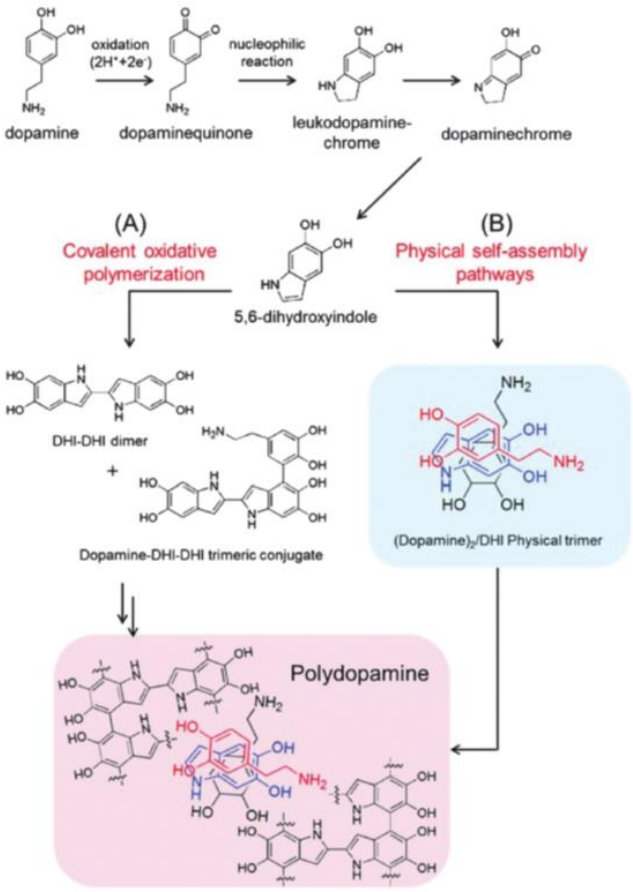


**Figure 2.1** Self polymerization mechanism proposed for dopamine. Reprinted with permission from ref. 104. Copyright (1982) American Chemical Society.

Polymerization of the aminoacid 3,4-dihydroxyphenylalanine (DOPA) involves formation of 2-carboxylic acid-5,6-dihydroxyindole as intermediate product and addition to 5,6-dihydroxyindole in variable proportions depending on the particular reaction conditions. [22] Substitution at the 6 position of the catechol ring by Cl or $NO_2$ groups leads to a decrease in the pKa of the phenolic hydroxyls and in the oxidation potential of the catechol. As a result, Cl- and $NO_2$- substituted dopamines are less prone to oxidation, and polymerization. [23]

Free amine group in catecholamine derivatives leads internal cyclization. When catechol is coupled to another molecule from amino moiety, it turns into secondary amine from primary amine group. It decreases nucleophilicity and the probability of internal cyclization step in the self-oxidation. Figure 2.2 summarizes the self-oxidation steps of catecholamine derivatives when they are attached to another molecule from its amine group.

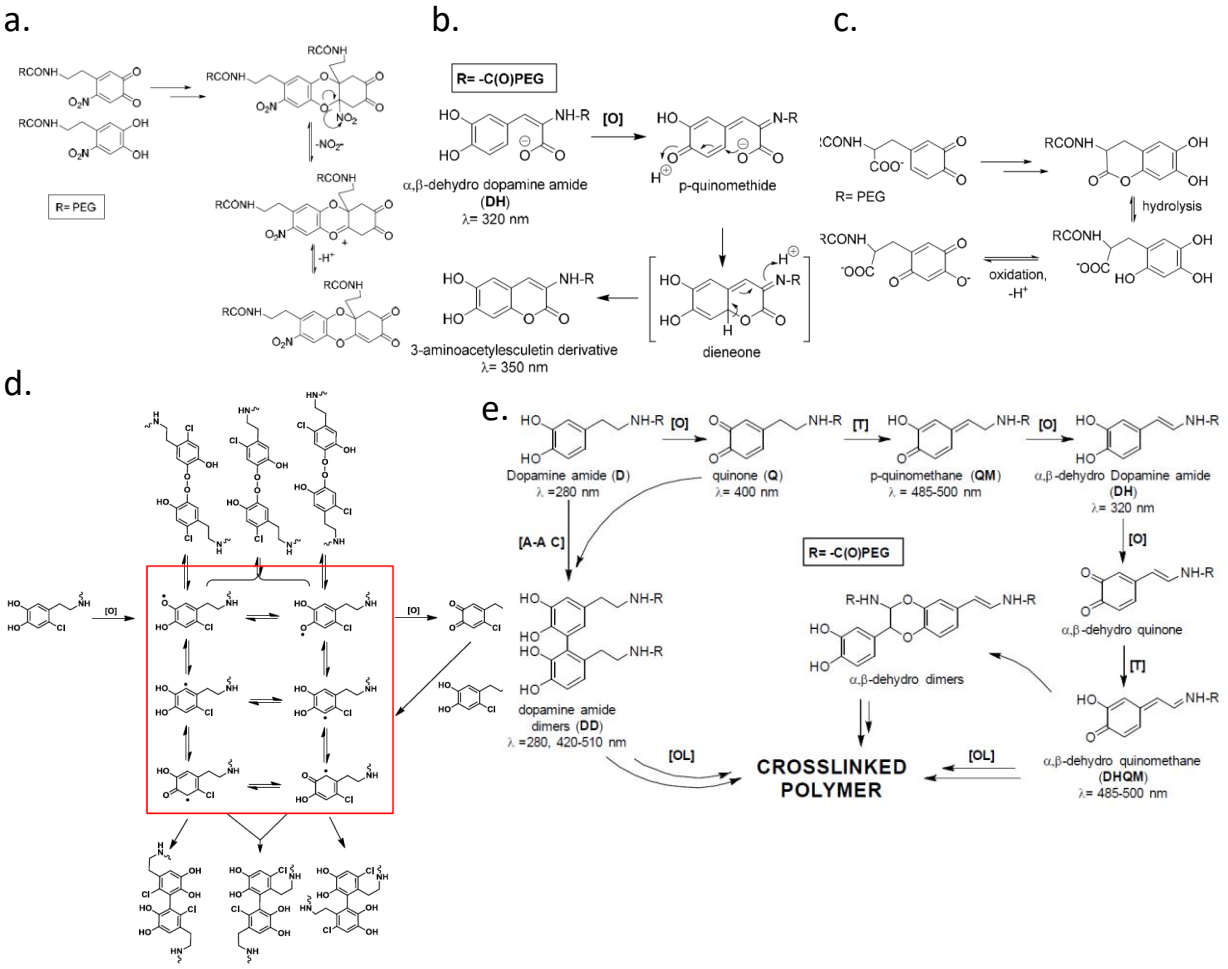


**Figure 2.2** Proposed crosslinking mechanisms for PEG-catecholamine derivatives

In light of the different reactivity of catecholamines depending on their molecular structure, different crosslinking products and kinetics are expected from each catecholamine modified PEG. In this chapter, the polymerization kinetics and the final mechanical properties of star-PEG hydrogels functionalized with dopamine, 2-chloro-4,5-dihydroxyphenylalanine, 6-nitro dopamine, 3,4-dihydroxyphenylalanine, and norepinephrine are studied and compared under different polymerization conditions.(Figure 2.3) This study should identify the most appropriate catechol-PEG derivative for applications requiring long vs. short curing times, or high vs. low mechanical strength of the final hydrogel. Moreover, it should demonstrate if mixing of different

catecholamine-PEG derivatives allows adjusting the crosslinking time and the mechanical stability of the hydrogel.

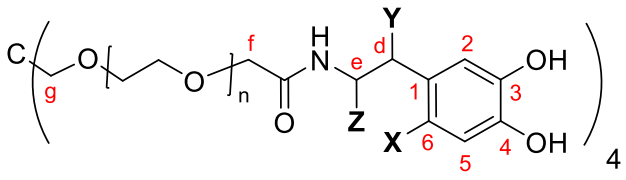


**PEG-Dop**: X=H, Y=H, Z=H
**PEG-ClDop**: **X=Cl**, Y=H, Z=H
**PEG-NDop**: **X=$NO_2$**, Y=H, Z=H
**PEG-DOPA**: X=H, Y=H, **Z=COOH**
**PEG-NE**: X=H, **Y=OH**, Z=H

**Figure 2.3** Chemical structures and nomenclature of catecholamine PEG derivatives

## 2.3 Results and Discussions

### 2.3.1 Selection of Oxidant and Polymer Concentration

First of all, PEG-catecholamine derivatives were kindly synthesized by Dr. Julieta Paez, Dr. Xuan Anh Ton, and Dr. Zahid Shafiq. The crosslinking kinetics of the PEG-catechol homopolymers was tested by measuring their mechanical properties during curing by piezorheology. A solution of PEG-catechol (100 mg $mL^{-1}$) was mixed with different concentrations of $NaIO_4$ oxidant (5-9 mM) and placed between the two plates of the piezorheometer. The shear moduli (storage modulus, G', and loss modulus, G'') were measured until the crosslinking was completed, i.e. a stable plateau was reached in the rheological curves. Figure 2.4a shows the data obtained for PEG-Dop at increasing oxidant concentrations. During the first 40 minutes G' and G'' values were very low (<1Pa) and almost not detectable for the equipment. After 40 min for 9 mM oxidant concentration or 2 hours for 5 mM oxidant concentration, a steep increase in the shear moduli was observed, as expected in a crosslinking process. The formation of stable crosslinking points upon reaction of the catechol units led to stiffening of the mixture. The rheological curve presented a sigmoidal profile, characteristic of network formation processes in gels and elastomers. A plateau value of the shear moduli was achieved after 4 hours in the mixture with 5 mM oxidant and after 10 hours when 9mM oxidant concentration was used. These data demonstrate that crosslinking kinetics (i.e. the time to achieve the plateau value of the shear moduli) is faster at higher oxidant concentrations within the studied range. The final shear modulus achieved at higher oxidant concentrations is also higher, i.e. a higher degree of crosslinking is achieved. A previous study has shown that an increase in oxidant concentration leads to a faster kinetics when the oxidant:catechol exceeds 1, but to a lower kinetics if the ratio is <1. [24] In the further experiments, concentration of oxidant was chosen as 9 mM in order to have a comfortable curing time for experimental measurements.

Figure 2.4b shows the rheology curves during crosslinking of PEG-Dop at increasing polymer concentration (between 25 and 100 mg $L^{-1}$) and constant oxidant concentration (9 mM). The samples with 25 and 50 mg/mL did not achieve crosslinking degrees detectable for the rheometer. At polymer concentration of 75 and 100 mg $L^{-1}$, gel formation was faster and the final gel was mechanically stronger. 75 mg $L^{-1}$ of PEG-Dop reached plateau at storage modulus of 800 Pa and $10^4$ Pa were achieved 60 h after the mixing polymer and crosslinker.

These results evidence that the changes in the oxidant, or polymer concentration have an influence in the polymerization kinetics and in the final mechanical stability of the hydrogel, simultaneously. This is a negative point of the system, since applications that might require long-term curing would end with a very weak gel. In the following, alternatives to change only one of the two parameters will be searched.

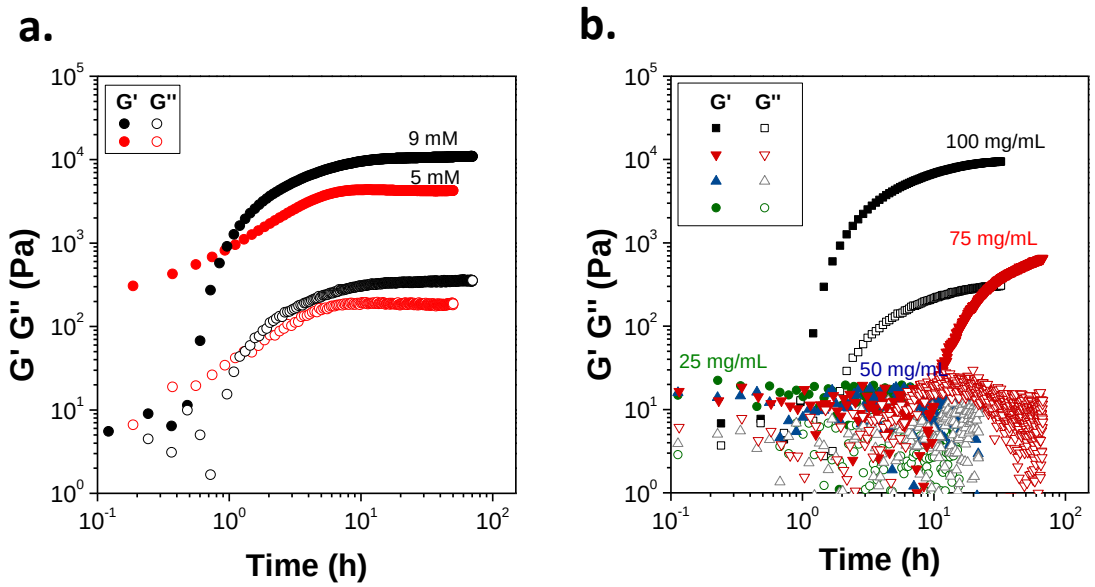


**Figure 2.4 a.** Shear moduli (G', G") of 100 mg $mL^{-1}$ *PEG-Dop* in water with various oxidant (*$NaIO_4$*) concentrations as a function of crosslinking time. The noise level of the rheological measurements is ~10 Pa. **b.** Shear moduli (G', G") of *PEG-Dop* in water at 9 mM oxidant, *$NaIO_4$,* concentration with decreasing polymer concentrations as a function of crosslinking time. The noise level of the rheological measurements is ~10 Pa.

### 2.3.2 Comparison of rheology curves of the different PEG-catecholamine derivatives

Different PEG-catechol derivatives were used as starting polymers for similar studies. The mixtures of 100 mg $mL^{-1}$ polymer concentration and 9 mM $NaIO_4$ concentration were used for

the measurements. These conditions allowed a comfortable time window for experimentation and a comparison of the crosslinking kinetics between all systems.

The crosslinking kinetics and the mechanical properties of the crosslinked gel significantly varied with the type of catecholamine end-group functionalization.(Figure 2.5) PEG-ClDop and PEG-Dop achieved the highest G' after completion of crosslinking ($10^4$ Pa). However, curing was complete within a few minutes in the case of PEG-ClDop, but it took almost 10 hours for PEG-Dop. PEG-NDop reached a lower G' after crosslinking (~ $3\times10^3$ Pa) than PEG-Dop and PEG-ClDop. The rheological curve showed an interesting profile. G' reached a maximum value of $5\times10^3$ Pa after 3-4 hours of crosslinking, but it decreased for longer crosslinking times until it reached the plateau value after 10 hours. This behavior was reproducible. Such curve suggests a gelation process where two crosslinking mechanisms with different kinetics compete. A fast crosslinking reaction of PEG-NDop (time scale 1-2 hours) is reflected in the steep initial slope in the rheological curve. A second, slower crosslinking mechanism contributed to the stiffening of the hydrogel in a time scale of 5-10 hours under these experimental conditions. The reason for the partial drop in the shear modulus observed after 4 hours before the plateau value of G' is reached remains unclear at this point. It is important to note that the fast crosslinking mechanism of PEG-NDop was already visible during sample preparation. While all other solutions of PEG-catechol derivatives maintain their fluid properties right after mixing with the oxidant for at least a few seconds (PEG-ClDop) to hours (all the others), the PEG-NDop does no longer flow right upon mixing with the oxidant. This observation is in agreement with recently published work on PEG-NDop gels by Lee et al[25] who observed faster gelation on PEG-NDop than on PEG-Dop (tested by inverting the vial), but lower shear modulus in the final PEG-NDop gel. These authors suggested that NDop mainly forms dimers through oxidative crosslinking while unsubstituted Dop can form higher crosslinked products. (Figure 2.5) The data obtained here complement this picture by providing information about the kinetics of the crosslinking mechanism. However, the nature of the cluster forming intermediates and that of the slower crosslinks remains to be elucidated. A possible explanation for the anomalous behavior of PEG-NDop can be found in the mechanism of polymerization of nitrodopamine and nitrocatechols reported in previous studies. [26] According to those reports, the electron-withdrawing nitro group decreases the oxidation potential of the catechol ring, which accounts for a greater stability to autoxidation. However, once semiquinone or quinone intermediates are generated under forcing conditions due to the addition of oxidant, oxidative coupling may occur at rather fast rates leading to dimeric species. These latter may then evolve via slower processes

involving nucleophilic attack of the phenolic -OH groups onto the quaternary nitro-substituted 6-position of the aromatic ring, possibly in a quinonoid form, with $sp^2$ to $sp^3$ conversion. (Figure 2.5) The overall outcome of this process is the weakening of the C-N bond causing the possible release of nitrite ions with rearrangement of the dimer structure and an alteration of the overall properties of the crosslinked product. [26]

The rheological curves of 100 mg $mL^{-1}$ of PEG-NE and PEG-DOPA showed a pronounced sigmoidal shape, typical of processes with slow crosslinking kinetics. Full crosslink was achieved after 20 and 80 hours respectively. A G´ of ~ $3\times10^3$ Pa was observed after curing, significantly lower than the final G´ of PEG-Dop under comparable experimental conditions.

From these data it could be concluded that the introduction of substituents 1 (-Cl, $-NO_2$) in the catechol ring, or in the alkyl chain of the catecholamines (-COOH, -OH) strongly affects the crosslinking kinetics and crosslinking degree of the PEG-catecholamine derivatives. The crosslinking kinetics followed the sequence: PEG-ClDop >>> -NDop, -Dop > -NE > -DOPA. The crosslinking degree (i.e. the final G´ and the cohesiveness of the material) followed the sequence: PEG-ClDop ≈ -Dop > -NDop, -DOPA, -NE.

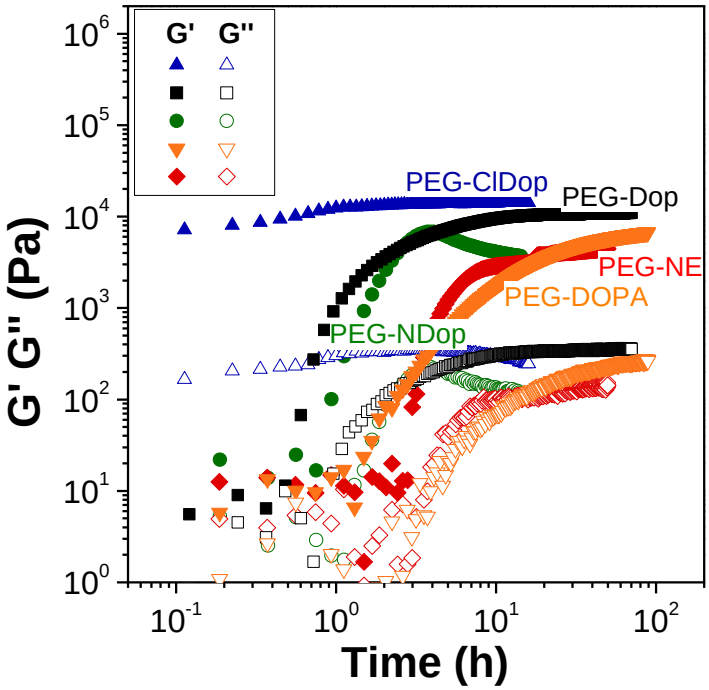


**Figure 2.5** Comparison of curing process of the different PEG-catecholamine derivatives at 100 mg $mL^{-1}$ polymer concentration and 9 mM oxidant concentration, (4:1) catechol:$NaIO_4$ molar ratio. The noise level of the rheological measurements is ~10 Pa.

In summary, the kinetics and extent of crosslinking of PEG-catecholamines strongly varies with the chemical nature of the catechol group, as reflected in the rheological data.[27] This is a consequence of the differences in their oxidation, acidity and reactivity. Given the complexity of catechol chemistry and the combined action of these parameters, the observed differences cannot be explained in terms of single molecular mechanisms but are likely to reflect concurrent competing pathways. However, some general conclusions can be drawn. The crosslinking kinetics measured for the different PEG-catechol derivatives via rheology indicates that curing kinetics of catecholamine functionalized materials can be followed in the described system. From the chemical viewpoint, different effects were observed depending on the site and type of functionalization. Ring functionalization allowed for effective tuning of the crosslinking process both with regard to kinetics and product features. In particular, the chloro substituent in PEG-ClDop induced a faster crosslinking relative to PEG-Dop, while the nitro group in PEG-NDop exerted an opposite effect. In the latter, the formation of dimers instead of high order crosslinks [26] and their subsequent evolution by slow processes may account for the observed rheology. Conversely, chain functionalization resulted invariably in a decrease in the reaction kinetics and

degree of crosslinking, as evidenced by the slow reactions observed with PEG-NE and PEG-DOPA. In these latter cases, side reactions such as chain breakdown in PEG-NE and cyclization for PEG-DOPA may be exploited to achieve more complete control over crosslinking degree and kinetics. Finally, it is worth noting that all these catechol derivatives have been extensively proved valuable for biocompatible and non-cytotoxic biomaterials preparation and an adhesive for tissues. [12, 28-35] Quinones, obtained after catechol oxidation, can undergo Michael reaction and/or Shiff base reaction with amine and thiol groups of organic materials under basic conditions. It gives high adhesive strength to catechol derivatives. Moreover, under ambient conditions, there might be noncovalent interactions such as metal coordination or chelating, π-π stacking, and quinhydrone charge transfer complexes with surface molecules. [36-39] (Figure 2.6)

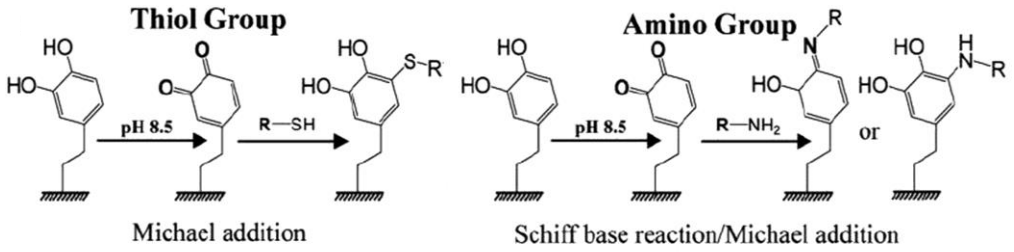


**Figure 2.6** Possible reactions between dopamine and amine and thiol groups in organic materials. [12]

### 2.3.3 Tuning Elastic Strength and Curing Time by mixing of different catechol derivatives

The possibility of tuning the kinetics of PEG gelation using mixtures of catecholamine-PEGs with different curing kinetics was tested. The fast crosslinking catechol derivative, PEG-ClDop was selected and mixed with the slower catechol crosslinking derivative PEG-Dop in different ratios (ClDop:Dop = 100:0, 75:25, 50:50, 25:75, 0:100) keeping a constant solid content of the gel (100 mg $mL^{-1}$). As controls, the curing kinetics of the monocomponent gels at different solid contents, i.e. ClDop:Dop = 75:0, 50:0, 25:0 and 0:75, 0:50, 0:25 was measured. Figure 2.7a presents the curing curves of the mixtures as measured by piezorheology. The fast polymerization kinetics of PEG-ClDop was successfully slowed down in a 25:75 mixture with PEG-Dop, while the final mechanical properties of the gel ($10^4$ Pa) were retained. This demonstrates that the rheological behavior of the 25:75 mixture reflects the synergy effect of the two comonomers during crosslinking that can be exploited for the control of polymerization kinetics without compromising the mechanical properties of the final gel. The following mechanism behind the observed rheological behavior is proposed: the fast crosslinking ClDop

groups form gel clusters within the sample at low crosslinking times and cluster aggregation to form the stable gel is done by the Dop groups at a slower rate. Interestingly, polymer mixtures with higher concentrations of ClDop (50:50, 25:75) did not show a significantly slower kinetic than the homopolymer PEG- ClDop gel, only a lower G' after curing. At these higher ClDop concentrations the clusters quickly formed by the ClDop reactive sites seem to have hindered the motion of the Dop groups in such a way that they could not find reaction partners on different chains. Whether this led to dangling ends or to intrachain reactions is unclear. Nevertheless, these bonds did not contribute to the shear modulus, they were not force-carrying bonds. From the rheological data we however conclude that too dense clusters formed by the ClDop groups hinder the efficiency of the Dop groups in forming force-carrying bonds. As control, Figure 2.7b shows the polymerization kinetics for 75:0 mixture (i.e. without PEG-Dop), which occurs as rapidly as in 100:0 but achieves lower mechanical strength, reflecting only a dilution effect.

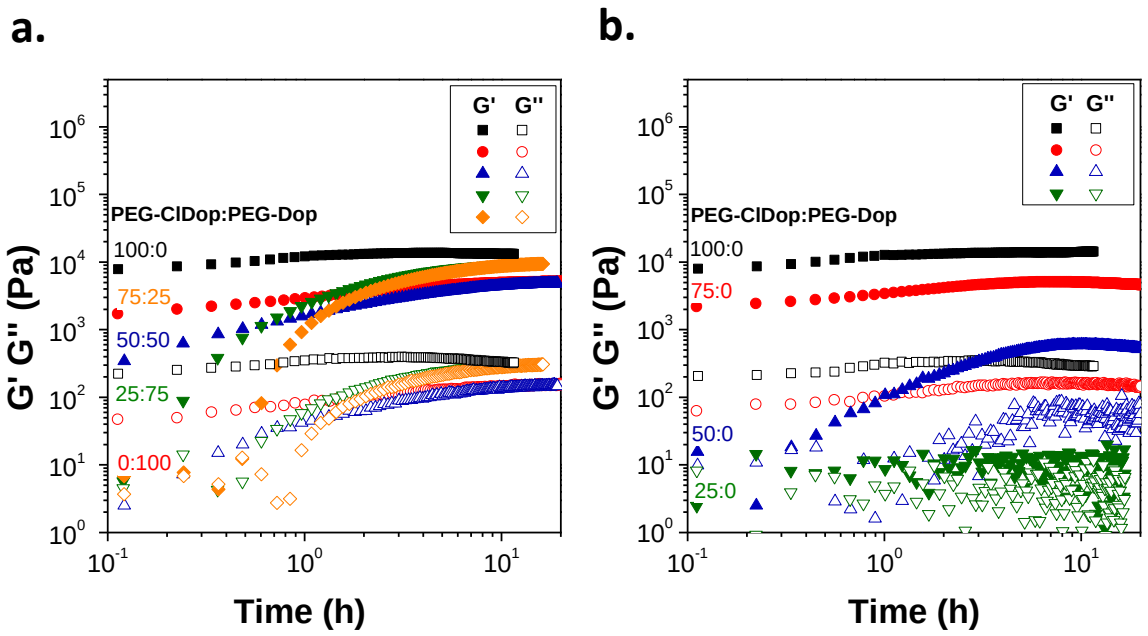


**Figure 2.7** Shear moduli (G´, G´´) of PEG-ClDop/PEG-Dop mixtures at **a.** different ClDop:Dop ratios and **b.** only PEG-ClDop as a function of crosslinking time (100 mg $mL^{-1}$ polymer concentration and 9 mM oxidant concentration, (4:1) catechol:$NaIO_4$ molar ratio). The noise level of the rheological measurements is ~10 Pa.

## 2.4 Conclusion

Functionalization of catecholamines has been explored as a convenient strategy to gauge and tune crosslinking kinetics in catechol-PEG derivatives for new design rules. Comparing the polymerization kinetics and final mechanical properties of PEG gels obtained by polymerization of catecholamine end-functionalized star-PEGs with different substituents at specific ring and chain positions, it was possible to draw some general rules for controlling and tuning crosslinking processes and product properties. In particular, installation of PEG-Dop PEG-ClDop an electron-withdrawing but pi-electron donating chloro substituent on the catechol ring resulted in faster and more efficient crosslinking, while opposite effects were observed with the strongly electron-withdrawing nitro group. Chain substitution, on the other hand, interfered with the process by slowing down the kinetics and hindering crosslinking, due either to chain breakdown (beta-OH group) or intramolecular cyclization (alpha-carboxyl group). Interesting perspectives derive from use of mixtures of catecholamine-PEG precursors offering further opportunities for fine tuning.

## References


1. Lee, H., et al., *Mussel-inspired surface chemistry for multifunctional coatings.* Science, 2007. **318**(5849): p. 426-430.
2. Sun, I.C., et al., *Heparin-Coated Gold Nanoparticles for Liver-Specific CT Imaging.* Chemistry-a European Journal, 2009. **15**(48): p. 13341-13347.
3. Guvendiren, M., et al., *Adhesion of DOPA-Functionalized Model Membranes to Hard and Soft Surfaces.* Journal of Adhesion, 2009. **85**(9): p. 631-645.
4. Faure, E., et al., *Catechols as versatile platforms in polymer chemistry.* Progress in Polymer Science, 2013. **38**(1): p. 236-270.
5. Hong, S., et al., *Non-Covalent Self-Assembly and Covalent Polymerization Co-Contribute to Polydopamine Formation.* Advanced Functional Materials, 2012. **22**(22): p. 4711-4717.
6. Laachachi, A., et al., *Diffusion of Polyphosphates into (Poly(allylamine)-montmorillonite) Multilayer Films: Flame Retardant-Intumescent Films with Improved Oxygen Barrier.* Langmuir, 2011. **27**(22): p. 13879-13887.
7. Metters, A. and J. Hubbell, *Network formation and degradation behavior of hydrogels formed by Michael-type addition reactions.* Biomacromolecules, 2005. **6**(1): p. 290-301.
8. Sawicki, L.A. and A.M. Kloxin, *Design of thiol-ene photoclick hydrogels using facile techniques for cell culture applications.* Biomaterials Science, 2014. **2**(11): p. 1612-1626.
9. Polizzotti, B.D., B.D. Fairbanks, and K.S. Anseth, *Three-dimensional biochemical patterning of click-based composite hydrogels via thiolene photopolymerization.* Biomacromolecules, 2008. **9**(4): p. 1084-1087.
10. Hu, B.H., J. Su, and P.B. Messersmith, *Hydrogels Cross-Linked by Native Chemical Ligation.* Biomacromolecules, 2009. **10**(8): p. 2194-2200.

11. Ehrbar, M., et al., *Enzymatic formation of modular cell-instructive fibrin analogs for tissue engineering.* Biomaterials, 2007. **28**(26): p. 3856-3866.
12. Liu, Y., K. Ai, and L. Lu, *Polydopamine and Its Derivative Materials: Synthesis and Promising Applications in Energy, Environmental, and Biomedical Fields.* Chemical Reviews, 2014. **114**(9): p. 5057-5115.
13. Miserez, A., et al., *The transition from stiff to compliant materials in squid beaks.* Science, 2008. **319**(5871): p. 1816-1819.
14. Floriolli, R.Y., J. von Langen, and J.H. Waite, *Marine surfaces and the expression of specific byssal adhesive protein variants in Mytilus.* Marine Biotechnology, 2000. **2**(4): p. 352-363.
15. Palumbo, A., et al., *Nitrite- and Peroxide-Dependent Oxidation Pathways of Dopamine: 6-Nitrodopamine and 6-Hydroxydopamine Formation as Potential Contributory Mechanisms of Oxidative Stress- and Nitric Oxide-Induced Neurotoxicity in Neuronal Degeneration.* Chemical Research in Toxicology, 1999. **12**(12): p. 1213-1222.
16. Palumbo, A., G. Astarita, and M. d'Ischia, *Inhibition of neuronal nitric oxide synthase by 6-nitrocatecholamines, putative reaction products of nitric oxide with catecholamines under oxidative stress conditions.* Biochemical Journal, 2001. **356**: p. 105-110.
17. Yang, J., M.A.C. Stuart, and M. Kamperman, *Jack of all trades: versatile catechol crosslinking mechanisms.* Chemical Society Reviews, 2014. **43**(24): p. 8271-8298.
18. Kang, S.M., et al., *Norepinephrine: Material-Independent, Multifunctional Surface Modification Reagent.* Journal of the American Chemical Society, 2009. **131**(37): p. 13224-13225.
19. Felix, C.C. and R.C. Sealy, *o-Benzosemiquinone and its metal chelates. Electron spin resonance investigation of radicals from the photolysis of catechol in the presence of complexing metal ions.* Journal of the American Chemical Society, 1982. **104**(6): p. 1555-1560.
20. Dreyer, D.R., et al., *Elucidating the Structure of Poly(dopamine).* Langmuir, 2012. **28**(15): p. 6428-6435.
21. Lin, S.C., et al., *Tuning heterogeneous poly(dopamine) structures and mechanics: in silico covalent cross-linking and thin film nanoindentation.* Soft Matter, 2014. **10**(3): p. 457-464.
22. Edge, R., et al., *Dopaquinone redox exchange with dihydroxyindole and dihydroxyindole carboxylic acid.* Pigment Cell Research, 2006. **19**(5): p. 443-450.
23. Cui, J., et al., *Dopamine-Based Coatings and Hydrogels: Toward Substitution-Related Structure–Property Relationships.* Macromolecular Chemistry and Physics, 2014. **215**(24): p. 2403-2413.
24. Cencer, M., et al., *Effect of pH on the Rate of Curing and Bioadhesive Properties of Dopamine Functionalized Poly(ethylene glycol) Hydrogels.* Biomacromolecules, 2014. **15**(8): p. 2861-2869.
25. Cencer, M., et al., *Effect of nitro-functionalization on the cross-linking and bioadhesion of biomimetic adhesive moiety.* Biomacromolecules, 2015. **16**(1): p. 404-10.
26. Palumbo, A., et al., *Oxidative conversion of 6-nitrocatecholamines to nitrosating products: A possible contributory factor in nitric oxide and catecholamine neurotoxicity associated with oxidative stress and acidosis.* Chemical Research in Toxicology, 2001. **14**(9): p. 1296-1305.
27. Paez, J.I., et al., *Gauging and Tuning Cross-Linking Kinetics of Catechol-PEG Adhesives via Catecholamine Functionalization.* Biomacromolecules, 2015. **16**(12): p. 3811-3818.
28. Shafiq, Z., et al., *Bioinspired Underwater Bonding and Debonding on Demand.* Angewandte Chemie-International Edition, 2012. **51**(18): p. 4332-4335.

29. Garcia-Fernandez, L., et al., *Antibacterial Strategies from the Sea: Polymer-Bound Cl-Catechols for Prevention of Biofilm Formation.* Advanced Materials, 2013. **25**(4): p. 529-533.
30. Madhurakkat Perikamana, S.K., et al., *Materials from Mussel-Inspired Chemistry for Cell and Tissue Engineering Applications.* Biomacromolecules, 2015. **16**(9): p. 2541-55.
31. Ko, E., et al., *Polydopamine-assisted osteoinductive peptide immobilization of polymer scaffolds for enhanced bone regeneration by human adipose-derived stem cells.* Biomacromolecules, 2013. **14**(9): p. 3202-13.
32. Wei, Q., et al., *Multivalent anchoring and cross-linking of mussel-inspired antifouling surface coatings.* Biomacromolecules, 2014. **15**(8): p. 3061-71.
33. Zhu, Y., et al., *A robust graft-to strategy to form multifunctional and stealth zwitterionic polymer-coated mesoporous silica nanoparticles.* Biomacromolecules, 2014. **15**(5): p. 1845-51.
34. Duarte, A.P., et al., *Surgical adhesives: Systematic review of the main types and development forecast.* Progress in Polymer Science, 2012. **37**(8): p. 1031-1050.
35. Kim, E., et al., *Sticky "delivering-from" strategies using viral vectors for efficient human neural stem cell infection by bioinspired catecholamines.* ACS Appl Mater Interfaces, 2014. **6**(11): p. 8288-94.
36. Ye, Q., F. Zhou, and W.M. Liu, *Bioinspired catecholic chemistry for surface modification.* Chemical Society Reviews, 2011. **40**(7): p. 4244-4258.
37. Pop-Georgievski, O., et al., *Nonfouling Poly(ethylene oxide) Layers End-Tethered to Polydopamine.* Langmuir, 2012. **28**(40): p. 14273-14283.
38. Li, S.C., et al., *Hydrogen Bonding Controls the Dynamics of Catechol Adsorbed on a TiO2(110) Surface.* Science, 2010. **328**(5980): p. 882-884.
39. Anderson, T.H., et al., *The Contribution of DOPA to Substrate-Peptide Adhesion and Internal Cohesion of Mussel-Inspired Synthetic Peptide Films.* Advanced Functional Materials, 2010. **20**(23): p. 4196-4205.

# 3

# Chemical Strategies to Tune Mechanical Properties of Hydrogels by Light

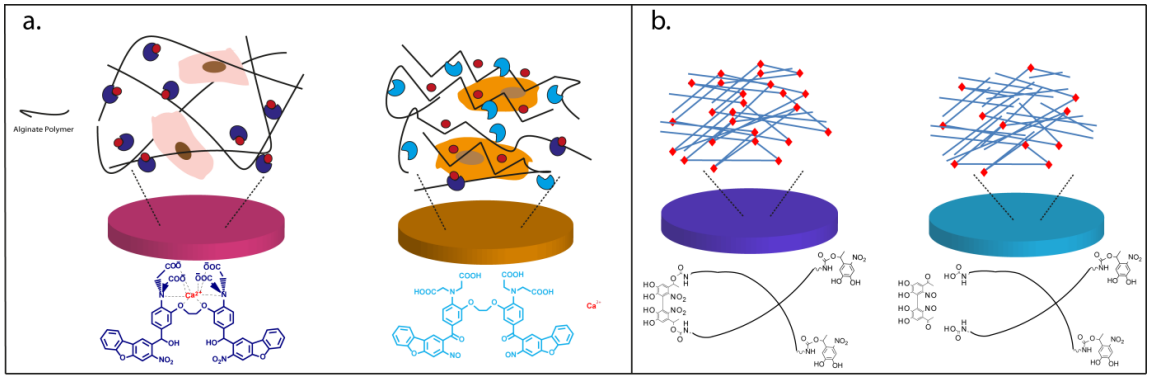


Light triggered **a.** stiffening and **b.** softening of hydrogel

## 3.1 Abstract

The mechanical properties of living tissues are dynamic in a sense that changing over time i.e. aging. It can be changed during diseases such as tumor formation. Therefore, the systems with dynamic mechanical properties are needed to study the properties of biological tissues or processes. Two light controlled systems were studied in this chapter. First one is based on a cage $Ca^{2+}$ molecule, Nitr-T, which liberates $Ca^{2+}$ ions upon light exposure. It was mixed with a biopolymer crosslinking with $Ca^{2+}$ ions, alginate. However, only very limited change in modulus of alginate-Nitr-T hydrogel was observed upon light exposure. The second system is based on the PEG functionalized with photosensitive nitro-catechol derivative or nitrobenzyl derivative.

## 3.2 Introduction

Cells are able to sense mechanical properties of cellular microenvironment and alter their activity according to it. [1] Therefore, there is an urge to tune mechanical properties of ECM mimetic materials *in situ* to understand and control their behavior. Such stiffness changes should occur within physiologically relevant ranges, i.e. between 0.1 and 50 kPa.

Responsive hydrogels for biomedical applications typically undergo stiffness changes in response to temperature or pH variations.[2] However, these changes are typically associated to the collapse of the polymer chains, which occurs drastically and cannot be spatially localized. These limitations can be overcome with light responsive hydrogels. To design a system for this purpose, it is important to select photosensitive molecules that can be photoactivated at wavelengths and doses compatible with living cells.

To control the stiffness of hydrogels, two new light responsive materials have been recently developed; 1) A photocrosslinkable alginate containing caged $Ca^{2+}$ molecules to increase stiffness,[3] 2) A photodegradable biopolymer functionalized with nitro-catechol derivatives to decrease stiffness.[4] These systems will be described in the following paragraphs.

### 3.2.1 Light Responsive Alginate Hydrogels

Two strategies have described to tune the mechanical properties of alginates with light. One possibility is the photorelease of $Ca^{2+}$ from a chelator molecule embedded in liposomes which are contained in the gel.[5] This system has been used for preparing stiffness gradients and patterns in an alginate hydrogel. Changes of the storage modulus between ~1 and ~3 kPa were obtained and applied to regulate the morphology of fibroblasts. Moreover, the system was

compatible with in vivo environments. Near infrared light was used to modulate the stiffness externally. (see section 1.5)

Previous work in the group A. del Campo has demonstrated a light-based strategy to change the stiffness of alginate hydrogels by using a caged calcium molecule, Nitr-T. (Figure 3.1 and 3.2) [3] (see section 1.5)

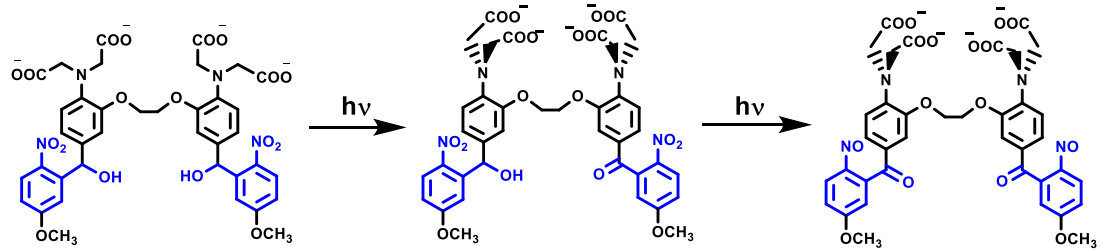


**Figure 3.1** Photoproducts of caged $Ca^{2+}$ molecule, Nitr-T

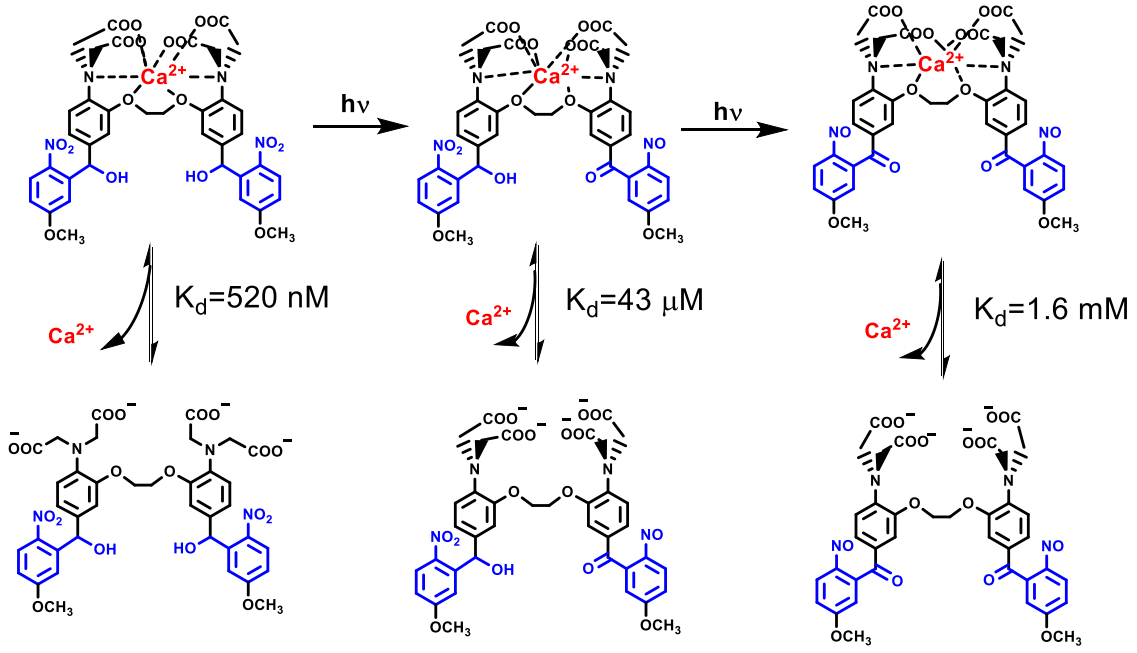


**Figure 3.2** Complex formation of $Ca^{2+}$ with Nitr-T, and its photolytic products.

### 3.2.2 Photodegradable Hydrogels Based on Nitro-Catechol Derivatives

In the last 5 years, different examples of photodegradable hydrogels based on the use of photocleavable o-nitrobenzyl groups have been reported. These chromophores are introduced in the polymer chains and mediate light-induced depolymerization reactions. In this way, photodegradable hydrogels with tunable mechanical properties by light have been developed

based on different polymeric backbones: poly(ethylene glycol),[6-13] acrylates,[14-17] dextran,[18] hyaluronan,[19] or agaros [20, 21]. These systems have been applied to release cells,[13] bioactive molecules,[21] and potential drugs[11], to photodegrade hydrogels to spatiotemporally control the mechanical properties of hydrogels[10, 22] or to prepare complex structures with mechanical and topographical cues,[23] or 3D channels to control migration of cells with 2 photon photolithography.[7, 8]

In most reported examples, photocleavable groups derived from o-nitrobenzyl group have been used. The photolysis mechanism, particularized for a protected amine, is shown in Figure 4.3. The photochemical reaction starts with radical formation at nitro moiety upon light excitation. After rearrangement, cyclization occurs between hydroxyl moiety of nitro group and benzylic carbon. The molecule rearranges again with cleavage of bond between nitrogen and oxygen in the ring and oxygen and benzylic carbon to form a ketone or aldehyde and carbamic acid. With rearrangement of carbamic acid, carbon dioxide and an amine are formed. (Figure 3.3)

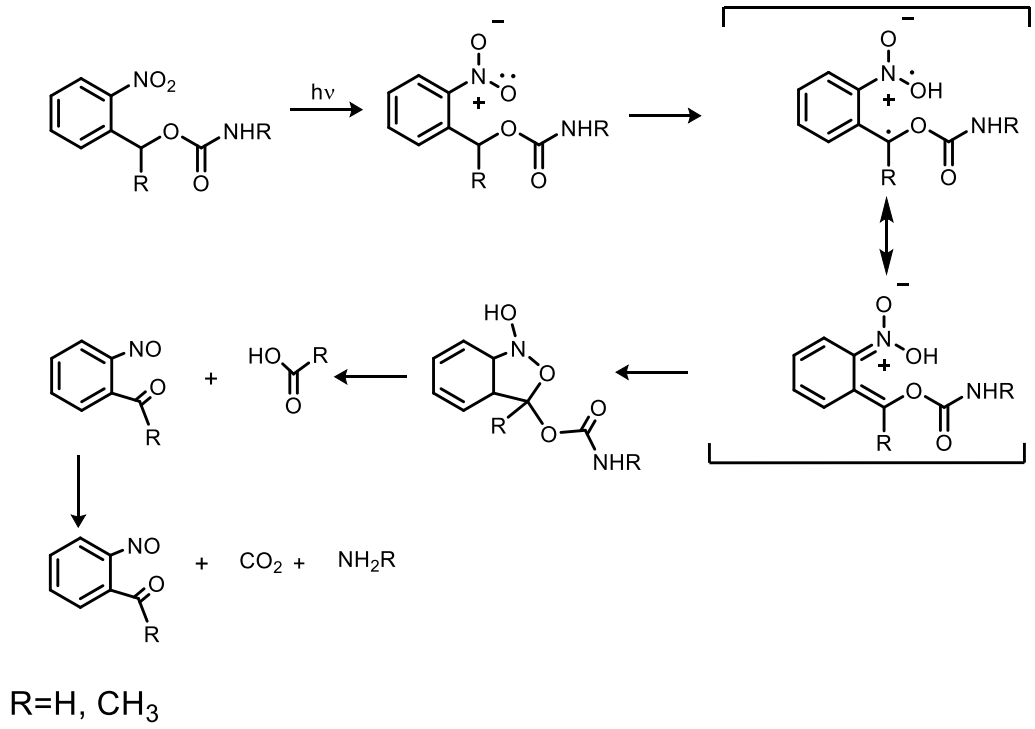


**Figure 3.3** Photoisomerization mechanism of *o*-nitrobenzyl alcohol derivatives. [5]

Photoactive variants of the o-nitroalkyl unit are also present in nature. For example 6-nitrodopamine (NDop, Figure 3.4), which takes part in nitric oxide metabolism and neural system.[25] In this case, an o-nitrophenylethyl group is the photocleavable moiety.[24, 26-28]

The photochemical mechanism is shown in Figure 3.5.[27] The photolysis of o-nitrophenylethyl derivatives starts with formation of the aci-nitro intermediate by intramolecular H-transfer from the exocyclic α-position (with respect to the aryl moiety) to the nitro group. Then the second step is protolytic dissociation of the aci-nitro derivative and release of the caged functional group.[28] In the case of o-nitrophenylethyl derivative, α-substituent prevents the side reactions between the photoproduct and amine to form an imine.

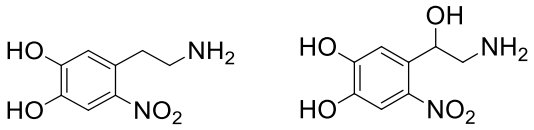


**Figure 3.3** Chemical structures of NDop and NNEN

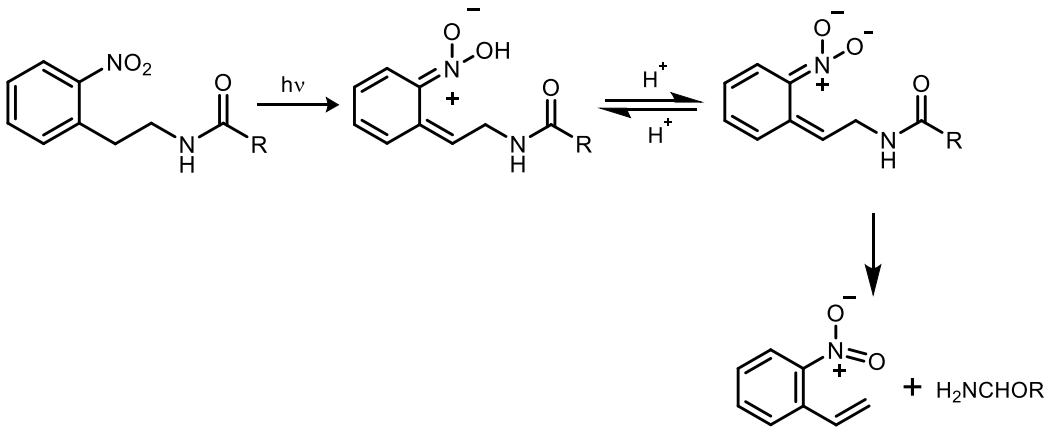


**Figure 3.4** Photoisomerization mechanism of *o*-nitrophenylethyl derivatives.

NDop has recently been used as end-functional group in PEG chains to form photodegradable hydrogels.[6] This molecule has the advantage of being able to self-polymerize and react with nucleophiles under physiological conditions. When attached to a biopolymer, catechol groups can be used for crosslinking under mild conditions, to generate physically crosslinked hydrogels with interest for biomedical applications.[7-9] In particular, NDop end-functionalized 4-armed star PEG has been reported to form hydrogels under physiological conditions, and can be depolymerized by light exposure to UV irradiation. (Figure 3.6)[4] As a result, the stiffness of the hydrogel network can be decreased gradually in response to light at increasing doses. However, the exposure dose required for the photodegradation of NDop crosslinked PEG was too high and not compatible with the presence of living cells in the hydrogel.[6] An important reason for the low photosensitivity of this derivative is the type of bond between NDop and PEG: the amide

bond is not a good leaving group and the photolysis reaction shows a poor quantum yield. In this chapter an alternative chromophore with higher photosensitivity based on the nitronorepinephrine (NNEN, Figure 3.4) molecule will be presented.

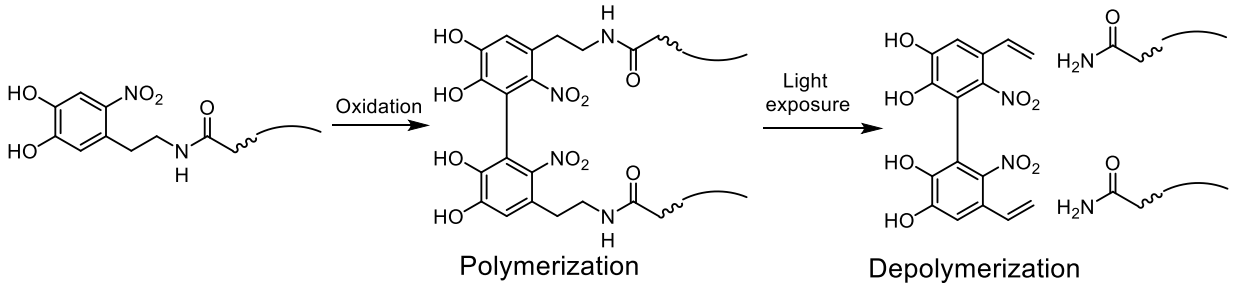


**Figure 3.5** Polymerization and depolymerization of NDop functionalized polymer.

## 3.3 Aim and Objectives

The aim of this chapter was to develop two different strategies to tune mechanical properties of ECM mimetic hydrogels at doses compatible with living cells. Two strategies are presented: 1) photostiffening of alginates using a photoactivatable $Ca^{2+}$ chelator and 2) photosoftening of PEG- hydrogels using NNEN derivative as photodegradable crosslinker.

In previous reported work with Nitr-T, a moderate increase in modulus of alginate hydrogel, from 0.01 to 1.5 Pa, was achieved after full photoconversion of Nitr-T.[3] According to calculations of free $Ca^{2+}$ concentration based on dissociation constants of Nitr-T and its photoproducts, a maximum concentration of 4 mM of $Ca^{2+}$ ions could be released from a 40 mM concentration of Nitr-T-$Ca^{2+}$ complex upon 100% photoconversion. Taking into account that the maximum solubility of Nitr-T-$Ca^{2+}$ at physiological conditions is 50mM, it seems not possible to obtain significantly higher stiffness changes only by increasing nitro-T-$Ca^{2+}$ concentration. Another possibility could be using alginates with higher content of G units, since in the reported studies alginate types with low G content (<70%) were used. However, the commercially available alginates with the highest G content have also high molecular weight. These alginates form very viscous solutions which are difficult to mix with $Ca^{2+}$ crosslinker to achieve homogeneous gels. It has been reported that mixture of high and low molecular weight of alginates can achieve higher modulus than individual alginate networks with higher cell viability due to low viscosity of pre-gel solution.[10-12] Therefore, a mixture of high and low molecular weight alginate was proposed to reach highest modulus with limited free $Ca^{2+}$ released from Nitr-T-$Ca^{2+}$ complex upon light

irradiation. The formulation of this system and the rheological characterization of the photomediated mechanical changes are described in this chapter.

In the second section, the use of NNEN as alternative photocleavable molecule to NDop is described. Coupling of NNEN through a carbamate bond to the PEG polymer chain is expected to provide a better leaving group (amide) for the photolysis reaction, and to exploit the o-nitrobenzyl cleavage vs. the o-nitrophenylethyl mechanism of NDop. This design is expected to produce gels with higher photosensitivity that allows photodegradation in the presence of living cells without causing photodamage. The synthesis and the characterisation of the photochemical properties of the new hydrogels will be described in this chapter.

## 3.4 Results and discussion

### 3.4.1 Light Responsive Alginate Hydrogels

#### 3.4.1.1 Alginate solutions with high G content but reduced viscosity by ɣ irradiation

A commercially available alginate with highest possible G content was selected (Pronova UP MVG, FMC BioPolymers). This alginate has a G content of 60% and a molecular weight of 188000 g/mol. When dissolved in water, highly viscous solutions are obtained already at 1 wt. % alginate content. In order to reduce viscosity, and improve workability of the solution, the molecular weight of the alginate was reduced by exposure to ɣ irradiation.[12] This treatment causes breakage of glycosidic bonds and creates shorter chains. γ-treated alginate solutions were analyzed by GPC to quantify the change in the molecular weight ($M_w$) of the chains with the increasing γ dose. The average number molecular weight of alginate ($M_n$) before irradiation was 187601 g/mol and it was reduced to 53237 g/mol after 12 h exposure. (see Table 3.1) Samples with $M_n$=53000 g/mol showed appropriate viscosity for mixing with $CaSO_4$ suspensions to at 50 mM concentration.

**Table 3.1** *$M_n$ and $M_w$* of alginate samples before and after γ irradiation

| Alginate | $M_n$ (g/mol) | $M_w$ (g/mol) |
|---|---|---|
| Untreated<br>*High molecular weight (HMW) alginate* | 188000 | 572000 |
| As Powder (4 h, 0.72 Mrad) | 150000 | 348000 |
| In Solution (1.5 wt %)(4 h, 0.72 Mrad) | 102000 | 329000 |
| In Solution (1.5 wt %)(8 h, 1.44 Mrad) | 68000 | 15000 |

| | | |
|---|---|---|
| In Solution (1.5 wt %)(12h, 2.16 Mrad)<br>*Low molecular weight (LMW) alginate* | 53000 | 11000 |

### **3.4.1.2** Preparation of alginate hydrogel films with different stiffness

Solutions of the high molecular weight (HMW) alginate were mixed with solutions of the alginate with the low molecular weight (LMW, $M_n$=53000 g/mol) in order to obtain workable solution with the maximum alginate content. The maximum concentration of HMW alginate to obtain a workable solution was 1 wt. %. To this solution, LMW alginate was added. Concentrations of LMW up to 4 wt. % rendered workable mixtures of HMW and LMW alginate.

The mechanical properties of different alginate mixtures after addition of $Ca^{2+}$ were measured with a piezorheometer. The aim of this experiment was to identify the $Ca^{2+}$ concentration for obtaining alginate hydrogels with elastic modulus within physiologically relevant values, i.e. between 1 and 30 kPa. The stiffness of LMW and HMW alginate mixtures after addition of 25 mM $Ca^{2+}$ was measured first. Figure 3.7 shows the Elastic Modulus (G') at equilibrium after mixing with the $CaSO_4$ solution. The increase in G' with time reveals the progress of the crosslinking reaction and the consequent increase in stiffness during dissolution of the $CaSO_4$ salt, which is concluded after ca. 30 minutes. At this $Ca^{2+}$ concentration the HMW alginate and the mixture 1 wt.% HMW+ 4 wt.% LMW gave the highest elastic moduli (3.8 and 4.5kPa respectively, Figure 3.7). Higher contents of LWM alginates gave softer gels, i.e. the shorter chains did not support the network at low crosslinking degrees.

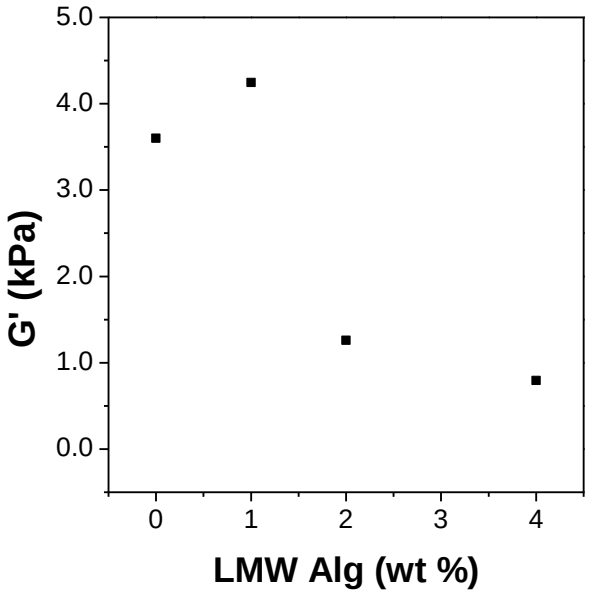


**Figure 3.6.** Changes in the storage and loss moduli (G', G'') with time corresponding to different mixtures of HMW and LMW alginate after mixing with 25 mM $CaSO_4$ at pH 7.4.

The mechanical properties of the alginates were also measured at higher [$Ca^{2+}$] between 5 and 50mM. In this case, the stiffness of the 1wt.% HMW + 1 wt.% LMW alginate mixture showed the steepest stiffness change with increasing $Ca^{2+}$ concentration: from 1 to 26 kPa when [$Ca^{2+}$] increased from 25 mM to 35 mM.(Figure 3.8) The contribution of the short alginate chains to the network became notable at higher crosslinking degrees. This mixture was selected for further studies and it was named 1+1 Alg.

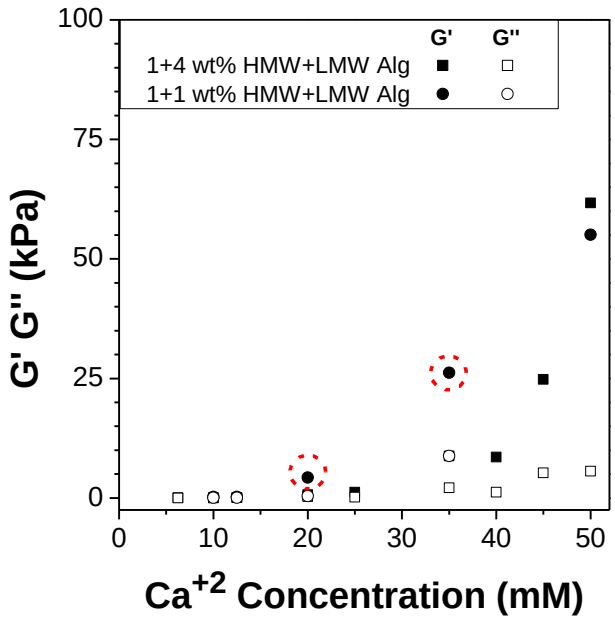


**Figure 3.7** Change in G' and G'' with [$Ca^{2+}$] for different alginate mixtures: 1wt. % HMW+1 wt. % LMW and 1 wt. % HMW+4 wt. % LMW.

### 3.4.1.3 Preparation and characterization of Nitr-T containing alginate solutions and films

Alginate solutions and films containing the photosensitive $Ca^{2+}$ chelator Nitr-T were prepared. The presence and photolysis of Nitr-T in solution and in the alginate film was tested by UV spectroscopy.

Nitr-T solutions with or without $Ca^{2+}$ were prepared in buffer at pH 7.4. Nitr-T spectrum in solution at pH 7.4 shows a maximum absorbance at 298 nm. This maximum shifted to 285 nm upon addition of an equivalent of $Ca^{2+}$ ions, and an extra peak appeared at 315 nm. A mixture of 1+1 Alg, $CaSO_4$ and Nitr-T+$Ca^{2+}$ in buffer at pH 7.4 showed a similar UV spectrum to the Nitr-T+$Ca^{2+}$ solution, indicating that $Ca^{2+}$ remain chelated by Nitr-T also in the presence of Alg. After exposure of light at 365 nm, the Nitr-T peaks at 285 and 315 nm disappeared and a strong peak showed up at 365 nm, indicating that the photochemical reaction occurred. (Figure 3.9)

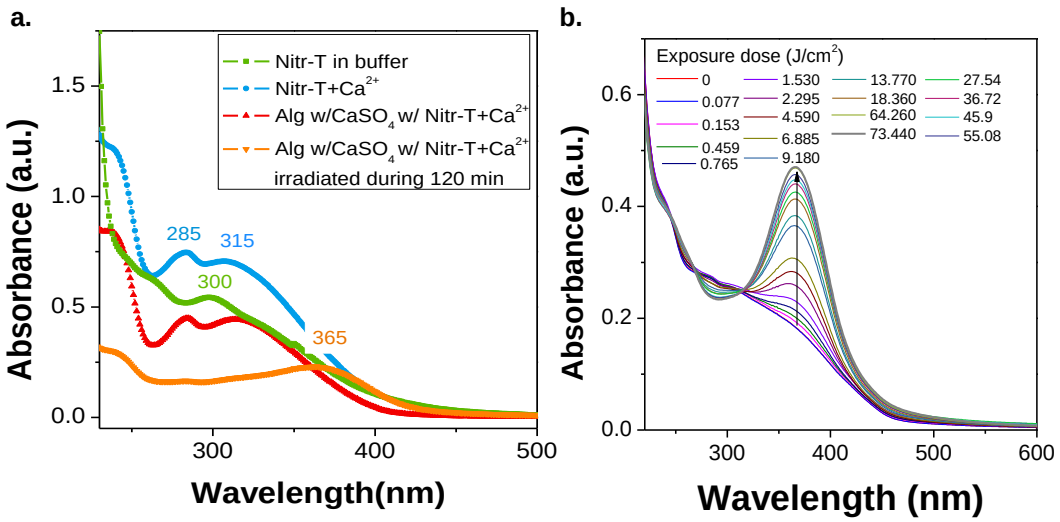


**Figure 3.8 a.** UV spectra of Nitr-T w/ or w/o Alg and $Ca^{2+}$ solutions. **b.** UV spectra of solution of Nitr-T w/ Alg and $Ca^{2+}$ which was irradiated over time. The photoreaction and complexation of Nitr-T with $Ca^{2+}$ can be followed by the change in the absorption maxima in the UV spectra. The photosensitivity of the Alg/Nitr-T-$Ca^{2+}$ solution was tested with light exposure. (LUMOS 43 lamp LED source 360 nm Power: 4.7 mW $cm^{-2}$)

The spectrum of hydrogel film prepared on quartz substrates showed a maximum at 315 nm and the appearance of another maximum at 365 nm upon light exposure. (Figure 3.10) This change reflects that a photoreaction took place, and expectedly with a similar mechanism to the reaction observed in solution. These results indicate that the loss of solvent does not change the photochemical properties. The changes were analogous to those reported for Nitr-T in solution,[13] indicating that the presence of alginate does not significantly change the stability and photochemical properties of Nitr-T.

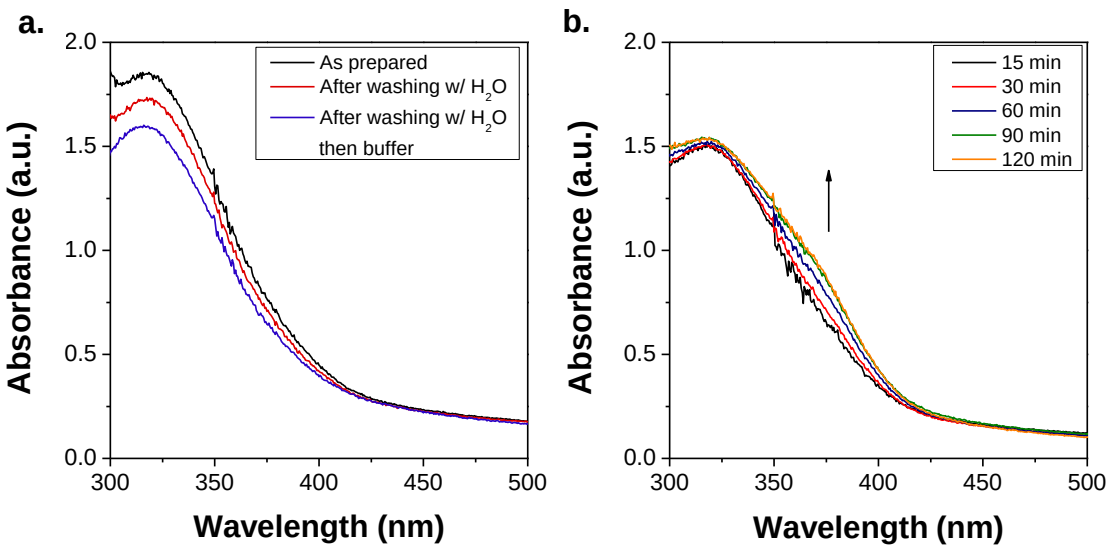


**Figure 3.9**: UV spectra of thin films of Alg/nitr-T-$Ca^{+2}$. **a.** Thin film prepared with 2 wt. % (1 wt. % LMW+ 1wt. % HMW) alginate with 12.5 mM $CaSO_4$ and 25 mM Nitr-T/$CaCl_2$. Sample was irradiated with polychrome V lamp at 360 nm with power 2.55 mW $cm^{-2}$.

### 3.4.1.4 Formulation and light-triggered stiffening of Alg+Nitr-T+ $Ca^{2+}$ hydrogel

The first step for the formulation of the Alg+NitrT+$Ca^{2+}$ mixture was the estimation of the amount of $Ca^{2+}$ ions and Nitr-T necessary to achieve a stiffness change between 1 and 30 kPa upon light exposure in the 1+1 Alg composition. From the rheological analysis in Figure 3.9, it was known that a $Ca^{2+}$ concentration of 25 mM formed hydrogels with a modulus of 1 kPa, which is at the lower limit for physiologically relevant hydrogels. A $Ca^{2+}$ concentration of 50 mM formed hydrogels with G'~ 65kPa. Therefore, 1+1 Alg samples were prepared with a basal $Ca^{2+}$ concentration by mixing CaSO4 with the Alg solution to approach the lower stiffness limit with physiologically relevance, and the photoliberated $Ca^{2+}$ from nitro-T photolysis was used only for the dynamic stiffening.

The low solubility of Nitr-T in the alginate solution at pH 7.4 sets a limit for Nitr-T concentration in the alginate at 50 mM. Note that the dissociation constant of the complex formation between alginate and $Ca^{2+}$ is $9.3x10^{-5}$ mM. [14] It is lower than $K_d$ of photoproduct and cage molecule ($1.5x10^{-6}$ and $520x10^{-6}$ mM respectively). In consequence, the photoliberated $Ca^{2+}$ ions are expected to be complexed by the alginate.

A solution of equimolar concentrations of $CaCl_2$ and Nitr-T was mixed with 1+1 Alg and 12.5 or 25mM $CaSO_4$. 1+1 Alg with 12.5 or 25 mM $CaSO_4$ forms weak hydrogels of 0.2 or 0.9 kPa respectively, which can be still mixed with nitr-T/$CaCl_2$ solution to form homogenous samples. The storage modulus of this mixture was measured with a piezorheometer before and after

irradiation for increasing times. (Figure 3.11) The storage modulus of 1+1 Alg/12.5 mM $CaSO_4$ mixed with 25 mM Nitr-T+$CaCl_2$ was 0.2 kPa, and it gradually increased to 0.7 kPa upon full exposure, indicating an increase in the crosslinking degree as a consequence of the photoliberated $Ca^{2+}$. (Figure 3.11a) When using a lower equivalent of $CaCl_2$ (16mM) in the Nitr-T solution, a lower initial value and increase of the storage modulus was observed, from 0.01 to 0.16 kPa, as a result of the complexation of $Ca^{2+}$ from $CaSO_4$ by the free Nitr-T. (Figure 3.11a) In order to extend the change in stiffness upon irradiation, the initial concentration of $CaSO_4$ in the 1+1Alg gel was increased to 25mM and the concentration of Nitr-T/$Ca^{2+}$ was increased to 33.3 and 50mM (Figure 3.11b). The initial stiffness of the resulting hydrogel was 0.4 kPa, and raised to 1.2 kPa after full exposure using 50 mM Nitr-T/$Ca^{2+}$concentration. (Figure 3.11b) It is worth to note that initial modulus of alginate-Nitr-T was lower than the modulus of alginate hydrogel prepared with the same amount of $Ca^{2+}$ ions. This result belonged to single measurement.

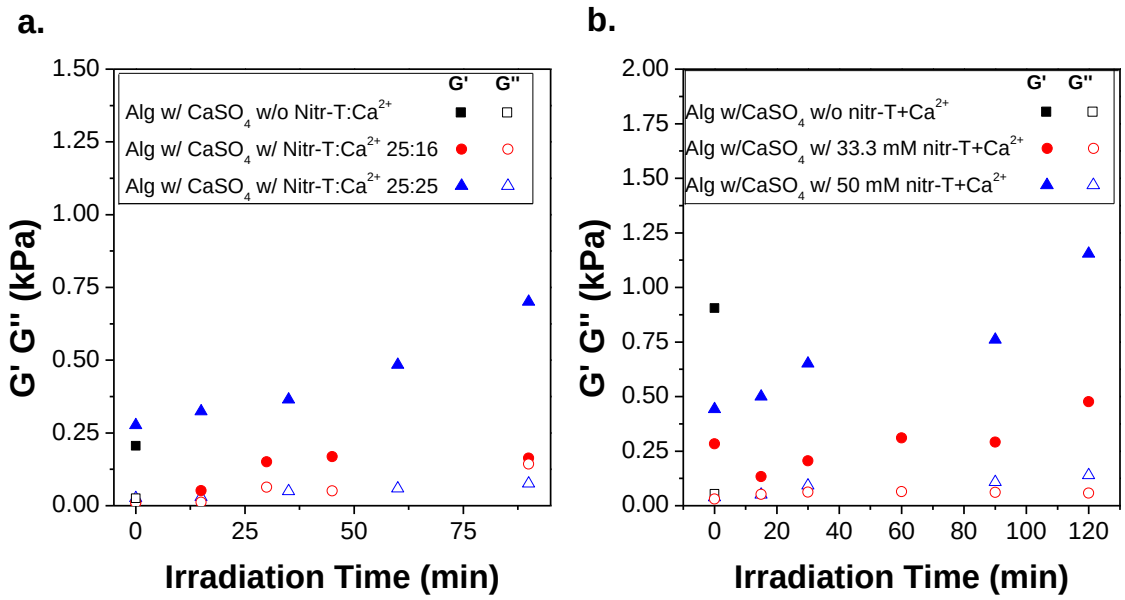


**Figure 3.10** Storage and loss modulus measured for 1+1Alg with **a.** 12.5 mM, **b.** 25 mM CaSO4 mixed with different concentrations of Nitr-T+$CaCl_2$ in DPBS buffer after different light exposure times at λ=365 nm.

These results show that, although HMW/LMW alginate mixtures with high G content lead to stiffer gels at lower $Ca^{2+}$ concentrations, they do not allow steeper changes of hydrogel stiffness with photoliberated $Ca^{2+}$ at the concentrations possible with Nitr-T chelator. Alternative photoactivatable chelators would be required, with higher solubility and a larger difference in the

dissociation constants of chelator and photoproduct. This strategy would require extensive synthetic effort and was no longer followed in this Thesis.

### 3.4.2 Photodegradable hydrogels based on Nitro-catechol Derivatives

#### 3.4.2.1 Nitrocatechol derivatives photoactivity of nitro-norepinephrine and comparison with nitrodopamine

Preliminary experiments were performed to compare the photoactivity of NDop and NNEN molecules, in order to check if NNEN could be a more photosensitive chromophore than the previously reported NDop to be used as photodegradable crosslinker. Solutions of both chromophores were irradiated at 420 nm and the changes in the UV spectra associated to the structural change of the chromophore during photolysis were analyzed. Figure 3.12 shows the spectra of the solutions of NDop and NNEN in PBS buffer at pH 7.5. Both chromophores show a $\lambda_{max}$ at 425 nm. Note that this peak shifts with the pH of the solution, as the ionization state of the catechol changes.[6] Upon light exposure, the intensity of the absorbance peak at $\lambda_{max}$ = 425 nm decreased and new peaks appeared at 270 and 325 nm and a very weak absorbance above 500 nm in the case of NNEN, and at 280 nm in the case of NDop. These changes suggest the disappearance of the initial chromophore and the appearance of the photobyproducts. In NDop, the intensity of the band at 425 nm decreased to half value after 10 h irradiation, whereas in NNEN the absorbance decay was completed in 90 min. These results demonstrate a significant difference in photoefficiency between the chromophores, and suggest that NNEN could potentially be a better candidate than NDop to be used in photodegradable polymers.

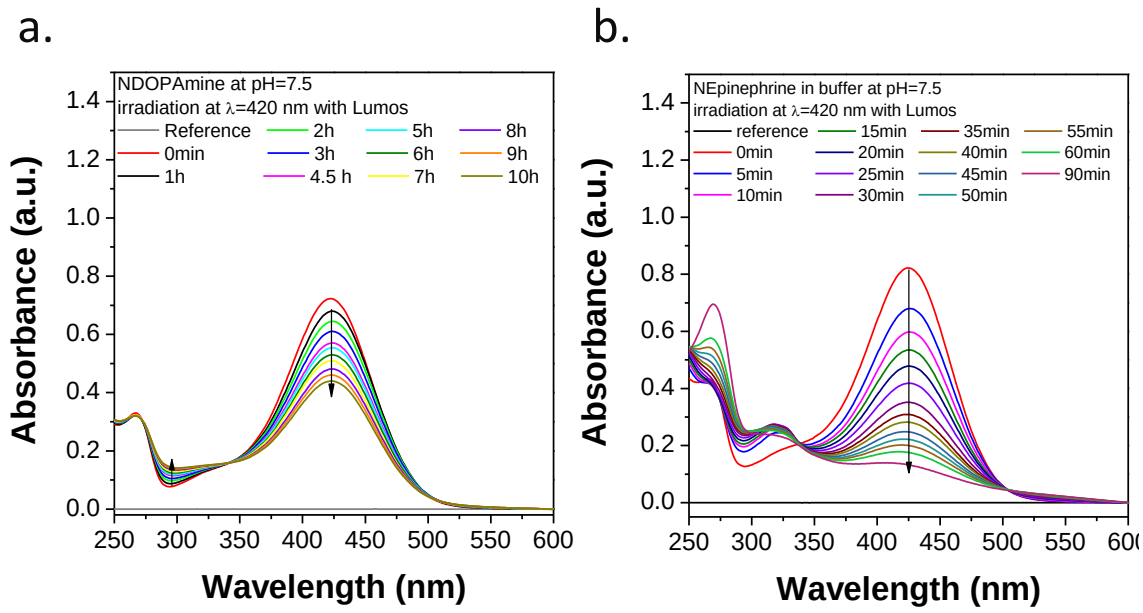


**Figure 3.11** UV absorbance spectra of NDop and NNEN solutions prepared at PBS buffer at pH 7.5 before and after irradiation with LUMOS 43 lamp LED source at 420 nm with power of 4.7 mW $cm^{-2}$.

It should be noted that NNEN can undergo photolysis in two different ways: as an *o*-nitrophenylethyl if it cleaves at the $NH_2$, or as *o*-nitrobenzyl if it cleaves by the OH group. A priori it is difficult to decide which reaction will take place. However, o-nitrobenzyl cleavage typically leads to a photobyproduct showing absorbance at longer wavelengths than the chromophore. This could be the reason for the very weak band appearing above 500 nm, which is absent in NDop. Therefore, the OH group was selected as position to attach to the polymer.

### **3.4.2.2** Synthesis of nitronorepinephrine conjugated to PEG

#### a. Protection strategies of norepinephrine

In order to join the PEG chain to the hydroxyl group of NNEN through a good leaving and proteolytically stable anchoring group, a carbamate bond was selected. For this purpose, the hydroxyl group of NNEN has to be reacted with an isocyanate terminated PEG. This step requires previous protection of the amine and the catechol moieties, which can also react with the isocyanate. Different combinations of protecting groups and reaction steps were tested. (Figure 3.13)

The protection of NNEN with methyl trifluoroacetate (MTFA) did not work, although this reaction was successful in dopamine molecule, suggesting that the presence of the nitro group hinders reaction at the amine group. Reaction of the amine group with *N*-(tert-Butoxycarbonyloxy) succinimide (boc-Osu) resulted in boc protected NNEN (**4)** in 27% yield after prep-HPLC

purification. For catechol protection, **4** was refluxed in 2,2-dimethoxypropane (DMP), but the boc- moiety was cleaved under the reaction conditions. In a last attempt, the amine group of NNEN was reacted with 9-fluorenylmethyl N-succinimidyl carbonate (Fmoc-Osu) to obtain Fmoc protected NNEN **(3)** with 67% yield after purification. **3** was reacted with DMP for catechol protection, but no reaction was observed, according to ESI-MASS analysis. Catechol protection was also attempted using *tert*-Butyldimethylsilyl chloride (TBDMS-Cl) in the presence of different catalysts: 1,5,7-Triazabicyclo[4.4.0]dec-5-ene (TBD) and 1,8-Diazabicyclo[5.4.0]undec-7-ene (DBU). The reaction with DBU did not work. In the presence of TBD the catechol protection reaction took place in 14 h, but partial cleavage of the fmoc- group occurred as well.

In summary, protection of the amine and catechol groups of NNEN before reaction of the hydroxyl group did not work in any of the tested variants. These were surprising results, since some of these reactions have been reported to work for dopamine derivatization. We hypothesized that the nitro group was hindering reaction at the amine group. Therefore, new reaction conditions were tested where nitration was performed after amine and catechol protection.

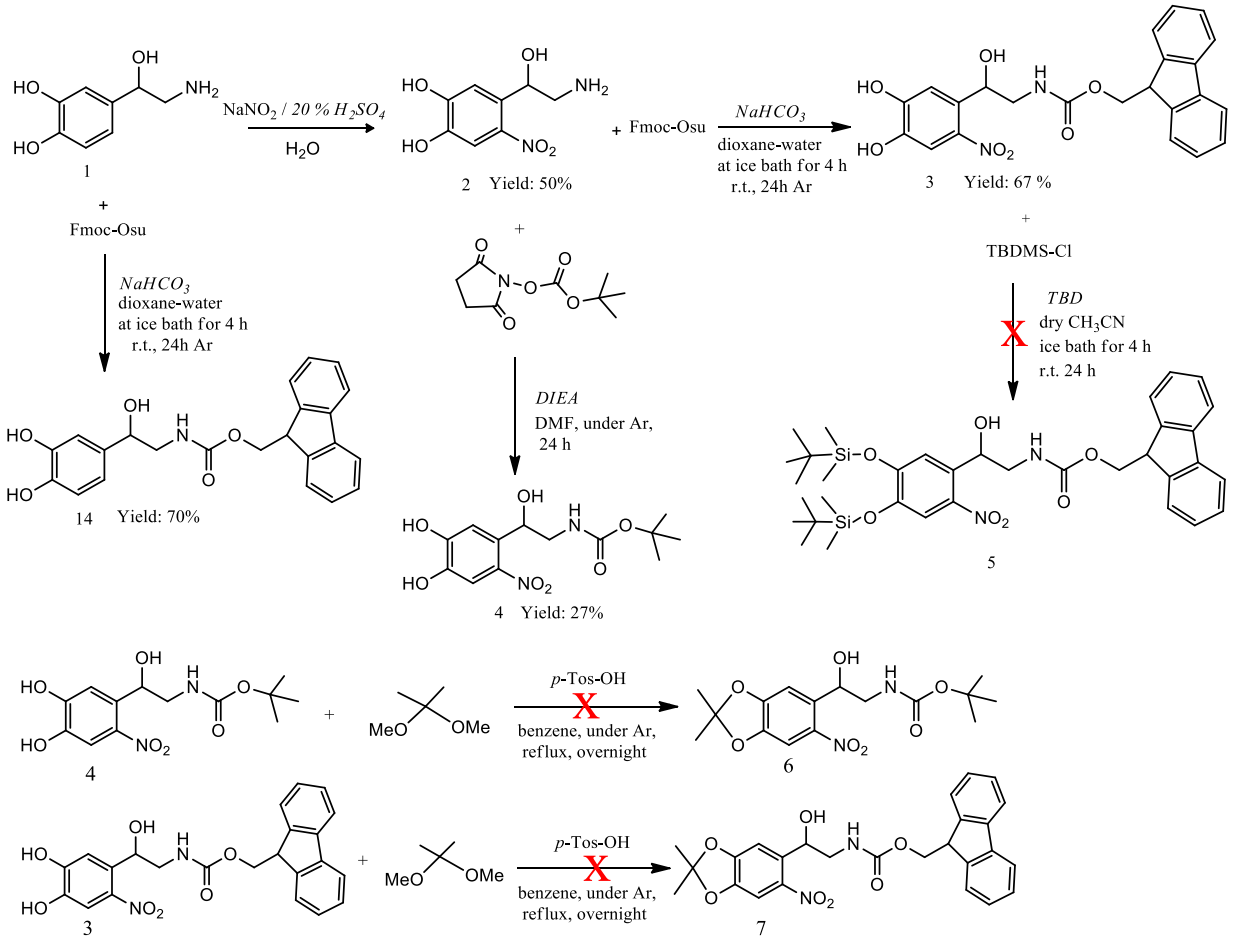
NaNO2 / 20 % H2SO4
H2O
2 Yield: 50%
+ Fmoc-Osu
NaHCO3
dioxane-water
at ice bath for 4 h
r.t., 24h Ar
3 Yield: 67 %
TBDMS-Cl
TBD
dry CH3CN
ice bath for 4 h
r.t. 24 h
5
Fmoc-Osu
NaHCO3
dioxane-water
at ice bath for 4 h
r.t., 24h Ar
14 Yield: 70%
DIEA
DMF, under Ar,
24 h
4 Yield: 27%
p-Tos-OH
benzene, under Ar,
reflux, overnight
6
7

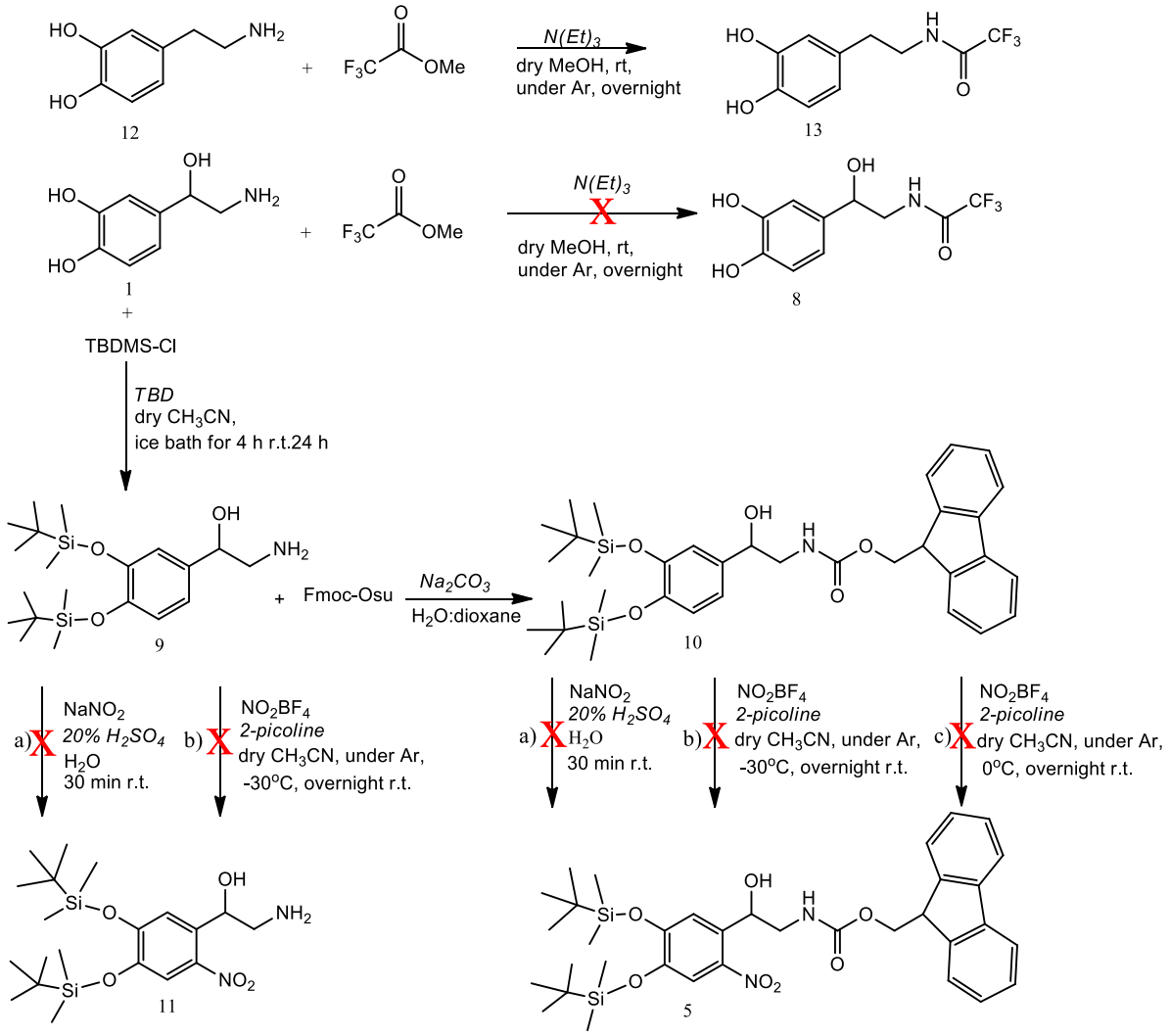


**Figure 3.12** Summary of reactions that were performed for synthesis of NNEN with protected amine and catechol groups.

Reaction of NEN (**1)** with TBDMS-Cl afforded the protected catechol product **9**. Nitration of **9** with $NO_2BF_4$ and $NaNO_2$ did not work because of the lack of solubility of **9** in the nitration conditions. Protection of the amine group of **9** with Fmoc-Osu worked with 95% yield, but nitration of **10** failed again because of insolubility of the starting material. In a different protection strategy, Fmoc- protected NEN, **14**, was synthesized with 70% yield, but **14** was insoluble in nitration conditions (nitration with $NO_2BF_4$ and $NaNO_2$). In conclusion, nitration of protected NEN failed in all cases because of the lack of solubility of protected NEN in the water-based reaction conditions.

b. Coupling of amine protected nitro-norepinephrine to PEG-4NCO

In a last alternative, the direct coupling of Fmoc-protected NNEN (**3)** to isocyanate terminated PEG without protection of the catechol groups was attempted. The free hydroxyl group of **3** should react with isocyanate group of PEG resulting a carbamate bond. Therefore, a change in the $^{1}$H NMR signal corresponding to C**H**-OH proton is expected. Moreover, ONC-C**H**$_2$ protons will be affected due to the change of neighbouring group. A preliminary test using a model molecule was run using n-Butyl isocyanate (butylNCO) to react with **3** in the presence of dibutyltin dilaurate (DBTDL) as catalyst (Figure 3.14). The changes in the 1H-NMR peak at 3.4 ppm, corresponding to ONC-C**H**$_2$ protons, were followed. After 5 h reaction, no significant changes were observed in the 1H NMR spectrum. The reaction was repeated in THF and DMF. However, neither product formation nor reactant consumption was observed attending to the $^{1}$H NMR spectra. (Figure 3.14 and 3.15)

After the failed synthetic attempts with NNEN, a different variant of the photosensitive catechol had to be found.

**Figure 3.13:** Coupling reaction of **3** with butylNCO in catalysis of DBTDL in deuterated DMF and corresponding $^{1}$H NMR spectra of reaction at time 0 and 5 h in addition to $^{1}$H NMR spectrum of **3**.

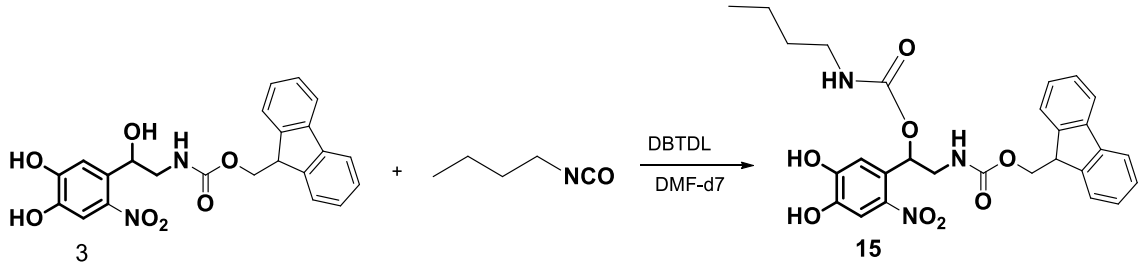

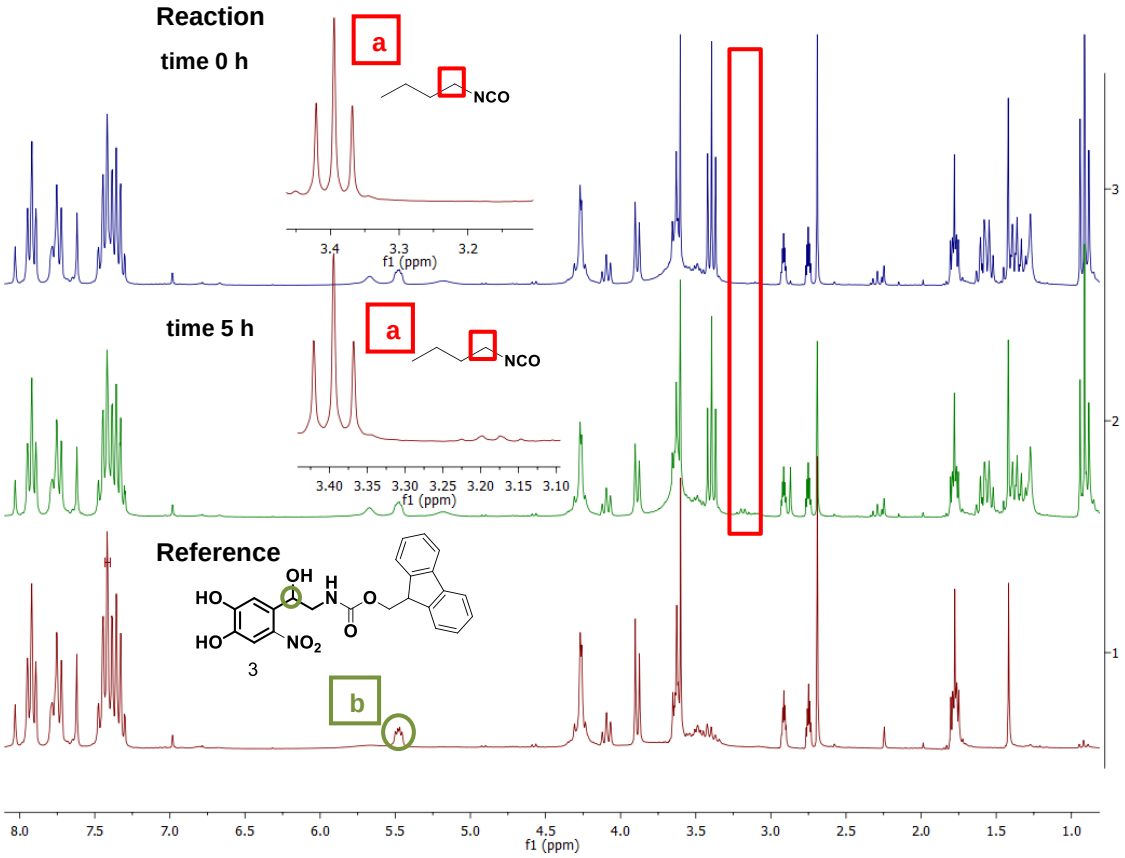
Reaction
time 0 h
a
NCO
3.4
3.3
3.2
f1 (ppm)
time 5 h
a
NCO
3.40 3.35 3.30 3.25 3.20 3.15 3.10
f1 (ppm)
Reference
OH
H
N
O
HO
HO
NO2
O
3
b
3
2
1
8.0
7.5
7.0
6.5
6.0
5.5
5.0
4.5
4.0
3.5
3.0
2.5
2.0
1.5
1.0
f1 (ppm)

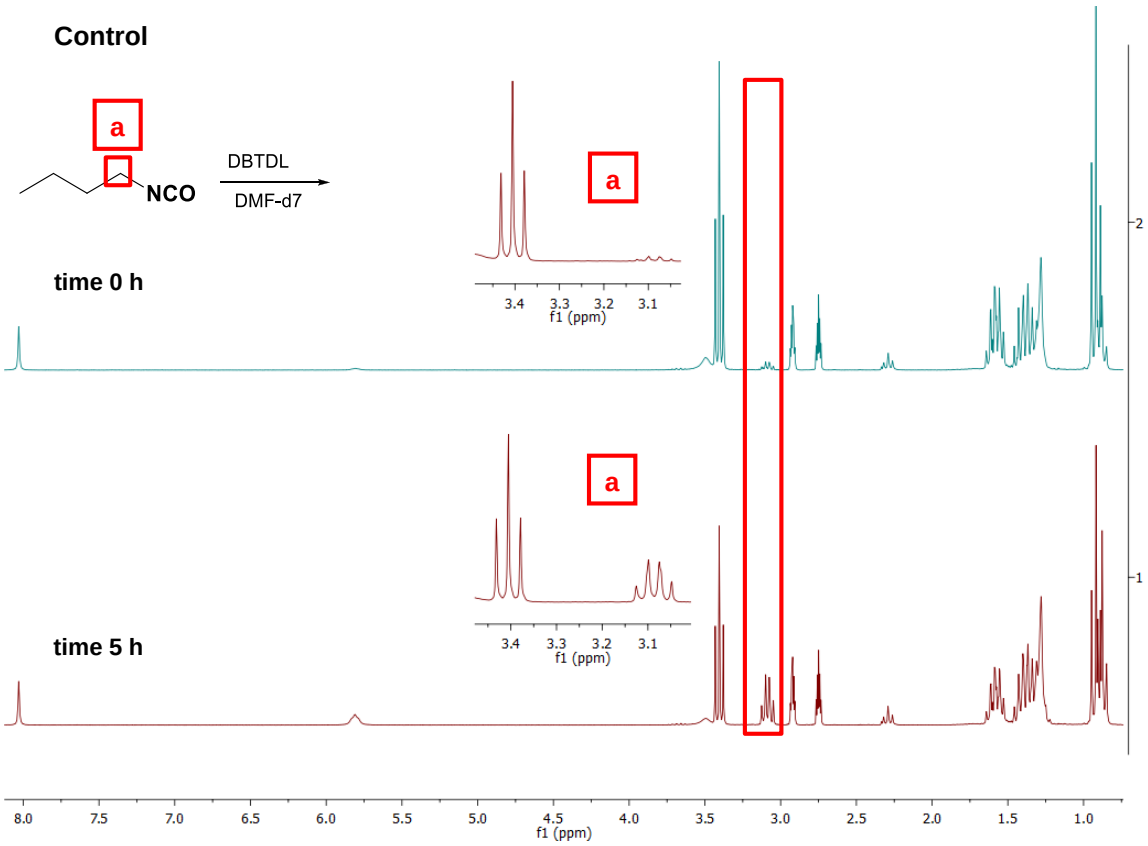


**Figure 3.14** [1]HNMR spectra of butylNCO in the presence of DBTDL at time 0 and 5 h as control reaction.

### 3.4.2.3 Alternative photosensitive nitrocatechols

The 4-(1-hydroxyethyl)-5-nitrobenzene-1,2-diol molecule (16) was selected as alternative to NNEN. (Figure 3.16)

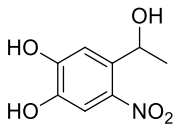


16

**Figure 3.15:** 4-(1-hydroxyethyl)-5-nitrobenzene-1,2-diol molecule (16)

This molecule can be obtained by reduction of the commercially available 6-nitropiperonal, where the catechol group is already protected as dioxymethylene. Previous experience in the group had shown that removal of the dioxymethylene group required harsh acidic conditions (48% HBr) that could also cleave the carbamate bond after PEG coupling. Therefore, a variant with the methoxymethyl (MOM) protecting group was also tested, where 1-(benzo[d][1,3]dioxol-5-yl)ethanone was first nitrated and the methylene moiety was replaced by the methoxymethyl

group followed by ketone reduction. These molecules were kindly synthesized by Dr. J. Paez and S. Koynova at MPIP.(Figure 3.17)

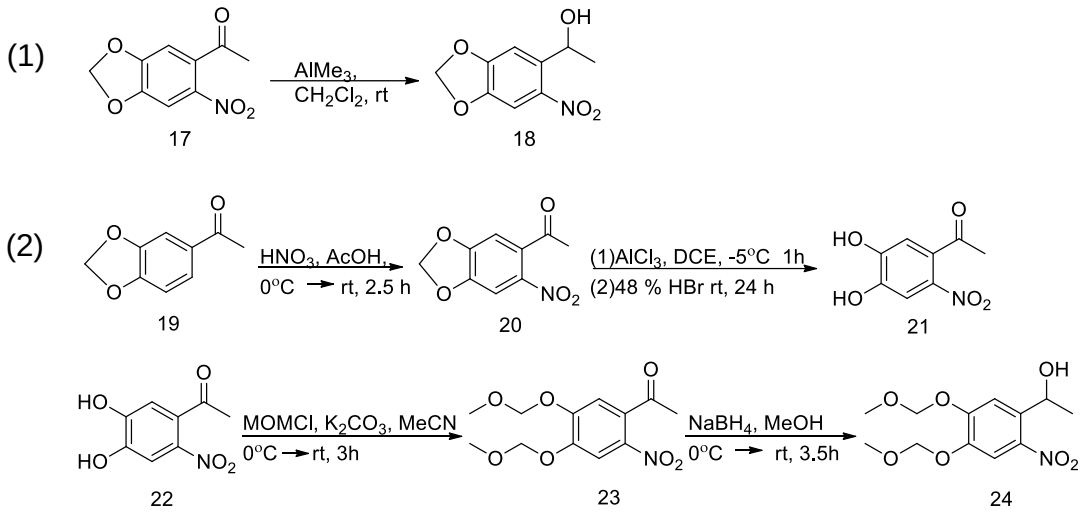


**Figure 3.16** Reaction scheme to synthesize protected 16 with two different protecting groups; **18** and **24**.

a. NMR studies with alternative molecule for adjusting coupling conditions

In order to test the reaction conditions for the coupling of **18** and **24** to the isocyanate terminated star PEG, NMR studies with n-butylisocyanate as model molecule were performed. (Figure 3.18 and 3.19) When **18** was mixed with n-butyl isocyanate with catalysis of DBTDL, clear changes in NMR peaks were observed after 2h. A change in the triplet at δ=3.41 ppm associated to the ONC-C**H**$_2$ protons of butylNCO, and a change in the multiplet at 5.39 – 5.22 associated to the C**H**OH proton in **18** were observed. Moreover, a new doublet at δ=5.54 ppm appeared during reaction. The multiplicity of the peak at δ=5.31 ppm associated to the **CH** proton of **18** changed from quartet to multiplet. After 2 h reaction time no further changes were observed, indicating that reaction was completed.

**Figure 3.17** Coupling reaction of **18** with butylNCO in catalysis of DBTDL in deuterated DMF and corresponding $^1$H NMR spectra of reaction at time 0 and 2 h in addition to $^1$H NMR spectrum of **18**.

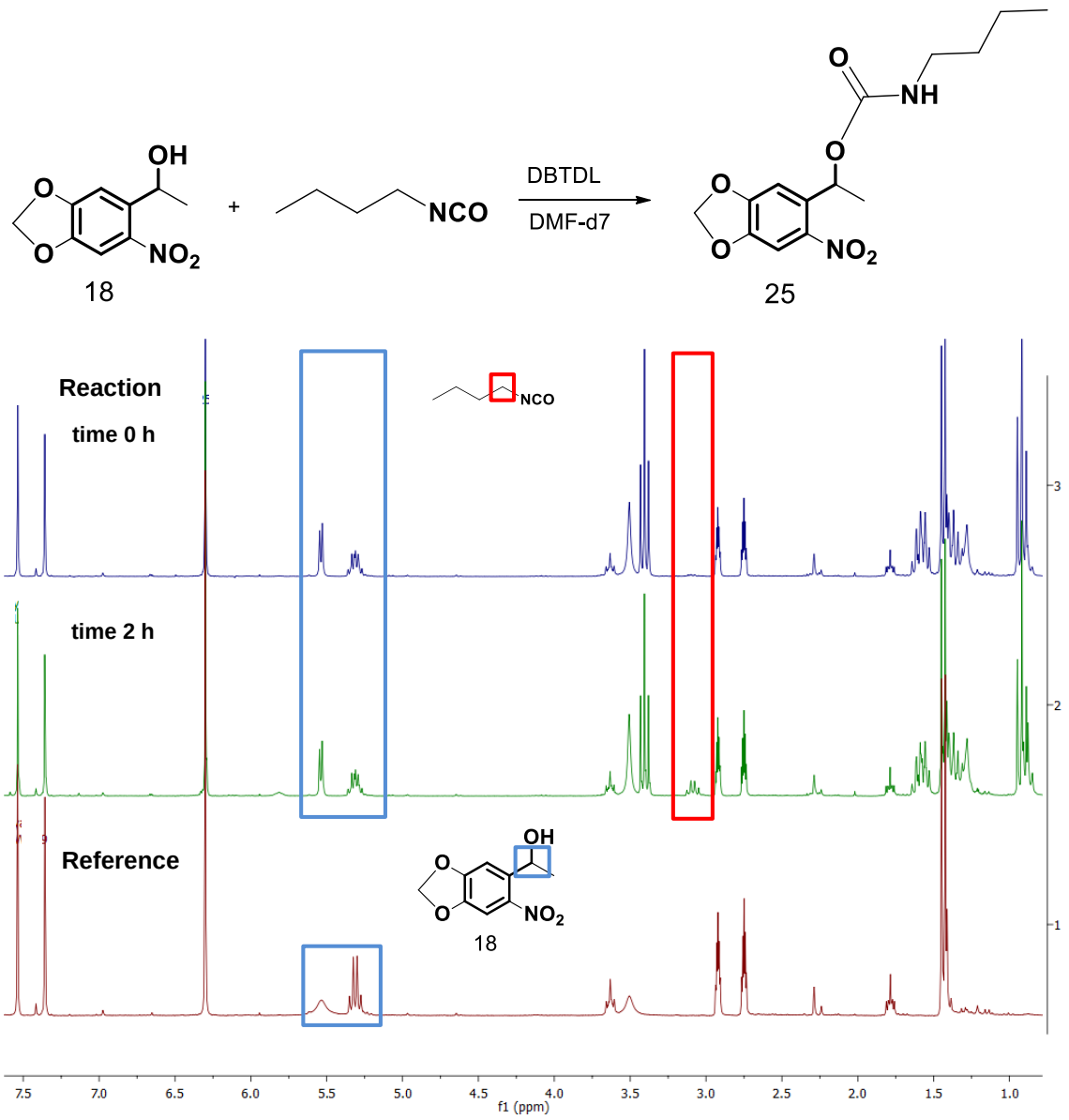
OH
O
O
NO2
18
+
NCO
DBTDL
DMF-d7
O
NH
O
O
O
NO2
25
Reaction
time 0 h
NCO
time 2 h
Reference
OH
O
O
NO2
18
7.5
7.0
6.5
6.0
5.5
5.0
4.5
4.0
3.5
3.0
2.5
2.0
1.5
1.0
f1 (ppm)

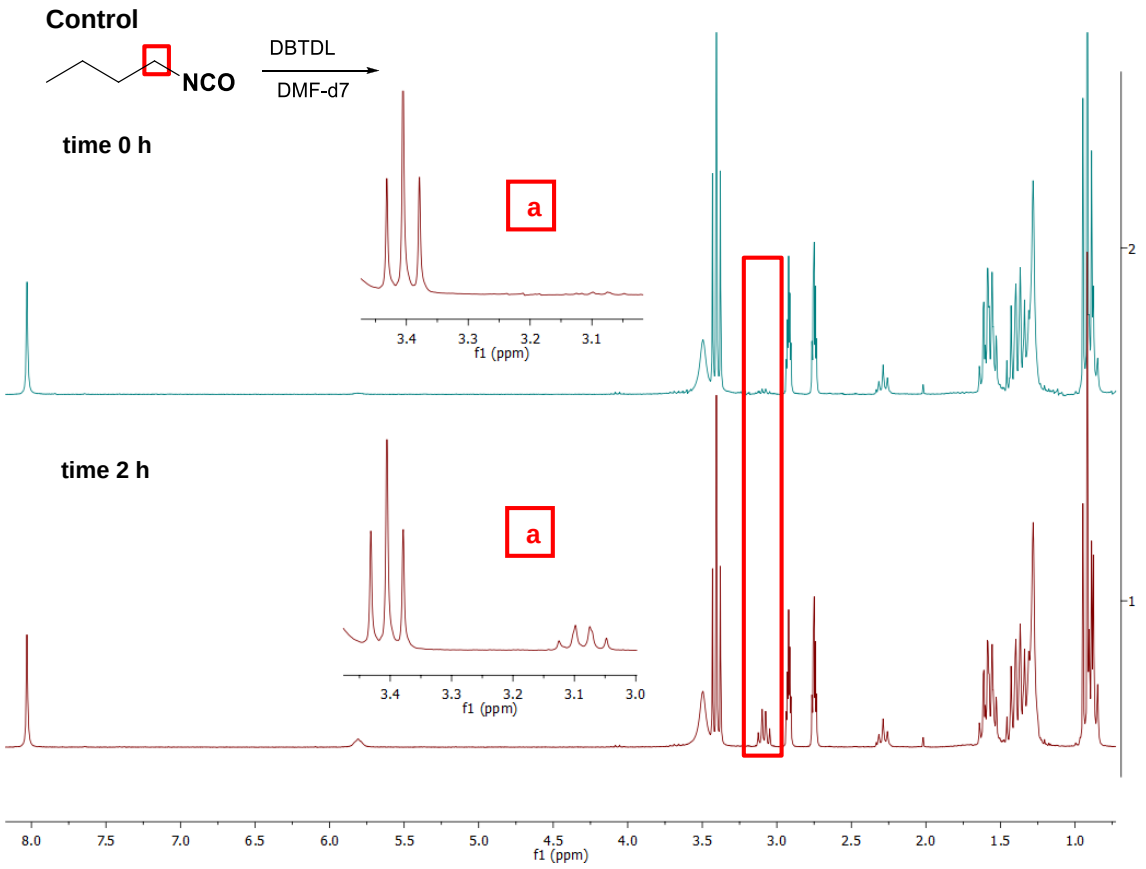


**Figure 3.18** NMR spectra of butylNCO with DBTDL at time 0 and 2 h as control reaction.

## b. Coupling of molecule to PEG polymer (NMR)

After adjusting the optimum coupling conditions with the model molecule, compounds **18** and **24** were coupled to PEG-$(NCO)_4$. The coupling was monitored by the NMR signals at δ=5.0-5.5 ppm corresponding to the C**H**-OH proton of **18**. (Figure 3.20 and 3.21) After 2 hours reaction time these signals did not change any further, the reaction was stopped and the functionalized polymer was purified with dialysis in MeOH. In order to determine the purity of the product and the coupling efficiency, $^1$H NMR spectra of the dialyzed polymers were taken. (Figure 3.22 and 3.23) In the coupling of **18**, the doublet signal at δ=5.54 ppm and multiplet at δ=5.39 – 5.22 disappeared and a new quartet peak at δ=5.36 appeared after dialysis, indicating the change in C**H** proton of **18**. (Figure 3.22) In the case of **24**, the changes in the chemical environment of the C**H** proton of **24** upon coupling was visualized by the change of the multiplet at δ=5.43 ppm to a quartet at δ=5.46 ppm. (Figure 3.23)

**Figure 3.19** Coupling reaction between **18** and isocyanate terminated star PEG in catalysis of DBTDL in deuterated DMF and corresponding $^{1}$H NMR spectra of reaction at time 0 and 2 h in addition to $^{1}$H NMR spectrum of **18**.

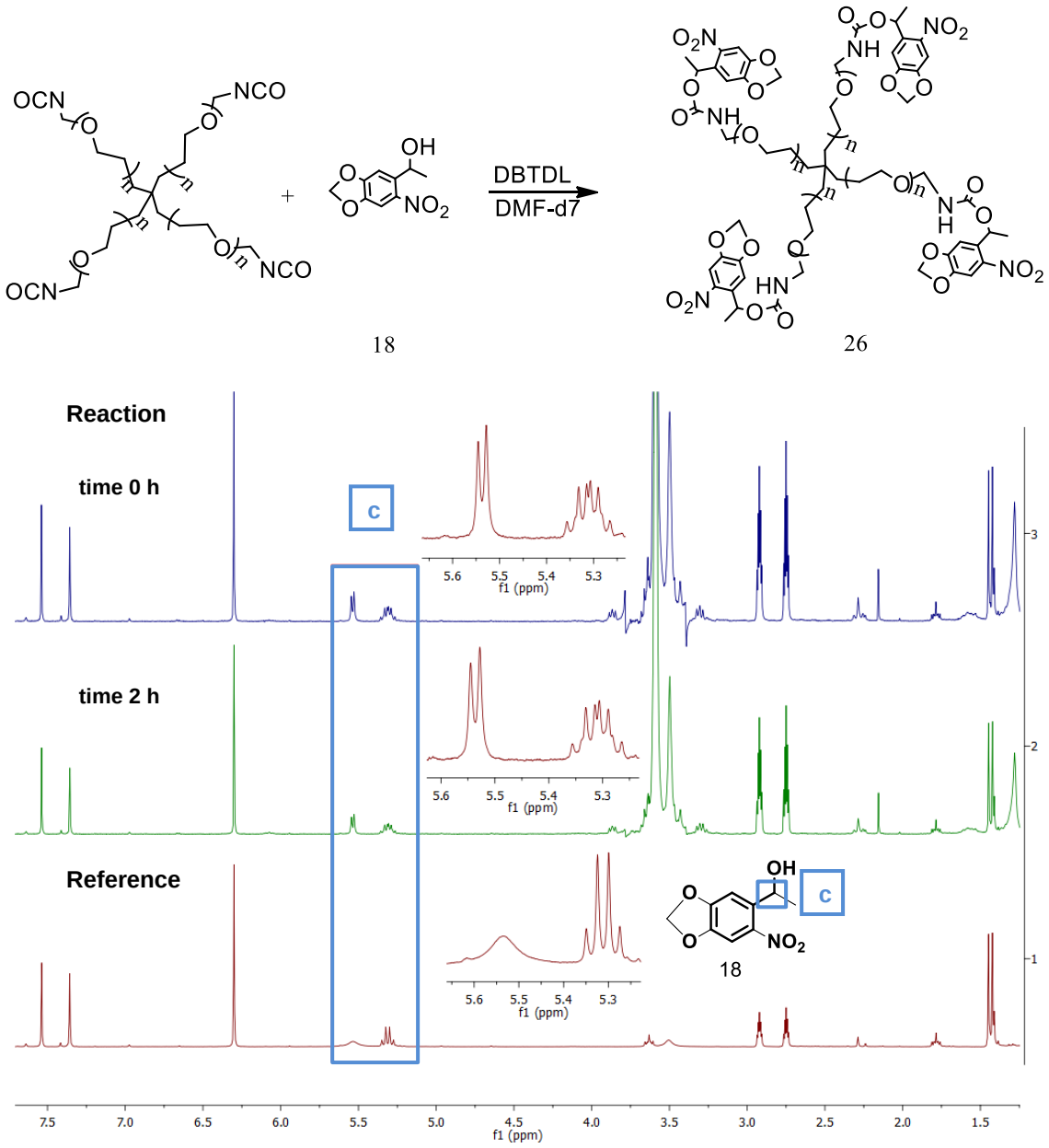

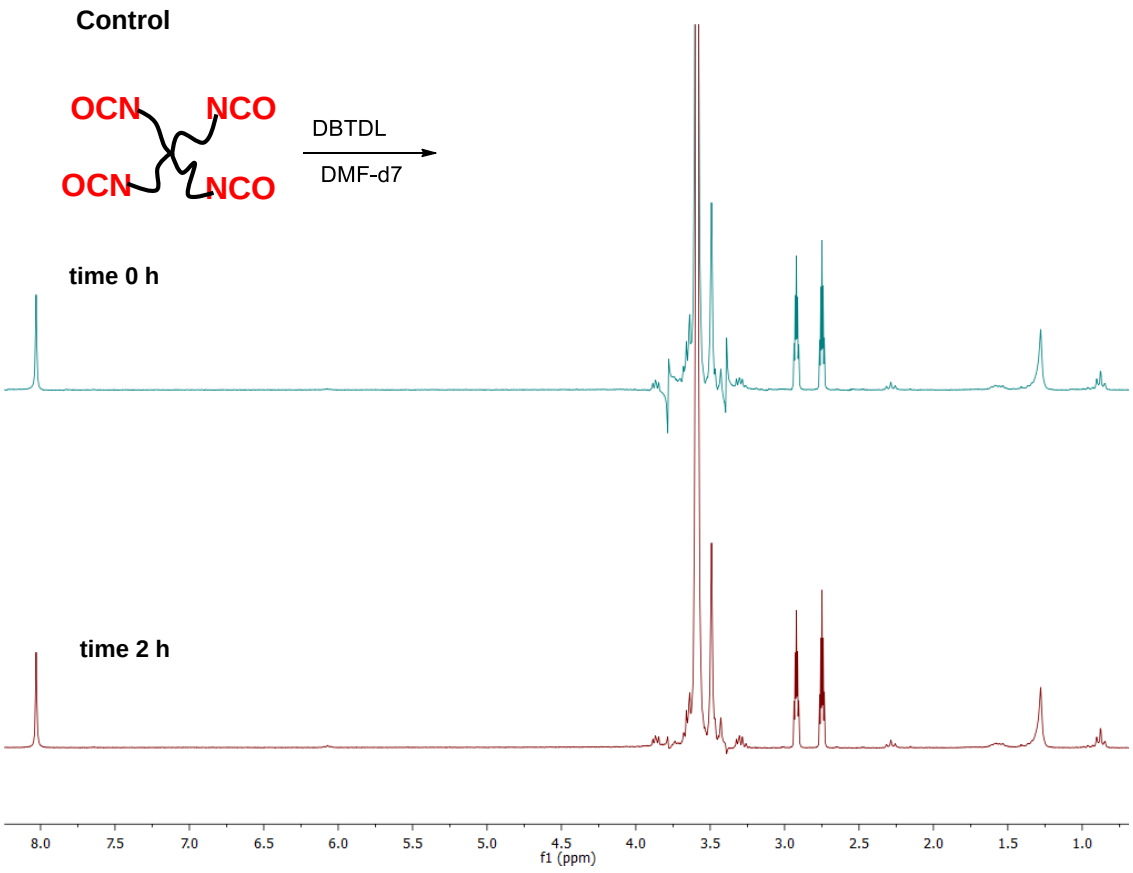


**Figure 3.20** $^{1}$H NMR spectra PEG-$(NCO)_4$ in the presence of DBTDL as control reactions at time 0 and 2 h.

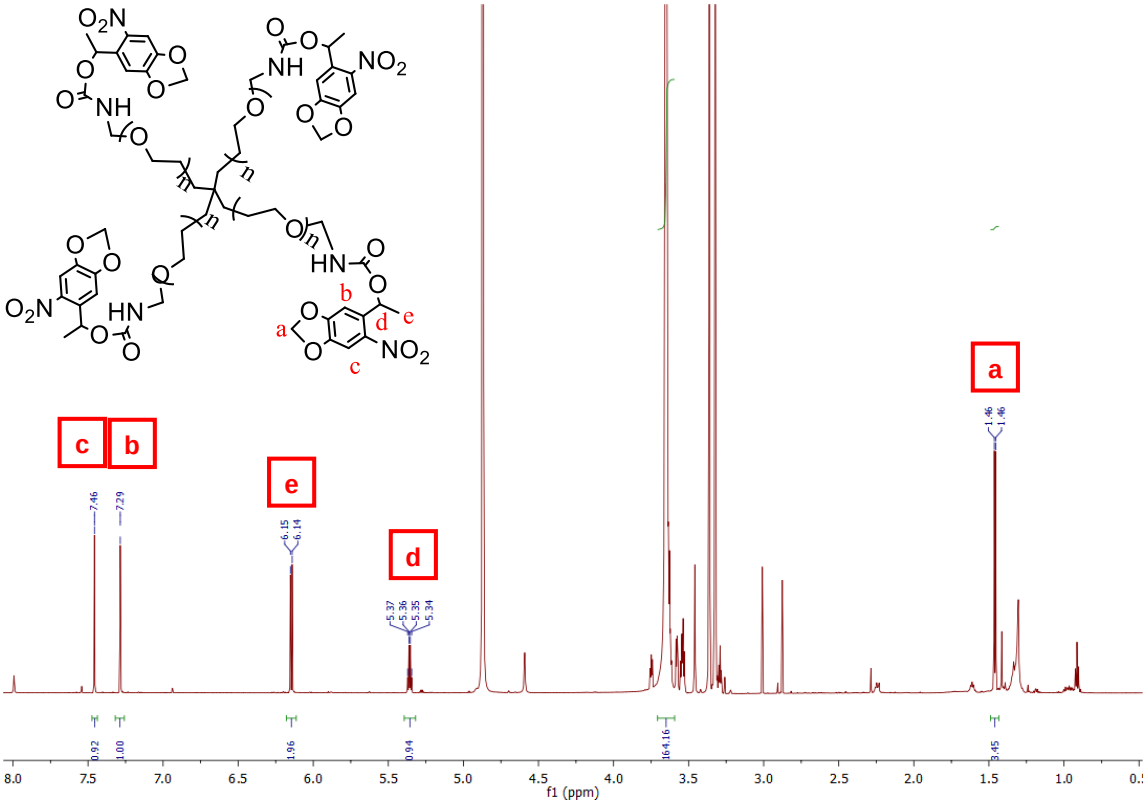


**Figure 3.21** $^{1}$H NMR spectrum after dialysis of reaction of **18** and PEG-$(NCO)_4$ with DBTDL. It corresponds to chemical structure of **26.**

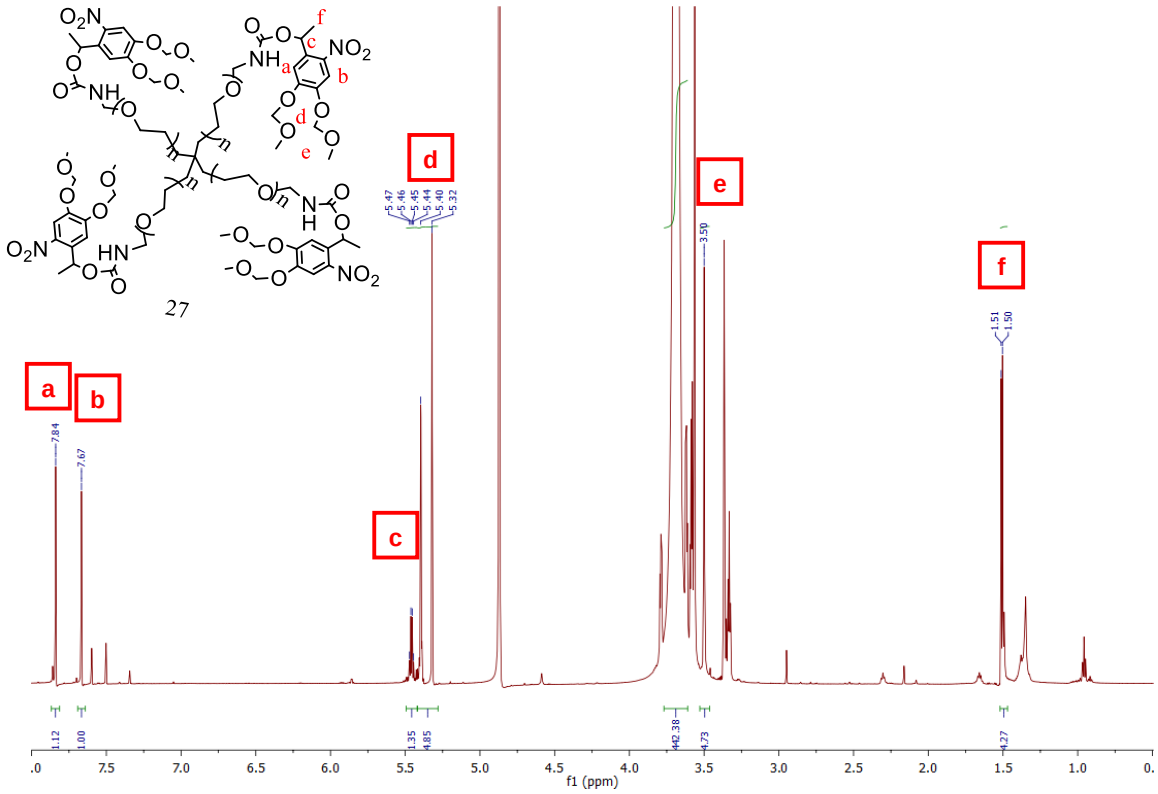


**Figure 3.22** $^{1}$H NMR spectrum after dialysis of reaction of **24** and PEG-$(NCO)_4$ with DBTDL. It corresponds to chemical structure of **27.**

## c. Deprotection conditions of functionalized polymer (NMR results)

The cleavage of the methylene moiety in **26** and MOM moiety in **27** was performed in strong acidic conditions. (Figure 3.24) $^{1}$H NMR analysis of the deprotected polymer in presence of 48% HBr and after dialysis revealed catechol deprotection, but also parallel cleavage of the carbamate bond. We couldn't observe peaks belonging to **18** in NMR analysis even after 1h deprotection. It indicates the cleavage of carbamate bond and disposal of **18** during dialysis.

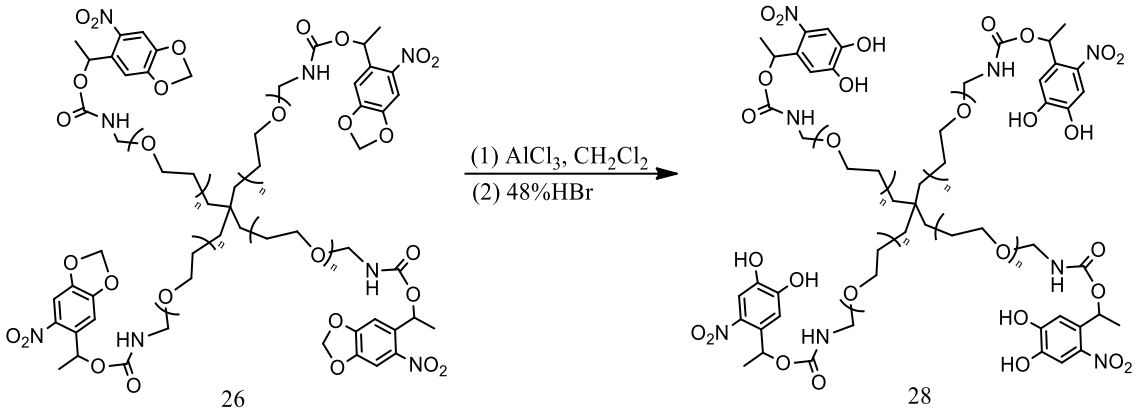


**Figure 3.23** Deprotection of catechol moiety of **26.**

In the case of **27**, the carbamate bond was stable during 5h deprotection while catechol moiety of **24** was deprotected in a remarkable amount.(Figure 3.25) Deprotection of **27** was followed in mixture of $CHCl_3$:TFA in 1:1 ratio to deprotect catechol moiety without breaking carbamate bond. Samples were taken at certain time intervals (1, 3, 4, and 5 h) and dialyzed in MeOH. Deprotection amount was monitored with NMR by monitoring changes at peaks at around δ=5.0-5.5 ppm. Two singlet peaks at around δ=5.40 and 5.32 ppm indicate presence of **$CH_2$** moiety of MOM group. Therefore, decrease in these peaks was monitored during deprotection with NMR. After 5 h deprotection, one peak singlet completely disappeared indicating the presence of **$CH_2$** at MOM moiety and intensity of the other one decreased 80% so **27** was deprotected 90% after 5 h deprotection reaction. However, approximately 6% of carbamate bond left after 5 h of deprotection. (Figure 3.25)

**Figure 3.24** Deprotection reaction of **27 and** $^1$H NMR spectra after deprotection reaction and dialysis of **27** at different reaction time intervals.

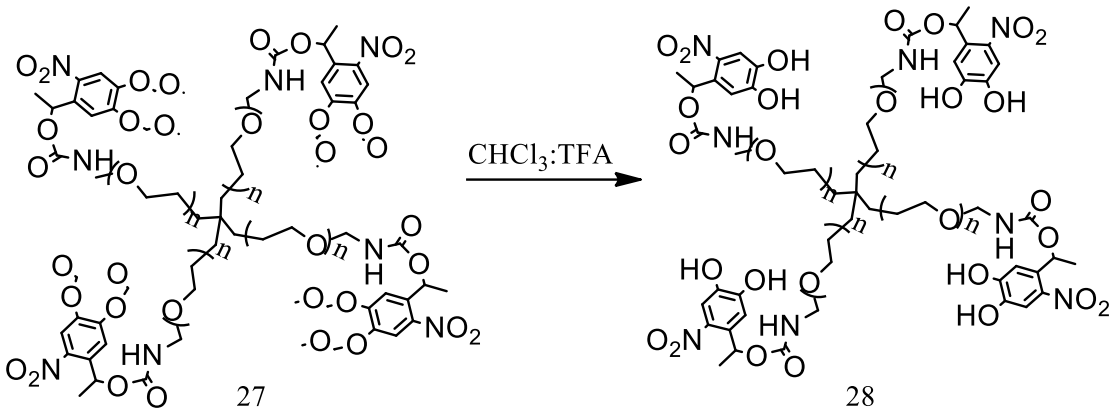


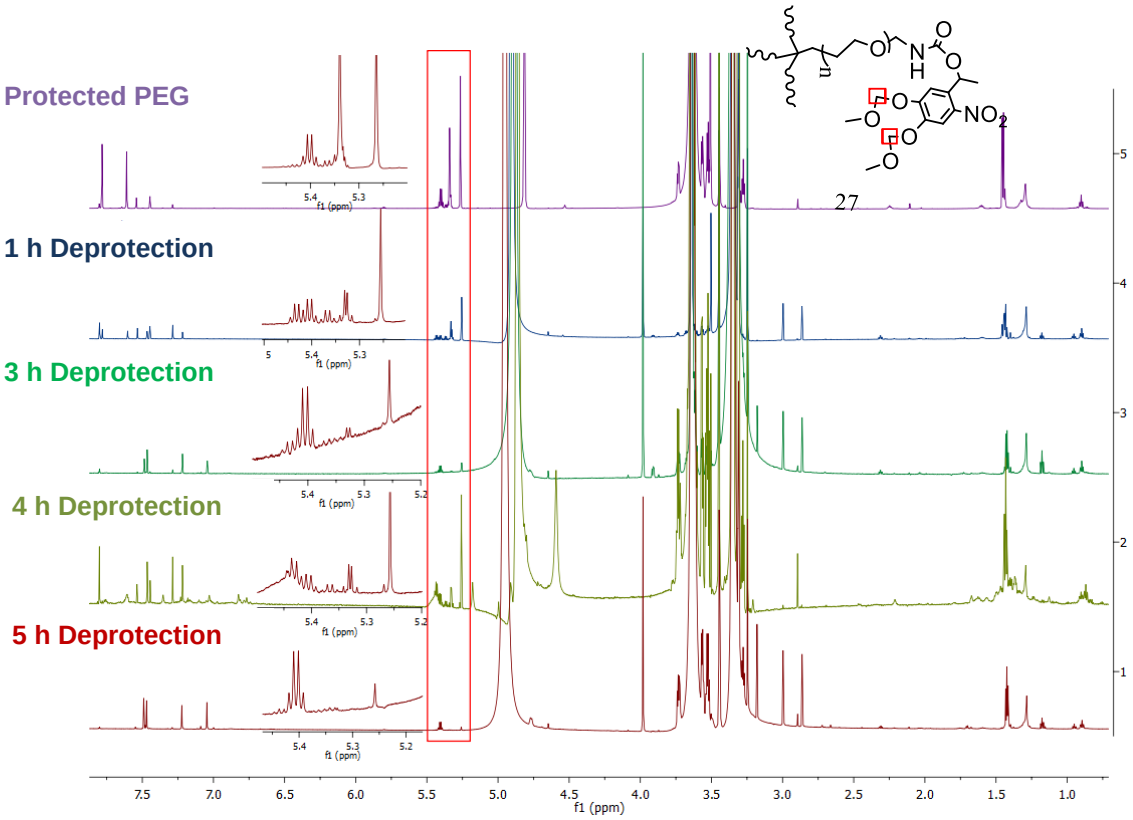


### 3.4.2.4 UV studies

The photoactivity of **28** was monitored by UV spectroscopy measurements of irradiated solutions. The UV spectrum of **28** is shown in Figure 3.26a. It shows a maximum absorbance peak at 425 nm corresponding to the nitrocatechol group. A solution of 0.05 mM 25 in DPBS at pH 7.4 was irradiated with LUMOS 43 lamp LED source at 420 nm with power of 4.7 mW $cm^{-2}$. The absorbance of the peak at 425 nm decreased while a new peak at 320 nm appeared (Figure 3.26a). The spectrum did not show further changes at exposure times longer than 45 min, indicating that the photoreaction was completed. For comparison, the photolysis of PEG-

$(NDop)_4$ was tested under similar conditions.(Figure 3.26b) Light exposure more than 4 h was required for completing photolysis. These results indicate a difference in photoefficiencies between both products higher than 10 fold. They also demonstrate that **28** is a promising polymer for obtaining hydrogels with photocontrolled stiffness.

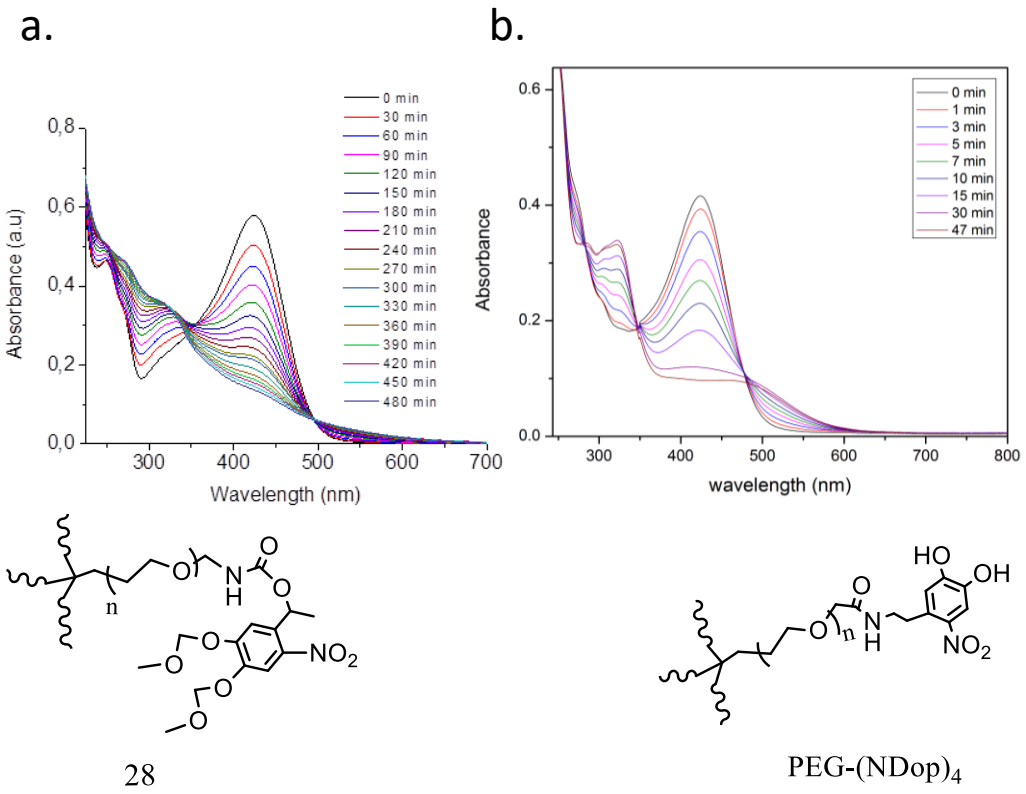


**Figure 3.25** UV absorbance of **28** and PEG-$(NDop)_4$ solutions at PBS buffer at pH 7.4 before and after irradiation at 420 nm with LUMOS 43 lamp LED source at 420 nm with power of 4.7 mW $cm^{-2}$.

### 3.4.2.5 Film Preparation

Thin films of **28** supported on glass substrates were prepared (see appendix for a description of the experimental procedure). Films were prepared and imaged with confocal microscope in order to characterize film thickness. Surfaces with less than 1 μm thickness could be prepared.(Figure 3.27 and 3.28)

a. b. c.

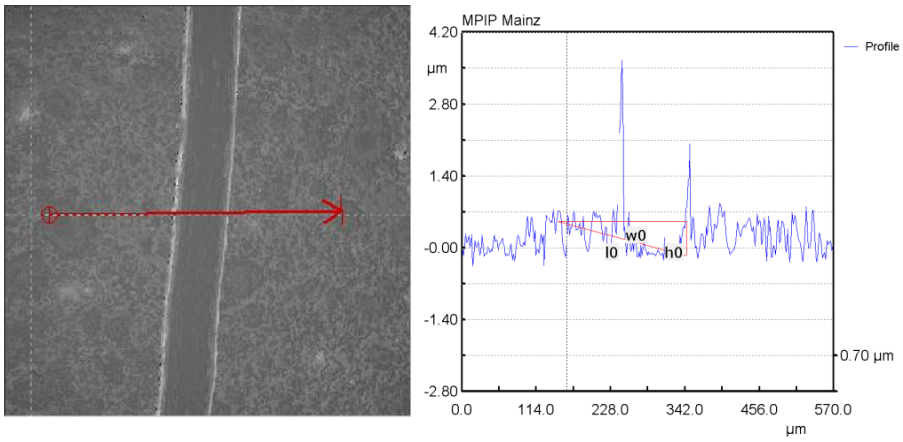


| Profile Values | |
|---|---|
| **Width** | 197.0 µm |
| **Height** | 0.669 µm |
| **Length** | 197.0 µm |

**Figure 3.26** Microscopic image and thickness profile of **28** spin-coated surface.

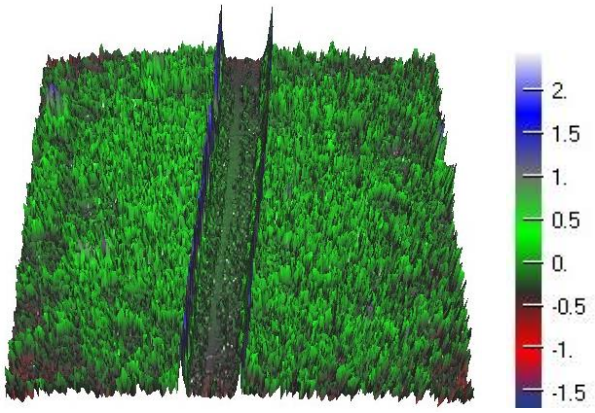


**Figure 3.27** 3D image of **28** spin-coated surface.

### 3.4.2.6 Gelation studies

However, during deprotection reaction of **27**, NMR spectra showed that functionalization of polymer decreased as a consequence of carbamate bond cleavage. Functionalization amount of PEG, **27**, was 55%. However, after 5 h deprotection reaction, functional groups of PEG, **28**, decreased dramatically to 6%. Following hydrogelation experiments with **28** did not result with hydrogel formation. (see appendix for the experimental procedure) Therefore, prepared thin films of **28** were washed off with immersion in water and buffer at pH 7.4.

## 3.5 Conclusions and Outlook

Alginate solutions with appropriate viscosities for forming homogeneous hydrogels were developed. The hydrogels had elastic modulus within the physiologically relevant range (1-30

kPa) which could be controlled by the concentration of the ionic crosslinker, $Ca^{2+}$. Nitr-T+$Ca^{2+}$ complex was introduced into the gels at different concentrations. The resulting hydrogel was exposed upon light at 365 nm. UV spectroscopy analysis of the film showed that Nitr-T photoconverted to its photoproduct. However, rheological experiments showed modest stiffness increase. At 50mM concentration of nitr-T-$Ca^{2+}$ complex, a stiffness increase from 0.4 kPa to 1.2 kPa was measured after full photoconversion of nitr-T. A possible reason for the modest stiffness changes might be the initial crosslinking of Alg by the basal concentration of free $Ca^{2+}$ that did not allow for enough movement of the high molecular weight alginate chains to allow effective crosslinking of the photoliberated $Ca^{2+}$ ions after irradiation.

Nitrocatechol functionalized polymers with improved photosensitivity versus reported nitrodopamine ones were achieved. The synthetic difficulties faced while working with the promising molecule nitronorepinephrine forced a strategy change to 4-(1-hydroxyethyl)-5-nitrobenzene-1,2-diol. The photosensitive PEG derivative **28** was successfully synthesized and the improved photosensitivity vs. the nitrodopamine analog was confirmed in UV spectroscopy. However, gelation experiments in the stated conditions did not result with hydrogel formation due to low degree of functionalization.

## References


1. Engler, A.J., et al., *Matrix Elasticity Directs Stem Cell Lineage Specification.* Cell, 2006. **126**(4): p. 677-689.
2. Rehmann, M.S. and A.M. Kloxin, *Tunable and dynamic soft materials for three-dimensional cell culture.* Soft Matter, 2013. **9**(29): p. 6737-6746.
3. Cui, J.X., et al., *Light-Triggered Cross-Linking of Alginates with Caged Ca2+.* Biomacromolecules, 2013. **14**(5): p. 1251-1256.
4. Shafiq, Z., et al., *Bioinspired Underwater Bonding and Debonding on Demand.* Angewandte Chemie International Edition, 2012. **51**(18): p. 4332-4335.
5. Zhao, H., et al., *o-Nitrobenzyl Alcohol Derivatives: Opportunities in Polymer and Materials Science.* Macromolecules, 2012. **45**(4): p. 1723-1736.
6. Shafiq, Z., et al., *Bioinspired Underwater Bonding and Debonding on Demand.* Angewandte Chemie-International Edition, 2012. **51**(18): p. 4332-4335.
7. Mizrahi, B., et al., *A Stiff Injectable Biodegradable Elastomer.* Advanced Functional Materials, 2013. **23**(12): p. 1527-1533.
8. Lee, C., et al., *Bioinspired, Calcium-Free Alginate Hydrogels with Tunable Physical and Mechanical Properties and Improved Biocompatibility.* Biomacromolecules, 2013. **14**(6): p. 2004-2013.
9. Fullenkamp, D.E., et al., *Mussel-inspired silver-releasing antibacterial hydrogels.* Biomaterials, 2012. **33**(15): p. 3783-3791.
10. Kong, H.J., M.K. Smith, and D.J. Mooney, *Designing alginate hydrogels to maintain viability of immobilized cells.* Biomaterials, 2003. **24**(22): p. 4023-4029.

11. Huebsch, N., et al., *Harnessing traction-mediated manipulation of the cell/matrix interface to control stem-cell fate.* Nature Materials, 2010. **9**(6): p. 518-526.
12. Kong, H.J., K.Y. Lee, and D.J. Mooney, *Decoupling the dependence of rheological/mechanical properties of hydrogels from solids concentration.* Polymer, 2002. **43**(23): p. 6239-+.
13. Cui, J.X., et al., *New Photolabile BAPTA-Based Ca2+ Cages with Improved Photorelease.* Journal of the American Chemical Society, 2012. **134**(18): p. 7733-7740.
14. Fang, Y.P., et al., *Multiple steps and critical behaviors of the binding of calcium to alginate.* Journal of Physical Chemistry B, 2007. **111**(10): p. 2456-2462.

# 4

# Alginate/pAAm Interpenetrating Networks with Long-Term Mechanical Stability at Physiological Conditions

## 4.1 Abstract

The interpenetrating networks (IPNs) offer unusually strong mechanical properties. In that sense, they are promising cell substrates. In this chapter, the long term mechanical stability of alginate/pAAm IPNs were studied in term of crosslinker concentrations of alginate and pAAm, and molecular weight of alginate in physiological conditions. Mechanically stable alginate/pAAm IPNs within physiologically relevant ranges were obtained.

## 4.2 Introduction

Hydrogels are interesting materials for biomedical applications, i.e. as wound dressings, depots for drug delivery, or as scaffolds for cell culture, cell therapies or tissue engineering. Hydrogels show low mechanical stability, typically in the sub-MPa range, though this is not surprising since they are mainly composed of water. For some applications, hydrogels need to present higher mechanical robustness. Hydrogel architectures formed by interpenetrating networks (IPNs) have been demonstrated to be effective towards improving mechanical stability of hydrogels.[1, 2] An IPN consists of two independent polymer networks that can be formed either sequentially or simultaneously. One of the networks is highly crosslinked and provides the mechanical stability, while the other is weakly crosslinked and provides high swelling to the IPN, effectively stretching the rigid network. Two aspects are important in the design of IPNs. The first being that one network is able to maintain the original shape of hydrogel after deformation. The second is that the other network is able to dissipate mechanical energy, which can be achieved with loose or transient crosslinking.[3] As a result of the binary composition, IPNs can show elastic moduli of 0.1-1 MPa, tensile strengths up to 10 MPa, compressive failure stress up to 60 MPa and tearing fracture energies of 100-1000 $J/m^2$.[3] The improved balance of high strength and toughness is based on the contrasting network structures. Accordingly, IPNs can dissipate energy while maintaining high elasticity. [2-4]

One distinct example of IPNs that demonstrate high toughness is the Alginate/pAAm system. It comprises covalently crosslinked, robust poly(acrylamide) (pAAm) interpenetrated with an ionically, reversibly crosslinked alginate (Alg) network.[1] While pAAm provides mechanical stability, alginate network dissipates energy by reversible opening and re-closing ionic crosslinkers upon deformation. It has been demonstrated that Alg/pAAm IPNs can sustain deformations of more than 20 times their initial length without rupturing and can possess fracture toughness values close to natural rubber.[5] Moreover, the starting materials are commercially available and the properties of the network can be tailored easily by tuning the concentration of the bifunctional acrylate crosslinker, the $Ca^{2+}$ concentration and the solid

weight of the polymer.[6-8] These substrates have been proposed as relevant model systems for culturing cells and for the study of cell-materials interactions, in particular in the context of cells response to the mechanical properties of the substrate.[9]

Alg/PAAm IPNs with tunable mechanical properties have been obtained by using different cations for ionic crosslinking.[10] $Na^{+,}$ $Ca^{2+}$, $Sr^{2+}$, $Ba^{2+}$, $Al^{3+}$ and $Fe^{3+}$ ions were tested. Alginate/pAAm hydrogels were initially prepared by polymerization of acrylate monomers in the presence of Alg and monovalent $Na^{+}$. Then, hydrogels were incubated in $Ca^{2+}$, $Sr^{2+}$, $Ba^{2+}$, $Al^{3+}$ or $Fe^{3+}$ ion solutions for ion exchange and ionic crosslinking. Alginate/pAAm hydrogels showed greater elastic modulus when incubated with trivalent cations than with divalent cations. IPN with $Fe^{3+}$ and $Al^{2+}$ showed elastic moduli of 250 and 170 kPa respectively, whereas IPNs with $Ba^{2+}$, $Sr^{2+}$ or $Ca^{2+}$ ions showed elastic moduli of 70, 40 and 50 kPa respectively. Another approach to tune the mechanical strength of Alginate/pAAm hydrogel was by mixing alginates with long and short chains.[11] With this approach systems with an unconventional relationship between toughness and stiffness were generated. A general rule in classical materials is that toughness decreases when stiffness increases. Alginate/pAAm hydrogels prepared with long alginate chains have fracture energies of 9 kJ $m^{-2}$ and elastic moduli of a couple of kPa. In the contrary, Alg/pAAm hydrogels with short and long chains of alginate showed higher fracture energy, ~16 kJ $m^{-2}$, and higher elastic modulus, ~1 MPa.

A recent report describes Alg/PAAm IPNS with different elasticity and stress relaxation response.[12] Alg/pAAm IPNs were prepared using a time dependent crosslinking system. Final concentration of alginate varied from 1.27 to 2.73 wt.% whereas the alginate to acrylamide ratio was 1:10. The final polymer concentration was 14-30 wt.% of the total solution. The solution of alginate and acrylamide was prepared by dissolving the solid content in water. Then, the crosslinker for alginate and initiators for polymerization reaction of acrylamide were added to this mixture. Here, calcium carbonate mixed with D-glucono-δ-lactone (GDL) was used as crosslinker of alginate. GDL hydrolyzes to form an acid to dissolve calcium carbonate and slowly liberate free $Ca^{2+}$ ions. In this way, homogenous alginate crosslinking was achieved. IPNs with tunable mechanical properties were prepared. The mechanical stability of the systems after soaking in PBS, water, or $CaCl_2$ baths for different times was studied. A decrease in elastic modulus and stress-relaxation behavior of the samples was observed after soaking in PBS or water for 72 h. Soaking in 100 mM $CaCl_2$ solution for 72 h led an increase in elastic modulus of the IPN and stress-relaxation. Yet, there was little study on the effect of soaking Alg/pAAm IPN in different solutions of $CaCl_2$ on their stress relaxation behavior.

Studies of long term stability of Alginate/pAAm IPNs under physiological conditions have also been reported.[9] No significant difference in Young's moduli of Alg/PAAm hydrogels after soaking between 1 and 50 days in cell culture conditions was observed. IPNs were first soaked in cell culture medium (containing 1.8 mM $CaCl_2$) up to 50 days and then used to culture D1 mouse stem cells retaining the conditioning medium. Proliferation assays showed a significant reduction in cell proliferation ratio in IPN samples with 0.06 wt% and 0.03 wt% crosslinker and also in Alg samples. At shorter incubation times (17 days) cell proliferation was only lower on the Alg sample. Similar results were observed for metabolic activity. Authors analyzed the concentration of acrylamide in the medium after 40 days incubation by high performance liquid chromatography. 1 mM acrylamide was detected. The decrease in cell proliferation was then associated with the increase of acrylamide in solution. However, no explanation was found for the proliferation decrease in the medium conditioned only with alginate. Similar gels were implanted into rats for 8 weeks. Limited inflammatory response in the tissue surrounding the gels was observed. The continuous fluid flow *in vivo* dilutes the released acrylamide and decreases the local toxicity effects.

In order to understand the mechanical stability of Alg/pAAm IPN, it is worth to look into the mechanical stability of each network individually. With alginate being ionically crosslinked, $Ca^{2+}$ ion exchange with the solution may change crosslinking degree and IPN properties.[13, 14] In fact, treatment of the IPN in physiological conditions has been shown to decrease the compression and shear moduli of Alg/PAAm IPNs.[15] On the contrary, tensile modulus has been shown to increase in the first 7 days and reach equilibrium thereafter. [16]

In this work the mechanical stability of Alg/pAAm IPNs under different experimental conditions is investigated. A significant difference in elastic moduli between as-prepared Alg/pAAm IPN and post-treated Alg/pAAm IPN was observed. The mechanical properties of Alg/pAAm IPNs as a function of the degree of crosslinking in the pAAm network, the $Ca^{2+}$ concentration, the molecular weight of alginate and of post-treatment in physiological conditions and soaking in solutions with different $Ca^{2+}$ concentration were investigated. The elastic modulus of Alg/pAAm IPNs decreased to the level of pAAm prepared with the same amount of crosslinker after soaking in solutions with lower $Ca^{2+}$ concentration than the crosslinking $Ca^{2+}$ concentration. It is demonstrated that by increasing the molecular weight of the alginate, the modulus of the Alg/pAAm hydrogel increases and reaches an equilibrium value upon soaking in solutions of low $Ca^{2+}$ concentration. Finally, by tuning the fraction of long and short chain alginates in the IPN

stable hydrogels with tunable elastic modulus can be achieved. These materials can be then regarded as mechanically stable IPNs for long-term cell culture experiments.

## 4.3 Results and Discussion

### 4.3.1 Preparation and Characterization of Alginate/pAAm IPNs

Alg/pAAm IPN samples were prepared using the procedure at the paper Zang et al. [1] (Figure 4.1a) Morphology of resulting IPN samples was visualized with SEM (Figure 4.1b). Pre-gelled samples were poured into silicon wafer and polymerized putting a glass on top. Images were taken from top and side of hydrogels. SEM micrographs showed that pAAm/Alginate IPN hydrogel had homogeneous, fibrillar morphology.

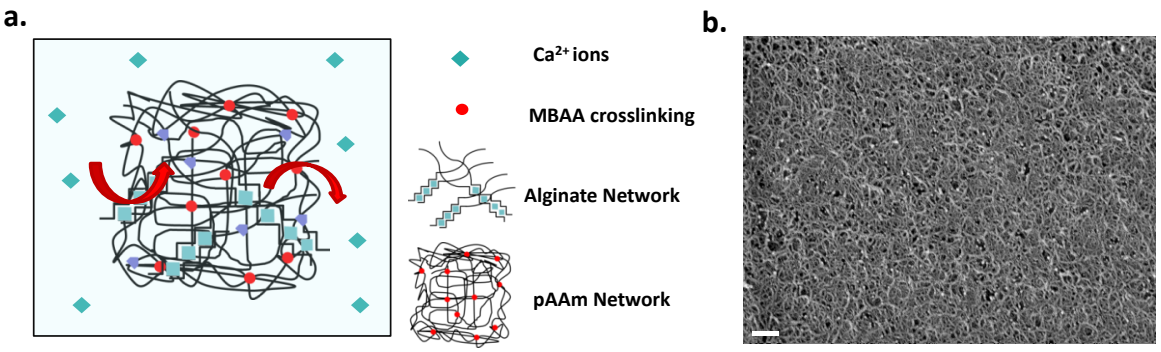


**Figure 4.1: a.** Schematic of diffusion of $Ca^{2+}$ ions from hydrogel to solution and solution to hydrogel. **b.** SEM image of IPN. Image shows homogeneity of the sample. Scale bar is 200 nm.

In the characterization of mechanical properties of IPNs, as first step pAAm hydrogels were prepared with different concentrations of MBAA. Disks of homogeneous pAAm hydrogels with 12 wt.% AAm and increasing concentrations of MBAA crosslinker between 0.015 and 0.9 wt.% were prepared by photoinitiated radical polymerization. The shear modulus of the samples (G) was characterized in a plate-plate rheometer.(Figure 4.2a) Young's modulus, $E$, was calculated from the shear data by the relation $E=2G(1+\nu)$, taking $\nu=0.5$. The Young's modulus of pAAm gels increased from 5 to 80 kPa with increasing MBAA concentration between 0.015 and 0.9 wt.%, as expected consequence of the higher crosslinking degree. Disks of Alginate/pAAm were prepared by adding 2 wt. % alginate concentrations to the polymerization mixture. Curiously, the Alg/pAAm IPNs with MBAA crosslinker concentration below 0.9 wt.% showed similar values of shear modulus to the pAAm networks (Figure 4.2a), whereas IPNs with higher MBAA concentrations (0.9 wt.%) showed a lower shear modulus than the PAAm network. We hypothesize that the presence of the Alg hinders diffusion of the propagating PAAm macroradicals during polymerization, resulting in a lower crosslinking degree of the PAAm

network in the IPN. This effect becomes stronger in the networks with higher crosslinking degrees, and translates in a lower shear modulus.

The obtained IPNs with MBAA concentrations below 0.4 wt. % were transparent. At higher MBAA concentrations, pAAm hydrogels became opaque.(Figure 4.2b) Transparency did not change upon addition of alginate to the polymerization mixture in the IPNs.
The mechanical properties of $Ca^{2+}$ crosslinked alginate hydrogels were measured using a piezorheometer. This allowed to minimize the amount of material (costly Alg medical grade) required for the measurements (Figure 4.2c) vs. the conventional plate-plate rheometer used before. 2 wt.% alginate hydrogels prepared with a concentration of $Ca^{2+}$ ions of 25 mM and 50 mM showed a Young's Modulus of 4 kPa and 13 kPa, reflecting higher mechanical strength with increased ionic crosslinking, Alginate hydrogels prepared in the presence of acrylamide monomer showed a slight decrease in the modulus (3 and 9 kPa respectively). This is likely only associated with the dilution effect due to the increase in the solid fraction of the final gel. Solid fraction increased from 2 wt.% to 14 wt.%.

The mechanical properties of Alg/pAAm IPNs prepared with different concentrations of $Ca^{2+}$ ionic crosslinker were evaluated by tensile testing. Samples with a concentration of 0.3 wt. % MBAA and 1.8 or 25 mM $Ca^{2+}$ concentration were studied. (Figure 5.2d) IPNs with Young's Modulus of 16 and 60 kPa were obtained. Notably, the modulus of the IPN crosslinked with 25mM $Ca^{2+}$ was significantly higher than the modulus of either constituent separately (18 kPa for PAAm with 0.3 wt.% MBBA and 4 kPa for 2 wt.% Alg), reflecting the effect of the double network in strengthening the hydrogel. The addition of alginate crosslinked with 1.8 mM $Ca^{2+}$ had little effect in the PAAm network**.**

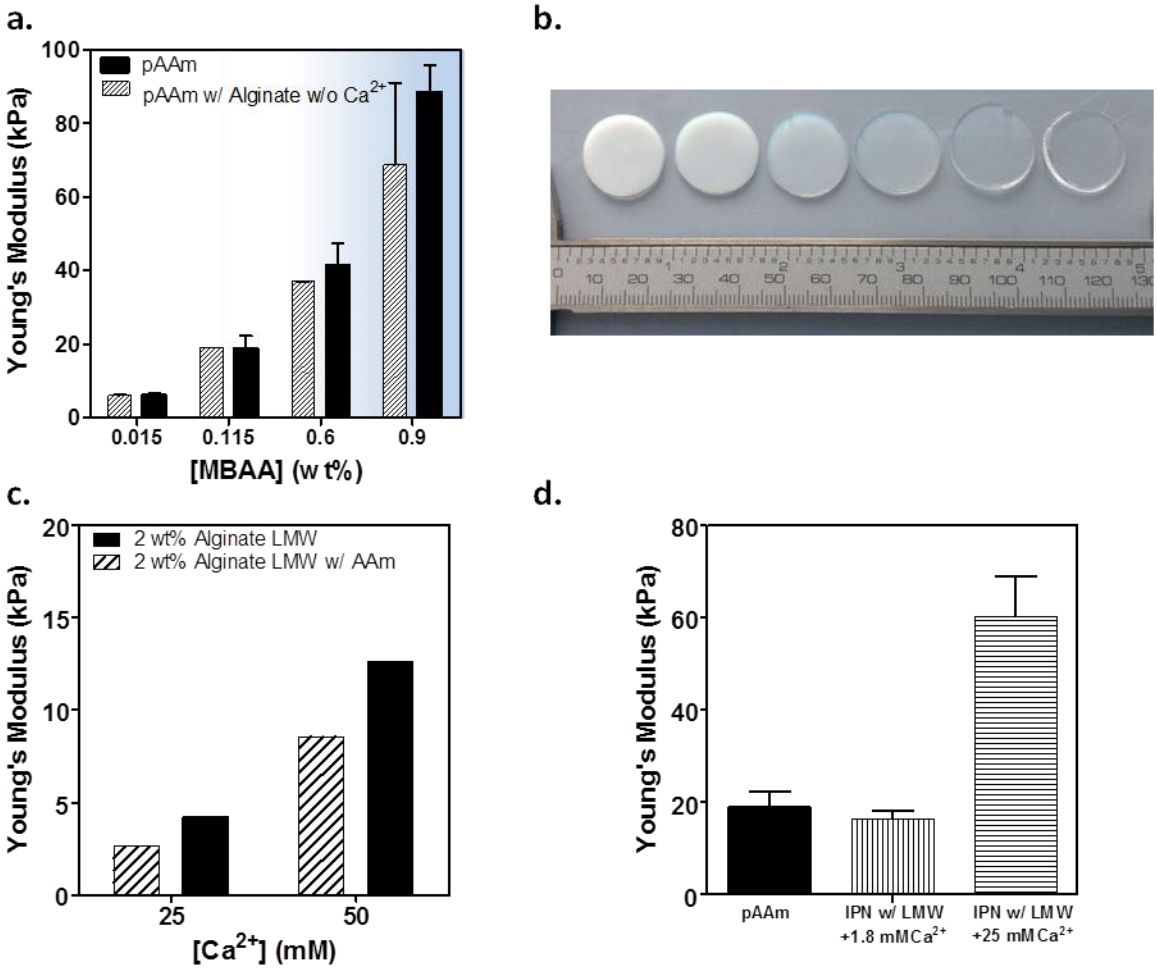


**Figure 4.2**: **a.** Young's moduli and transparency of pAAm with and without uncrosslinked Alginate. Young's modulus was derived from shear modulus obtained in a plate-plate rheometer (n=3, mean ± SD). **b. .** Photographs of pAAm hydrogels with varying MBAA concentrations from 0.9 to 0.1 wt. %. **c**. Young's moduli of Alg LMW with or without uncrosslinked AAm with different concentrations of $CaSO_4$. Measurements were performed with piezorheometer and *E* was derived from shear modulus. **d.** *E* of as-prepared hydrogels with 25 or 1.8 mM $CaSO_4$ and 0.115 wt. % MBAA. *E* was calculated from the linear region of stress vs. strain curves of tensile testing. (n=3, mean ± SD)

### 4.3.2 Effect of Long Term Soaking in Watery Media on The Mechanical Properties of The IPNs

In order to analyze the stability of the IPNs in close-to physiological conditions, the IPN samples with 0.3 wt. % MBAA and 1.8 or 25 mM $CaSO_4$ were soaked in cell culture medium (DMEM, containing 1.8 mM $Ca^{2+}$) at 37 °C up to 4 days.(Figure 4.3) This soaking reproduces typical cell culture conditions in biological experimentation. The modulus of the IPN with 1.8 mM $CaSO_4$ dropped from 16 to 14 kPa after 1 day of incubation and remained constant after 4 days of soaking.(Figure 4.3a) The modulus of IPNs prepared with 25 mM $CaSO_4$ dropped from 60

kPa to 14 kPa after 1 day of incubation, i.e. to the same value of the IPN prepared with 25 mM $CaSO_4$. This result shows that the modulus of IPN samples reaches a constant value after incubation in cell culture medium during in 1 day, independently of the initial concentration of $Ca^{2+}$. In the following experiments, all IPN samples were soaked for 1 day before further experimentation in order to deal with mechanically stable gels.

In order to address if $Ca^{2+}$ concentration of the soaking solution influences the final properties of the IPNs, the samples crosslinked with 25 mM $CaSO_4$, were soaked in DPBS (-,-) or in 25 mM $CaCl_2$ solutions. The mechanical properties after soaking were measured in uniaxial tensile tests.(Figure 4.3b and Table 4.1) Young's modulus decreased from 60 to 13 kPa when the sample was soaked in DPBS (0.4 mM $Ca^{2+}$ from the formulation), and it increased to 125 kPa when the sample was soaked in 25 mM $CaCl_2$ solution. The higher modulus can be attributed to a higher crosslinking of the Alg network, presumably by diffusion of $Ca^{2+}$ ions from soluble $CaCl_2$ to inside the gel during the long soaking time. Under the same conditions, pAAm gels did not show significant changes in the mechanical properties while 2 wt.% Alg samples crosslinked with 25 mM $Ca^{2+}$ showed an increase in Young's modulus from 1.8 to 55 kPa after soaking in 25 mM $Ca^{2+}$ for 1 day.(Table 4.1) The alginate sample after soaking in DPBS was too fragile to measure in tensile tester. These measurements show that the concentration of $Ca^{2+}$ ions in the soaking solution is critical for the mechanical properties of Alg/pAAm IPNs.

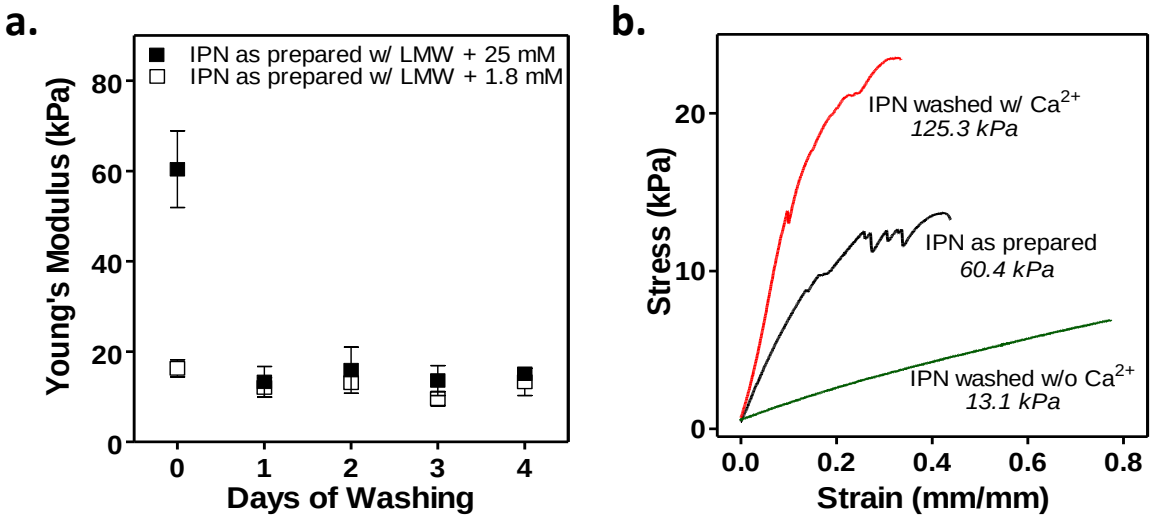


**Figure 3.3:** *Effects of soaking on mechanical properties of IPNs*. **a.** Change in elastic modulus of IPN samples prepared with 25 or 1.8 mM $CaSO_4$ and 0.115 wt. % MBAA as-prepared and after soaking in cell

culture conditions (n=3, mean ± SD) **b.** Stress vs. strain curve of IPN as-prepared or with different soaking conditions.

**Table 4.1** Comparison of Young's moduli of pAAm, alginate and IPN samples in different conditions.

| | Young's Modulus | | |
|---|---|---|---|
| **Sample** | **Without Soaking (kPa) mean ± SD** | **Soaking w/o $CaCl_2$ (kPa) mean ± SD** | **Soaking w/ 25 mM $CaCl_2$ (kPa) mean ± SD** |
| **IPN** | 60.4±8.5 | 13.1±2.2 | 125.3±68.7 |
| **pAAm** | 18.8 ±3.4 | 14.0±7.1 | --- |
| **Alginate** | 1.8±0.8 | --- | 55.0±11.8 |

In order to investigate if an increased initial $Ca^{2+}$ concentration in the IPN affects stability during soaking, IPN samples with 50 mM $Ca^{2+}$ were also prepared.(Figure 4.4a) In this experiment the concentration of MBAA was 0.015 wt.%. The Young's modulus of the IPN dropped from 20 to 1.8 kPa after 1 day of soaking in cell culture medium. The Young's Modulus of pAAm gel without Alg was 2.4 kPa and remained unchanged after soaking under the same conditions. In conclusion, the initial concentration of $Ca^{2+}$ in the gel does not play a major role for the mechanical properties of the IPN after soaking in watery solutions.

### 4.3.3 Tuning IPN Mechanical Properties by Changing the Concentration and Molecular Weight of Alginate Component

Kong et al.[17] reported that the mechanical properties of alginate hydrogels can be improved using higher concentrations of alginate or alginates with higher molecular weight. Taking into account this information, we tested if an increase in the concentration of alginate lead to an increase in the modulus and possibly higher stability of the hydrogels during long term soaking. (Figure 4.4b) IPNs prepared with 4 wt.% Alg and 25 or 50 mM CaSO4 showed Young's Modulus of 2.6 and 38 kPa respectively. After 1 day soaking in cell culture medium, values of ~1 and 2 kPa were obtained. These values are similar to those of PAAm network with the same AAm/crosslinker concentrations. These results demonstrate that an increase in the Alg concentration in the IPN does not prevent the decrease in Young's modulus to a few kPas after long term soaking.

To test the effect of molecular weight, IPNs with alginate of $2.9x10^5$ (denoted as Alg LMW) or $5.7x10^5$ g $moL^{-1}$ (denoted as Alg HMW) were prepared. Note that Alg LMW was used in experiments previously described due to the easier mixing as a consequence of lower viscosity. Alg LMW was obtained from Alg HMW by $\gamma$-irraditation.(Table 4.2) IPN samples with 12 wt.%

pAAm, 2 wt.% Alg (LMW or HMW) and 50 mM $CaSO_4$ were prepared. Initial Young's modulus of 38 kPa and 113 kPa for LMW and HMW dropped to ~1 and 30 kPa respectively after 1 day soaking in cell culture medium.(Figure 4.4c) This result illustrates that IPNs with HMW Alg can be used to obtain hydrogels with higher mechanical properties after soaking, up to 30 kPa, which is in the upper range of physiological relevance. However, the softening upon soaking (from 130 kPa to 30 kPa in this case) seems to be an unavoidable issue in Alg/PAAm IPNs.

Finally, IPNs including mixtures of Alg HMW and Alg MMW were prepared and their stability before and after soaking was tested.(Figure 4.4d). As the weight fraction of HMW Alg increased in the IPN hydrogel, the elastic moduli increased before and after 1 day soaking. IPNs with tunable and stable elastic moduli between 15 and 30 kPa were obtained. It should be noted that samples in Figure 4d were prepared with a different batch of alginate. Although alginate was commercial and purchased from the same company, *E* of IPN prepared with 100% Alg HMW and 50 mM $Ca^{2+}$ slightly varied from the one in Figure 4.4c.

**Table 4.2** Molecular weight of alginate before and after ɣ-irradiation.

| Alginate Type | Mn (g/mol) | Mw (g/mol) |
|---|---|---|
| Alg HMW | 467000 | 1232000 |
| Alg MMW | 188000 | 83000 |
| Alg LMW | 65000 | 17000 |

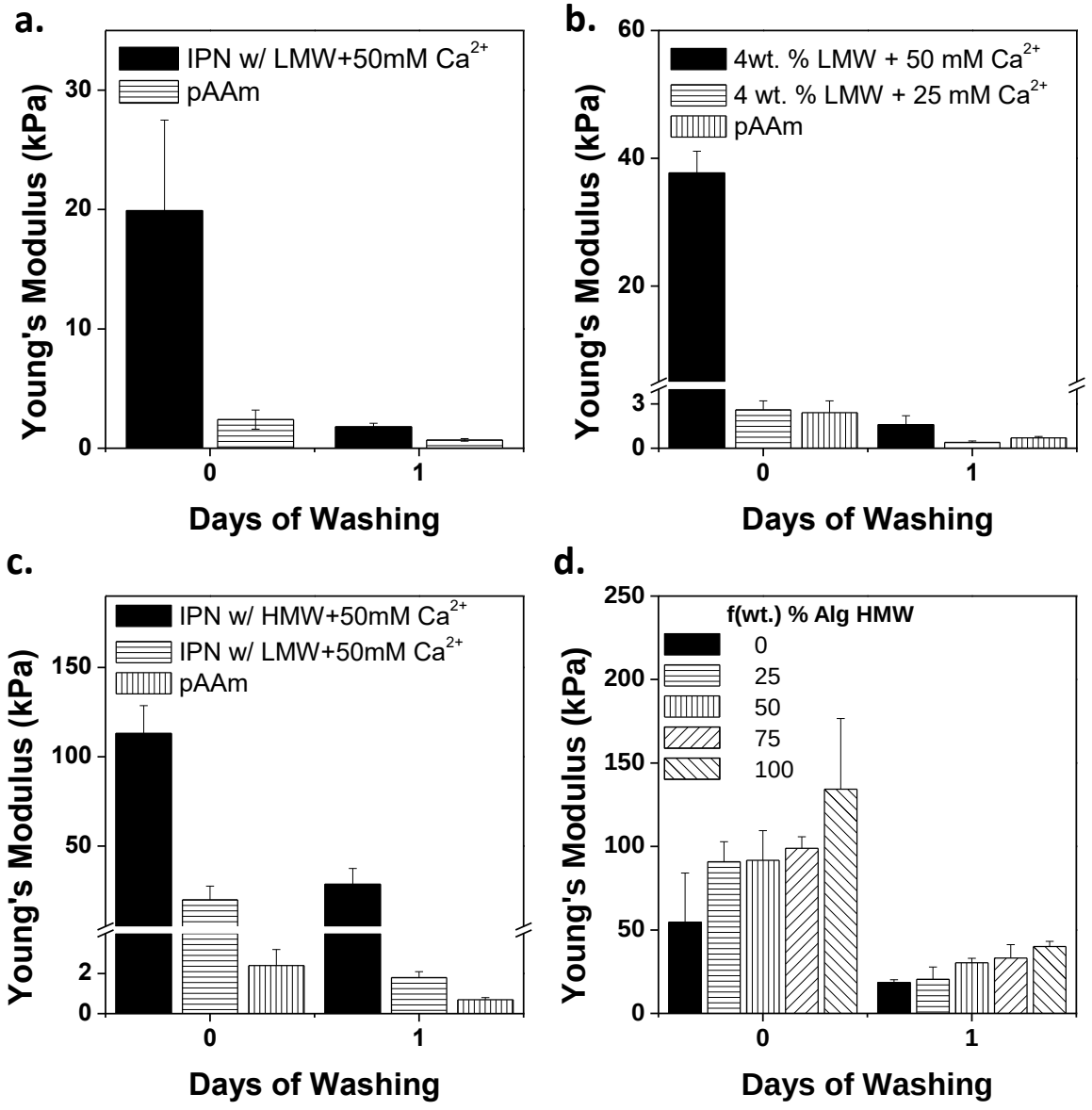


**Figure 4.4:** *Tuning the modulus by the alginate network.* **a.** Change in stiffness of pAAm with 0.015 wt. % MBAA and IPN sample prepared with 50 mM $CaSO_4$ and 0.015 wt. % MBAA as-prepared and after soaking in cell culture conditions (n=3, mean ± SD). **b.** Change in stiffness of IPN with increased alginate content, 4 wt. %. pAAm sample was prepared with 0.015 wt. % MBAA and IPN samples were prepared with 50 and 25 mM $CaSO_4$ and 0.015 wt. % MBAA and soaked in cell culture conditions (n=3, mean ± SD).**c.** Comparison of stiffness of IPN with HMW and LMW alginate (n=3, mean ± SD). Concentration of MBAA was used as 0.015 wt. % MBAA in pAAm and IPN. Concentration of $CaSO_4$ was 50 mM. **d.** Change in stiffness of IPN HMW to IPN with MMW alginate prepared with 50 mM $CaSO_4$ 0.015 wt. % MBAA and soaked in cell culture conditions.

The decrease in the mechanical stability of the IPN during soaking can be a consequence of the diffusion of $Ca^{2+}$ ions outside of the hydrogel to the solution, or to the diffusion of alginate chains out of the IPN during soaking. We evaluated the solid weight of IPN hydrogels prepared with

various fractions of LMW and HMW alginate.(Figure 4.5) However, weight loss did not follow any systematic trend. Sample preparation method for dry weight determination needs to be optimized for reliable data.

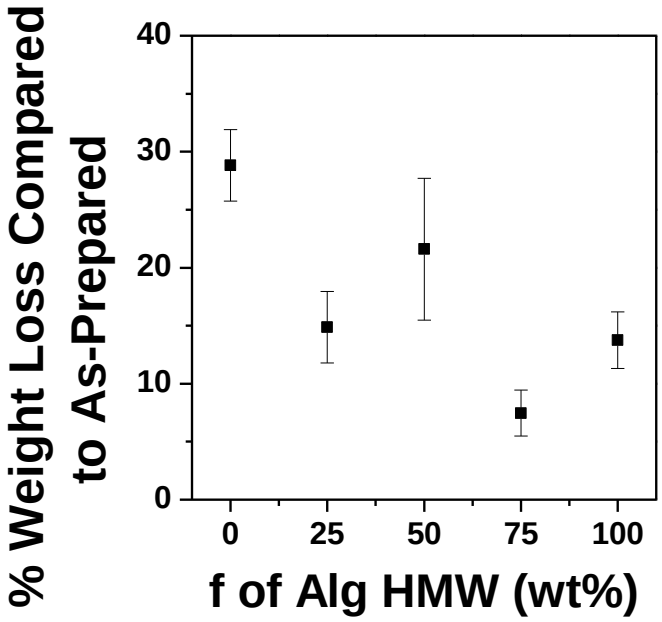


**Figure 4.5:** *Change in weight after 1 day soaking***.** Decrease in solid weight after 1 day in cell culture conditions of IPNs of Alg HMW mixed with Alg MMW was calculated compared to solid weight of as-prepared samples (n=3, mean ± SD). IPN samples were prepared with 50 mM $CaSO_4$ and 0.015 wt. % MBAA and different weight fractions of Alg HMW and Alg MMW.

## 4.4 Conclusion

IPN hydrogels comprised of polyacrylamide and alginate were prepared and mechanically characterized. Gels with different crosslinker concentrations and including alginates of two different molecular weights were prepared. Young's modulus of as-prepared IPN samples was increased with the $Ca^{2+}$ concentration that increased ionic crosslinking of the Alg network. However soaking of gels in cell culture medium conditions ($Ca^{2+}$ concentration 0.4 mM) significantly decreased the modulus of the hydrogel within hours. Samples prepared with higher alginate concentrations led to higher Young's modulus. Yet after soaking in cell medium, the modulus dropped. A possibility to increase the post-soaking modulus of Alg/pAAm hydrogels was using alginate with higher molecular weight. Additionally, using various fractions of different molecular weights of alginate provides a route to precise control of the post-treatment elastic modulus of IPN hydrogels in constant ionic concentration solutions.

## References


1. Sun, J.Y., et al., *Highly stretchable and tough hydrogels.* Nature, 2012. **489**(7414): p. 133-136.
2. Gong, J.P., et al., *Double-network hydrogels with extremely high mechanical strength.* Advanced Materials, 2003. **15**(14): p. 1155-+.
3. Zhao, X.H., *Multi-scale multi-mechanism design of tough hydrogels: building dissipation into stretchy networks.* Soft Matter, 2014. **10**(5): p. 672-687.
4. Chen, Q., et al., *Engineering of Tough Double Network Hydrogels.* Macromolecular Chemistry and Physics, 2016. **217**(9): p. 1022-1036.
5. Dragoni, E. and G. Medri, *Fracture toughness evaluation of natural rubber.* Theoretical and Applied Fracture Mechanics, 1988. **10**(1): p. 79-83.
6. Wen, J.H., et al., *Interplay of matrix stiffness and protein tethering in stem cell differentiation.* Nature Materials, 2014. **13**(10): p. 979-987.
7. Chaudhuri, O., et al., *Substrate stress relaxation regulates cell spreading.* Nature Communications, 2015. **6**.
8. Chaudhuri, O., et al., *Hydrogels with tunable stress relaxation regulate stem cell fate and activity.* Nature Materials, 2016. **15**(3): p. 326-+.
9. Darnell, M.C., et al., *Performance and biocompatibility of extremely tough alginate/polyacrylamide hydrogels.* Biomaterials, 2013. **34**(33): p. 8042-8048.
10. Yang, C.H., et al., *Strengthening Alginate/Polyacrylamide Hydrogels Using Various Multivalent Cations.* ACS Applied Materials & Interfaces, 2013. **5**(21): p. 10418-10422.
11. Li, J.Y., et al., *Hybrid Hydrogels with Extremely High Stiffness and Toughness.* Acs Macro Letters, 2014. **3**(6): p. 520-523.
12. Fitzgerald, M.M., et al., *Tunable Stress Relaxation Behavior of an Alginate-Polyacrylamide Hydrogel: Comparison with Muscle Tissue.* Biomacromolecules, 2015. **16**(5): p. 1497-1505.
13. Zhang, X.Z., D.Q. Wu, and C.C. Chu, *Synthesis, characterization and controlled drug release of thermosensitive IPN-PNIPAAm hydrogels.* Biomaterials, 2004. **25**(17): p. 3793-3805.
14. Mandal, B.B., S. Kapoor, and S.C. Kundu, *Silk fibroin/polyacrylamide Semi-interpenetrating network hydrogels for controlled drug release.* Biomaterials, 2009. **30**(14): p. 2826-2836.
15. LeRoux, M.A., F. Guilak, and L.A. Setton, *Compressive and shear properties of alginate gel: Effects of sodium ions and alginate concentration.* Journal of Biomedical Materials Research, 1999. **47**(1): p. 46-53.
16. Drury, J.L., R.G. Dennis, and D.J. Mooney, *The tensile properties of alginate hydrogels.* Biomaterials, 2004. **25**(16): p. 3187-3199.
17. Kong, H.J., K.Y. Lee, and D.J. Mooney, *Decoupling the dependence of rheological/mechanical properties of hydrogels from solids concentration.* Polymer, 2002. **43**(23): p. 6239-+.

# 5

# 3D Printing of Alginate Scaffolds with Tunable Mechanics

## 5.1 Abstract

The morphology of biological tissues varies depending on the tissue. Therefore, mechanically tunable biomaterials with desirable morphology are needed. In this chapter, mechanically tunable 3D alginate scaffolds were prepared by 3D printing technique. The mixtures of alginate and gelatin were used as the ink. While alginate is used to control mechanical properties, gelatin provided cell adhesive cures to be used in biomedical applications. The printing parameters were studied for fast printing and mechanical stability. The windows for printability using different compositions, temperature and ionic concentration of the printing bath were studied. Alginate/gelatin 3D scaffolds with enhanced stability in watery media were printed in the chitosan/$Ca^{2+}$ printing bath. Chitosan formed a polyelectrolyte complex with alginate on the outer part of the alginate/gelatin scaffold. It formed a shell to protect and encapsulate cells inside the scaffolds. This printing strategy led printing biocompatible alginate/gelatin scaffolds with high fidelity.

## 5.2 Introduction

3D printing for biomedical applications is a fast growing-field.[1] New printing technologies and instruments are under continuous development.[2] One recent approach is the development of the core/shell printing method. It allows the coaxial deposition of two component, with printed strands containing different inner (core) and outer (shell) properties.[3, 4] Materials with different mechanical properties can be combined at the core and at the shell to enhance the mechanical strength of the final material. Moreover, drugs can be included in the ink formulations and controlled released independently, from the core and/or from the shell. Alternatively, the shell material can be designed to encapsulate cells and protect cells in the tubular core, to be used in biomedical applications.

The first application of core/shell extrusion based 3D bioprinting method was reported by Moroni and co-workers.[5] Polymer melts with different viscosities, poly[(ethylene oxide) terephthalate-co-poly(butylene) terephthalate] and poly(ethylene glycol) segments were used. The one with higher viscosity was encapsulated inside the polymer melt with low viscosity. Core/shell microfibers with clinically relevant sizes, a couple of micrometers and physicochemical properties were manufactured. In a different study, core/shell microfibers of ECM protein containing cells/ calcium alginate hydrogels were deposited to construct 2- and 3-dimensional structures.[6]

Alginate is one of the most widely used biopolymer in biomedical applications. It can form self-supporting structures when crosslinked with $Ca^{2+}$ ions or chitosan.[7, 8] After crosslinking, the structures keep their morphology. In order to use alginate printed scaffolds for supporting cell growth, the alginate molecules have to be supplemented with bioadhesive cues.[9] For this purpose, cell adhesive peptide sequences can be covalently attached to the alginate chain.[10] Another option is to co-print an extracellular matrix protein with alginate, like collagen,[11] fibrin[12] or fibrinogen[13]. The ECM proteins contain adhesive sequences and favor attachment of cells to the alginate construct. Gelatin, the hydrolyzed form of collagen, is the most commonly used for this purpose. It has excellent biocompatibility. It is a liquid at physiological temperature and forms gels at temperatures below ~30 °C.

Different literature reports describe different printing conditions and final properties of printed alginate based structures. Luo et al. enhanced the mechanical properties of alginate/gelatin scaffold by covalently crosslinking gelatin in a two-step deposition method.[14] First alginate/gelatin scaffolds were extruded on a plate at room temperature. Then, the scaffold was incubated in $CaCl_2$ solution to crosslink alginate. A second incubation in a solution of *N*-(3-dimethylaminopropyl)-*N′*-ethylcarbodiimide, EDC, and *N*-hydroxysuccinimide, NHS, allowed covalent crosslinking of the amino acids in gelatin with the carboxylic acids of alginate and gelatin. After the crosslinking process, the scaffold was mechanically stable. Cells seeded on the scaffold were able to migrate and colonize the inner parts of it. In a different strategy, $Ca^{2+}$ ions were simultaneously co-deposited with alginate.[15] The alginate treads were printed into 3D scaffolds and incubated in chitosan solution. Chitosan is a positively charged polycation that can form a polyelectrolyte complex with the alginate polyanion. Further enhancement of the mechanical stability was achieved by crosslinking with EDC and genipin.

In this chapter, the two methods described in the literature were combined in one to develop an alginate based ink which that is mechanically stable and favors cell attachment. For fast printing, the ink was deposited directly in a crosslinking solution. The ink formulation was a mixture of alginate and gelatin. Alginate hydrogel provides mechanical support and gelatin offers cell adhesive cues and facilitates printability. The extrusion of alginate/gelatin into a $Ca^{2+}$/chitosan solution allowed fast and stable crosslinking of the alginate and lead to high fidelity printing of microsized threads and 3D scaffolds.

## 5.3 Results and Discussion

### 5.3.1 3D printing of alginate/gelatin scaffolds

The first step in the 3D printing of hydrogel precursors is the determination of the printing conditions. The viscosity of the ink and the solidification mechanism and kinetics are the most relevant parameters. The ink should be fluid enough to allow flow during extrusion, but viscous enough to be deposited as a continuous line without significant loss. The solidification mechanism should be fast enough to maintain the shape of the extruded thread and keep shape fidelity of the printed structures.

In a first approach, printed alginate threads were crosslinked by mixing a 2 wt. % alginate solution with 2 mM $CaSO_4$ to form soft hydrogel threads with storage modulus of ~50 Pa (Data not shown). (For the properties of alginate, see Appendix 5.1.1) The threads were deposited using 70-150 kPa pressure with a metal nozzle with a diameter of 150 µm. However, threads were inhomogeneous and contained liquid-like and gel-like areas. The soft hydrogel was not able to flow properly and was squeezed out of the needle during printing. In a second attempt, the 2 wt.% alginate solution was deposited on glass slides at a speed of 10-20 mm/s and subsequently crosslinked by addition of a drop of 10-50 mM $CaCl_2$ solution after each printed layer. The $CaCl_2$ solution was removed with a micropipette before deposition of the next layer. However, although the shape fidelity with the width of 300 µm was conserved at the first layer (on the glass substrate), the thread spread and lost shape in subsequent ones.(Data not shown) A similar approach was repeated with a 8wt% gelatin and 2 wt.% alginate mixture. The printing cartridge was heated to 40 °C for liquefying gelatin, and the printing plate was cooled to 10 °C for fast gelation of the gelatin. The ink was deposited with a metal nozzle with the diameter of 200 µm at 70-100 kPa pressure and 10-20 mm/s speed. In the first layer, gelatin/alginate was deposited with the width of 300 µm successfully due to fast gelation of gelatin on the cooled glass slide at 10 °C.(Figure 5.1a) However, on the subsequent layers, the cooling effect was slower and the gelatin/alginate spread and shape fidelity was lost.

In a third approach, a 2 wt.% alginate solution was directly deposited into a 5 mM $CaCl_2$ bath at room temperature. The expected fast crosslinking of alginate in contact with the $CaCl_2$ solution was expected to provide enough mechanical strength to the alginate to form a 3D structure. The alginate threads were successfully extruded, though they could not be retained on the glass substrate but floated in the $CaCl_2$ solution. To solve this problem, the glass surface was coated with chitosan solution. In this way, the ionic interaction between chitosan and alginate was

expected to stabilize the printed threads on the substrate. 2 wt. % alginate solution was deposited in 5 mM $CaCl_2$ solution on chitosan coated glass surfaces with a pressure of 70-100 kPa and a speed of 10-20 mm/s. 3 layers of alginate threads could be successfully printed in an area of 1 cmx1 cm with high fidelity and remained attached to glass.(Figure 5.1b)

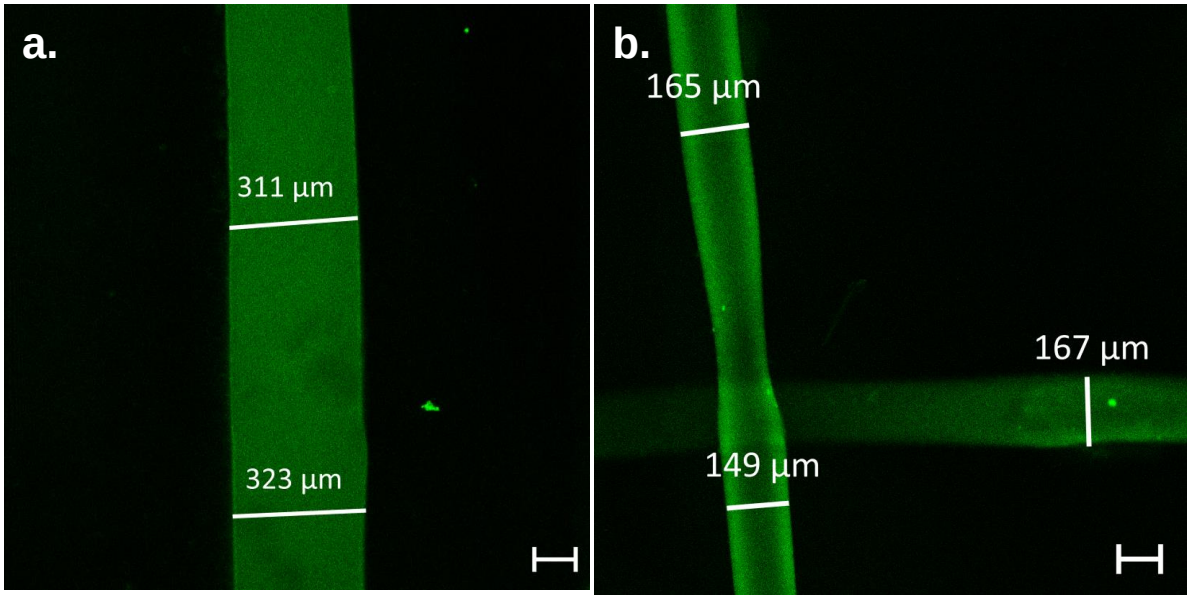


**Figure 5.1** Confocal microscope images of **a.** alginate/gelatin on the 1st layer and **b.** the alginate threads on the 3rd and 2nd layers.

The deposition of 8wt.% gelatin+2wt.% alginate threads in a 5 mM $CaCl_2$ bath was also tested using chitosan coated glass surfaces at room temperature. The fast crosslinking of alginate in the $CaCl_2$ solution was complemented by the gelation process of gelatin at room temperature. However, the gelation of gelatin occurred so fast that the tip of the cartridge immediately clogged. To solve this problem, the temperature of the $CaCl_2$ bath was increased to 35 °C and the solution was heated in the cartridge to 45°C. In this way, gelation of gelatin was slowed down, or even inhibited at 35 °C. 8wt.% gelatin+2 wt.% alginate solution heated to 45°C in the cartridge was printed in 5 mM $CaCl_2$ solution on chitosan coated glass slide at 35 °C. The deposited threads formed structures with high fidelity. Scaffolds of three layers were successfully printed over 1 cmx1cm areas. The disadvantage of this system is the uncontrolled release of gelatin from the printed structures due to deposition at 35 °C in the $CaCl_2$ bath. This issue was solved by adding chitosan to the crosslinking solution. It is expected that chitosan would form a polyelectrolyte complex on the outer surface of the alginate/gelatin threads during printing, and prevent the release of gelatin. Moreover, the chitosan could behave like a “glue” joining alginate/gelatin threads of consecutive layers via ionic interactions. Varying

concentrations of chitosan were added to $CaCl_2$ solution. At high concentrations of chitosan ($1x10^{-2}$ and $5x10^{-3}$ wt.%), alginate/gelatin scaffolds formed opaque structures due to strong interaction between chitosan and alginate and gelatin.(Figure 5.2a and 5.3a) However, scaffolds turned to transparent after soaking them in PBS for more than 1 day.(Figure 5.2d, 5.2g, 5.3d, and 5.3g) Similar phenomena was observed for lower concentration of chitosan, $5x10^{-4}$ wt.% and $2x10^{-4}$ wt.%.(Figure 5.2b and 5.3b) Scaffolds printed in high concentration of chitosan, structures were transparent after 1 day of soaking in DPBS. (Figure 5.2e, 5.2h, 5.3e and 5.3h) In the printing of alginate/gelatin scaffolds without any chitosan in printing solution, the scaffolds were transparent.(Figure 5.2c, 5.2f, 5.2i, 5.3c, 5.3f, and 5.3i) The most striking difference between scaffolds was the high fidelity of the structures and thus, the difference in swelling capacity. Fidelity is defined with the variation in the width of the printed structures. The average width of the printed threads calculated from the microscopic images of the scaffolds.(Figure 5.4) 3D printing of the scaffolds resulted in a small variation in the width.

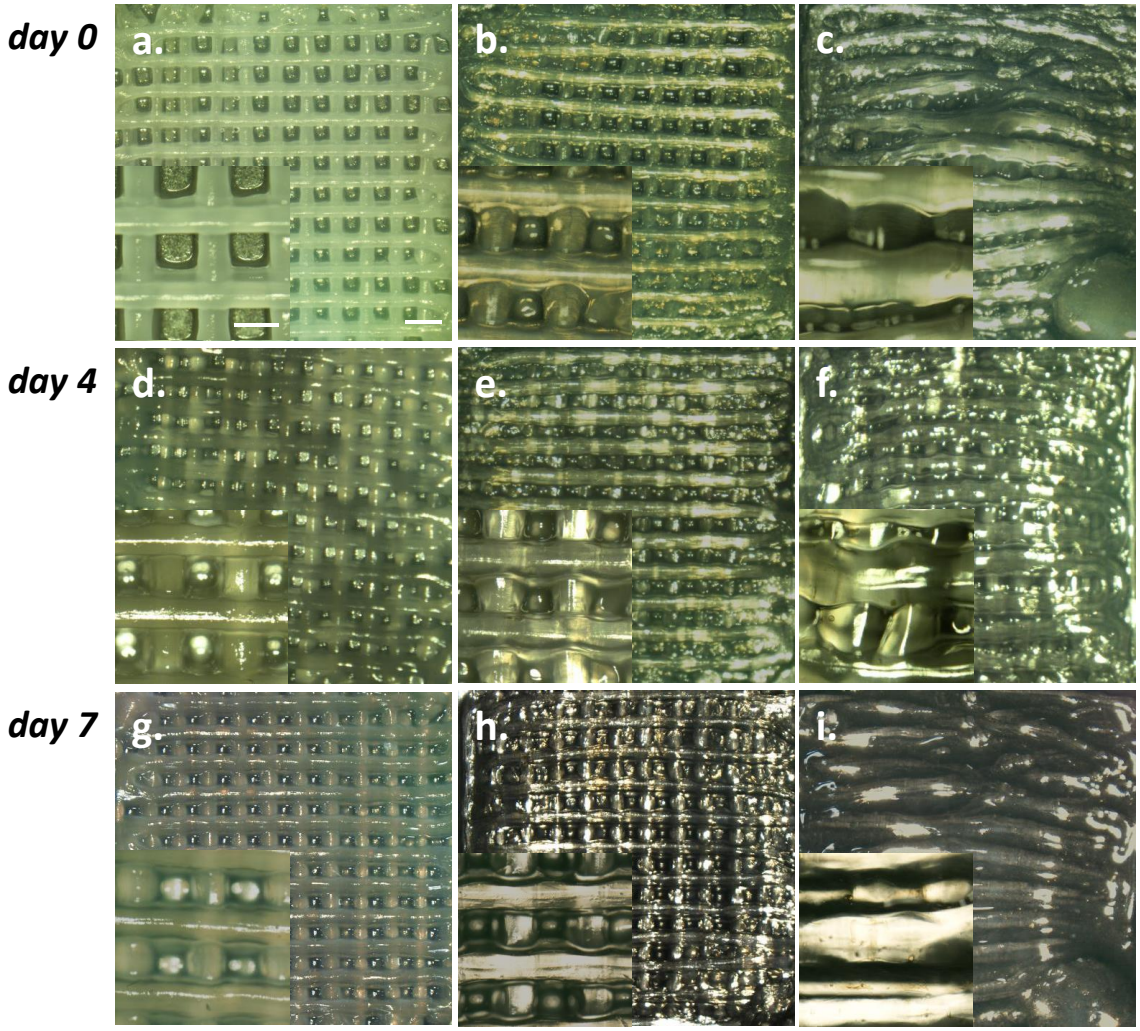


**Figure 5.2** *Effect of chitosan addition to printing solution.* 3D printed alginate/gelatin scaffolds in solutions of **a.** $5x10^{-3}$ wt.% chitosan+5 mM $CaCl_2$ **b.** $5x10^{-4}$ wt.% chitosan+5 mM $CaCl_2$ and **c.** 5 mM $CaCl_2$ with scale of 500 µm between a-c and 1 mm between d-f. Images at day 0 were taken 2 h after incubation in printing solutions. Then, printing solution was removed and replaced with DPBS.

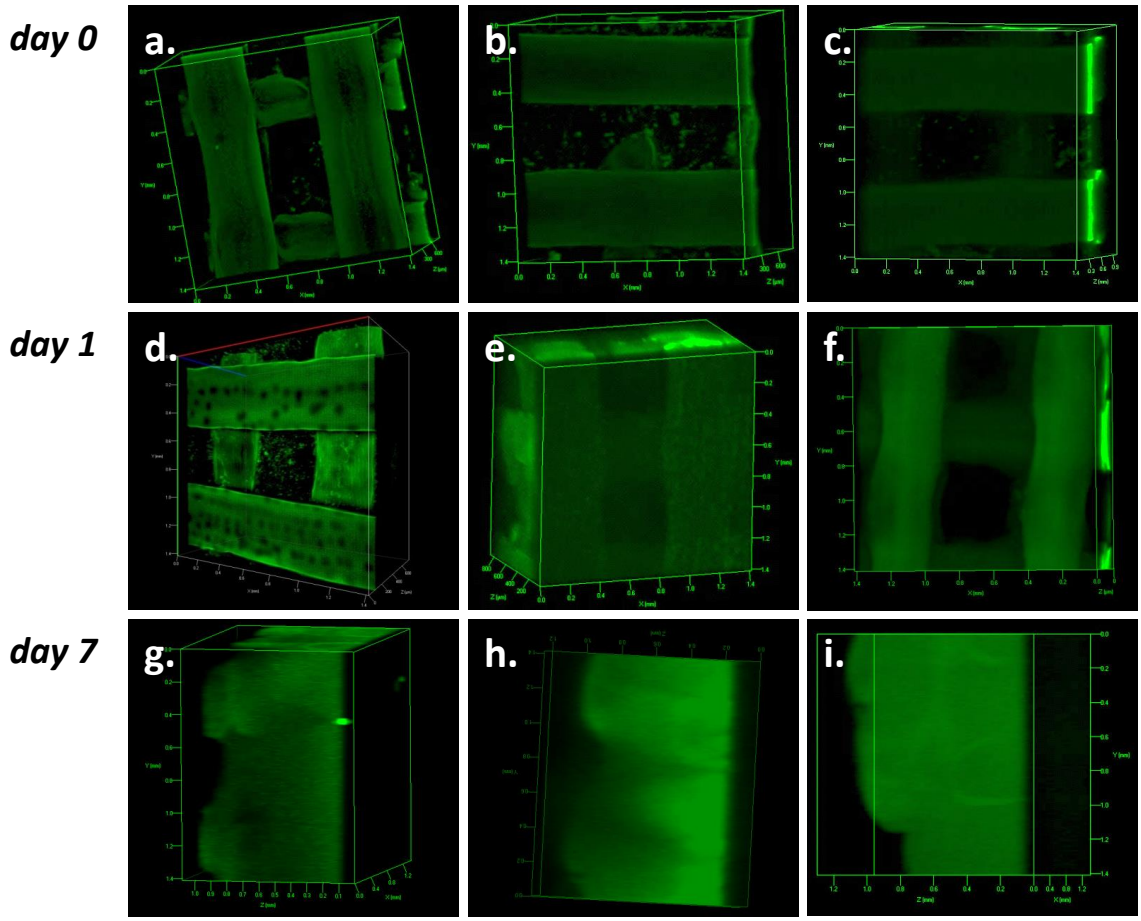


**Figure 5.3** *Effect of chitosan addition on swelling of scaffolds. Confocal* microscope images of 3D printed alginate/gelatin scaffolds in solutions of **a.** 0.005 wt.% chitosan+5 mM $CaCl_2$ **b.**0.0005 wt.% chitosan+5 mM $CaCl_2$ and **c.** 5 mM $CaCl_2$ with scale of 500 µm between a-c and 1 mm between d-f. Images were taken 4 days after incubation in PBS following 1 day incubation printing solutions.

### 5.3.2 Comparison of Degree of Swelling

The swelling degree of the printed structures was measured by imaging the scaffolds with confocal microscopy. The width of the printed structures before and after soaking in PBS was imaged and compared.(Figure 5.4) Fluorescein was conjugated to the alginate for this purpose. Since the scaffolds printed in high concentration of chitosan were opaque, only the width at the first layer was used to compare. (Figure 5.4a) At high concentration of chitosan, $5x10^{-3}$ wt.%, the width of the threads were ~370 µm when it was deposited using a nozzle with the diameter of 200 µm. After soaking in PBS, the width increased to ~400 µm. The increase in width after 7 days soaking in PBS is attributed to the removal of chitosan from the outer surface of alginate/gelatin scaffold. As a result, higher water absorption might occur. The scaffolds printed in $5x10^{-4}$ wt.% chitosan solution had no significant width changes before or after soaking in

PBS. The scaffolds deposited into $CaCl_2$ solution (no chitosan) swell so much that the borders of the threads were not distinguishable anymore. It should be noted that the scaffolds were deposited on the glass coated with chitosan. Therefore, the similarity in the width of the threads of the first printed layer was not unexpected.

Since the scaffolds printed with high concentration of chitosan were opaque, it was not possible to analyze the width of the threads at second and third layers with confocal microscope. Therefore, the width of the threads at the last, 4$^{th}$, layer was analyzed with optical microscope before and soaking in PBS.(Figure 5.4b) For the scaffolds printed in 5x10$^{-3}$ wt.% chitosan, the width of the lines increased slightly as it was observed in the first layer. The scaffolds printed in 5x10$^{-4}$ wt.% chitosan had no difference in the width of the threads. The width of the scaffolds printed without chitosan was almost 50% higher than the ones printed with chitosan.

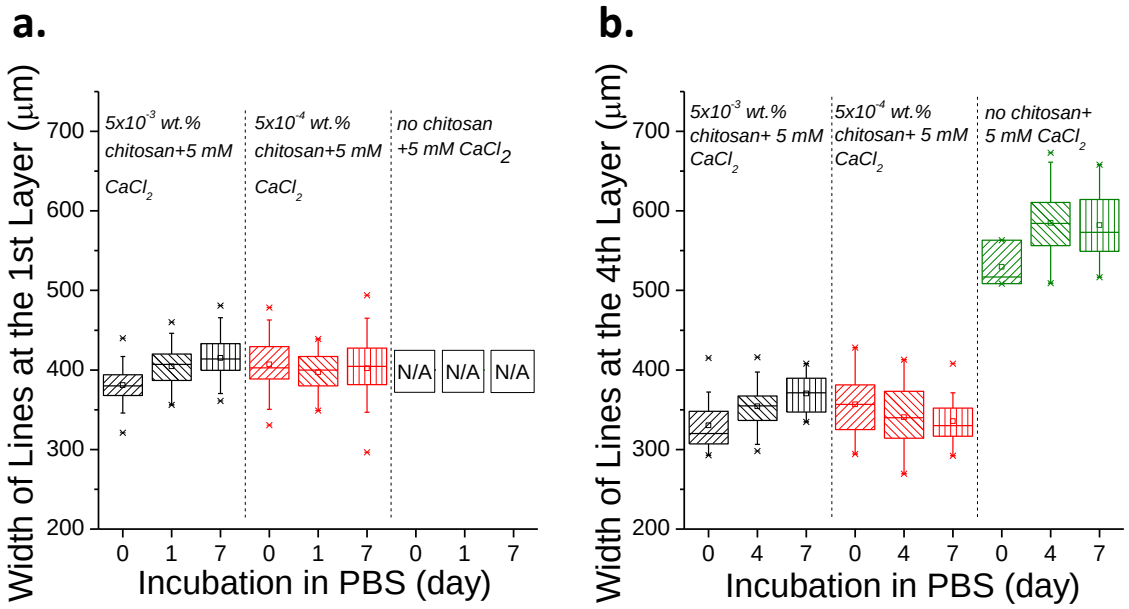


**Figure 5.4** *Effect of swelling on the width of lines.* Width of lines at the last layer of alginate/chitosan scaffolds printed in 5x10$^{-3}$ wt.% chitosan and 5 mM $CaCl_2$, 5x10$^{-4}$ wt.% chitosan and 5 mM $CaCl_2$, and 5 mM $CaCl_2$ before and after incubation in PBS. **a.** The width of the lines at the first layer analyzed with confocal microscope. **b.** The width of the lines at the last, 4$^{th}$, layer analyzed with optical microscope. Three replicates of each scaffold type were used to make statistics. At least 5 points were measured from each thread and at least 5 threads were used for statistics.

### 5.3.3 Degradation of Scaffolds

The addition of chitosan to the printing solution provides and additional crosslinking strategy to the alginate/gelatin system, in parallel to ionic crosslinking of alginate and gelation of gelatin at

lower temperature. Thus, it is expected to influence the stability and degradability of the scaffolds. The degradation rates of the scaffolds were measured by the amount of released alginate conjugated with fluorescein from the alginate/gelatin scaffolds.(Figure 5.5) The scaffolds were printed in $5x10^{-3}$ wt.% chitosan and 5 mM $CaCl_2$, $5x10^{-4}$ wt.% chitosan and 5 mM $CaCl_2$, and 5 mM $CaCl_2$. Then, the scaffolds were removed from the printing solution and rinsed with PBS for 15 min. These rinsing solutions were used as the solution at day 0. The absorbance at 494 nm was measured to detect the amount of the fluorescein. When the absorbance values of each scaffold at day 0 were compared, the lowest absorbance was obtained from the alginate/gelatin scaffold printed in $5x10^{-3}$ wt.% chitosan and 5 mM $CaCl_2$ at day o and day 7. At the scaffolds printed in $5x10^{-4}$ wt.% chitosan and 5 mM $CaCl_2$, absorbance at 494 nm was higher than the one printed in $5x10^{-3}$ wt.% chitosan and 5 mM $CaCl_2$ at day 0 and day 7. The absorbance for alginate/gelatin printed without chitosan was the highest at day 0 and day 7. Assuming there is direct correlation between the absorbance at 494 nm and amount of released alginate, the scaffolds printed without chitosan released more alginate to PBS during 7 day incubation than the scaffolds printed in chitosan/$Ca^{2+}$ bath. The concentration of chitosan in printing solution affected the amount of released alginate. The alginate/gelatin scaffolds printed in low concentration of chitosan released less alginate than the alginate/gelatin scaffolds printed in high concentration of chitosan.

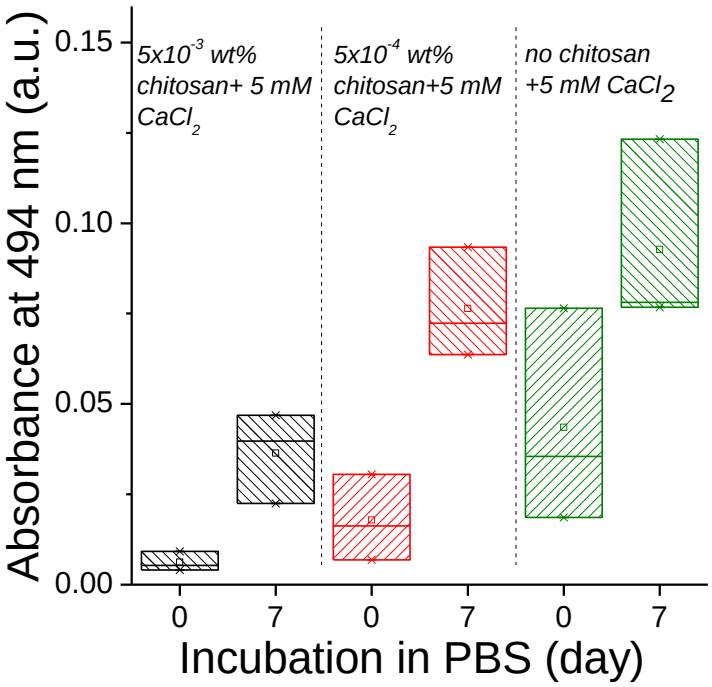


**Figure 5.5** *Comparison of degradation rate of alginate/gelatin scaffolds printed in different conditions.* UV spectra of solutions taken from alginate/gelatin scaffolds printed in different conditions. Absorbance at 494 nm corresponds to absorbance of fluorescein. Three replicates of each scaffold type were used to make statistics.

### 5.3.4 Mechanical Strength of the Printed Scaffolds

The mechanical strength of the printed scaffolds was measured by indentation test. (Figure 5.6a) in order to quantify the effect of adding chitosan to the crosslinking bad. In this test, an indenter with the diameter of 2 mm approached to the scaffolds until the strain was 50% and, then retracted while the force was measured during this movement. As the indenter moved towards the scaffolds laterally, the measured force was increased till ~80-100 mN with small variations. The scaffolds with 3 printed layers over an area of 1x1 $cm^2$ were used. An indenter with diameter of 2 mm was used for the testing and 3 points from each sample and 3 replicates from each scaffold type were measured. 5 mN preload was applied. The indentation was applied until the strain of 50%. The resulting forces vs. strain% curves were showed in Figure 5.6b. Each line was showed with its standard error. According to the result from the indentation test, there was no significant difference in the mechanical properties between the 3D printed scaffolds with different chitosan concentrations. The hardening with chitosan seems to be a superficial effect and chitosan does not seem to penetrate within the threads of the scaffold.

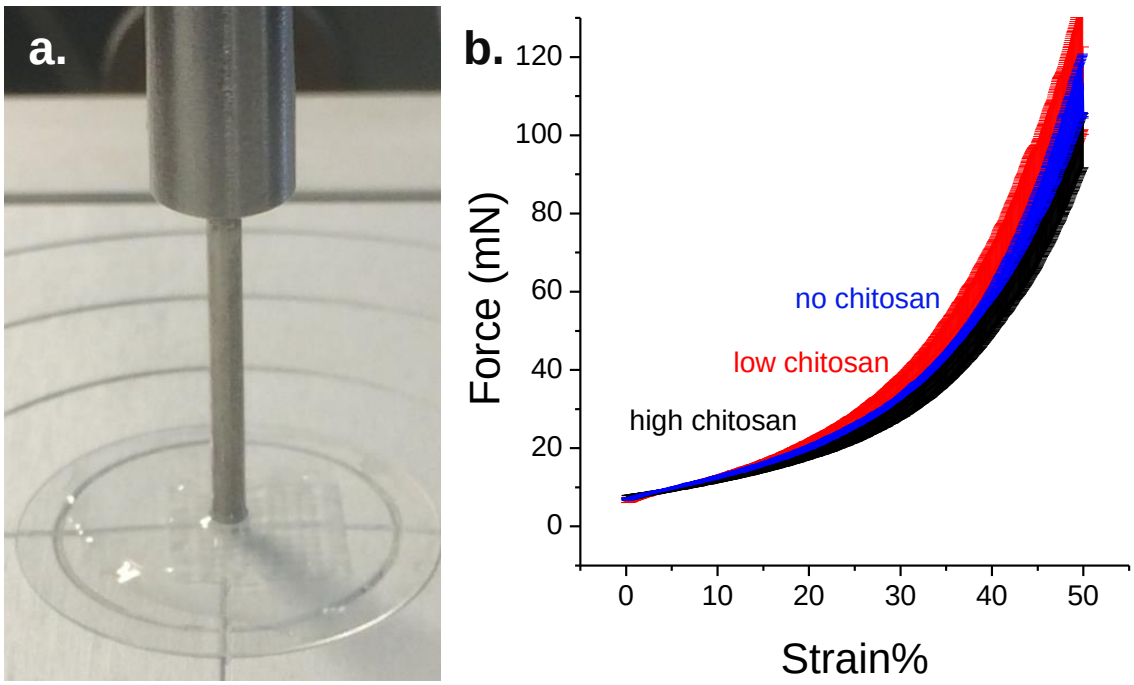


**Figure 5.6 a.** Photograph of indentation set-up with 3 layers of 3D printed alginate/gelatin scaffold. **b.** Force vs strain% curve of the scaffolds, printed in $5x10^{-3}$ wt.% chitosan and 5 mM $CaCl_2$, $5x10^{-4}$ wt.% chitosan and 5 mM $CaCl_2$, and 5 mM $CaCl_2$ with indentation test.

### 5.3.5 Effect of Temperature on the Scaffolds

The behavior of the alginate/gelatin scaffolds at 37 ˚C was investigated with confocal microscope.(Figure 5.7) The alginate/gelatin scaffolds were prepared with 0.3 wt.% alginate conjugated with fluorescein. Then, scaffolds were printed in $1x10^{-2}$ wt.% chitosan and 5 mM $CaCl_2$, $2x10^{-3}$ wt.% chitosan and 5 mM $CaCl_2$, and 5 mM $CaCl_2$. 1 day after soaking in keeping in printing solution, scaffolds were removed from the printing solution and washed with PBS. The temperature of the scaffolds was increased to 37 ˚C to melt the gelatin and observe the change in the morphology. At 37 ˚C, the transparency of the alginate/gelatin scaffolds printed at high chitosan concentration was regained while 3D structure was kept.

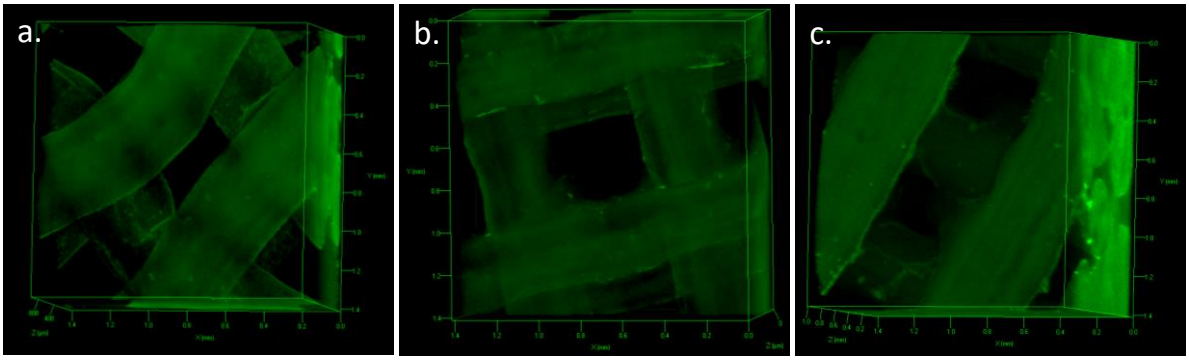


**Figure 5.7** *Transparency regained and high fidelity kept at 37 ˚C.* Confocal microscope images of alginate/gelatin scaffolds printed in **a.** 0.01 wt.% chitosan and 5 mM $CaCl_2$, **b.** 0.002 wt.% chitosan and 5 mM $CaCl_2$, and **c.** 5 mM $CaCl_2$. Scaffolds were kept in printing solution for 1 day. Then they were washed with PBS and imaged at 37 ˚C. At 37 ˚C, scaffolds kept high fidelity although gelatin melted. Scaffold printed in $CaCl_2$ solution without chitosan swelled so much that lines in the first two layers merged.

## 5.4 Conclusion

Alginate/gelatin based scaffolds were prepared with high fidelity with using 3D extrusion method. The scaffolds were deposited into the solution of $Ca^{2+}$ and chitosan. The alginate/gelatin scaffolds 3D-printed into solution with high chitosan concentration was nontransparent. As the concentration of chitosan in crosslinking solution decreased, the scaffold got transparent. The alginate/gelatin scaffolds deposited in chitosan solution had higher fidelity. The alginate/gelatin scaffolds printed in chitosan solution had higher swelling degree than the one deposited into solution without chitosan. Also, their degradation rates were lower than the one deposited into solution without chitosan. Their compressive strengths did not differ from each other in the indentation test. Finally, at 37 ˚ C, the scaffolds deposited into solution with or without chitosan kept their structures after melting of gelatin.

## References


1. Włodarczyk-Biegun, M.K. and A. del Campo, *3D bioprinting of structural proteins.* Biomaterials, 2017. **134**: p. 180-201.
2. Hinton, T.J., et al., *Three-dimensional printing of complex biological structures by freeform reversible embedding of suspended hydrogels.* Science Advances, 2015. **1**(9): p. e1500758.
3. Kim, G., et al., *Coaxial structured collagen-alginate scaffolds: fabrication, physical properties, and biomedical application for skin tissue regeneration.* Journal of Materials Chemistry, 2011. **21**(17): p. 6165-6172.
4. Ashwini Rahul, A., et al., *A versatile method for combining different biopolymers in a core/shell fashion by 3D plotting to achieve mechanically robust constructs.* Biofabrication, 2016. **8**(4): p. 045001.
5. Moroni, L., et al., *Design of biphasic polymeric 3-dimensional fiber deposited scaffolds for cartilage tissue engineering applications.* Tissue Engineering, 2007. **13**(2): p. 361-371.
6. Onoe, H., et al., *Metre-long cell-laden microfibres exhibit tissue morphologies and functions.* Nature Materials, 2013. **12**(6): p. 584-590.
7. Saether, H.V., et al., *Polyelectrolyte complex formation using alginate and chitosan.* Carbohydrate Polymers, 2008. **74**(4): p. 813-821.
8. Lee, K.Y. and D.J. Mooney, *Alginate: Properties and biomedical applications.* Progress in Polymer Science, 2012. **37**(1): p. 106-126.
9. Suárez-González, D., et al., *Controlled nucleation of hydroxyapatite on alginate scaffolds for stem cell-based bone tissue engineering.* Journal of Biomedical Materials Research Part A, 2010. **95A**(1): p. 222-234.
10. Yu, J., et al., *The use of human mesenchymal stem cells encapsulated in RGD modified alginate microspheres in the repair of myocardial infarction in the rat.* Biomaterials, 2010. **31**(27): p. 7012-7020.
11. Wu, Z., et al., *Bioprinting three-dimensional cell-laden tissue constructs with controllable degradation.* 2016. **6**: p. 24474.

12. Xu, Y. and X. Wang, *Fluid and cell behaviors along a 3D printed alginate/gelatin/fibrin channel.* Biotechnology and Bioengineering, 2015. **112**(8): p. 1683-1695.
13. Yu, Z., et al., *Three-dimensional printing of Hela cells for cervical tumor model in vitro.* Biofabrication, 2014. **6**(3): p. 035001.
14. Luo, Y., et al., *Concentrated gelatin/alginate composites for fabrication of predesigned scaffolds with a favorable cell response by 3D plotting.* RSC Advances, 2015. **5**(54): p. 43480-43488.
15. Colosi, C., et al., *Rapid prototyping of chitosan-coated alginate scaffolds through the use of a 3D fiber deposition technique.* Journal of Materials Chemistry B, 2014. **2**(39): p. 6779-6791.

# 6 Conclusion and Outlook

In this PhD thesis various strategies to tune mechanical properties of synthetic/natural hydrogels to be applied for advanced *in vitro* cell cultures were established. The mechanical properties of alginate hydrogels were enhanced by fabricating interpenetrate network (IPN) with hard polyacrylamide hydrogels. The mechanical properties of alginate hydrogels were spatiotemporally controlled by incorporation of the light activatable $Ca^{2+}$ chelator Nitr-T. A strategy to fabricate mechanically robust 3D alginate scaffolds was developed based on chitosan coatings that prevented dissolution and improved stability in solution. Moreover, catechol-derivatized star-PEG hydrogels with tunable curing kinetics and mechanics and phototunable stiffness were attempted.

The following are major conclusions from this work

1. The mechanical stability of ionically crosslinked alginate hydrogels can be enhanced by building interpenetrating networks with covalently crosslinked polyacrylamide. The mechanical properties of Alg/pAAm IPN can be adjusted using varying concentration of $Ca^{2+}$ ion, molecular weight of alginate and post-gelation modifications to mimic the mechanical properties of the cellular microenvironment.

2. The stiffness of soft alginate hydrogels depends on the concentration of $Ca^{2+}$ ions in the gel. The stiffness of alginate hydrogel can be regulated by light by releasing $Ca^{2+}$ ions from photoactivatable Nitr-T chelating complex embedded in the gel. This system can be used to enhance the mechanical properties of alginates upon irradiation at 365 nm. A 3-fold increase in local stiffness of alginate network was realized in this work. The solububility of Nitr-T and the affinity of the photolytic byproduct for the Ca2+ ions limit the amount of Ca2+ that can be delivered to the system.

3. The long term mechanical stability of alginate hydrogels can be an issue when culturing cells in mechanically controlled microenvironments. Independently of initial Ca2+ crosslinking degree in the alginate hydrogel. The concentration of Ca2+ in the culture solution strongly determines the long-term mechanical properties of the hydrogel.

4. Stable 3D scaffold of alginate hydrogels can be fabricated by 3D bioprinting a solution of alginate with gelatin a sacrificial component. Coating of the alginate scaffold with

chitosan enhances long term stability of the alginate scaffold by preventing leaching of $Ca^{2+}$ from the alginate network. The stability of alginate scaffold in the presence of chitosan was demonstrated after thermal degradation of gelatin.

5. Catechol functionalized PEGs can be used to create gels with tunable stiffness and crosslinking kinetics by introducing substituents at 6 positions in the catechol ring. The electron donating Cl substitution enhances the polymerization kinetics, while the strongly electron-withdrawing -NO2 substituent shows the reverse effect.

# 7 Appendix (Experimental)

## Chapter 2: Approaches to Adjust the Mechanical Properties and Curing Kinetics of PEG-catechol Hydrogels

## 2.1 Experimental

### 2.1.1 Rheological Measurements

The shear moduli of PEG-catechol and oxidant mixtures were measured with a homemade piezorheometer[308].The sample was placed between two glass slides connected to two piezoactuators: one piezoactuator applied the shear deformation to the sample and the other one measured the stress transmitted from sample. The gap between the glass slides was 100 µm, and it was filled with 15 µl of a solution of the polymer at 100 mg $mL^{-1}$ concentration. The applied voltage for these measurements was 9.5 V. The measurements were performed at room temperature and 0.32% strain. In the time sweep measurements, moduli at 10 rad/s - were used. In order to prepare the polymer solution, the PEG-catechol derivatives were dissolved at 200 mg $ml^{-1}$ concentration in water and mixed with 18 mM $NaIO_4$ in water at 1:1 ratio, unless otherwise stated. The mixtures were fluid when they were placed to the sample chamber. To avoid drying of hydrogels during measurements, hydrogels were sealed with polydimethylsiloxane oil (PDMS). The catechol:$NaIO_4$ molar ratio was (4:1).

### 2.1.2 Preparation of PEG-ClDop:PEG-Dop Mixtures

In preparation of PEG-catechol mixtures, total solid content in solution was kept constant. Solutions of PEG-catechol derivatives were prepared in volume of 10 µl and mixed at 1:3, 1:1 or 3:1 ratio. To this mixture 18 mM $NaIO_4$ oxidant in water at 1:1 volume ratio was added.

## Chapter 3: Chemical Strategies to Tune Mechanical Properties of Hydrogels by Light

## 3.1 Light Responsive Alginate Hydrogels

### 3.1.1 Experimental

#### 3.1.1.1 Cleavage of alginate chains

A commercially available alginate with highest possible G content was selected (Pronova UP MVG, FMC BioPolymers). This alginate has a G content of 60% and a molecular weight of 187601 g/mol. Alginate polymer was dissolved in water at concentration of 1.5 wt. % and

irradiated at different time intervals with Gammacell 2000 irradiator. After irradiation, alginate solution was freeze-dried and chain length was measured with GPC with a pump of PSS SECcurity with 1.0 mL/min flow rate in 0.1 M $NaNO_3$ buffer. Column was chosen as Suprema Linear M and detector was Shodex RI 101. Molecular weight was determined with using polyethylene oxide as reference.

#### 3.1.1.2 Preparation of samples

Nitr-T has low solubility in buffer at pH 7.4 and water. In order to increase solubility in aqueous conditions and physiological pH, a sodium salt of Nitr-T was prepared by dissolving Nitr-T in 4 equivalent of NaOH and freeze-drying. A stock solution of Nitr-T and $CaCl_2$ was prepared in buffer at pH 7.4 in concentration of 100 mM. If it was necessary, pH value of stock solution was increased with addition of NaOH solution. Concentration of Nitr-T+$Ca^{2+}$was decreased by addition of buffer into stock solution in some cases. Afterwards, $CaSO_4$ solution was mixed with Nitr-T+$Ca^{2+}$ complex to prevent preparing viscous alginate solution before introducing Nitr-T+$Ca^{2+}$ complex. This mixture was added to 2+2 wt% HMW+LMW Alg solution and mixed with pipetting and sonication. pH value of final solution was adjusted to 7.4.

#### 3.1.1.3 Thin film preparation

Quartz substrates were cleaned with $O_2$ plasma chamber 0.1 mbar for 10 min. Substrates were immediately immersed into 10 mg/ml dopamine solution in 10 mM TRIS buffer at pH 8.5 for 30 min. This treatment generates an adhesive primer layer to covalently attach to the hydrogel and stabilize the film on the glass slide. A solution of 1 wt% alginate HMW with 0.5 wt% dopamine in DPBS (-,-) was mixed with $CaSO_4$ solution to have concentration of 25 mM. A mixture of 100-150 µL were added to dopamine coated substrates depending on the dimensions. Approximately 3 h after, hydrogels were dried up with $N_2$ gun to have a thin film, washed with water and dried. Substrates were ready for further treatment.

A solution of 10 or 20 µL from 1+1 wt% HMW+LMW Alg mixed with 12.5 mM $CaSO_4$ with 25 mM Na-Nitr-T+25 mM $CaCl_2$ was added to treated substrates and incubated in room temperature for overnight to have stabile films. Afterwards, UV spectra of thin films were taken with or without irradiation or washing steps.

#### 3.1.1.4 UV Analysis

Agilent Cary 2000 was used in measuring UV spectra of Nitr-T in solution and thin film. Nitr-T was dissolved with or without $Ca^{2+}$ in buffer at pH 7.4 in the concentration of 0.5 mM. An equivalent of $Ca^{2+}$ ions was used in Nitr-T in buffer at pH 7.4. A solution of 1+1 Alg+$CaSO_4$+Nitr-

T+$CaCl_2$ was prepared with dissolving the sample as described in “preparation of samples” section in buffer at pH 7.4. A UV spectrum of irradiated Alg+$CaSO_4$+Nitr-T+$Ca^{2+}$ sample used in mechanical characterization was recorded. Sample was prepared with 1+1 wt% HMW+LMW Alg, 25 mM $CaSO_4$, 25 mM Nitr-T+$Ca^{2+}$. Then, it was irradiated with light at 365 nm with exposure dose of 110160 J/$cm^2$ when it was in sample chamber of piezorheometer. After measurement, it was dissolved in buffer at pH 7.4 in ratio of 1:100.

For the UV analysis of thin films, thin film of Alg+Nitr-T hydrogels was irradiated with polychrome V lamp at 360 nm with power 2.55 mW $cm^{-2}$. Then, a UV spectrum of Alg+Nitr-T hydrogels was measured.

#### 3.1.1.5 Mechanical Characterization

For measurements, 5 µL of Nitr-T+$Ca^{2+}$ solution was mixed with 0.907 µL of $CaSO_4$ in DPBS(-,-). Then, this solution was added to 5 µL of 2+2 wt% HMW+LMW Alg in DPBS (-,-). pH of solution was adjusted to 7.4 with addition of 1 M HCl. Sample was placed into transparent part of sample chamber. It was sealed with PDMS to avoid evaporation of water. Stiffness was measured with varying frequency values between 0.1 and 100 Hz with 0.32 % strain at room temperature.

## 3.2 Photodegradable Hydrogels Based on Nitro-Catechol Derivatives

### 3.2.1 Experimental

#### 3.2.1.1 Synthesis

**4-(2-amino-1-hydroxyethyl)-5-nitrobenzene-1,2-diol (2)**

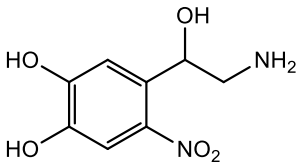

2

**1** was dissolved in water under Ar in ice bath and a few drops of concentrated HCl were added. (2 eq) $NaNO_2$ was dissolved in water and added slowly. 20 % $H_2SO_4$ was added slowly. Reaction time was 30 minutes. Solvent was reduced with rotavapor. Product was isolated preparative RP-HPLC. Solvents were water (0.1% TFA) and acetonitrile (MeCN) (0.1% TFA). LC was run for 40 min for each sample and it started with 100% $H_2O$ for 3 minutes. Then, gradient MeCN concentration reached to 100 % in 33 minutes. Finally, it kept running for 7 minutes. $^1$H NMR (250 MHz, $D_2O$) δ = 7.59 (s, 1H), 7.17 (s, 1H), 5.53 – 5.41 (m, 1H), 3.33 (dd, J = 13.0, 3.0 Hz, 1H), 2.97 (dd, J = 13.1, 8.7 Hz, 1H).

**(9H-fluoren-9-yl)methyl (2-(4,5-dihydroxy-2-nitrophenyl)-2-hydroxyethyl)carbamate (3)**

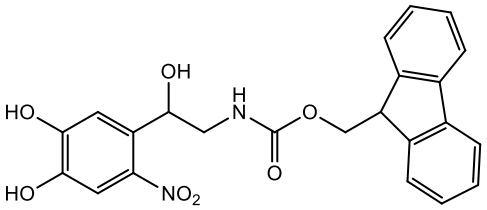

3

**2** was dissolved in water in ice bath. (1.1 eq) Fmoc-Osu was dissolved in dioxane and added to mixture. Sodium carbonate was added slowly. Reaction run at ice bath for 4 h then r.t for 24 h. Product was extracted with ether and dried with rotavapor. Product was purified by preparative RP-HPLC. Solvents were water (0.1% TFA) and MeCN (0.1% TFA). LC was run for 40 min for each sample and it started with 80% $H_2O$ and and 20% MeCN for 3 minutes. Then, gradient MeCN concentration reached to 100 % in 33 minutes. Finally, it kept running for 7 minutes. $^1$H NMR (250 MHz, DMSO-d6) δ 7.01 (d, *J* = 7.0 Hz, 8H), 6.82 (d, *J* = 7.3 Hz, 3H), 6.58 – 6.41 (m, 4H), 4.24 (t, *J* = 5.0 Hz, 1H), 3.16 (t, *J* = 7.0 Hz, 1H), 2.89 (dd, *J* = 6.9, 4.6 Hz, 2H).

**tert-butyl (2-(4,5-dihydroxy-2-nitrophenyl)-2-hydroxyethyl)carbamate (4)**

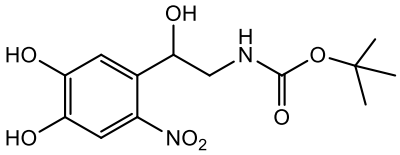

4

**2** and (1.1 eq) Fmoc-osu were mixed in DMF in catalysis of DIEA (2 eq) saturated with Ar for 10 min and left for 24 h at room temperature. Samples were taken from reaction mixture and checked with ESI-MS. Then, product was purified with preparative RP-HPLC. Solvents were water (0.1% TFA) and MeCN (0.1% TFA). LC was run for 40 min for each sample and it started with 80% $H_2O$ and and 20% MeCN for 3 minutes. Then, gradient MeCN concentration reached to 100 % until 33 minutes. Yield was 27%. ESI-MS: $[M+Na]^+$ (observed)=337.10, $[M+Na]^+$ (calculated)=337.10, $[M+K]^+$ (observed)= 353.11, $[M+K]^+$ (calculated)=353.08, $[2M+Na]^+$ (observed)=651.23, $[2M+Na]^+$ (calculated)=651.22

**(9H-fluoren-9-yl)methyl(2-(3,4-bis((tert-butyldimethylsilyl)oxy)phenyl)-2-hydroxyethyl)carbamate (5)**

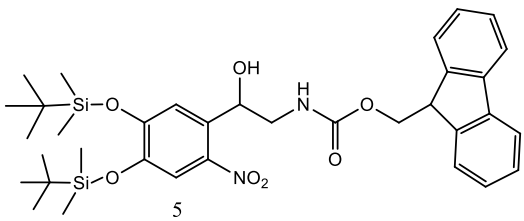

5

(2 eq) TBDMS-Cl in dry MeCN was saturated with Ar for 30 min. **3** was added a saturated with Ar for 10 min. (1.5 eq) TBD was added. Reaction ran at ice bath for 4 h then r.t for 24 h. It was centrifuged and the precipitate was collected. ESI-MS at 24 h : M (observed) 459.12, 380.24 and 334.11 [M] (calculated)= 664.30 $[M+Na]^+$ (calculated)= 688.29

**tert-butyl (2-(2,2-dimethyl-6-nitrobenzo[d][1,3]dioxol-5-yl)-2-hydroxyethyl)carbamate (6)**

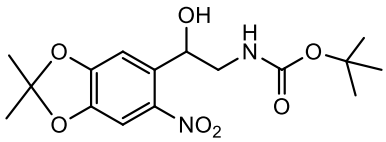


6

**4** and DMP were mixed in benzene and saturated with Ar for 10 min. Then, it was heated for reflux (105 °C). Then, *p*-Tos-OH was added to mixture. Reaction ran for overnight. After 24 h, benzene was evaporated. The results were checked with ESI-MS. Mass analysis did not show either reactant or product.

**(9H-fluoren-9-yl)methyl (2-(2,2-dimethyl-6-nitrobenzo[d][1,3]dioxol-5-yl)-2-hydroxyethyl)carbamate (7)**

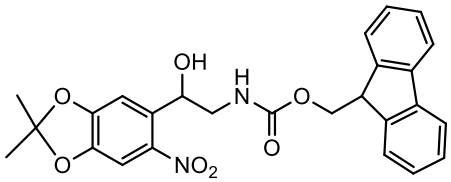


7

**3** and (4 eq) DMP were mixed in benzene and saturated with Ar for 10 min. Then, it was heated for reflux (105 °C). Then, *p*-Tos-OH (4.5 mol %) was added to mixture. Rxn run for overnight. After 24 h, benzene was evaporated. The results were checked with ESI-MS. ESI showed mass of starting material **3**. [$M_3$\2+Na](observed) = 241.17 [$M_3$\2+Na](calculated)= 241.17

**N-(3,4-dihydroxyphenethyl)-2,2,2-trifluoroacetamide (13)**

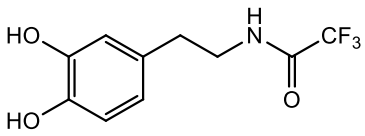


13

**12** solution in dry MeOH was saturated with Ar for 30 min. MTFA was added an saturated with Ar for 10 min. Then, $N(Et)_3$ was added slowly. Rxn run for 16 h. Solvents were evaporated with rotavap. Residue was treated with HCl for pH 1 and extracted with EtOAc. Organic layer was washed and dried with $MgSO_4$. Solvent was removed. The results were checked ESI-MS. $[M+Na]^+$ (observed)= 272.05 $[M+Na]^+$ (calculated)= 272.06

**N-(2-(4,5-dihydroxy-2-nitrophenyl)-2-hydroxyethyl)-2,2,2-trifluoroacetamide (8)**

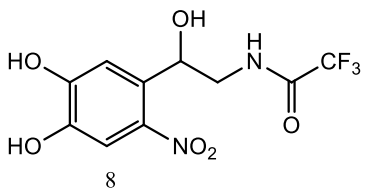


8

Solution of **1** in dry MeOH was saturated with Ar for 30 min. MTFA was added a saturated with Ar for 10 min. Then, $N(Et)_3$ added slowly. Rxn run for 16 h. Solvents were evaporated wit rotavap. Residue was treated with HCl for pH 1 and extracted with EtOAc. Organic layer was washed and dried with $MgSO_4$. Solvent was removed. Mass didn't show trifluoroacetyl signal. It indicated a mass lighter than **8**. M (observed)=239.24

**2-amino-1-(3-((tert-butyldimethylsilyl)oxy)-4-((isopropyldimethylsilyl)oxy)phenyl)ethanol (9)**

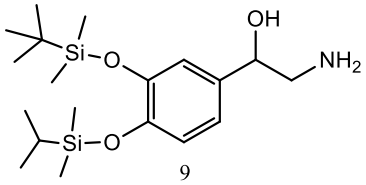

9

(2 eq) TBDMS-Cl was saturated with Ar for 30 min in dry MeCN. **1** was added a saturated with Ar for 10 min. (1.5 eq) TBD was added. Reaction ran at ice bath for 4 h then r.t for 24 h. It was centrifuged and the precipitate was collected. The results were checked ESI-MS. $[M]^+$ (observed)= 380.22 $[M]^+$ (calculated)= 380.25

**(9H-fluoren-9-yl)methyl (2-(3,4-bis((tert-butyldimethylsilyl)oxy)phenyl)-2-hydroxyethyl)carbamate (10)**

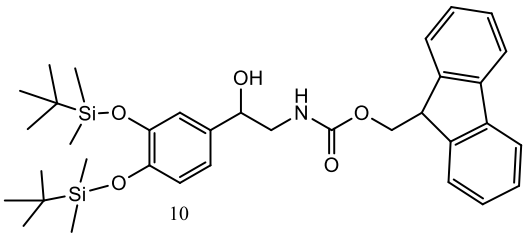

10

**9** was dissolved in water in ice bath. (1.1 eq) Fmoc-Osu is dissolved in dioxane and added. Finally, (2 eq) sodium carbonate was added slowly. Rxn run at ice bath for 4 h then r.t for 24 h. Product was extracted with ether and collected with rotavapor. The results were checked ESI-MS. $[M+Na]^+$ (observed)= 643.33 $[M+Na]^+$ (calculated)= 642.30

**2-amino-1-(4,5-bis((tert-butyldimethylsilyl)oxy)-2-nitrophenyl)ethanol (11)**

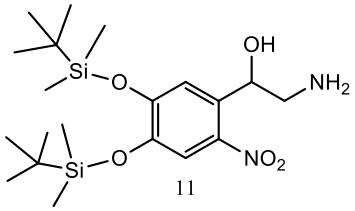

11

**9** was dissolved in water under Ar in ice bath. Then, a few drops of conc HCl was added. $NaNO_2$ was dissolved in water added slowly. 20 % $H_2SO_4$ was added slowly. **9** did not dissolve in solvent even at strong acidic conditions.

**(9H-fluoren-9-yl)methyl (2-(4,5-bis((tert-butyldimethylsilyl)oxy)-2-nitrophenyl)-2-hydroxyethyl)carbamate (5)**

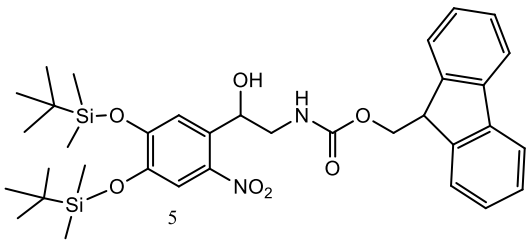

5

(2 eq) Nitronium tetrafluoroborate was dissolved in dry acetonitrile at -30 °C under argon for 30 min. Then, (1.5 eq) 2-picoline was added to the solution and mixed for 10 min. Finally, **10** was added to the mixture at -30 °C under argon. Reaction was allowed to warm overnight. However, **10** was partially soluble at this conditions. Next day, ESI sample showed 5% coupling.

### (9H-fluoren-9-yl)methyl (2-(3,4-dihydroxyphenyl)-2-hydroxyethyl)carbamate (14)

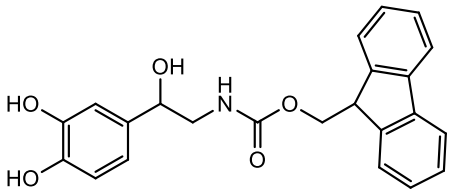

14

**1** was dissolved in water in ice bath. (1.1 eq) Fmoc-Osu is dissolved in dioxane and added. Finally, (2 eq) sodium carbonate was added slowly. Rxn run at ice bath for 4 h then r.t for 24 h. Product was extracted with ether and collected with rotavapor.

The results were checked ESI-MS. $[M+Na]^+$ (observed)= 414.11 $[M+Na]^+$ (calculated)= 414.13 $[2M+Na]^+$ (observed)= 805.26 $[2M+Na]^+$ (calculated)= 805.28

### 1-(6-nitrobenzo[d][1,3]dioxol-5-yl)ethanol (18)

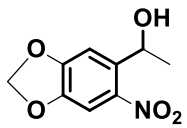

18

**18** was kindly synthesized by Dr. Julieta Paez and Sirma Koynova.

$^1$H NMR (250 MHz, DMF-d7) δ 7.54 (s, 1H), 7.36 (s, 1H), 6.30 (s, 2H), 5.31 (q, *J* = 6.2 Hz, 1H), 1.44 (d, *J* = 6.2 Hz, 3H).

### 1-(6-nitrobenzo[d][1,3]dioxol-5-yl)ethyl butylcarbamate (25)

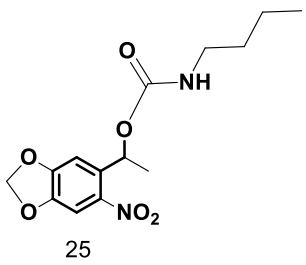

25

**18** and (1.05 eq) butylNCO were mixed in DMF-d7 in catalysis of (0.013 eq) DBTDL in an NMR tube. Reaction was monitored with NMR during certain time intervals. *All of the coupling reactions were performed with the same equivalency with the one used in this reaction.* After 2 h reaction $^1$H NMR (250 MHz, DMF-d7) δ 7.54 (s, 1H), 7.35 (d, *J* = 1.9 Hz, 1H), 6.30 (s, 2H), 5.54 (d, *J* = 4.3 Hz, 1H), 5.40 – 5.19 (m, 1H), 3.40 (td, *J* = 6.6, 2.2 Hz, 2H), 3.09 (q, *J* = 6.7 Hz, 0H), 1.65 – 1.49 (m, 3H), 1.49 – 1.21 (m, 9H), 0.90 (dt, *J* = 10.2, 7.3 Hz, 5H).

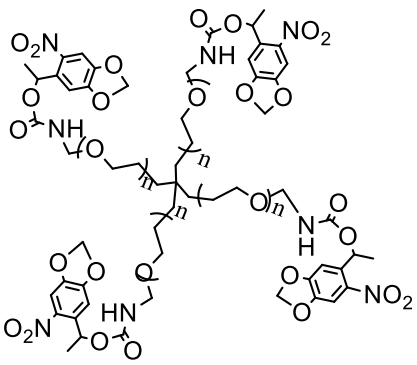

26

### Poly(ethylene glycol) functionalized with 1-(6-nitrobenzo[d][1,3]dioxol-5-yl)ethanol (26)

After 2 h reaction $^1$H NMR (250 MHz, DMF-d7) δ 7.54 (s, 1H), 7.36 (s, 1H), 5.54 (d, *J* = 4.3 Hz, 1H), 5.30 (td, *J* = 6.2, 4.3 Hz, 1H), 1.48 – 1.38 (m, 3H).

After dialysis $^1$H NMR (700 MHz, Methanol-d4) δ 7.46 (s, 0H), 7.29 (s, 0H), 6.15 (d, *J* = 8.3 Hz, 1H), 5.36 (q, *J* = 6.3 Hz, 1H),

1.46 (d, *J* = 6.3 Hz, 1H).

### 1-(4,5-bis(methoxymethoxy)-2-nitrophenyl)ethanol (24)

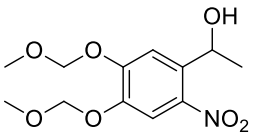

24

**24** was kindly synthesized by Dr. Julieta Paez and Sirma Koynova.

$^1$H NMR (300 MHz, Methanol-d4) δ 7.80 (s, 1H), 7.62 (s, 1H), 5.42 (q, *J* = 6.3 Hz, 1H), 5.35 (s, 3H), 5.27 (s, 2H), 1.47 (d, *J* = 6.3 Hz, 3H).

### Poly(ethylene glycol) functionalized with 1-(4,5-bis(methoxymethoxy)-2-nitrophenyl)ethanol (27)

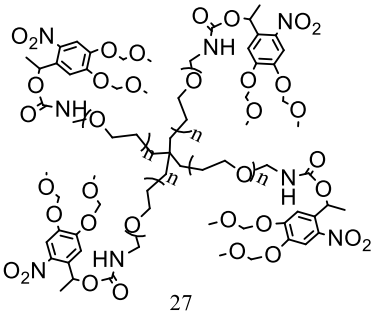

27

After dialysis $^1$H NMR (700 MHz, Methanol-d4) δ 7.84 (s, 0H), 7.67 (s, 1H), 5.46 (q, *J* = 6.3 Hz, 0H), 5.40 (s, 0H), 5.32 (s, 1H), 1.51 (d, *J* = 6.3 Hz, 1H).

***Deprotection of 26:*** (3 eq) $AlCl_3$ was poured into cold (-5 °C) $CH_2Cl_2$ and mixed with **26** under argon. After 1 h 48% HBr was added to solution. Samples were taken at certain time intervals (1, 3, 5 and overnight) and dialyzed in MeOH. In NMR analysis, even the sample at 1 h did not contain NMR signal belonging to **18**.

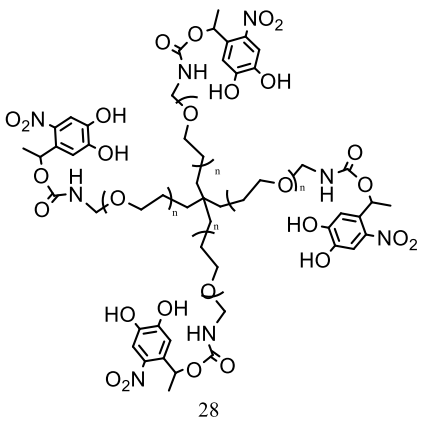

28

### Poly(ethylene glycol) functionalized with 4-(1-hydroxyethyl)-5-nitrobenzene-1,2-diol

Deprotection of **27**: **27** was deprotected in mixture of $CHCl_3$:TFA in 3:1 ratio. Samples were taken at some certain time intervals and dialyzed in MeOH. Sample at 5 h $^1$H NMR (700 MHz, Methanol-d4) δ 7.40 (d, *J* = 14.5 Hz, 2H), 7.14 (s,

1H), 6.96 (s, 1H), 5.32 (d, *J* = 6.3 Hz, 1H), 5.17 (s) 1.34 (t, *J* = 5.8 Hz, 7H).

### 3.2.1.2 Film preparation

Quartz substrates were cleaned in ethanol and subsequently treated in an oxygen plasma chamber. Clean substrates were immersed for 30 min in a 10 mg/mL solution of dopamine in 10 mM Tris-HCl (pH 8.5). The substrates were then washed with water and dried under/with $N_2$ stream. A mixture of 3 µl of a 200 mg/ml PEG-ND4 solution in water, 3 µl of 10 mM NaIO4 in water and 6 µl of TRIS buffer at pH 8.5 was spin coated onto the substrate at 1000 rpm and left for drying overnight.

### 3.2.1.3 Hydrogel formation

500 mg/ml solution of **28** in water was mixed with 330 mM $NaIO_4$ in water, or with 330 mM $NaIO_4$ in 10 mM TRIS-HCl buffer at pH 8.5, or with 200 mg/ml $H_2N$-PEG-$NH_2$, or with 200 mg/ml PEG-$4NH_2$ or with 500 mg/ml PEG-$4NH_2$. or with 500 mg/ml $H_2N$-PEG-$NH_2$ in water, or with buffer at pH 8.5. Also, 200 mg/ml solution of **28** was mixed with 500 mg/ml PEG-$4NH_2$ or 500 mg/ml $H_2N$-PEG-$NH_2$ in water or in buffer at pH 8.5. Formulations for the prepared mixtures were summarized below. The mixtures were prepared in an eppendorf and poured into a glass slide to follow the gelation by eye. The gelation was followed by eye. However, in the conditions explained above, no gelation was observed.

[**28**]=200 or 500 mg/ml in water (PEG-Nitro)
[PEG-$4NH_2$]=200 or 500 mg/ml in water (PEG-Amine)
[$NaIO_4$]= 330 mM in water, or in TRIS buffer pH 8.5 or pH 10

| Experiment | PEG-Nitro (µl) | PEG-Amine (µl) | $NaIO_4$ (µl) | pH |
|---|---|---|---|---|
| **1** | 3 | 3 | - | 5.0 |
| **2** | 3 | 3 | 3 | 5.0 |
| **3** | 3 | 1.5 | 1.5 | 5.0 |
| **4** | 3 | 3 | 3 | 8.5 |
| **5** | 3 | - | 3 | 8.5 |
| **6** | 3 | 1.5 | 1.5 | 8.5 |
| **7** | 3 | - | 3 | 10 |
| **8** | 3 | 3 | 3 | 10 |
| **9** | 3 | 1.5 | 1.5 | 10 |

# Chapter 4: Alginate/pAAm Interpenetrating Networks with Long-Term Mechanical Stability at Physiological Conditions

## 4.1 Experimental

### 4.1.1 Materials

Acrylamide, N,N'-methylenebisacrylamide (MBAA), ammonium persulfate (APS), calcium chloride, calcium sulfate and 3-(Trimethoxysilyl)propyl acrylate were purchased from Sigma Aldrich. Tetramethylenediamine (TEMED) was purchased from Alfa Aesar. Alginate, PRONOVA UP MVG, was purchased from Novamatrix. Glass cover slips with diameter of 25 mm were purchased from VWR.

Dulbecco's modified Eagle's medium (DMEM) and Dulbecco's phosphate-buffered saline no calcium, no magnesium (DPBS (-,-)) were purchased from Thermo Fisher Scientific.

### 4.1.2 Preparation of IPN Samples

1:6 weight ratio of alginate and acrylamide were mixed as powder to achieve a 14 wt. % concentration and pH was adjusted to 8.0. MBAA was added to this solution to a concentration of 0.015 to 0.9 wt. %. The mixture was degassed under vacuum for 10 min in order to eliminate $O_2$ that interferes with radical polymerization. Ammonium persulfate (APS) was added from a 10 wt. % stock solution in DPBS (-,-) at 1 v/v % concentration. Then, tetramethylethylenediamine (TEMED) was added to this solution to a final concentration of 0.1 v/v %. 180, 250 or 500 mM $CaSO_4$ slurry in DPBS (-,-) was added to the final solution to achieve a final concentration of 1.8, 25 or 50 mM $CaSO_4$ ($Ca^{2+}$ to alginate ratio 5 or 10 wt. %) respectively. The mixture was vortexed and sonicated for a few seconds to disperse $CaSO_4$ in solution. IPN samples were polymerized in a Stratagene UV Stratalinker 2400 Crosslinker, with a power of 15 watts and exposed at 254 nm for 40 min.

For preparation of low molecular weight alginate (Alg LMW), a solution of 1.5 wt% Alg HMW in water was treated with a Gammacell-2000 irradiator with $^{60}Co$ with 96 krad.[187] This treatment breaks glycosidic bonds and creates shorter chains. The samples were freeze-dried after irradiation.

IPN samples with different ratios of Alg MMW and Alg LMW were prepared by keeping the alginate concentration constant at 2 wt. %. 12 wt.% acrylamide was mixed with 2 wt.% Alg HMW, 1.5 wt% Alg HMW+0.5 wt.% Alg MMW, 1 wt% Alg HMW+1wt.% Alg MMW, 0.5 wt.% Alg

HMW+1.5 wt.% MMW and 2 wt.% Alg MMW. $Ca^{2+}$ concentration was chosen as 50 mM. Concentration of MBAA was 0.015 wt. %.

### 4.1.3 Gel Permeation Chromatography

The molecular weight distribution of alginate before and after ɣ-irradiation was characterized by gel permeation chromatography (GPC) with a pump of PSS SECcurity. The column was Suprema Linear XL from PSS Polymer Standards Service GmbH. The eluent was controlled with differential refractometer Shodex RI 101. A buffer solution of 0.1 M $NaNO_3$ was used as an eluent with a flow rate of 1 ml/min. The molecular weight distribution was calculated using a polyethylene oxide calibration standard.

### 4.1.4 Analysis of IPN Morphology by SEM

Hydrogel samples were prepared on silicon wafer surfaces and critical point dried to remove solvent while preserving the morphology of the network. The swollen hydrogel samples were incubated in isopropanol/ water solutions with increasing isopropanol concentration from 0 to 100 v/v % for 3-5 min. The samples were kept in isopropanol for at least 30 min before transfer to the critical point dryer to remove the isopropanol. A Scanning Electron Microscope Zeiss LEO Gemini 1530 was used for imaging with an acceleration voltage of 1 kV.

### 4.1.5 Rheology Measurements

Rheological measurements were performed with a TA ARES rotational rheometer. The two glass slides sandwiching the hydrogel samples were glued to the rheometer plates using a double sided tape. In order to prevent drying water loss during the measurement, the samples were covered with water during the measurements. The measurements were performed at strain of 0.5 % and angular frequency of 0.1 to 100 rad/s at room temperature.

Hydrogel disks were prepared between two 25 mm acryl-silanized glass slides using a ring with a diameter of 20 mm and a thickness of 1.5-2 mm. The ring was placed on one acryl-silanized glass slide. Then, 330 µl of solution was dropped in it. In this way, the solution was confined inside the ring and the dimensions were fixed. Another acryl-silanized glass slide was placed on top of solution. The pAAm hydrogel was covalently attached to the glass slides during its polymerization via acrylic groups. When polymerization was completed, the ring was removed. The solutions of the acrylic monomers at 12 wt. % concentration containing MBAA concentrations varying from 0.0115 to 0.9 wt. % were prepared and polymerized in the system described above.

The shear modulus of alginate hydrogels was measured with a custom-built piezorheometer.[308] The sample was placed between two glass slides connected to two piezoactuators: one piezoactuator applied shear deformation to the sample and the other one measured the stress transmitted from sample. The gap between the glass slides was 100 µm. 13.5 µl 2.0 wt% alginate was mixed with 1.5 µl of 250 mM (final concentration of 25 mM $Ca^{2+}$) or 500 mM $CaSO_4$ (final concentration of 50 mM $Ca^{2+}$) quickly. The solution was poured into the cell and sealed with PDMS to avoid drying during measurement. The voltage was 9.5 V. The measurements were performed at room temperature and 0.32% strain. When G' reached to plateau, *E* was calculated with the G' at 1.25 rad/s.

*Preparation of acryl-silanated glass slides:* 25 mm glass slides were rinsed with ethanol and water and incubated in a solution of 0.5 v/v% 3-(Trimethoxysilyl)propyl acrylate in 95% ethanol/water for 16 h. Glass slides were rinsed with water and ethanol and baked at 80 °C for 1 h in a vacuum oven. These slides were used for preparing hydrogel samples.

### 4.1.6 Tensile Testing

Measurements were performed with a Zwick Roell Z005 tensile machine. IPN Samples were prepared in molds of 7.5x5x0.1 $cm^3$ as described above. Before measurement, samples were stored in a humid box at 37 °C for at least 16 h. Then samples were cut with stamps with a gauge length and width of 20 and 9.6 mm, respectively. Hydrogel stripes were glued to glass slides with UHU sekundenkleber and stretched at a speed of 20 mm/min. The Young's modulus was calculated from the linear part of the stress vs strain curve in the low strain regime.

### 4.1.7 Determination of Solid Content of Hydrogels After Soaking

IPN samples were prepared in molds of 7.5x5x0.1 $cm^3$ in size as prepared for tensile tests. Samples were stored in a humid box at 37 °C for at least 16 h for equilibration of the networks. They were cut with stamps in dimensions of 20x9.6 $mm^2$. As-prepared samples were weighted and the mass was noted as swollen weight. Then, each sample was freeze-dried in order to obtain solid weight of as-prepared samples. At least 3 samples were measured. Samples were then soaked in cell culture medium conditions for 24 h and then washed in DPBS for 15 min and weighted again.

## Chapter 5: 3D Printing of Alginate Scaffolds with Tunable Mechanics

### 5.1 Experimental

### 5.1.1 Materials and Reagents

In this study, alginate was supplied from Fraunhofer Institute for Biomedical Engineering (IBMT) Department of Medical Biotechnology Clinical Stem Cell Technologies, Sulzbach. Alginate for fluorescence imaging was purchased from Novamatrix under the name of Alginate PRONOVA UP MVG. 1-Ethyl-3-(3-Dimethylaminopropyl)carbodiimide, N-Hydroxysuccinimide, gelatin from porcine skin gel strength 300 Type A, and 6-Aminofluorescein were purchased from Sigma Aldrich. Dulbecco's phosphate-buffered saline (DPBS (+,+)) with $CaCl_2$ and $MgCl_2$ was from Thermo Fischer. Glass cover slips with diameter of 25 mm were purchased from VWR. 3D printing was conducted with Gesim Bioscaffolder 3.1.

### 5.1.2 Preparation of the Ink and Printing Solution

Alginate was mixed with $ddH_2O$ at 2 wt.% concentration and placed in a shaker at 500 rpm overnight for getting a homogeneous solution. Gelatin powder was added to the alginate solution at 8 wt.% gelatin concentration and mixed at 50 °C in a magnetic stirrer for at least 2 h until gelatin was dissolved. If imaging was necessary, alginate conjugated with fluorescein was added to the formulation at concentration of 0.3 wt.%.

0.1 wt.% chitosan stock solution was prepared by dissolving 5 mg chitosan in 100 µl acetic acid and 4.9 mL $ddH_2O$ at 60 °C for 3 h and at room temperature overnight. 100 mM $CaCl_2$ stock solution was prepared in $ddH_2O$. Chitosan and $CaCl_2$ stock solutions were diluted to prepare solutions at targeted concentrations.

*Preparation of Alginate-Fluorescein*: 100 mg alginate PRONOVA UP was dissolved in 10 mL $ddH_2O$ by stirring for 2 h. Then, it was mixed with 23 mg 1-Ethyl-3-(3-Dimethylaminopropyl)carbodiimide, hydrochloride for 30 min. 7.5 mg N-Hydroxysuccinimide was added to this solution. 43 mg 6-aminofluorescein in 70 v/v % ethanol in $ddH_2O$ was added to the final solution. It was allowed to mix for overnight. It was dialyzed in $ddH_2O$ for 2 d.

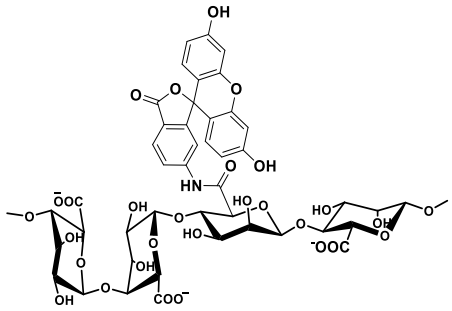

After dialysis $^1$H NMR (850 MHz, $D_2O$) δ = 9.06 (s), 7.82 (s), 7.46–7.43 (m), 5.07 (s), 4.52 (s), 4.15-3.76 (m), 3.22-3.10 (m), 1.92-1.89 (m)

*UV spectra of Alginate-Fluorescein Solution:* Solutions of 6-aminofluorescein, alginate-flurorescein and alginate were prepared in water in concentration of 1 mg $mL^{-1}$. The aim was to confirm the fluorescent activity of fluorescein after coupling to alginate-fluorescein.(Figure 7.1)

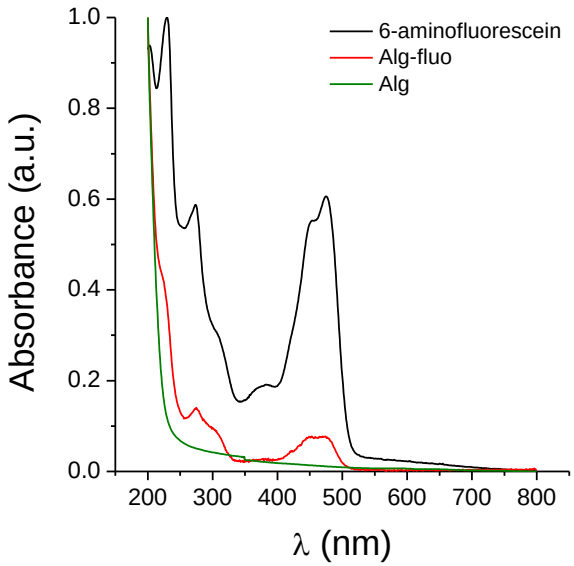


**Figure 7.1:** *UV absorbance of alginate-fluorescein, fluorescein and alginate.* Broad absorbance peak of fluorescein between 400 and 500 nm was kept after coupling to alginate. It confirmed that alginate-fluorescein was suitable to use to image alginate scaffolds in confocal microscope with the photoproperties of fluorescein.

*Preparation of Chitosan Coated Glasses:* Glass slides with diameter of 25 mm were sonicated in ethanol for 15 min. Then, they were rinsed with dd$H_2O$, ethanol, and dd$H_2O$, respectively. Glass slides were dried at ambient conditions. 400 µL of 0.1 wt.% chitosan solution was poured into each glass slide. Chitosan solution was kept on the glass slides for 15 min. Then, chitosan solutions were removed from glass slides. The glass slides were shortly rinsed in 0.1 M NaOH. Then, excess reagents were removed with rinsing in dd$H_2O$. The chitosan coated glass slides were dried at ambient conditions.

### 5.1.3 Calculation of Degree of Swelling

3D printed alginate/gelatin scaffolds were imaged with Zeiss LSM 880 Axio Observer, EC Plan-Neofluar 10x/0.3 M27 at 488 nm for excitation and 559 nm emission. The scaffolds were kept in DPBS (+,+) at room temperature during imaging. Three replicates of each scaffold type were used to make statistics. At least 5 points were measured from each thread and at least 5 threads were used for statistics.

### 5.1.4 Degradation Rate of Scaffolds

3 replicates of 2 layered alginate/gelatin scaffolds were used. Their printing solutions were removed after deposition. The scaffolds were rinsed with 1 mL of DPBS with $CaCl_2$ and $MgCl_2$ for 15 min. This solution was used as solution at day 0. Then, 1 mL of DPBS (+,+) was added to each sample. 7 days after the deposition of the scaffolds, the absorbance of the rinsing solutions at 494 nm was measured with Agilent Cary 2000.

### 5.1.5 Quantifying the Difference in Mechanical Strength

Zwick Roell Z005 tensile machine was using with its indenter accessory. 3 layered alginate/gelatin scaffolds with size of 1x1 cm were used in this test. Indenter with diameter of 2 mm was used to apply force with preload of 5 mN. The indentation was applied until the strain of 50%. 3 points from each sample and 3 replicates from each scaffold type were measured.

### 5.1.6 Effect of Temperature on Scaffolds

Alginate/gelatin scaffolds were placed in petri dishes filled with DPBS (+,+). Then, they were imaged during 1 h at Zeiss LSM 880 at 37 °C. 3D reconstructed images were taken after 1 h incubation in DPBS (+,+) at 37 °C.